The Embryological Origin of Resident Vascular Stem Cells – Implications for Vascular Disease

A dissertation submitted for the degree of Ph.D.

Mariana Soledad Di Luca, B.Sc (Hons)

School of Biotechnology

Dublin City University

Under the supervision of

Prof. Paul A. Cahill

Dr. Dermot Walls

September 2019

Declaration

I hereby certify that this material, which I now submit for assessment on the programme of study leading to the award of Ph.D. is entirely my own work, that I have exercised reasonable care to ensure that the work is original, and does not to the best of my knowledge breach any law of copyright, and has not been taken from the work of others save and to the extent that such work has been cited and acknowledged within the text of my work.

Signed: _____ ID No.: 10709317 Date: _____

Publications and Presentations

Publications

Collins, L.E., DeCourcey, **Di Luca M,** K. Rochfort D, Loscher CE, 2015. An Emerging Role for SNARE Proteins in Dendritic Cell Function. *Frontiers in Immunology*, 6 (133). DOI: 10.3389/fimmu.2015.00133

Molony C, **Di Luca M,** McIntyre J, Hennelly B,. Byrne MJ, and Cahill PA, 2016. Abstract 573: Vibrational Spectroscopy Discriminates Differentiated Vascular Smooth Muscle Cells From Mesenchymal Stem Cells and Their Vascular Progeny. *American Heart Association, Inc., Arteriosclerosis, Thrombosis, and Vascular Biology*, 36(1), page A573.

Hakimjavadi R, Burtenshaw D, Fitzpatrick E, **Di Luca M,** Casey G, Redmond EM, and Cahill PA, 2016. Abstract 143: Enrichment of Dimethylation of Lysine 4 on Histone 3 and Resident Vascular Stem Cell Transition to Vascular Smooth Muscle Cells. *American Heart Association, Inc., Arteriosclerosis, Thrombosis, and Vascular Biology*, 36(1), page A143.

Hakimjavadi R, Olayinka A, **Luca M Di,** Guha S, Walls D, Redmond EM, Cahill PA. 2017 "Pathogenetic Mechanisms in Alagille Syndrome," in *eLS* (Chichester, UK: John Wiley & Sons, Ltd), 1–10.

Di Luca M, Fitzpatrick E, Liu W, Morrow D, Redmond EM, Cahill PA. 2018 Characterisation of resident multipotent vascular stem cells (MVSCS) from susceptible and non-susceptible arteriosclerotic regions of the mouse aorta. *Heart* **104**:A10–A10.

Fitzpatrick E, Liu W, Alshamrani M, Helt JC, Hakimjavadi R, Harman S, Olayinka A, Burtenshaw D, Corcoran E, **Di Luca M,** Lally C, Redmond EM, Cahill PA 2018. Hedgehog responsive stem cell antigen-1/S100β resident vascular stem cells contribute to neointimal formation *Heart*;104:A7.

Hakimjavadi R, Burtenshaw D, Fitzpatrick E, **Di Luca M,** Corcoran E, Casey G, Redmond EM, Cahill PA. 2018. Stem-cell derived myogenic progeny enrich for vascular smooth muscle cell epigenetic marks at the myosin heavy chain 11 promoter in vitro. *Heart,* 104 (Suppl 4) A9

Corcoran E, Olayinka A, **Di Luca M**, O'Connor B, Cahill PA 2019. The role of N-glycosylation in the myogenic differentiation of stem cells to vascular muscle cells. *Heart* (in press)

Di Luca M, Hakimjavadi R, Burtenshaw D, Fitzpatrick E, Mathiue P, Lally C, Redmond EM. Cahill PA, 2018. The Dichotomy of Vascular Smooth Muscle Differentiation/De-differentiation in Health and Disease, in K. Sakuma (ed) *Muscle Cell and Tissue Current Status of Research Field.* IntechOpen: London. Available at https://www.intechopen.com/books/muscle-cell-and-tissue-current-status-of-research- field/the-dichotomy-of-vascular-smooth-muscle-differentiation-de-differentiation-in- health-and-disease.

Fitzpatrick E, **Di Luca M**, Liu W, Helt JC, Hakimjavadi R, Harman S, Olayinka A, Burtenshaw D, Corcoran E, Lally C, Redmond EM, Cahill PA 2019. The calcium binding protein S100β marks hedgehog-responsive perivascular stem cells that contribute to intimal thickening following iatrogenic flow-restriction. *Cell Stem Cell* (under review).

Molony C, King D, Lourdes A.N. Julius, Fitzpatrick E, **Di Luca M,** Casey G, Hakimjavadi R, Burtenshaw D, Healy K, Canning D, Kernan D, Llobera A, Liu W, Morrow D, Downing T, Redmond EM, Ducree J, Cahill PA 2019. PA Injury-Activated Vascular Cells Share a Common Photonic Fingerprint with Stem Cell-Derived Myogenic Progeny following Interrogation. *Stem Cell Reports* (under review).

Presentations: Poster

Notch Activation of resident multipotent vascular stem cells. The Notch Meeting IX, 8th – 12th October 2015, Athens, Greece

Resident multipotent vascular stem cell transition to vascular smooth muscle cells by Notch Signalling Activation. 8th Annual SoBT Research, 29th January 2016, Dublin, Ireland.

Enrichment of dimethylation of lysine 4 on histone 3 following resident vascular stem cell transition to vascular smooth muscle cells *in vivo.* 2nd Annual Epigenetics Discovery Congress, 8th – 9th September 2016, London, UK.

Resident multipotent vascular stem cells (MVSC) isolated from susceptible and non-susceptible arteriosclerotic regions of the mouse aorta are Sca-1/S100/Nestin+ and respond similarly to the same myogenic inductive stimulus. Annual SoBT Research Day, 26th January 2018. Dublin, Ireland.

Resident multipotent vascular stem cells (MVSC) isolated from susceptible and non-susceptible arteriosclerotic regions of the mouse aorta are Sca-1/S100/Nestin+ and respond similarly to the same myogenic inductive stimulus. Scottish Cardiovascular Forum, 3rd February 2018. Dublin, Ireland.

Resident multipotent vascular stem cells (MVSC) isolated from susceptible and non-susceptible arteriosclerotic regions of the mouse aorta are Sca-1/S100/Nestin+ and respond similarly to the same myogenic inductive stimulus. ATVB-PVD 2018 Scientific Sessions, 10th – 12th May 2018. ATVB-PVD

Presentations: Oral

The Embryological Origin of resident vascular stem cells - Applications for vascular diseases, 7th Annual SoBT Research, January 2015, Dublin, Ireland.

Finalist on "Why does vascular disease develop in specific areas of the aorta?". Tell-it-Straight Competition, 29th April 2015, Dublin, Ireland.

Dedication

This thesis is wholeheartedly dedicated to my Mam and Dad who always showed me immense patience, love and support, throughout the trials and tribulations of my studies. There are no words to describe my gratitude to you and I only hope you know this would not have been possible without you.

Acknowledgments

Firstly, I would like to sincerely thank my supervisor and advisor Professor Paul Cahill, for providing me the opportunity to complete my research under his excellent stewardship. I am very grateful for the support and advice you offered me throughout the completion of my work and most importantly the continued patience you extended to me. It was a pleasure working with you. I would also like to thank Dr. Dermott Walls for his support throughout my studies.

Many thanks to all the technical staff within the School of Biotechnology for their constant help. Also, to Damian O'Donohue and Carolyne from DCU BRU for their unconditional assistance and advice throughout the years. You have provided me with the knowledge and confidence to carry on my work into the future.

To all my friends and colleagues, within the School of Biotechnology and the Vascular Biology and Therapeutics Lab, who have contributed in so many ways to this thesis through their unconditional support, advice and guidance, including Abidemi Olayinka, Roya Hakimjavadi, Flavio Ferreira, Burca Gunes, Arun Decano, Emma Fitzpatrick, Claire Moloney, Roa Bashmail, Denise Burtenshaw, Eoin Corcoran, Yusof Gusti, Susan Harman and Joseph Mackle.

To my best friends Julieta, Silvia, and Patricia for answering my calls at any time of the day and night regardless the time differences, only to listen and give me the strength to continue working when I thought of giving up.

Thank you to Tommy and Pauline for the talks, calls and meals-on-wheels, they were all much needed.

A very special thanks is owed to my boyfriend Richard, who showed me unwavering support even on my most stressful days.

To my brothers Esteban and Zaki, my family back home and my extended family here in Ireland for believing in me and being so understanding and supportive throughout all these years.

Contents

Declaration ii
Publications and Presentations iii
Dedication vi
Acknowledgments vii
List of Figures xiii
List of Tables xviii
Abbreviations xix
Units xxii
Abstract xxiii
Chapter 1 1
1.1 The Vascular System 2
1.2 Cardiovascular Diseases 4
1.2.1 Arteriosclerosis 4
1.2.2 Current therapies for cardiovascular disease 4
1.2.2.1 In-stent restenosis 6
1.3 Smooth Muscle Cells (SMCs) 8
1.3.1 Vascular Smooth Muscle Cell Heterogeneity and Plasticity 8
1.3.2 Vascular Smooth Muscle Cell Origin 10
1.3.3 Epigenetic modifications involved in Vascular Smooth Muscle Cell Differentiation 13
1.3.4 The molecular signals involved in SMC differentiation 16
1.3.5 Signalling involved in Vascular Smooth Muscle Cell Development and Differentiation 26
1.4 Smooth Muscle Cell Progenitors 34
1.4.1 De-differentiated SMCs 34
1.4.2 Circulating Progenitors, and BM-derived Stem Cells 35
1.4.3 SMC Progenitor Cells from the Adventitia 37
1.4.4 SMC Progenitor Cells from Tunica Media 38
1.4.5 SMC Progenitor Cells from Endothelium 39
1.5 The use of animal models in research 39
1.5.1 Use of animal models in cardiovascular research 39
1.5.1.1 Use of injury models in cardiovascular research 40
1.5.1.2 The lineage tracing studies that have mostly contributed to our knowledge of SMC progeny in the murine neointima 45
1.6 Aim of this Study 64
Chapter 2 65

2.1 Biological Materials 66
2.1.1 Commercial Cell Lines & Tissue-derived Cells 66
2.1.2 Antibodies 67
2.1.3 Primers used in this study 69
2.1.4 Chemical and Biological agents used in this study 70
2.2 RNA Manipulation 72
2.2.1 RNA Storage 72
2.2.2 Total RNA Extraction from tissue and cultured cell samples 72
2.2.3 RNA Measurements 74
2.3 Real Time Reverse-Transcriptase Polymerase Reaction Chain 75
2.3.1 Real Time One-Step RT-PCR by QIAGEN 76
2.3.3 Real Time One-Step RT-PCR by BioLine 79
2.3.4 Relative expression ratio analysis by the REST© tool 81
2.4 Chromatin Immunoprecipitation (ChIP) followed by Polymerase Chain Reaction (PCR) 82
2.4.1 Chromatin Extraction 83
2.4.2 Chromatin Immunoprecipitation (ChIP) 84
2.4.3 Real Time Polymerase Chain Reaction (PCR) 86
2.5 Immunocytochemistry 87
2.6 Flow Cytometry 89
2.7 Scanning Electron Microscopy (S.E.M.) 90
2.8 Cell Culture Methods 91
2.8.1 Cell lines 91
2.8.2 Cell Subculture and Expansion 98
2.8.3 Cell Counting 99
2.8.4 Cryogenic preservation and recovery of cells 100
2.9 Animal work 101
2.9.1 Animal Models 101
2.9.2 Injury Models 108
2.9.3 Immunohistochemistry 111
2.9.3.1 Method 1 111
2.9.3.2 Method 2 114
2.9.4 Morphometric Analysis 115
2.10 Data Analysis 116
Chapter 3 119
3.1 Introduction 120
3.2 Strategy 123
3.2.1 Determine the presence of vSCs in healthy and diseased vessels using Sca-1-EGFP and S100β-EGFP transgenic mice 123
3.2.2 Perform cell fate mapping of S100β cells within the vessel wall

following vascular injury 124
3.2.3 Determine whether or not the S100β progeny, S100β-tdT$^+$ within the neointima are also Sca-1$^+$ 124
3.2.4 Methodology 125
3.3 Results 127
3.3.1 Morphometric analysis of sham and ligated vessels reveals vascular remodelling concomitant with an increase in the number of S100β-EGFP$^+$ and Sca-1-EGFP$^+$ cells within the media and neointima of injured vessels 127
3.3.1.1 Morphometric analysis of the left carotid artery (LCA) and right carotid artery (RCA) in sham and ligated vessel 21 days post ligation 127
3.3.1.2 Increased number of S100β-eGFP and Sca-1-EGFP cells within injured vessels post ligation 127
3.3.2 Lineage tracing analysis using tamoxifen-inducible S100β-EGFP/cre /ERT2/ROSA26RtdTomato animals reveals the presence of S100β-derived cells (S100β-tdT+) in the neointimal and medial layers of ligated vessels 21 days post-ligation. 137
3.3.3 Co-localisation of a Sca-1$^+$ cell population with S100β-tdT$^+$ cells in the neointima and media of ligated vessels after injury 143
3.3.3.1 Lineage tracing studies reveal the presence of S100β-derived Sca-1$^+$ cells (S100β-tdT$^+$ Sca-1-white$^+$) in the neointima of ligated vessels after 21 days post ligation..... 143
3.3.4 Co-localisation of a αSMA$^+$ cell population with S100β-tdT$^+$ cells in the neointima and media of ligated vessels after injury. . 152
3.3.5 Summary 157
3.4 Discussion 158
Chapter 4 165
4.1 Introduction 166
4.2 Strategy 169
4.2.1 Isolate vascular stem cells from the tunica media of murine aortic tissue using an altered enzymatic dispersion protocol..... 169
4.2.2 Characterize the isolated vascular stem cells (vSCs) from both neuroectodermal (NE), and the paraxial mesodermal (PM) regions of the murine aorta 170
4.2.3 Compare the embryological origin of the isolated vSCs to that of the resident tissue..... 170
4.2.4 Identification of the vascular stem cell niche in the aorta – “tunica media versus tunica adventitia” 171
4.2.5 Methodology 171
4.3 Results 174
4.3.1 Isolation of vascular stem cells from the tunica media of murine

aortic tissue 174
4.3.2 Characterization of isolated stem cells from the tunica media of murine aortic tissue 176
4.3.3 Murine stem cells from the tunica media of the aortic arch and thoracic aorta are of a neuroectodermal origin 182
4.3.4 Identification of the location of vascular stem cells 194
4.3.4.1 Histochemical analysis for the presence of cells on the external lamina of the adventitial medial boundary following removal of the adventitia 194
4.3.4.2 Scanning Electron Microscopy (SEM) analysis for the presence of cells on the external lamina of the adventitial medial boundary after enzymatic removal of the adventitia..... 194
4.3.5 Summary 197
4.4 Discussion 198
Chapter 5 201
5.1 Introduction 202
5.2 Strategy 205
5.2.1 Determine whether or not mAA-vSCs are capable of differentiating into mature SMC by culturing them for 7 days in 10%FBS-supplemented DMEM (DM). 205
5.2.2 Compare the differentiation levels of both mAA-vSCs and mTA-vSCs to the SMC phenotype when exposed to TGF-β1 and the Jagged1-activated Notch signalling. 206
5.2.3 To examine the effect of TGF-β1 on Jagged1/Notch-induced SMC differentiation, and vice versa. 207
5.2.4 Determine whether or not mAA-vSCs are capable of differentiating into mature SMC upon activation of the Hh and Wnt/β-catenin signalling pathways..... 208
5.2.5 Methodology 208
5.3 Results 210
5.3.1 mAA-vSCs are capable of differentiating into SMC in 10% FBS-supplemented DMEM for 7 days 210
5.3.2 Jagged1-dependent Notch signaling but not TGF-β1 drives differentiation of mAA-vSCs and mTA-vSCs into mature SMCs. 214
5.3.2.1 Vascular stem cells from murine aortic arch and thoracic aorta respond similarly to TGF-β1 signalling. 214
5.3.2.2 Vascular stem cells from murine aortic arch and thoracic aorta respond similarly to Jagged1-activated Notch signalling 215
5.3.3 Interaction studies between the TGF-β1 and Jagged1 signalling suggested that both pathways may be required for SMC

induction, but Jagged1 activation is directly involved in SMC differentiation of vSCs. 239
5.3.3.1 TGF-β1-induced myogenic differentiation of vascular stem cells from murine aortic arch is prevented by the SMAD/TGF-β signalling inhibitor, SB431542 239
5.3.3.2 Jagged1-induced myogenic differentiation of vascular stem cells from murine aortic arch is prevented by the secretase inhibitor, DAPT 240
5.3.3.3 The TGF-β and Jagged1-dependent Notch signalling pathways work synergistically to transition vascular stem cells (vSCs) to SMCs, but Jagged1-activated Notch is critical in the SMC maturation process of vSCs. 241
5.3.4 Wnt4 and Sonic Hedgehog treatment on mAA-vSCs 268
5.3.4.1 Murine recombinant Wnt4 does not induce myogenic differentiation of vascular stem cells from murine aortic arch 268
5.3.4.2 Murine recombinant Shh does not induce myogenic differentiation of vascular stem cells from murine aortic arch 269
5.3.5 Summary 279
5.4 Discussion 281
Chapter 6 287
6.1 The Involvement of S100β$^+$ and Sca-1$^+$ in Vascular Disease 289
6.2 Isolated vascular progenitor cells from the athero-prone (aortic arch) and athero-resistant (thoracic aorta) regions of the murine aorta are neuroectodermal in origin 295
6.3 Jagged1-activated Notch signaling directly mediates SMC differentiation in vascular stem cells 298
Future work 303
Bibliography 305

List of Figures

Figure 1.1. Composition of Arteries and Veins. 3
Figure 1.2. Embryological origin-specific SMCs. 12
Figure 1.3. Cartoon depicting epigenetic changes in mature SMCs. 16
Figure 1.4. SMAD/TGF-β Signalling Pathway. 18
Figure 1.5. Canonical Notch Signalling Pathway. 21
Figure 1.6. Wnt/β-catenin Signalling Pathway. 23
Figure 1.7. Hedgehog Signalling Pathway in Vertebrates. 25
Figure 2.1. Obtaining the tunica media by following a series of steps. 94
Figure 2.2. Tissue pieces on a CellStart pre-coated 6-well plate. 96
Figure 2.3. Schematic illustration of the seeding step on a CellStart pre-coated 6-well plate after cell enzymatic dissociation. 97
Figure 2.4. Schematic illustration of the seeding steps of the modified enzymatic dispersion protocol. 98
Figure 2.5. Schematic of a haemocytometer cell counting (Provost & Wallert Research, 2015). 100
Figure 2.6. Genetics of the S100β-EGFP/cre-ER^{T2}/Rosa26td^{Tomato} animals used in the *in vivo* tracing study. 104
Figure 2.7. Tamoxifen-inducible Cre-loxP technology. 105
Figure 2.8. Cre-recombination Efficiency. 106
Figure 2.9. Representation of the Sca-1-EGFP transgene. Expression of the EGFP protein is driven by the Sca-1 promoter when active. 108
Figure 2.10. Supine position and Surgical incision. 110
Figure 2.11. Schematic representation of the Neck and Carotid Triangle. 110
Figure 2.12. Schematic representation of Complete and Partial Carotid Artery Ligation. 111
Figure 3.1. Morphometric analysis of adventitial medial, intimal and luminal volumes in RCA vessels from S100β-EGFP/cre/ERT2/ROSA26RtdTomato transgenic mice 21 days post ligation. 129
Figure 3.2. Morphometric analysis of adventitial medial, intimal and luminal volumes in LCA vessels from S100β EGFP/cre/ERT2/ROSA26RtdTomato transgenic mice 21 days post ligation. 130
Figure 3.3. S100β-GFP expression in sham and ligated RCA from S100β-EGFP/cre/ERT2/ROSA26RtdTomato transgenic mice. 131
Figure 3.4. S100β-GFP expression in sham and ligated LCA from S100β-EGFP/cre/ERT2/ROSA26RtdTomato transgenic mice. 133
Figure 3.5. Sca-1-EGFP expression in sham and ligated LCA from the Sca-1-EGFP transgenic mice 14 days after partial carotid artery ligation. 135
Figure 3.6. S100β-tdTomato expression in sham and ligated LCA of S100β-EGFP/cre/ERT2/ROSA26R^{tdTomato} transgenic mice after 21 days that were pre-treated with corn oil for 5 days prior to ligation after 2 weeks. 138

Figure 3.7. S100β-tdTomato expression in sham and ligated RCA of S100β-EGFP/cre/ERT2/ROSA26R^{tdTomato} transgenic mice 21 days that were pre-treated with tamoxifen for 5 days prior to ligation after 2 weeks. 139
Figure 3.8. S100β-tdTomato expression in sham and ligated LCA of S100β-EGFP/cre/ERT2/ROSA26R^{tdTomato} transgenic mice after 21 days that were pre-treated with tamoxifen for 5 days prior to ligation after 2 weeks. 141
Figure 3.9. S100β-tdTomato expression in RCA and LCA of ligated S100β-EGFP/cre/ERT2/ROSA26RtdTomato transgenic mice after 21 days that were pre-treated with tamoxifen for 5 days prior to ligation after 2 weeks. 145
Figure 3.10. Profile of Sca-1+ cells in RCA and LCA of ligated S100β-EGFP/cre/ERT2/ROSA26RtdTomato transgenic mice after 21 days that were pre-treated with tamoxifen for 5 days prior to ligation after 2 weeks. 147
Figure 3.11. Co-localisation of S100β-tdT+ and Sca-1+ cells in RCA and LCA of ligated S100β-EGFP/cre/ERT2/ROSA26RtdTomato transgenic mice after 21 days that were pre-treated with tamoxifen for 5 days prior to ligation after 2 weeks. 149
Figure 3.12. Co-localisation of S100β-tdT+ and alpha-SMA+ cells in RCA and LCA of ligated S100β-EGFP/cre/ERT2/ROSA26RtdTomato transgenic mice after 21 days that were pre-treated with tamoxifen for 5 days prior to ligation after 2 weeks. 153
Figure 3.13. S100β-EGFP and S100β-tdTomato expression in bone-marrow. 161
Figure 4.1. Enzymatic dissociation and expansion of murine vascular stem cells (vSCs) isolated from aortic arch and thoracic aorta. 175
Figure 4.2. Flow Cytometry analysis of murine vSCs isolated from aortic arch (mAA-vSCs) and thoracic aorta (mTA-vSCs). 178
Figure 4.3. Immunocytochemical analysis of murine vSCs isolated from the medial layer of thoracic aorta. 179
Figure 4.4. Immunocytochemical analysis of murine vSCs isolated from the medial layer aortic arch. 180
Figure 4.5. ChIP-PCR analysis of mAA-vSCs on H3K4me2, H3K27me27 histone modifications and TET-2 binding at the SM-MHC promoter. 181
Figure 4.6. Relative S100β mRNA expression levels in mAA-vSCs and mTA-vSCs compared to SMC controls. 184
Figure 4.7. Relative Nestin mRNA expression levels in mAA-vSCs and mTA-vSCs compared to SMC controls. 185
Figure 4.8. Relative Sox10 mRNA expression levels in mAA-vSCs and mTA-vSCs compared to SMC controls. 186
Figure 4.9. Relative SM-MHC mRNA expression levels in mAA-vSCs and mTA-vSCs compared to neural stem cell mNE-4C controls. 187
Figure 4.10. Relative CNN1 mRNA expression levels in mAA-vSCs and mTA-vSCs compared to neural stem cell mNE-4C controls. 188
Figure 4.11. Relative Tbx6 mRNA expression levels in mAA-vSCs and mTA-vSCs compared to mNE-4C controls. 189
Figure 4.12. Relative Pax1 mRNA expression levels in mAA-vSCs and mTA-vSCs

compared to mNE-4C controls. 190
Figure 4.13. Relative Pax6 mRNA expression levels in mAA-vSCs and mTA-vSCs compared to mC3H-10T1/2 controls. 191
Figure 4.14. Relative Nkx2.5 mRNA expression levels in mAA-vSCs and mTA-vSCs compared to mNE-4C controls. 192
Figure 4.15. Relative KDR mRNA expression levels in mAA-vSCs and mTA-vSCs compared to mNE-4C controls. 193
Figure 4.16. Cells are still present on the adventitia-side external laminar after enzymatic adventitia removal. 195
Figure 4.17. Adventitial tissue/cells are still present on the external lamina after enzymatic removal of the adventitial layer. 196
Figure 5.1. Myogenic differentiation of mouse aortic arch vascular stem cells (mAA-vSCs) in response to 10% FBS-containing DMEM (DM) for 7 days. 211
Figure 5.2. Myogenic differentiation of mouse aortic arch vascular stem cells (mAA-vSCs) in 10% FBS-containing DMEM (DM) for 7 days. 212
Figure 5.3. The cell number of mouse aortic arch vascular stem cells (mAA-vSCs) decreased 7 days after in 10% FBS-containing DMEM (DM). 213
Figure 5.4. Calponin1 mRNA levels significantly increased on mAA-vSC 7 days after TGF-β1 treatment. 218
Figure 5.5. Calponin1 protein levels significantly increased on mAA-vSC 7 days after TGF-β1 treatment. 219
Figure 5.6. The fraction of cells positively expressing Calponin1 significantly increased on mAA-vSC 7 days after TGF-β1 treatment. 220
Figure 5.7. The cell number of mAA-vSCs decreased 7 days after TGF-□1 treatment. 221
Figure 5.8. Calponin1 mRNA levels significantly increased on mTA-vSC 7 days after TGF-β1 treatment. 222
Figure 5.9. Calponin1 protein levels significantly increased on mTA-vSC 7 days after TGF-β1 treatment. 223
Figure 5.10. The fraction of cells positively expressing Calponin1 significantly increased on mTA-vSC 7 days after TGF-β1 treatment. 224
Figure 5.11. The cell number of mTA-vSCs decreased 7 days after TGF-β1 treatment. 225
Figure 5.12. Hey1, Calponin1 and Sm-mhc mRNA levels significantly increased on mAA-vSC 7 days after Jagged1-activated Notch signalling. 226
Figure 5.13. Calponin1 and SM-MHC protein levels significantly increased on mAA-vSC 7 days after Jagged1-activated Notch signalling. 227
Figure 5.14. The fraction of cells positively expressing Calponin1 and SM-MHC significantly increased on mAA-vSC 7 days after Jagged1-activated Notch signalling. 228
Figure 5.15. The cell number of mAA-vSCs decreased 7 days after Jagged1-activated Notch signalling. 229
Figure 5.16. The histone modification H3K4me2 is enriched at the SM-MHC gene locus after Jagged1-activated Notch signalling on mAA-vSCs. 230
Figure 5.17. The histone modification H3K27me3 is enriched at the SM-MHC gene

locus after Jagged1-activated Notch signalling on mAA-vSCs. 231
Figure 5.18. TET-2-binding at the SM-MHC gene locus after Jagged1-activated Notch signalling on mAA-vSCs.....232
Figure 5.19. Hey1, Calponin1 and Sm-mhc mRNA levels significantly increased on mTA-vSC 7 days after Jagged1-activated Notch signalling. 233
Figure 5.20. Calponin1 and SM-MHC protein levels significantly increased on mTA-vSC 7 days after Jagged1-activated Notch signalling. 234
Figure 5.21. The fraction of cells positively expressing Calponin1 significantly increased on mTA-vSC 7 days after Jagged1-activated Notch signalling. 235
Figure 5.22. The cell number of mTA-vSCs decreased 7 days after Jagged1-activated Notch signalling.....236
Figure 5.23. The SMAD/TGF-β signalling inhibitor, SB431542 attenuates the effect of TGF-β1 on the Bcl2l1 and Cnn1 gene expression in mAA-vSC. 245
Figure 5.24. The SMAD/TGF-β signalling inhibitor, SB431542 attenuates the effect of TGF-β1 on the CNN1 protein expression in mAA-vSC. 246
Figure 5.25. The SMAD/TGF-β1 signalling inhibitor, SB431542 reduces the effect of TGF-β1 on the fraction of $CNN1^+$ cells in mAA-vSC. 247
Figure 5.26. The SMAD/TGF-β1 signalling inhibitor, SB431542 reduces the effect of TGF-β1 on cell number in mAA-vSC. 248
Figure 5.27. The γ-secretase inhibitor, DAPT downregulates the effect of Jag1-Fc on Hey1 gene expression in mAA-vSC.....249
Figure 5.28. The γ-secretase inhibitor, DAPT downregulates the effect of Jag1-Fc on Cnn1 gene expression in mAA-vSC.....250
Figure 5.29. The γ-secretase inhibitor, DAPT downregulates the effect of Jag1-Fc on Sm-mhc gene expression in mAA-vSC.....251
Figure 5.30. The γ-secretase inhibitor, DAPT downregulates the effect of Jag1-Fc on CNN1 and SM-MHC protein expression in mAA-vSC. 252
Figure 5.31. The γ-secretase inhibitor, DAPT reduces the effect of Jag1-Fc on the fraction of $CNN1^+$ cells in mAA-vSC. 253
Figure 5.32. The γ-secretase inhibitor, DAPT reduces the effect of Jag1-Fc on the fraction of SM-MHC^+ cells in mAA-vSC. 254
Figure 5.33. The γ-secretase inhibitor, DAPT reduces the effect of Jag1-Fc on cell number in mAA-vSC. 255
Figure 5.34. The γ-secretase inhibitor, DAPT attenuates the effect of TGF-β1 on Cnn1 gene expression in mAA-vSC. 256
Figure 5.35. The γ-secretase inhibitor, DAPT does not alter the effect of TGF-β1 on Sm-mhc gene expression in mAA-vSC. 257
Figure 5.36. The SMAD/TGF-β inhibitor, SB431542 enhances the effect of Jag1-Fc on Hey1 gene expression in mAA-vSC.....258
Figure 5.37. The SMAD/TGF-β inhibitor, SB431542 enhances the effect of Jag1-Fc on Cnn1 gene expression in mAA-vSC.....259
Figure 5.38. The SMAD/TGF-β inhibitor, SB431542 enhances the effect of Jag1-Fc on

Sm-mhc gene expression in mAA-vSC. 260
Figure 5.39. Relative Tgf-β1 gene expression in mAA-vSCs at different time points after Jag1-Fc treatment. 261
Figure 5.40. Relative Col3a1 gene expression in mAA-vSCs at different time points after Jag1-Fc treatment. 262
Figure 5.41. Relative Hey1 gene expression in mAA-vSCs increases with time after Jag1-Fc treatment. 263
Figure 5.42. Relative Sm-mhc gene expression in mAA-vSCs peaks 72 hours after Jag1-Fc treatment. 264
Figure 5.43. Relative Cnn1 gene expression in mAA-vSCs increases 7 days after Jag1-Fc treatment. 265
Figure 5.44. Relative Jag1 gene expression in mAA-vSCs 24 hour and 7 days after TGβ1 treatment. 266
Figure 5.45. Relative Col3a1 gene expression in mAA-vSCs 24 hour and 7 days after TGβ1 treatment. 267
Figure 5.46. Wnt4 signalling increases the expression levels of the Wnt target gene Runx1 in mAA-vSC 7 days post-treatment. 270
Figure 5.47. Wnt4 signalling increases the expression levels of Cnn1 in mAA-vSC 7 days post-treatment. 271
Figure 5.48. Wnt4 signalling does not have an effect on the expression levels of Sm-mhc in mAA-vSC 7 days post-treatment. 272
Figure 5.49. Wnt4 signalling increases the expression levels of Fzd-1 in mAA-vSC 7 days post-treatment. 273
Figure 5.50. The effect of rmWnt4 on the Wnt target genes Runx1 and Fzd-1 in mAA-vSCs 48 hours after treatment. 274
Figure 5.51. The effect of rmWnt4 on the SMC genes Cnn1 and Sm-mhc in mAA-vSCs 7 days after treatment. 275
Figure 5.52. The effect of rmShh on the Shh target gene Gli1 in mAA-vSCs 48 hours after treatment. 276
Figure 5.53. The effect of rmShh on the SMC target gene Cnn1 in mAA-vSCs 7days after treatment. 277
Figure 5.54. The effect of rmShh on the SMC target gene Sm-mhc in mAA-vSCs 7days after treatment. 278
Figure 5.55. The myogenic effect of Wnt4 signalling on mTA-vSC cultured in 10% FBS-containing medium. 284
Figure 5.56. The myogenic effect of Shh signalling on mTA-vSC cultured in 10% FBS-containing medium. 285

List of Tables

Table 1-1. Classification of Arteriosclerosis.....6
Table 1-2. Morphology of contractile and synthetic SMCs.....10
Table 1-3. The HERP family (Iso, Kedes and Hamamori, 2003).....19
Table 2-1. Cells used during the course of study.....66
Table 2-2. Antibodies and their corresponding dilutions used in immunocytochemistry. 67
Table 2-3. Antibodies and their corresponding dilutions used in immunohistochemistry. 67
Table 2-4. Antibodies and their corresponding dilutions used in Chromatin Immunoprecipitation (ChIP). 68
Table 2-5. Antibodies and their corresponding dilutions used in Flow Cytometry.....68
Table 2-6. Customised primers used in this study from Integrity DNA Technology (IDT).....69
Table 2-7. Primers used in this study from QIAGEN.....69
Table 2-8. Chemical and Biological Agents used in this study. 70
Table 2-9. Components supplied in the Rotor-Gene SYBR® Green RT-PCR Kit. 76
Table 2-10. Preparation of a single Reaction Tubes. 78
Table 2-11. Cycling Condition Setup. 78
Table 2-12. Components supplied in the SensiFAST™ SYBR® No-ROX One-Step Kit. 79
Table 2-13. Preparation of a single Reaction Tubes. 80
Table 2-14. Cycling Condition Setup. 80
Table 2-15. ChIP reaction components.....85
Table 2-16. Preparation of a single Reaction Tubes. 87
Table 2-17. Cycling Condition Setup. 87
Table 2-18. Neuroectodermal Maintenance Medium (NE-MM).....93
Table 2-19. Collagenase Solution. 95
Table 2-20. CellStart Dilution for a 6-well plate. 96
Table 2-21. Collagenase/Elastase Solution.....97
Table 5-1. Responsiveness of mAA-vSCs and mTA-vSCs to myogenic differentiation according to gene expression.....237
Table 5-2. Responsiveness of mAA-vSCs and mTA-vSCs to myogenic differentiation according to protein expression.....238

Abbreviations

β-arr	beta-arrestin
β-TrCP	beta-transducin repeat-containing protein
BMS	Bare Metal Stents
BSA	Bovine Serum Albumin
ChIP	Chromatin Immunoprecipitation
CNN1	Calponin1
CO_2	Carbon Dioxide
CVD	Cardiovascular Disease
DAPI	4',6-diamidino-2-phenylindole
DEPC	Diethylpyrocarbonate
DES	Drug Eluting Stents
DMEM	Dulbecco's Modified Essential Medium
DMSO	Dimethyl Sulfoxide
DNA	Deoxyribose Nucleic Acid
DPBS	Dulbecco's Phosphate Buffered Saline
tdT	tdTomato
EC	Endothelial Cell
ECM	Extra Cellular Matrix
EMEM	Eagle's Minimum Essential Medium
EndMT	Endothelial-Mesenchymal Transition
FBS	Fetal Bovine Serum
Fu	Serine/ Threonine Kinase Fused
GFP	Green Fluorescent Protein
GRK2	G protein couple receptor kinase 2
GSK3β	Glycogen Synthase Kinase 3β
HERP	HES-related Repressor Protein
HES	Hairy and Enhancer Split
HPF	High Power Field

IMT	Intimal Medial Thickening
ISR	In-stent Restenosis
Kif3a	Kinesin family member 3a
Kif7	Kinesin family member 7
mAA-vSC	mouse Aortic Arch vascular Stem Cell
MSC	Mesenchymal Stem Cell
mTA-vSC	mouse Thoracic Aorta vascular Stem Cell
MVSC	Multipotent Vascular Stem Cell
MYOCD	Myocardin
NICD	Notch Intracellular Domain
NECD	Notch Extracellular Domain
NTMIC	Notch Transmembrane and Intracellular Domain
NEXT	Notch Extracellular Truncation
P/S	Penicillin-Streptomycin
PBS	Phosphate Buffer Saline
PCR	Polymerase Chain Reaction
PDGF	Platelet Derived Growth Factor
PTA	Percutaneous Transluminal Angioplasty
RNA	Ribo-nucleic Acid
S100β	S100 calcium-binding protein β
SCF	Skp, Cullin, F-box containing complex or multi-protein E3 ubiquitin ligase
$SCF^{\beta\text{-}TrCP}$	Skp, Cullin, β-TrCP containing complex
Sca-1	Stem Cell Antigen-1
Shh	Sonic Hedgehog
SM22α	Smooth Muscle 22 alpha
SMC	Smooth Muscle Cell
SMMHC	Smooth Muscle Myosin Heavy Chain
Sox10/17	SRY (sex determining region Y)-box 10/17
SRF	Serum Response Factor

Sufu	Suppressor of Fused
TGFβ	Transforming Growth Factor Beta
Tm	Tamoxifen
vSC	vascular Stem Cell
vSMC	Vascular Smooth Muscle Cell
αSMA	Smooth Muscle alpha Actin

Units

%	Percentage
°C	Degrees Celsius
cm	Centimetres
cm^2	Centimetres squared
cm^3	Centimetres cubes
g	Grams
kg	kilograms
mAmp	milliamperes
mg	Milligram
min	Minutes
ml	Millilitre
ng	Nanogram
nl	Nanolitre
nm	Nanometre
rpm	Revolutions per minute
sec	Seconds
x g	G force
µg	Microgram
µl	Microliter
µM	Micromoles

Abstract

The Embryological Origin of Resident Vascular Stem Cells – Implications for Vascular Disease

Mariana Soledad Di Luca

Intimal medial thickening (IMT) and vascular regeneration are hallmarks of arteriosclerosis disease. The source of lesional vascular smooth muscle (vSMC)-like cells contributing to the neointima thickening and the molecular mechanisms that dictate their fate and function have been the topic of much debate. Our lab along with other research groups have previously shown a putative role for re-capitulation of Notch and Hedgehog signalling components in promoting neointima thickening and progression of IMT in murine models of arteriosclerosis. In recent years, a population of smooth muscle myosin heavy chain (SM-SMHC)-negative multipotent vascular stem cells (MVSCs) have been isolated in the tunica media and shown to proliferate and differentiate into vSMCs and further invade the intima in animal models of vascular injury. The risk of vascular disease may depend, in part, on the embryological origin of vSMC progenitors; with vSMCs of neuroectodermal (NE) origin (ascending aorta, aorta arch and carotid artery) exhibiting a higher risk compared to their paraxial mesodermal (PM) counterpart (descending aorta).

Herein, we demonstrate that NE ($S100\beta^+$) stem cell-derived progeny substantially contribute to neointima thickening within carotid arteries of S100β-eEGP-$CreER^{T2}$-Rosa26-tdT transgenic mice following ligation-induced injury and regeneration *in vivo*. $S100\beta^+$ vascular stem cells (vSCs) of NE origin were successfully isolated and characterised from the two discrete embryological regions of arterial vessels (neuroectoderm versus mesoderm) *in vitro* and responded in the same manner to different myogenic stimuli including transforming growth factor-β1 (TGF-β1), the Notch ligand Jagged1 and the morphogens wnt4 and sonic hedgehog (Shh). The primary inductive stimulus for myogenic differentiation was the Jagged1/Notch signalling pathway, which was shown to enrich the H3K4me2 epigenetic mark at the SM-MHC locus. Furthermore, enhanced calponin1 (Cnn1) and Sm-mhc gene expression along with an increase in the number of CNN1 and SM-MHC positive cells was attenuated using γ-secretase inhibitor DAPT. In conclusion, neuroectodermal-derived ($S100\beta^+$) vSCs may be responsible for the progression of pathological vascular remodelling and ultimately cardiovascular disease through re-capitulation of the Notch signalling pathway by the ligand, Jagged1.

Chapter 1

Introduction

1.1 The Vascular System

The vascular system is responsible for the preservation of a healthy environment in all the tissues and cells of the body, and its function is mediated by the circulation of blood throughout the body. Components of the vascular system supply the body with nutrients and oxygen and remove waste from metabolic reactions. The function of a blood vessel is dictated by its structural composition. Arteries are complex vessels whose architecture depends on their location within the vascular system. On the other hand, veins do not require elastic fibres within their walls due to the reduced blood pressure within these vessels. Their large vessel diameter and thin layer of smooth muscle cells are sufficient to exert the mechanical force of contraction and expansion facilitating the return of large amounts of deoxygenated blood back to the heart (Freeman, 2011).

Arteries can be categorised into two main groups namely elastic and muscular arteries. Elastic arteries are the largest arteries of the body including the aorta and the common carotid, and are often located close to the heart. Elastic arteries usually withstand highly pressurised blood propelled by the heart into the systemic circulatory system. Muscular arteries are generally small to medium in diameter vessels including the coronary arteries and the radial artery. All arteries contain three distinct layers referred to as the tunics; the tunica intima, tunica media and the tunica adventitia as shown in Figure 1.1 (Freeman, 2011). Unlike veins, the endothelial cells of arteries sit on a membrane composed of extracellular matrix (EM) and proteoglycans. This layer is usually referred as the intima and it is surrounded by the internal elastic lamina. It acts as a barrier between the tunica intima and the tunica media. The tunica media of both arteries and veins consist mainly of densely packed vascular smooth muscle cells, type I and III collagen, fibronectin and proteoglycans, albeit much less densely packed in veins. The tunica media is the main structure of a vessel wall, and in the case of arteries, can be categorised as elastic or muscular depending on its composition, extracellular matrix content and SMCs. For example, multiple layers of elastin fibres are found in elastic arteries compared to the loose elastin and collagen composition of muscular arteries. The adventitia is the last layer composed of fibroblasts, type I

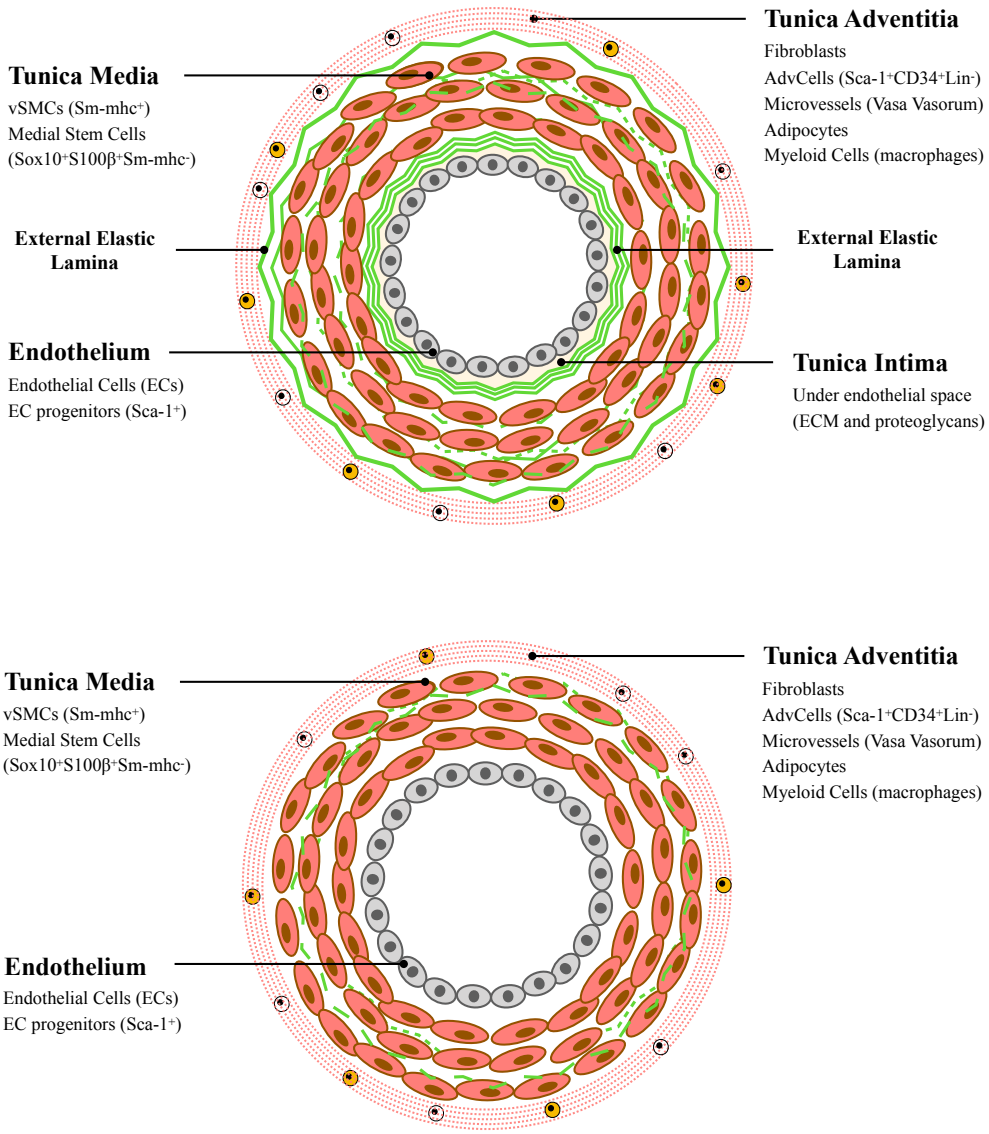

Figure 1.1. Composition of Arteries and Veins.

Arteries (top) and veins (bottom) consist of three main layers, a single-cell endothelium barrier between the lumen and the artery wall, a layer of smooth muscle cells (the media), and the outermost adventitial layer composed of fibroblasts.

collagen fibres, connective tissue and microvessels (vasa vasorum). In arteries, an external elastic lamina is the barrier between the adventitial and medial layer (Galkina and Ley, 2009) (Stocker and Keaney, 2004).

1.2 Cardiovascular Diseases

Cardiovascular Diseases (CVD) are renowned as one of the leading causes of death and morbidity worldwide. According to figures released by the World Health Organization (WHO), an estimated 31% of the global deaths are due to CVD. Of these fatalities, 85% were due to heart attacks and stroke. CVD are not only detrimental to the health of a population, but also affect the financial situation of thousands of families and have a huge impact on the economy of a country (WHO facts, 2017). According to a 2019 study, CVD are expected to cause the death of more than 23.6 million individuals globally by 2030. The medical cost of CVD are estimated to increase to $749 billion in 2035 (Benjamin et al., 2019).

CVD may develop in a patient with a genetic predisposition or develop gradually through their lifetime through a process known as *Atherosclerosis.* The term atherosclerosis itself has often been misused due to a lack of emphasis in establishing a classification system. In fact, atherosclerosis is a sub-type of *Arteriosclerosis* that indicates the class of arterial lesion. Therefore, progressive cardiovascular diseases originate through the process of arteriosclerosis and the subtype is determined by the nature of the arterial lesion (Fishbein and Fishbein, 2015).

1.2.1 Arteriosclerosis

The term of Arteriosclerosis defines a group of arterial lesions characterised by the thickening (symmetrical or asymmetrical) of the blood vessel wall resulting in partial obstruction of the blood flow. The current classification of Arteriosclerosis is shown in Table 1-1. As opposed to natural occurring vascular lesions, *iatrogenic lesions* usually occur after angioplasty and stenting, in bypass implantations, and transplants. Examples are intimal hyperplasia and restenosis (Fishbein and Fishbein, 2015) (Newby and Zaltsman, 2000).

1.2.2 Current therapies for cardiovascular disease

Despite having a genetic predisposition, CVD primarily occur naturally in the human population. However, there are numerous preventative measures that can delay its onset by adopting a healthy life-style. These are highly recommended for the normal

population, and of course patient cohorts who present either early or with advanced CVD symptoms. Medication is also prescribed to relieve symptoms by reducing high blood pressure and high LDL cholesterol levels.

Patients presenting with advanced atherosclerotic plaque formation commonly developed in coronary arteries are routinely subjected to surgical and non-surgical intervention. Percutaneous Transluminal Coronary Angioplasty (PTCA) followed by stenting is commonly used in the treatment of advanced CVD (Benjamin et al., 2019).

Balloon angioplasty is the surgical widening of an obstructed artery, due to the presence of an atherosclerotic plaque, by means of a balloon catheter. The technique consists of insertion of a collapsed balloon attached to a catheter into the obstructed site. Once the balloon catheter is in place, the balloon is inflated pushing the atheroma into the vessel wall re-establishing the blood flow. Most percutaneous coronary intervention (PCI) procedures involve the insertion of a metal mesh or *stent* after angioplasty to prevent elastic recoil after revascularization. However, the procedure introduces other issues such as re-occlusion of the vessel known as *in-stent restenosis (ISR).* The new lesion is classified as *iatrogenic* because it is due to intervention, and best known as *Intimal Hyperplasia* (Farooq *et al.*, 2011).

The introduction of the first-generation and second-generation Drug-Eluting Stents (DES) has significantly reduced re-occlusion rates of vessels when compared to their Bare-Metal (BMS) equivalents. However, ISR remains a major concern in the DES era, with re-occurrence rates up to 15% within the first year following PCI (MD et al., 2018). Secondary conditions to restenosis are ischemia, thrombosis and embolism (Mehta *et al.*, 2001). Patients undergoing either BMS- or DES-PCI receive a drug adjunctive treatment to reduce the risks while the artery heals (Giustino *et al.*, 2015).

Table 1-1. Classification of Arteriosclerosis

(Fishbein and Fishbein, 2015) (Newby and Zaltsman, 2000).

	Lesion(s)	Location	Description
Atherosclerosis	Atheroma or atherosclerotic plaque	Large and Intermediate Arteries. E.g.: Aorta and Coronary Arteries	The atheromatic plaque consists of lipoproteins, macrophages, platelets, T-cells, foam cells, smooth muscle cells, a necrotic core, and fibrous cap. Calcification of the plaque gradually occurs.
Medial calcification sclerosis	Calcification of the media	Elastic Arteries	Calcium begins to deposit in the medial layer of an artery forming a calcium plaque. The literature also suggests calcification of the internal elastic lamina.
Arteriolosclerosis	1) Hyperplastic lesion, and 2) Hyaline lesion	Arteries and Arterioles.	1) Intimal layer thickening characterised by the proliferation and migration of vascular smooth muscle cells at the site of the damaged endothelium; and 2) amorphous thickening of the wall of arterioles, characterised by deposits of plasma proteins, collagen and necrotic smooth muscle cells.

1.2.2.1 In-stent restenosis

In-stent restenosis also known as *clinical restenosis or neointima hyperplasia (NIH)* is mainly characterised by extensive proliferation and migration of smooth muscle cell like (SMC-like) cells into the intimal space of the stented artery resulting in the formation of a new (neo) intima (Indolfi, Mongiado, Curcio and Torella, 2003). The process of in-stent restenosis (ISR) appears to be a multi-factorial mechanism

involving:

Biological Factors - The immunomodulatory and antimitotic drugs, sirolimus and paclitaxel can activate drug resistance mechanisms in cells exposed to these agents due to their high cytotoxic effect. Additionally, the genetic make-up of a diseased population can significantly vary among individuals affecting the efficiency of a drug. Moreover, the stent material can cause a hypersensitivity reaction, and thus exacerbate the progression of the injury (Farooq *et al*, 2011).

Arterial Factors - Wall shear stress plays a critical role in neointima hyperplasia. Shear stress is highly dependent on the geometry of the vessel, and thus proportional to laminar blood flow. Shear stress contours the endothelium structure and triggers endothelial cells to express modulatory genes to maintain vascular homeostasis. For instance, under a normal physiological conditions endothelial cells release nitric oxide (NO), which it is essential to vasodilatation. Moreover, migration and proliferation of lesional cells are responsive to shear stress levels and thus blood flow. *In vivo* studies have shown that low shear stress level correlates with an increase of SMC density in the tunica intima of a vessel. Conversely, laminar blood flow prevents migration and proliferation of medial cells into the vessel intima (Guyton, and Hall, 2005) (Cunningham and Gotlieb 2005) (Farooq *et al*, 2011).

Stent Factors - The stent material, the type of drug, the elution profile and dose are all important factors when trying to control neointimal hyperplasia after implantation of a DES. The elution profile of the drug has a greater impact on neointima formation than the dose. (Farooq *et al*, 2011).

Implantation Factors - Failure to correctly expand the obstructed vessel also affects lesion formation. Although, the reasons aren't clear, under expansion or asymmetrical expansion of the lesion following stent implantation may contribute to greater ISR consequences (Farooq *et al*, 2011).

Molecular Mechanism – One of the downsides of angioplasty followed by stenting is the damage of the endothelium, which initiates a healing reaction. Neointima hyperplasia is characterised by large proliferation of SMCs-like cells, and a high accumulation of extracellular matrix (ECM) molecules in the tunica intima. Platelets

and leukocytes aggregate at the site of injury and secrete chemokines to trigger an immune response and the activation of SMC-like cells that contribute to lesion formation in response to mitogenic factors such as platelet-derived growth factor (PDGF) and transforming growth factor-β1 (TGF-β1) (Indolfi et al., 2003). The source of smooth muscle-like cells contributing to neointima hyperplasia is a topic of much controversy. Different schools of thought within the literature have been proposed about the cellular origin of these SMC-like cells in the neointima. (This topic is review later in this thesis).

1.3 Smooth Muscle Cells (SMCs)

Smooth muscle cells (SMCs) provide the structural support to hollow organs such as the bladder, the uterus, and organs of the gastrointestinal system. Additionally, they play a key physiological role in the contractility of blood vessels under normal conditions to maintain normal blood pressure and may be involved in pathological conditions, such as vessel remodelling during disease progression after injury. This subtype is known *vascular smooth muscle cells (vSMCs),* and its origin is diverse. Vascular smooth muscle cells are considered to be very heterogeneous due to their repertoire of functions and various embryological origins (Rensen, Doevendans and van Eys, 2007; Sinha, Iyer and Granata, 2014; Majesky, 2007; 2003; Gammill and Bronner-Fraser, 2003; Hao, Gabbiani and Bochaton-Piallat, 2003).

1.3.1 Vascular Smooth Muscle Cell Heterogeneity and Plasticity

SMCs were originally classified into two main phenotypes namely, *contractile* and *synthetic*, with notable differences apparent in their morphology (Table 1-2), and their gene expression profile (Rensen, Doevendans and van Eys, 2007). Subpopulations of SMCs observed within different vessels are derived from different embryological origins (mesoderm, neuroectoderm etc) and are thought to exhibit great plasticity and potentially switch between contractile, and migratory and proliferative phenotypes due to their non-terminally differentiated state (Sinha, Iyer and Granata, 2014).

The gene expression profile of both subpopulations of SMCs has been documented

and suggests that rather than having different biomarker expression, the level of expression of SMC differentiation markers may in fact vary between both states. For instance, markers such as smooth muscle-myosin heavy chain (SM-MHC) or MYH11, and smoothelin B (Smo) are typical of mature differentiated (contractile) SMCs; however, they are thought to be downregulated in synthetic SMCs. On the other hand, markers such as non-muscle MHC isoform-B (Smemb, smooth muscle-myosin heavy chain 10, Myh10), and cellular retinol binding protein-1 (CRBP-1) characteristic of proliferative SMCs, are found in synthetic SMCs (Rensen, Doevendans and van Eys, 2007).

Previous studies have isolated and characterised two morphologically distinct SMC populations from the tunica media of porcine coronary arteries by enzymatic dispersion and explant culture techniques namely elongated spindle-shaped (or contractile) and cobblestone (or synthetic) SMCs. Both were isolated from the tunica media but the elongated spindle-shaped cells were exclusively observed by enzymatic dispersion. After culturing explants, both phenotypes were found when the tissues were cultured on the luminal side, whereas only synthetic SMCs grew out from the tissue when the surface of the adventitia was placed face down.

These data agreed with prior studies performed on aortic media of healthy rats at different ages that suggested the density of synthetic SMCs may vary throughout life depending on factors such as age (Hao, Gabbiani and Bochaton-Piallat, 2003).

Subsequent gene expression studies indicated that when contractile SMCs are cultured *in vitro* over time, typical biomarkers (e.g.: SM-MHC and Smo) are downregulated, whereas expression of migratory and proliferative genes such as Smemb and CRBP-1 increase to resemble a synthetic phenotype. Additionally, serum concentration, and the presence of distinct bioactive molecules have phenotypic effects on SMCs *in vitro.* This suggests that even though SMCs can be maintained stably in culture, their phenotype may vary between the synthetic-contractile spectrum depending on the culture conditions, a process termed de-differentiation. This phenomenon was widely accepted, until recently and is referred to as a *modulated phenotype* or *phenotypic modulation/switching* of SMCs (Rensen, Doevendans and van Eys, 2007).

Table 1-2. Morphology of contractile and synthetic SMCs

(Rensen, Doevendans and van Eys, 2007).

	Contractile SMCs	Synthetic SMCs
Elongated spindle-shaped	Yes	No
Cobblestone (known as epithelioid or rhomboid cells)	No	Yes
Number of organelles producing proteins	Reduced	Increased
Number of contractile filaments	Increased	Reduced
Migratory and proliferative activity	Low	High

1.3.2 Vascular Smooth Muscle Cell Origin

Vascular smooth muscle cells (vSMCs) originate from different areas of the embryo during development and contribute to the formation of distinct tissues of the vasculature. It is widely accepted that vSMCs can arise from different mesodermal lineages such as lateral plate and paraxial mesoderm, as well as from the neural crest. The different embryological origins of the vSMCs comprising the tunica media of the aorta includes the cranial neural crest from where the aortic arch, ascending aorta, and branching carotid arteries are derived, and mesodermal background of the aortic root and annulus and descending (thoracic and abdominal) (Figure 1.2).

At embryonic day 6.5 (E6.5) in the mouse (at 3 weeks in humans), the formation of the primitive streak (PS) on the dorsal (back) / posterior region in the epiblast creates the left-right and cranial-posterior axis marking the beginning of gastrulation and germ layer development. Epithelial cells along the side of the primitive streak undergo mesenchymal transition (EMT) and invaginate inwards giving rise to the mesoderm and endoderm layers. Depending on how proximal or distal epithelial cells are from the primitive streak, different mesodermal derivatives develop as they sort and move

away from the proximal-distal plane towards the sides of the early embryo including paraxial, intermediate, and lateral plate mesoderm (Sinha, Iyer and Granata, 2014; Majesky, 2007; Parameswaran and Tam, 1995).

Neurulation also takes place during gastrulation by induction of the ectoderm, thus becoming divided in three neural regions: i) the neural ectoderm or neural plate, that will become the neural tube, and develops the neural system; ii) the non-neural ectoderm, which becomes the epidermis; and iii) the cells enclosed between the neural and non-neural ectoderm (cells of the neural folds), which in part give rise to the neural crest cells. Neural crest cells are neither a defined population nor from a very defined region, but they are mostly identified during their emigration from the neural folds or the dorsal region of the neural tube depending the organism at E8.5 (Sinha, Iyer and Granata, 2014; Gammill and Bronner-Fraser, 2003).

Different signalling factors and morphogen gradients are known to be involved in the induction of neural crest and mesoderm precursors including the wingless-type family (Wnt), fibroblast growth factor (FGF), Notch, and the TGF-β family such as bone morphogenic protein (BMP), nodal and activin. In vertebrates, neural crest precursors contribute to a number of cell types in the adult organism such as glial cells, peripheral neurons, and the pulmonary trunk. However, in the vasculature they are responsible for the formation of medial vSMCs in the ascending aorta, aortic arch, right and left carotid arteries, and the right subclavian artery. In contrast, the vSMCs within the tunica media of the descending aorta are predominantly derived from the paraxial mesoderm. Additionally, vSMCs of the coronary arteries, and aortic root are derived from the proepicardium and secondary heart field-derived cardiac progenitors (myocardium) (Wang et al., 2015; Majesky, 2003; 2007; Gammill and Bronner-Fraser, 2003; Sinha, Iyer and Granata, 2014).

This is important since it has been previously reported that certain cardiovascular diseases develop in specific areas of the vasculature. For instance, aneurysms usually

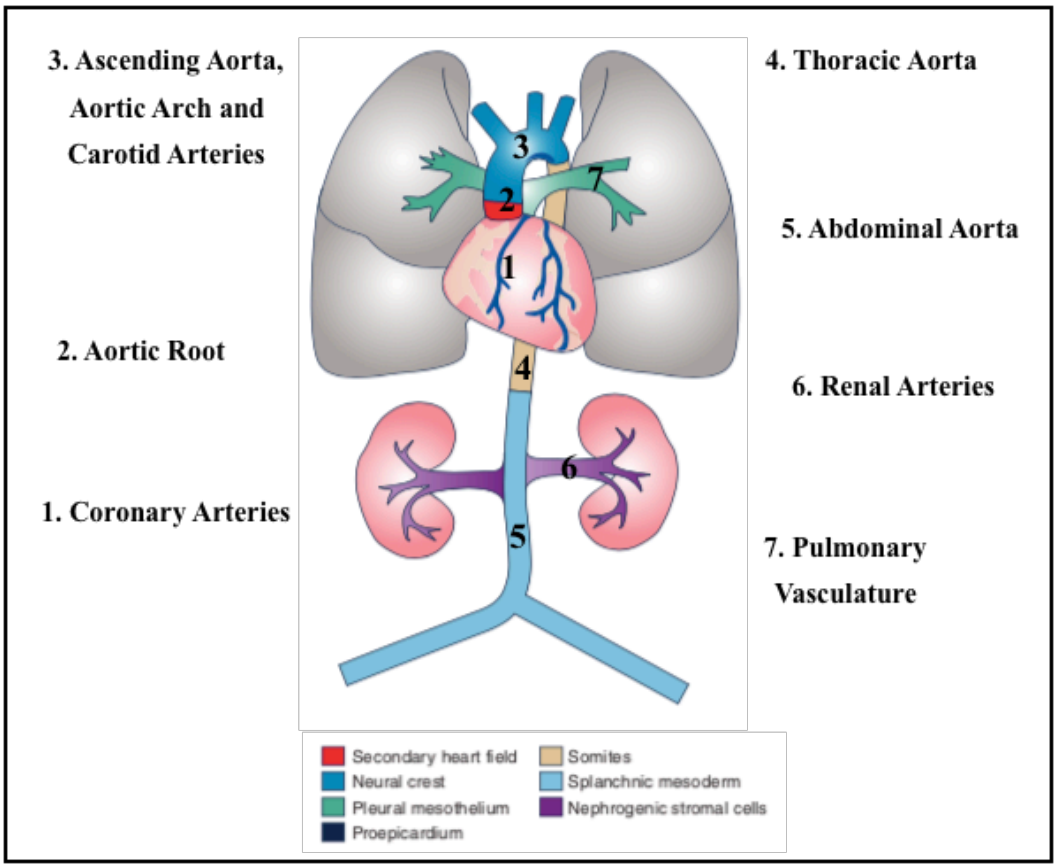

Figure 1.2. Embryological origin-specific SMCs.

Smooth muscle cells comprising the tunica media of the aorta including aortic root (2), ascending aorta, aortic arch and carotid arteries (3), thoracic aorta (4) and abdominal aorta (5) posses different embryological origins. SMCs of the coronary arteries (1), renal arteries (6) and pulmonary vasculature (7) also developed from distinct germ layers during embryogenesis (Wang, Jacquet, Karamariti and Xu, 2015).

occur in the abdominal stretch of the aorta; instead atherosclerosis is observed in places with a turbulent and pulsing blood flow such as the aortic arch, and arterial branches and bifurcation points.

Therefore, a possible relationship between the SMC embryonic lineage and vascular disease-site susceptibility has been proposed (Sinha, Iyer and Granata, 2014). High-throughput mRNA profiling of aortic arch (AA; atherosclerotic-prone) and thoracic aorta (TA; atherosclerotic-resistant) tissues harvested from wild-type (WT) and apoE-deficient (apoE-KO) mice revealed differential expression of a range of Homeobox

(Hox) genes in the TA and TA-SMCs compared to that of the AA and AA-SMCs, irrespective of the murine strain. Similar results were obtained in other animal models such as pigs and rats, suggesting that the difference in Hox gene expression may be region-dependent. Human neural ectodermal (NE)- and paraxial mesodermal (PM)-derived SMCs have since been generated from human induced pluripotent stem cells (hiPSCs) using chemically defined protocols to examine the mRNA expression levels of the HOX genes (Cheung, Bernardo, Pedersen and Sinha, 2014). In agreement with the animal models, the *in vitro* data suggest that human PM-SMCs possessed a higher expression of a range of HOX genes compared to the NE counterpart. Therefore, distinctive Homeobox gene expression patterns existed between the NE- and PM-derived SMCs composing the tunica medial of atherosclerotic-susceptible and atherosclerotic-resistant regions of the aorta. Moreover, DNA-binding activity of the pro-inflammatory transcription factor NF-κB was higher in the mouse and rat AA and AA-SMCs than in the TA and TA-SMCs and a feedback loop between NF-κB and HoxA9 was present where they reciprocally regulated each other (Trigueros-Motos et al., 2013; Bennett, Sinha and Owens, 2016).

1.3.3 Epigenetic modifications involved in Vascular Smooth Muscle Cell Differentiation

Epigenetics refers to the study of the dynamic biochemical modifications that control the expression of genes without altering the genetic code. These modifications known as epigenetic marks exert conformational changes in the chromatin structure resulting in the regulation of gene expression during smooth muscle cell differentiation. The chromatin is composed of genomic DNA and histone proteins. Two copies of histones H2A, H2B, H3 and H4 forms an octamer, where 146 base pairs of DNA wrapped around it, establishing the fundamental unit of chromatin known as the nucleosome. Linker DNA joints the nucleosomes giving rise to the primary packing level of chromatin known as beads-on-a-string chromatin. The histone N-terminal tails are projected from the nucleosome and are subjected to post-translational modifications including, acetylation, phosphorylation, methylation and ubiquitinoylation. Post-translational modifications of histone influence the conformation of the nucleosome thus controlling chromatin accessibility, which in turn regulates the activation or suppression of gene transcription (Handy, Castro and Loscalzo, 2011).

Histone modifications at the N-terminal tails alter the higher order chromatin structure by increasing or reducing the affinity of DNA to histone proteins. For instance, histone acetylation is associated with gene activation by loosening the compact chromatin structure allowing for binding of transcription factor complexes to the DNA molecule. Myocardin/serum response factor (SRF)/myocardin complex binding to CArG box [$CC(A/T)_6GG$] DNA sequence at SMC promoters is critical for SMC gene expression and thus differentiation. Interestingly, SRF binding to the CArG box at SMC marker genes occurs only if the regions are enriched in histone acetylation (Gomez, Swiatlowska and Owens, 2015; McDonald, Wamhoff, Hoofnagle and Owens, 2006). In addition, the histone methylation mark H3K4me2 (de-methylation of Lysin 4 on histone 3) on SMC marker genes such as αSMA, SM-MHC and TAGLN was enriched in mature SMCs and SMC progenitors during myogenic differentiation in contrast to embryonic stem cells or non-SMC somatic cells. Enrichment of H3K4me2 at the αSMA promoter was shown to be independent on SRF binding to CArG box sequence, and thus identifying this histone mark as a potential upstream regulator of SRF binding to CArG box chromatin. Thereafter, it was demonstrated that binding of SRF to the CArG box was specific to the physical interaction between myocardin/SRF and H3K4me2 and that SRF binding to CArG box was sensitive to the expression levels of myocardin (Gomez, Swiatlowska and Owens, 2015; McDonald et al., 2006). Gomez *et al.* (2013) performed an *in vivo* study using a novel technique, which combined *in situ* hybridisation and a proximity ligation assay (ISH-PLA) to reveal that enrichment of H3K4me2 on the SM-MHC promoter was restricted to mature SMCs and cells of a SMC lineage (Figure 1.3). Concordant with previous studies, they showed that the histone modification H3K4me2 at the SM-MHC promoter was retained in phenotypic modulated SMCs *in vivo*. The study concluded that the H3K4me2 on SMC marker genes is a restricted but stable epigenetic signature of SMCs independently of their state of differentiation (Gomez, Shankman, Nguyen and Owens, 2013; Gomez, Swiatlowska and Owens, 2015; McDonald et al., 2006).

Another epigenetic change that has been widely studied in smooth muscle cell differentiation is DNA methylation. In mammals, DNA methylation occurs at the 5'-cytosine in CpG islands (genomic regions with high concentration of CpG dinucleotides) through the actions of DNA methyltransferases, DNMT1, DNMT3A and DNAMT3B. Methylation at CpG-rich promoter sequences is typically associated

with gene silencing thus inhibiting the expression of genes in differentiated cells, especially genes specific to pluripotency (Jones and Takai, 2001). Several *in vivo* and *in vitro* studies have shown that DNA methylation is implicated in gene silencing of certain SMC genes during disease progression and SMC phenotypic switching. However, more evidence is required to define whether the role of DNA methylation in this process is casual (Liu, Leslie and Martin, 2015). Nevertheless, the mechanisms of DNA demethylation have been recently related to activation of gene expression through the role of the ten-eleven-translocation (TET) family of enzymes that catalyze the oxidative reactions of 5-methylcytosine (5-mC) to 5-hydroxymethylcytosine (5-hmC). The 5-hmC is then converted to unmethylated cytosine through the DNA repair pathway and thymine-DNA glycosylase (TDG) resulting in DNA demethylation and gene expression. Three TET isoforms are currently identified namely, namely TET1, TET2 and TET3; however, TET2 is the predominant enzyme in human coronary artery SMCs (hCASMCs) in cultures and is highly enriched in smooth muscle tissues. Liu *et al.* (2013) showed that TET2 was upregulated in hCASMCs following SMC differentiation and significantly reduced upon PDGF-BB-induced de-differentiation. The research group also demonstrated that knockdown of TET2 in hCASMCs reduced the expression levels of SMC contractile genes (SM-MHC, MYOCD, αSMA and SRF), while increasing the expression of makers associated to the synthetic SMC phenotype (e.g. KLF4 and MYH10) (Liu et al., 2013).

These observations were accompanied with enhanced cell proliferation and morphological changes. Concomitantly, the H3K4me2/H3K27me3 ratios at the MYH11, MYOCD and SRF promoters decreased contributing to gene silencing, whereas the levels of H3K4me3 enrichment was elevated at the KLF4 gene locus. These data suggest that TET2 demethylase plays a critical role in SMC differentiation by modifying histone methylation (Liu, Leslie and Martin, 2015; Liu et al., 2013).

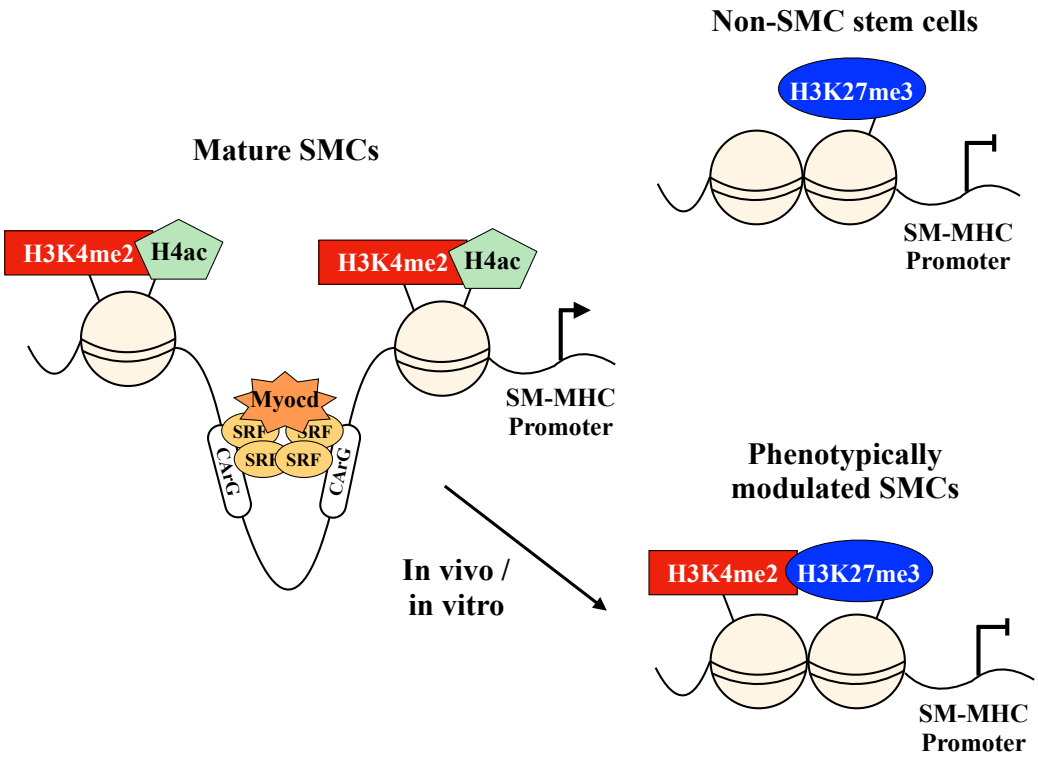

Figure 1.3. Cartoon depicting epigenetic changes in mature SMCs.

Diagram summarises the histone methylation and acetylation of the SM-MHC promoter at CArG sites in mature SMCs, phenotypically modulated SMCs and non-SMC stem cells. Image was modified from Gomez *et al.* (2013) (Gomez et al., 2013).

1.3.4 The molecular signals involved in SMC differentiation

Transforming Growth Factor-β (TGF-β) signalling pathways

Transforming Growth Factor-β (TGF-β) signalling is a versatile pathway important during embryonic development and adulthood that controls cell behaviour such as cell proliferation and differentiation, tissue homeostasis and tissue regeneration. TGF-β signalling consists of two principal pathways namely, the canonical and the non-canonical pathways. The canonical TGF-β signalling transduction is mediated by the activity of the membrane-bound receptors, secreted ligands and the signalling effectors SMAD proteins. The TGF-β family of ligand proteins is very extensive, with over 30 members identified in humans. They are classified into two subfamilies namely the

TGF-β-activin-Nodal and the Bone Morphogen Protein (BMP) subfamilies. TGF-β family of Ser/Thr kinase receptors consists of two receptor subfamilies defined as type I and type II, which create specific ligand-receptor combinations and thus activating a different signalling pathway. For instance, TGF-β binds exclusively to type I receptor TGFβR1 (also denoted ALK5 and TβRI) and TGFβR2. The SMAD family consist of eight proteins that regulate TGF-β signal transduction and thus transcription of the TGF-β target genes. SMAD proteins are activated by type I phosphorylation; however, the SMAD isoform that is activated depends on the ligand-receptor combination. For instance, SMAD2 and SMAD3 are targeted by TGFβR1 (Derynck and Zhang, 2003; Massagué, 2012).

Upon TGF-β binding to its receptors, a hetero-tetrameric receptor complex composed of two type I and two type II receptor components initiate activation of TGF-β signalling pathway. Thereafter, phosphorylation of type I by type II ensues and the signal is propagated by the phosphorylation of SMAD2 and SMAD3 effector proteins. These receptor-regulated SMAD proteins (R-SMADs) form a heterodimeric complex with SMAD4 in the cytoplasm, and subsequently translocate to the nucleus where they interact with other DNA-binding transcriptional factors and co-activators essentially CBP and p300 to transcriptionally activate target genes. The R-SMAD-SMAD4 trimer can also bind to co-repressors in order to repress the transcription of target genes. Therefore, the promoter targeted by the DNA-binding transcription complex is selected by the initial ligand-receptor combination (Figure 1.4) (Massagué, 2012; Derynck and Zhang, 2003).

In the absence of TGF-β ligands, the type I and type II receptors are present in the cell plasma membrane as homodimers preventing signal transduction. The overall effect of SMAD/TGF-β signalling varies depending on the activity of different ligands, receptors and regulators, as well as contextual determinants that further shape the activity of the SMAD/TGF-β pathway (Massagué, 2012; Derynck and Zhang, 2003).

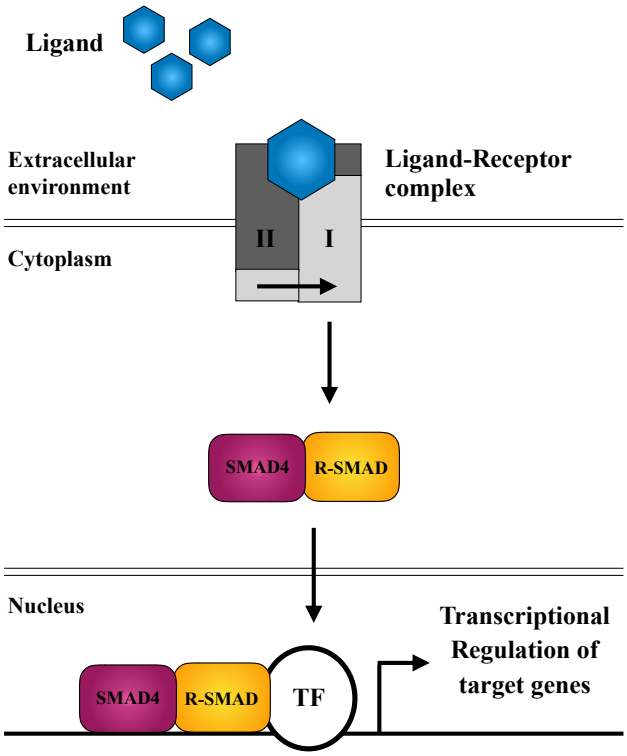

Figure 1.4. SMAD/TGF-β Signalling Pathway.

Assembly of the two type I and the two type II receptor components occurs upon binding of TGF-β ligands to the receptors. Subsequently, type II activates the TGF-β signalling by phosphorylation of the type I, which in turn phosphorylates SMAD proteins (R-SMAD). R-SMADs bind to SMAD4 and translocate to the nucleus where the trimer associates with partners transcription factors to activate or repress the transcription of target genes.

Notch signalling pathway

Notch signalling is an evolutionary conserved pathway across many species important for the regulation of embryonic development in many aspects as well as tissue homeostasis in several organs. Notch signalling consists of two principal pathways namely, the canonical and the non-canonical (ligand- or transcription-independent) pathways. In vertebrates, canonical Notch signalling transduction is mediated by the activity of the membrane-bound receptors and ligands. There are four Notch receptors (Notch1-4), four delta-like ligands (Dll1-4) and two jagged ligands (Jagged1 and

Jagged2) found in mammals up to date. The Notch receptors are heterodimers, which consist of an extracellular domain (NECD) subunit non-covalently bound to the transmembrane and intracellular domain (NTMIC) [NECD-NTMIC] (Kopan and Ilagan, 2009; Bray, 2006).

Upon receptor-ligand interaction between neighbouring cells, the ADAM family of metalloproteases initiate a proteolytic cleavage of Notch at site 2 (S2) resulting in the release of the extracellular domain from the heterodimer Notch receptor followed by its endocytosis by the ligand-presenting cell. In the Notch-activated cell, a membrane-tethered intermediate known as Notch extracellular truncation (NEXT) is proteolytically cleaved by γ-secretase, a multiprotein complex of cleaving proteases at site 3 (S3) and site 4 (S4), resulting in the release of the NICD into the cytoplasm. Subsequently, NICD translocates nucleus where it interacts with the DNA-binding protein RBPjκ (also known as CSL) recruiting the co-activator Mastermind (MAM), which in turn recruits the MED88 mediator transcription activation complex thus activating transcription of the Notch target genes. Notch target genes include the hairy enhancer of split (HES) and the HES-related repressor proteins (HERP) family (Table 1-3) that act as Notch effectors by negatively regulating the expression of downstream

Table 1-3. The HERP family (Iso, Kedes and Hamamori, 2003).

Abbreviations	Full Names	Species	Function
HERP1, HERP2 & HERP3	HES-related repressor protein	Mouse, rat, human	Transcriptional repressor
Hesr1, Hesr2 & Hesr3	Hairy/E(spl)-related	Drosophila, mouse, human	Transcriptional repressor
Hey1, Hey2 & HeyL	Hairy/E(spl)-related with YRPW	Drosophila, mouse, chicken, human	Transcriptional repressor

target genes encoding for tissue-specific proteins (Figure 1.5) (Kopan and Ilagan, 2009; Bray, 2006; Iso, Kedes and Hamamori, 2003). In the absence of a ligand, the initial cleavage of Notch receptor by ADAM metalloprotease is prevented by a unique negative regulatory region (NRR) within the NECD (Bray, 2006; Kopan and Ilagan, 2009).

In the absence of a ligand, the initial cleavage of Notch receptor by ADAM metalloprotease is prevented by a unique negative regulatory region (NRR) within the NECD (Bray, 2006; Kopan and Ilagan, 2009).

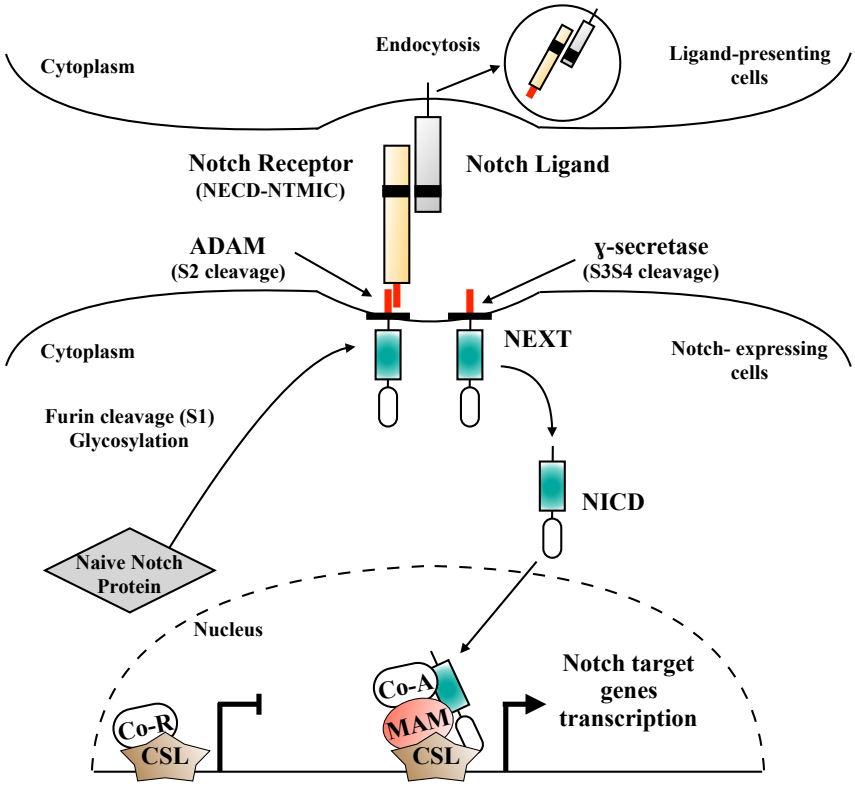

Figure 1.5. Canonical Notch Signalling Pathway.

The newly translated Notch protein undergoes a series of post-translational modifications including glycosylation and a furin-dependent proteolytic cleavage at site 1 (S1) producing the heterodimer Notch receptor, NECD non-covalently bound to the NTMIC. The functional receptor is transported to the plasma membrane, where it is activated upon its binding to the Notch ligands presented by a neighbouring cell. Once binding takes place, ADAM metalloprotease cleaves the Notch receptor at site 2 (S2) shredding its extracellular domain, which together with the ligand are endocytosed by the ligand-presenting cell. On the Notch-expressing cell, a membrane-anchored Notch extracellular truncation (NEXT) fragment is created that is subsequently cleaved by γ-secretase complex at site 3 (S3) and 4 (S4) freeing the NICD into the cytoplasm. Thereafter, the NICD localises to the nucleus where associates with the CSL complex recruiting Mastermind (MAM) and other co-activators (Co-A) to initiate Notch target gene transcription. In the absence of NICD, the CSL complex may associate with co-repressor (Co-R) proteins inhibiting translation. Image was modified from Kopan and Ilagan (2009) (Kopan and Ilagan, 2009).

Wnt signalling pathway

Wnt signalling consists of two principal pathways namely, the canonical and the non-canonical pathways. The canonical signalling is the most characterised pathway that mediates signal transduction by the activity of the frizzled receptor (Fzd), a co-receptor lipoprotein receptor-related protein (LRP) 5/6 (LPR5/6), the cytoplasmic protein Dishevelled (Dvl) and the transcription factor β-catenin. In humans, the Wnt family of 19 secreted proteins are post-transcriptionally modified via palmitoylation and glycosylation before they are released into the extracellular space (Ackers and Malgor, 2018; Tsaousi et al., 2011; Hua et al., 2014; Steinhart and Angers, 2018).

In the absence of Wnt protein, β-catenin is maintained at low levels in the cell cytoplasm due to a ubiquitin-dependent degradation process facilitated by a molecular machinery known as the β-catenin destruction complex. This complex consists of the scaffolding protein Axin and adenomatous polyposis coli (APC), casein kinase I (CKI) and glycogen synthase kinase 3β (GSK3β), and its function is to phosphorylate β-catenin leaving it marked for degradation. Phosphorylated β-catenin is recognised by an E3 ubiquitin ligase ($SCF^{\beta\text{-}TrCP}$), which prepares the protein for proteasomal degradation, resulting in the inhibition of the Wnt target genes' transcription (Figure 1.6, A) (Ackers and Malgor, 2018; Tsaousi et al., 2011; Hua et al., 2014; Steinhart and Angers, 2018).

In the presence of Wnt protein, Wnt ligand binds to the Fzd and LPR5/6 co-receptor complex triggering the recruitment of Dvl and the Axin-APC-GSK3β complex to the membrane where the intracellular domain of LPR5/6 co-receptor becomes phosphorylated by GSK3β, CKI and Cyclin Y kinases. Consequently, the destruction complex is disassembled and β-catenin levels in the cytoplasm increases. Elevated levels of β-catenin results in its translocation to the cell nucleus, where it acts as a co-activator with TCF/LEF to regulate the transcription of Wnt/β-catenin target genes (Figure 1.6, B) (Steinhart and Angers, 2018; Tsaousi et al., 2011; Hua et al., 2014; Ackers and Malgor, 2018).

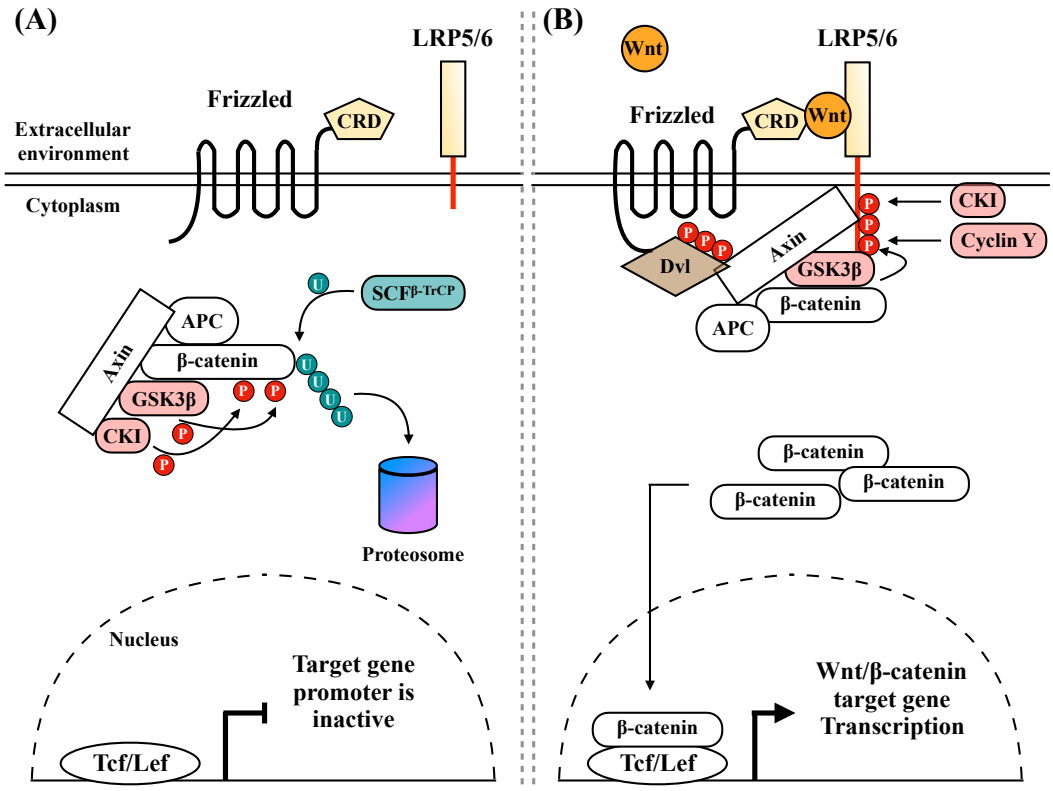

Figure 1.6. Wnt/β-catenin Signalling Pathway.

(A) In the absence of Wnt, β-catenin is sequestered and phosphorylated by the β-catenin destruction complex (Axin-APC-GSK3β-CKI). Recruitment of the E3 ubiquitin ligase ($SCF^{β\text{-}TrCP}$) ubiquitinates phosphorylated β-catenin marking it for proteasomal degradation and thus resulting in the transcriptional inhibition of the Wnt target gene. **(B)** In the presence of Wnt, Wnt protein binds to the Fzd-LRP5/6 receptor heterodimer and recruitment of the degradation complex as well as Dvl to the membrane occur. Dvl inhibits GSK3β resulting in the accumulation of β-catenin proteins in the cytoplasm. Active β-catenin proteins translocate to the nucleus where it serves as a co-activator with TCF/LEF to initiate transcription of the Wnt/β-catenin target genes. Image was modified from Steinhart and Angers (2018) (Steinhart and Angers, 2018).

Hedgehog signalling pathway

Hedgehog (Hh) signalling is an evolutionary conserved pathway across many species important for the development of several tissues and organs. In vertebrates, Hh signalling transduction is mediated by the activity of the transcription factors Gli (Gli1/2/3), the transmembrane receptors Patched 1 and 2 (Ptch1 and Ptch2), a second

transmembrane protein Smoothened (Smo), suppressor of fu (sufu) and kinesin family member 7 (Kif7). The Hh family of secreted cholesterol-modified proteins consists of Sonic (Shh), Indian (Ihh) and Desert (Dhh) hedgehog. These proteins act as morphogens by exclusively mediating different development process that depend on the dose and the time of secretion.

During embryogenesis, Dhh is primarily involved in the formation of the gametes and sex hormones. Because of its restricted expression to the reproductive glands (gonads) Dhh-deficiency does not exhibit phenotypic abnormalities, thus allowing for a normal embryo development, however, males are infertile. Moreover, Ihh is expressed during the formation of the yolk-sac vasculature, therefore gene knockdown is shown to cause lethality in approx. 50% of the cases during early development. The surviving embryos present bone mass and body structure defects as well as deficits in chondrocytes development. Shh is the most widely expressed protein and its knockdown is embryologically lethal in mice. For instance, it is expressed during neural patterning along the dorsal-ventral axis, cranial neural crest and smooth muscle cell patterning. During organogenesis, Shh is mainly involved in the development of epithelial tissues such as lung branching and kidney morphogenesis (Varjosalo and Taipale, 2008) (Morrow et al., 2009; Mooney et al., 2015; Hooper and Scott, 2005; Choudhry et al., 2014).

In the absence of Hh, the Gli proteins are attached to sufu and Kif7, which mediates binding to the microtubules in the cytoplasm thus forming the repressor complex. The complex then promotes the phosphorylation of the Gli full length protein (Gli-FL) by protein kinase A (PKA), glycogen synthase kinase 3β (GSK3β) and casein kinase I (CKI) causing the retention of Gli-FL protein in the cytosol. Phosphorylated Gli-FL is subsequently ubiquitinylated by an E3 ubiquitin ligase ($SCF^{\beta\text{-}TrCP}$) leading to Gli-FL partial degradation and thus rendering a truncated/repressor form of the Gli protein denoted Gli-R. Then Gli-R translocates to the nucleus, where it suppresses the activation of Hh targets genes including the Gli and the Ptch gene families, thus Gli and Ptch are both components and targets of the Hh signalling pathway (Mooney et al., 2015; Morrow et al., 2009; Choudhry et al., 2014; Hooper and Scott, 2005).

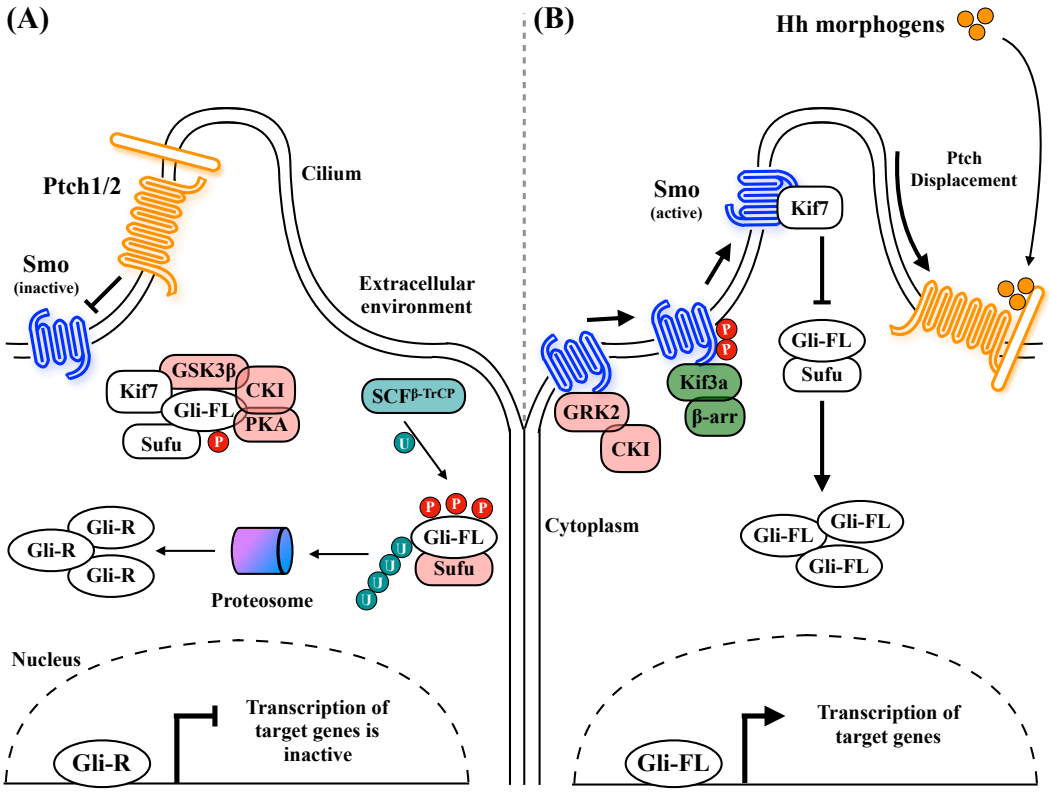

Figure 1.7. Hedgehog Signalling Pathway in Vertebrates.

(A) In the absence of Hh, patched (Ptch) receptor inhibits Smoothened (Smo) and so the Gli repressor complex composed of Gli full length proteins (Gli-FL), suppressor of Fu (Sufu) and kinesin family member 7 (Kif7) is formed. The repressor complex mediates the phosphorylation of Gli-FL by recruiting protein kinase A (PKA), glycogen synthase kinase 3β (GSK3β) and casein kinase I (CKI). Subsequently, Ubiquitination and partial degradation of phosphorylated Gli-FL are carried out by an E3 ubiquitin ligase ($SCF^{\beta TrCP}$) and the proteasome, respectively leading to the formation of the repressor form of Gli denoted Gli-R. Gli-R then translocate to the nucleus, where it suppresses the translation of Hh target genes. **(B)** In the presence of Hh, Hh ligand binds to Ptch causing the receptor to move out of the cilia and thus relieving its inhibitory effect of Smo. Then Smo is phosphorylated by G protein couple receptor kinase 2 (GRK2) and CKI allowing its trafficking to the cilia by β-arrestin (β-arr) and kinesin family member 3a (Kif3a). Thereafter, Smo promotes the disassembly of the repressor complex (Gli-FL-Sufu), and Gli-FL is then localised to the nucleus to activate target gene expression of Hh target genes. Image was modified from Mooney *et al.* (2015) (Mooney et al., 2015).

Upon binding of Hh signalling ligand the Ptch receptor through the interaction of the Ptch sterol-sensing domain (SSD) and the Hh cholesterol motif, the Ptch-Smo receptor complex dissociates and Smo is phosphorylated and activated. Phosphorylated Smo displaces Ptch receptor out from the microtubules and binds to Kif7 promoting disassembly of the Gli repressor complex. Consequently, Gli-FL is freed in the cell cytoplasm followed by its translocation to the nucleus, where it initiates the transcription of the Hh target genes (Morrow et al., 2009; Hooper and Scott, 2005; Mooney et al., 2015; Choudhry et al., 2014).

1.3.5 Signalling involved in Vascular Smooth Muscle Cell Development and Differentiation

Transforming Growth Factor β (TGFβ) Signalling

The TGF-β isoforms (TGF-β1, TGF-β2, and TGF-β3) as multipotent cytokines are involved in cell differentiation, proliferation, survival and apoptosis. *In vivo* experiments using different TGFβ/TGFβR null mice have shown early embryo lethality, reduced angiogenesis, abnormal vascular tube formation and SMC hypoplasia around the nascent dorsal aorta. On the other hand, *in vitro* studies demonstrated that the TGF-β1 isoform played an important role in embryonic-derived SMC development (Wang et al., 2015; Sinha, Iyer and Granata, 2014; Sinha et al., 2004; Xie et al., 2011). More recently, Cheung *et al.* (2014) published an *in vitro* protocol to drive human pluripotent stem cells (hPSCs: embryonic stem cells and induced pluripotent stem cells) towards the SMC phenotype by transitioning through embryological lineage-specific progenitors. This protocol involved the treatment of neuroectodermal or (paraxial and lateral plate) mesodermal progenitors with recombinant TGF-β1 protein thus confirming the involvement of TGF-β signalling in SMC maturation from embryonic cells *in vitro* (Cheung et al., 2014).

Various SMC differentiation systems have been used to study the effect of recombinant TGF-β1 *in vitro.* For instance, neural crest cell-derived models (Monc-1 and JoMa1 cells) and mesodermal-derived models (C3H/10T1/2) transition to the SMC phenotype after TGF-β1 treatment, resulting in both expression of the smooth muscle cell markers and phenotypic changes to the spindle-shaped morphology. Unlike the JoMa1, the Monc-1 cell line was also shown to express the mature SMC

marker SM-MHC (Xie et al., 2011). In adult vascular SMCs, TGF-β treatment was associated with reduced proliferation and increased SMC differentiation, favouring the contractile or spindle-shaped morphology (Hao, Gabbiani and Bochaton-Piallat, 2003). The TGF-β signalling seems to be an important mechanism of SMC differentiation and maintenance of stem cells and adult contractile vSMCs, respectively (Wang et al., 2015).

Platelet-derived Growth Factor (PDGF) Signalling

The platelet derived growth factor isoforms (PDGF-A, PDFG-B, ODGF-C, PDGF-D, PDGF-AB, PDGF-AA, and PDGF-BB) are strong mitogenic and chemoattractant ligands involved in development, inflammation and tissue repair. Their secretion is regulated by platelets and endothelial cells (ECs) to act on SMCs and mesenchymal-derived cells by binding to their corresponding tyrosine kinase receptors (PDGFR-α and PDGFR-β) (Westermark, Siegbahn, Heldin and Claesson-Welsh, 1990; Wang et al., 2015; Hellström et al., 1999).

Several studies have reported that PDGF signalling may play opposing roles in myogenic differentiation depending on the initial differentiation state of the target cells. In embryonic and adult undifferentiated stem cells, PDGF promotes myogenic differentiation to a SMC-like phenotype (Cheung et al., 2014; Xiao et al., 2007), whereas in differentiated SMCs, PDGF may promote de-differentiation to a more synthetic SMC phenotype (Corjay, Thompson, Lynch and Owens, 1989; Corjay, Blank and Owens, 1990).

PDGF-BB is the most powerful chemoattractant secreted by BAEs followed by PDGF-AB and PDGF-AA in studies using bovine aortic endothelial cells (BAE) and C3H 10T1/2 fibroblast mesenchymal cells in co-culture (Hirschi, Rohovsky and D'Amore, 1998). However, mC3H movement was inhibited by PDGF-B but not PDGF-A neutralising antibodies. Moreover, myogenic differentiation of mC3Hs results in increased expression of smooth muscle cell markers (αSMA, SM22α, Calponin1 and SM-MHC) and phenotypic transition to a more spindle-shaped morphology that required the co-culture with the BAEs and cell contact. Similarly, TGF-β1 treatment of mC3Hs exhibited similar results to those seen in the BAE-mC3H co-cultures. TGF-β neutralising antibodies attenuated these effects in BAE-mC3H cocultures and

decreased expression of αSMA and SM-MHC proteins. These data suggested that TGF-β promotes SMC differentiation while PDGF-B was responsible for cell recruitment (Hirschi, Rohovsky and D'Amore, 1998).

Similarly, primary cultures of stem cell antigen 1- Sca-1-positive (Sca-1^+) mesenchymal stem cells undergo myogenic differentiation to SMC lineage following PDGF-BB treatment and increases the expression of αSMA, SM22α, Calponin1 and SM-MHC proteins (Hu et al., 2004). In mouse embryonic stem (ES)-derived Flk1-positive (Flk1^+) cells specification towards the SMC phenotype is also governed by PDGF-B/PDGFR-β, while administration of the vascular endothelial growth factor (VEGF) favoured endothelial cell (EC) differentiation (Yamashita et al., 2000).

However, during adulthood, PDGF isoforms, PDGF-A and PDGF-B, are reported to stimulate contractile SMC transition to a more synthetic phenotype *in vitro* as evident by changes in morphology, gene expression profile along with migration and proliferation rates (Rensen, Doevendans and van Eys, 2007). *In vivo,* arterial SMC proliferation contributing to neointima thickening was coordinated by PDGF-B but not PDGF-A in balloon injury model of rabbit femoral arteries (FAs). PDGF-B and PDGFR-β was highly expressed in the neointima with trace amounts within the tunica media of injured FAs. Expression of PDGF-B in lesional cells peaked at 7 days concomitant with cell proliferation resulting in the formation of a large neointima by 21 days (Uchida et al., 1996; Wang et al., 2018).

Notch Signalling

The highly conserved Notch signalling pathway functions in many different developmental and homeostatic processes (Bray, 2016). In the canonical ligand-dependent pathway, Notch receptors (Notch1-4) undergo conformational changes upon ligand engagement (e.g. Jagged1, Jagged2, Serrate and Dll4), stimulated by a pulling-force on the extracellular fragment of Notch that results from endocytosis of the receptor-bound ligand into the ligand-expressing cell. These conformational changes in the receptor allow for two consecutive proteolytic cleavage events to occur, which release the intracellular region of the receptor into the cytoplasm where it then travels to the nucleus and induces Notch target gene transcription. However, there is accumulating evidence that other pathways may also induce Notch signalling. A

ligand-independent mechanism of Notch activation has been described in which receptor processing is initiated via cell-internal signals. These signals result in the internalization of Notch into endosomal compartments, where chemical changes existing in this microenvironment result in the conformational modifications required for receptor processing (Bray, 2016).

The role of the Notch signalling pathway in smooth muscle cell early development and the specific progenitor cell type activated remains unclear. However, *in vivo* and *in vitro* studies have reported the importance of Notch activation during smooth muscle cell specification of neural crest progenitors, and the separation of SMC, and blood cell (BC)/endothelial cell (EC) progenitors of ventral mesodermal cells (Shin, Nagai and Sheng, 2009; High et al., 2007; Wang et al., 2015).

Shin *et al.* (2009) carried out cell-fate tracing studies in chick embryos by inserting a construct constitutively expressing a GFP-tagged Notch receptor protein, whose tag was cleaved in Notch-expressing cells marking them indelibly. The constructs known as dENotch1 were electroporated at stage HH3 of the chick embryo, where mesodermal prospective epiblast cells are positioned at the primitive streak just before invagination occurs. At stage HH10, embryos were harvested and co-stained with alpha smooth muscle actin (αSMA) revealing that SMCs defined by their αSMA-positive (αSMA^{+}) staining, are derived from dENotch1-expressing cells. Moreover, the same group studied the expression of Notch and its pathway components during chick embryo gastrulation (HH3-HH10) using *in-situ* hybridisation analysis. The data showed that Notch1, Delta1 and Notch components (Hairy2, Herp2 and Lunatic-fringe) were strongly expressed at the posterior primitive streak during early ventral mesodermal formation (HH4). However, soon after invagination extensive migration and differentiation of the ventral mesodermal cells into SMC or BC/EC progenitors was governed by the expression of early progenitor-specific transcription factors, *dHand* and *Scl*, respectively. During this process, the Notch pathway becomes inactivated due to the attenuation or absence of protein expression. These studies reveal that Notch signalling is involved in SMC and BC/EC progenitor segregation of ventral mesodermal cells, but lineage specification was dictated by the early progenitor markers, dHand and Scl (Shin, Nagai and Sheng, 2009; López-Sánchez and García-Martínez, 2011).

The role of Notch in neural crest (NC) cells during cardiovascular development has also been addressed. Using cre-lox systems, Notch signalling did not affect NC cell migration towards the cardiac outflow track or mature aortic arch but was crucial for their specification and SMC differentiation. Inhibition of Notch signalling in neural crest cells resulted in the down regulation of notch target genes such as the HES-related transcription factors (HRTs) and a corresponding underdeveloped smooth muscle layer within the aortic arch. Additionally, the expression of the smooth muscle cell markers, SM22α (Transgelin; TAGLN) and alpha smooth muscle actin (αSMA) were decreased in the developing aortic arch arteries accompanied with a disorganised vessel architecture. This did not interfere with expression of the neural crest marker Plexin2, which is activated during migration and postmigration of NC cells, suggesting that Notch was not involved in an NC cell spreading event. The hearts of notch-deficient embryos were also examined at late-gestation exhibiting multiple cardiac and aortic arch patterning defects. Offspring did not survive or died within 2 weeks of birth. Finally, neural tube explant studies confirmed that Notch signalling promoted SMC differentiation in cardiac neural crest progenitors (High et al., 2007).

Since the Notch signalling pathway is known to play an important role in smooth muscle cell (SMC) growth, migration and apoptosis, the role of Notch has been intensively studied in the adult vasculature as a possible molecular mechanism to explain the extensive SMC migration and proliferation observed during vascular remodelling and repair. Various *in vitro* and *in vivo* studies have been carried out to determine the role of Notch signalling pathway in adult smooth muscle cells. Some studies suggested that activation of the Notch signalling pathway was related to SMC proliferation with loss of their contractile proteins and phenotype (Morrow et al., 2005a; Proweller, Pear and Parmacek, 2005; Havrda, Johnson, O'Neill and Liaw, 2006). Others have concluded that activation of Notch signaling by both overexpression of the constitutively activated form of Notch, Notch intracellular domain (NICD), and Jagged-1 (Jag-1) induction in cultured human aortic smooth muscle cells (SMCs) increased the expression of smooth muscle marker genes (SM-MHC and SM22α) and promoted a contractile phenotype at the expenses of proliferation in vascular SMCs (Boucher et al., 2011; Doi et al., 2006; Wang et al., 2015).

Despite these contradictory studies, Notch signalling is generally considered pro-myogenic in dictating SMC fate and differentiation in undifferentiated or poorly differentiated cells.

Wnt/β-catenin Signalling

The Wnt protein family, as a family of 19 lipid-modified glycoproteins, is known to be involved in embryogenesis and development as well as cell proliferation, migration and differentiation during adulthood. These signal molecules are widely known to be implicated in the pathophysiology of many tumours and its role in vascular restenosis has been recently addressed (Ackers and Malgor, 2018).

The role of Wnt protein through the activation of the canonical (Wnt/the β-catenin) pathway has been shown to induce cell proliferation, by increasing the expression of cell cycle genes such as cyclin D1 and p21, in vascular smooth muscle cells (vSMCs) *in vitro.* Moreover, inhibition studies using a canonical Wnt signalling antagonist, secreted frizzled related protein-1 (sFRP-1) reduced proliferation of vSMC in culture. Additionally, *in vivo* studies performed in rats demonstrated that the Wnt/β-catenin signalling was activated in balloon-injured carotid artery. Consequently, an increase in the expression of cyclin D1 as well as in vSMC proliferation were observed (Ezan et al., 2004; Tsaousi et al., 2011).

In vivo studies have identified key Wnt signalling molecules involved in vSMC proliferation during neointima hyperplasia. The expression of β-catenin signalling increased in the media and intima of mice 3 and 28 days after complete carotid artery ligation. Immunohistochemical studies revealed that Wnt4 expression was elevated in the media and intima of injured animals 3- and 28-days post-surgery, respectively. Using $Wnt4^{+/+}$ wild type (WT) and Wnt4-defitient ($Wnt^{+/-}$) mice after carotid ligation injury, the size of the intimal lesion and the rate of cell proliferation were reduced in the $Wnt^{+/-}$ animals compared to the WT 21 days post-surgery (Tsaousi et al., 2011).

Wnt pathway microarray analysis has also been carried out on vascular smooth muscle cell (vSMCs) mRNA samples. Quiescent and proliferative vSMCs isolated from explanted murine aortas were examined for significant upregulation of Wnt molecules. Wnt4 was constitutively expressed and the expression levels were significantly

upregulated in proliferative vSMCs compared to quiescent cells. Moreover, Wnt4 protein increased in vSMCs treated with platelet derived growth factor-BB (PDGF-BB) and basic fibroblast growth factor (b-FGF) after 24 hrs, an effect that was attenuated following siRNA knockdown of Wnt4. Concomitantly, recombinant Wnt4 protein promoted cell proliferation as well as the protein expression levels of β-catenin and cyclin D1 (a canonical Wnt target gene) (Tsaousi et al., 2011).

Similar *in vivo* studies in rats after balloon-wired injury of carotid arteries demonstrated that the expression of Wnt4 and β-catenin proteins was significantly increased in the injured animals compared to the sham-operation group (Hua et al., 2014).

Overall, Wnt/the β-catenin signalling has been implicated in vSMC proliferation *in vitro* and *in vivo* contributing to neointima hyperplasia. Among the Wnt family proteins, it appears that Wnt4 signalling molecule is a key player during vascular remodelling (Tsaousi et al., 2011; Ezan et al., 2004; Ackers and Malgor, 2018; Hua et al., 2014).

Hedgehog Signalling

Hedgehog (Shh) signalling, essential for proper embryonic development (Ingham and McMahon, 2001) also participates in adult homeostasis (Petrova and Joyner, 2014). This family of morphogens is known to be involved in cell differentiation, survival and growth. Hedgehog signalling is critical for early vascular development, and it has been shown to re-capitulate during vascular injury in adulthood (Hooper and Scott, 2005; Morrow et al., 2009). Canonical signalling is initiated when Shh binds to Ptch1 resulting in the removal of its' inhibitory effect on the smoothened receptor (SMO). SMO subsequently allows Gli family transcription factors to translocate to the nucleus and affect expression of Hh target genes, including Gli_1, Gli_2 and Ptch1 (Briscoe and Thérond, 2013). Previous studies highlighted a permissive role for Shh in atherosclerosis through increased lipid uptake by macrophages (Beckers et al., 2007). Moreover, in the Cardiogram C4 CAD genome wide associations study (GWAS), the hedgehog (Hh) interacting protein like-1 locus (HHIP1, a negative regulator of Hh signalling), was strongly associated with vascular disease (CARDIoGRAMplusC4D Consortium et al., 2013).

Seminal studies by Mark Majesky's group using Ptc^{lacZ} transgenic demonstrated that the Hh target gene Pcth1 was highly expressed in ascending aorta and pulmonary truck in neonatal mice (at 2 days; P2) by β-galactosidase-positive staining (β-gal^+) (Passman et al., 2008). Moreover, aortic cross-section revealed that β-gal^+ cells in P2 transgenic mice were only found within the tunica adventitia at the boundary between the tunica media and tunica adventitia. Immunolabelling of these sections with an anti-Shh antibody exhibited close proximity expression with the Ptc1-expressing cells at the adventitial side of the external lamina. Additionally, staining with an anti-Sca-1 antibody showed extensive overlapping expression with β-gal^+ cells in the aortic adventitia. The data, in support of previously reported Sca-1^+ cells in adventitia (AdvSca1), suggested a possible niche where these vascular Sca-1^+ progenitor cells may reside within the wall of vessels, and contact with Shh may, in part, maintain their stemness (Passman et al., 2008; Hu et al., 2004). Lastly, isolated aortic AdvSca1 were found to express genes of the Shh signalling pathway such as pcth1, pct2, smo, and Gli1/2/3. Confirmation of their SMC differentiation potential was carried out in 10% serum-containing DMEM, suggesting that these cells may serve as SMC progenitors *in vivo* (Passman et al., 2008).

Our research group along with other researchers have shown that Hh signalling controls 'de-differentiated' vSMC growth in cultured cells *in vitro* and neointimal formation *in vivo* (Morrow et al., 2007b; 2009; Redmond et al., 2013; Polizio et al., 2011). Targeted perivascular inhibition of the Hh receptor, Ptch1 attenuated neointimal formation following injury *in vivo* (Redmond et al., 2013). However, as Ptch1 is inhibitory in the absence of ligand, the directionality of Hh function following Ptch1 knockdown remains unclear. This signalling pathway can be blocked using cyclopamine that binds to SMO preventing it from signalling downstream. Interestingly, proliferative vSMCs not only exhibited increased protein expression of the Hh target Patch1 (Ptch1) but also increased levels of the Notch target genes/proteins Hairy-related transcription factors (Hey1, Hey2 and HeyL) 24 hours after Shh treatment (Morrow et al., 2009). Crucially, Shh has been implicated in the regulation of myofibroblasts, promoting their migration (Polizio et al., 2011). Furthermore, $Sca1^+$ stem cells co-localise in the healthy arterial vessel wall where Shh and its receptor, ptch1 are primarily expressed, i.e., at the adventitial medial boundary (Passman et al., 2008). Finally, recent lineage tracking studies have implicated Hh-

Gli-responsive stem cells in organ fibrosis and vascular lesion development (Kramann et al., 2016; 2015) while Hh activation of adventitial fibroblasts promotes neointimal formation (Dutzmann et al., 2017).

Overall, Hh signalling is re-capitulated during vascular remodelling contributing to neointima hyperplasia. Moreover, there is convincing evidence suggesting a possible role of Hedgehog (Shh) signalling in the maintenance of resident vascular stem/ progenitor cells (Huang and Kalderon, 2014)

1.4 Smooth Muscle Cell Progenitors

vSMCs accumulation is a key event leading to intimal thickening and lesion formation and an important marker of subclinical disease (Touboul PJ, 2015) yet the fundamental aspects of vascular cell accumulation, proliferation and the phenotypic changes within the vessel wall remain unresolved (Bennett, Sinha and Owens, 2016). Lineage tracing analysis has provided substantial evidence of the involvement of stem cell-derived progeny (Wan et al., 2012; Tang et al., 2012; Kramann et al., 2016) in addition to 'reprogrammed' differentiated SMC(Nemenoff et al., 2011; Herring, Hoggatt, Burlak and Offermanns, 2014; Chappell et al., 2016; Albarrán-Juárez et al., 2016), SMC derived from endothelial-mesenchymal transition (EndMT) (Cooley et al., 2014) and SMC derived from bone-marrow stem cells (Yu et al., 20111) in initiating and progressing intimal thickening as these cells become activated/reprogrammed, differentiate down vascular and myeloid lineages and subsequently dictate, in part, vessel remodelling.

1.4.1 De-differentiated SMCs

Depending on the environmental cues, vSMCs are purported to switch between two different phenotypes, from/to a contractile and quiescent state to/from a synthetic and proliferative phenotype. Therefore, it is commonly accepted that de-differentiated vSMCs contribute to not only to the secretion of extracellular matrix components but also to the SMC-like cells responsible for lesion formation during vascular remodelling and injury (Indolfi et al., 2003).

This dogma was originally reported by Ross (1999) as the result of an inflammation cascade initiated by a dysfunctional endothelium in order to maintain the local homeostasis. In this report, the transduction of contractile SMCs to the synthetic phenotype may occur by the secretion of factor molecules such as PDGF-BB, TGF-β, and Fibroblast growth Factor-2 (FGF-2), and changes in the ECM by metalloproteinase such as collagenase (Ross, 1999).

1.4.2 Circulating Progenitors, and BM-derived Stem Cells

Saiura *et al.* (2001) published the first article demonstrating the existence of SMC progenitors in the circulation. The study focused on cell lineage tracing studies to identify the cellular origin of the SMC-like cells found in transplant-associated arteriosclerosis (e.g. neointimal hyperplasia). Using cardiac transplantation from a wild-type to a LacZ transgenic mice, β-galactosidase-positive (β-gal^{+}) cells were found within the newly formed lesion 4 weeks post-transplantation. Co-staining analysis performed on tissue cross-sections revealed positive staining for the SMC markers, SM-MHC, calponin and α-smooth muscle actin (αSMA). To reinforce this finding, the heart of the LacZ transgenic mouse was transplanted into the wild-type mouse, and no lacZ-expressing cells were observed within the remodelled organ (Saiura et al., 2001).

Similar *in vivo* studies using transplantation models (e.g. aorta and kidney) have demonstrated that circulating bone-marrow derived progenitors are responsible for a significant number of SMC like cells within vascular lesions (Sata, 2003). However, the role of circulating bone-marrow derived stem cells has since been clarified (Hoglund, Dong and Majesky, 2010) and suggests that their involvement in the accumulation of SMCs leading to intimal thickening may be dictated by the degree of trauma to the vessel wall and the level of inflammatory cell infiltration at the site of injury (Daniel and Sedding, 2011).

Hematopoietic Stem Cells (HSCs)

Hematopoietic Stem Cells (HSCs) are well-known resident cells of the bone marrow that can replenish myeloid blood cells such as monocytes and lymphocytes. HSCs can also differentiate into SMCs and endothelial cells (Sata, 2003; Sata et al., 2002). In this context, HSCs (CD34^{+}c-Kit^{+}Sca-1^{+}Lin^{-}) from bone marrow of a LacZ-expressing

mouse were transplanted into wildtype irradiated mice before wire-induced injury of the femoral artery to reveal β-galactosidase-positive (β-gal^{+}) cells present in the neointima and medial layer of the host animal. Co-expression of αSMA and CD31 was observed by immunofluorescence (IF) (Sata et al., 2002).

Similarly, a recent study using the wire induced injury of the femoral artery in mice, demonstrated that expression of CD4^{5+} cells (hematopoietic lineage marker) decreased while αSMA+ cells increases as the neointimal thickening develops over time, respectively (Shoji *et al*, 2014). In addition, PDGF-BB promoted myogenic differentiation of adherent bone-marrow cells towards the smooth muscle cell lineage (Shoji, Koba and Kobayashi, 2014).

Mesenchymal Stem Cells (MSCs)

Mesenchymal stem cells are a heterogeneous group of multipotent stem cells capable of cell renewal and of differentiation into osteoblasts, adipocytes, and chondrocytes *in vitro*. MSCs are adherent and present a fibroblast-like morphology. Unlike other stem cells, MSCs are typically identified by a conventional criterion of markers (Shoji, Koba and Kobayashi, 2014).

The myogenic differentiation capacity of MSCs was confirmed by the expression of the smooth muscle cell marker αSMA (Kinner, Zaleskas and Spector, 2002). For instance, TGF-β1 treatment of cultured human MSCs showed an increase in the expression of the αSMA protein. However, the expression of αSMA protein in human MSCs decreased upon PBGF-BB treatment. These growth factors not only seem to affect the protein profile of hMSCs, but also their morphology characterised by a well-spread polygonal shape along with easily observable stress fibres (Kinner, Zaleskas and Spector, 2002; Talele et al., 2015).

In human mesenchymal stem cells (hMSCs,) gene expression profiling suggests that TGF-β1 induced Notch ligand Jagged 1 (JAG1) and SMC markers, including smooth muscle alpha-actin (ACTA2), calponin 1 (CNN1), and myocardin (MYOCD). This effect was dependent on the activation of SMAD3 and Rho kinase. In addition, knocking down JAG1 expression partially blocked ACTA2 and CNN1 expression and completely blocked MYOCD expression, suggesting that JAG1 plays an important

role in TGF-β-induced expression of SMC markers. These results suggest that hMSC transition to SMC differentiation may be mediated by TGF-β1-activated Notch pathway (Kurpinski et al., 2010).

1.4.3 SMC Progenitor Cells from the Adventitia

In 2002, Xu's group provided the first evidence *in situ* of resident SMC progenitors by performing vena cava isografts to carotid arteries between different sex-mismatched transgenic mice. Their data showed that 60% of the newly formed SMCs within the neointima belonged to the donor mouse (SM-LacZ reporter mouse), and the rest to the recipient (wild-type) animal. In order to confirm these values, they double stained for α-actin and the Y-chromosome within the neointimal lesion. Furthermore, other *in vivo* studies approached the question in a similar way, however this time SM-LacZ mouse bone marrow was transplanted into a recipient mouse containing an aortic homograft. After staining the homograft with X-gal, no β-gal positive staining was observed suggesting that the SMC progenitors did not come from the bone marrow (of the SM-LacZ donor mouse) (Torsney, Hu and Xu, 2005). This data therefore suggests that SMC progenitors are definitely present in the vessel, however, these cells are resident within the vessel wall.

Resident cells of the adventitial layer, the *Fibroblasts,* consist of a highly heterogenic cell population that can be isolated from each other by subculture of the primary cells, and exposing them to different growing conditions (e.g. adherent plates versus semi-solid media) (Stenmark and Mecham, 1997). Sections of aortic root from an ApoE-/- mouse were immunohistochemically stained for different stem cell markers. Notably, adventitia was the only aortic layer staining positive for stem cell antigen-1 (Sca-1) (abundant, 21%), c-kit (9%), CD34 (15%), and Flk-1 (4%), but they were negative for the embryonic stem cell marker SSEA-1, and less than 0.1% were positive for the bone marrow marker, CD133. Moreover, cultured adventitial cells varied in their morphologies, some of them showed a fibroblast-like phenotype, while others possessed a rounder shape (Hu et al., 2004) resembling the morphology of proliferative SMC-like cells such as myofibroblasts, and synthetic vSMCs. They have been shown to express Vimentin and non-muscular (NM)-Myosin, typical markers of proliferative SMC-like cells such as myofibroblasts, and synthetic vSMCs.

In vitro studies carried out using purified Sca-1$^+$ cells derived from adventitia explants and cultured in embryonic stem cell medium, demonstrated that they were able to differentiate into SMCs upon PDGF-BB stimulation. mRNA levels of SMC markers such as SMA, SM22, calponin and SMC-MHC were upregulated 3 days after stimulation. Similarly, purified Sca-1$^+$ cells derived from adventitia explants of SM22 promoter-driven LacZ transgenic mice exhibit positive β-gal staining after co-culturing the cells with PDGF-BB (Hu et al., 2004). *In vivo*, adult adventitial fibroblasts of the pulmonary artery are the earliest cells to respond to vessel injury and exhibit an intrinsic flexibility to undergo phenotypic changes and secretion of molecules such as type I collagen, fibronectin and elastin proteins (Stenmark and Mecham, 1997). These studies suggest the presence of a resident adventitial progenitor cell population characterised by the expression of stem cell markers (Sca-1$^+$ c-kit$^+$ CD133$^-$), and their potency to differentiate into SMCs after stimulation by PDGF-BB, a factor involved in activation of the endothelial after injury (e.g. in atherosclerosis).

Other studies have focused on the embryological origin of these diverse adventitial cell populations, and they were able to demonstrate that a subtype of arterial adventitial fibroblasts shares a common embryological origin with smooth muscle cells of tunica media. The lineage specification occurs by differentiation of epicardial mesothelium-derived undifferentiated MSCs in response to growth factors such as VEGF and PDGF-BB. Therefore, because of their clonogenicity, and their embryological origin variability, fibroblasts have been hypothesised to be not only the inhabitants of arterial adventitia, but also the source of synthetic SMCs found in the tunica media, and thus neointimal SMCs during pathology (Sartore et al., 2001).

1.4.4 SMC Progenitor Cells from Tunica Media

Seminal studies conducted by Song Li's group in Berkeley, CA identified a new peripheral SMC progenitor residing in the tunica media of blood vessels expressing protein markers associated with neuroectodermal stem cells. These cells were isolated and shown to be capable of not only myogenic differentiation but also other multilineages (adipogenic, osteogenic, chondrogenic and neural). These cells were considered multipotent vascular stem cells (MVSCs). This intensive work concluded that MVSCs rather than de-differentiated vascular SMCs were in part responsible for the cell progeny found within neointimal lesions (Tang et al., 2012).

In support with these findings, the same group reported the presence of a SM-MHC$^-$ cell in tunica media and adventitia of carotid arteries *in vivo* (Yuan et al., 2017; Sainz et al., 2006) that were SOX10-positive stem cells. These cells were able to proliferate and migrate upon vascular injury contributing to vascular remodelling and lesion formation (Yuan et al., 2017).

1.4.5 SMC Progenitor Cells from Endothelium

Endothelial cells have been proposed to contribute to vascular remodelling and neointimal lesions via an endothelial-to-mesenchymal transition (EndoMT), which involves the loss of endothelial markers such as CD31 and the acquisition of markers related to a mesenchymal phenotype (Wang et al., 2015). Cooley *et al.* (2014) carried out an extensive cell fate mapping study *in vivo* of vein grafting demonstrating that a large number of the neointimal cells are derived from the vein graft endothelial cells (Cooley, 2005).

1.5 The Use of Animal Models in Research

The use of animal models has been an essential tool for dissecting complex human phenotypes by investigating specific signalling pathways and genes contributing to disease states. The choice of animal and corresponding injury model employed is crucial when designing these studies. A number of considerations must be measured when selecting the most representative animal model for the desired study, and in some cases more than one animal model is necessary to investigate the disease state in question (Breckenridge, 2013).

1.5.1 Use of animal models in cardiovascular research

One of the first uses of animals for cardiovascular research took place in 1907 whereby the effect of a western diet on atheroma development within rabbit aortas was investigated. Since then, animal models have been used extensively to investigate the mechanisms of atherosclerosis and are the foundations of basic and preclinical research for numerous cardiovascular syndromes (Konstantinov and Jankovic, 2013; Chen, Shannon and Shen, 2013). The choice of animal model depends on numerous

factors including animal availability, cost, time constraints, and the scientific question under investigation. Animals such as mice and rats are often the choice selection for researchers due to their fast reproduction rates and basic maintenance requirements (Santos et al., 2015). Additionally, genetically modified mice have allowed us to investigate disease mechanisms by genetic manipulation (Chorro, Such-Belenguer and López-Merino, 2009).

1.5.1.1 Use of injury models in cardiovascular research

The choice of injury model selected is highly dependent on the human pathology under investigation as the lesion induced must mirro the normal cardiovascular and human pathology. To date, a variety of animals have been used for the modelling of cardiovascular disorders. However 90% of all *in vivo* work has been conducted within mice and rat models (Hasenfuss, 1998) (Liao, Huang and Liu, 2017) (Chen, Shannon and Shen, 2013).

The following sections review the most commonly used injury model systems performed in mice:

Models of atherosclerosis – Atherogenesis is a multifactorial disease believed to begin with high levels of low-density lipoproteins (LDL) followed by endothelium damage and subsequent immune response. Cell death, calcification at the vessel site, as well as smooth muscle cell (SMC) proliferation and migration are also characteristics of atherosclerosis. As a result, an asymmetric atheroma is formed within the luminal area of blood vessels obstructing the normal course of blood flow (Cunningham and Gotlieb, 2005; Galkina and Ley, 2009). Vulnerable plaques present a high-risk of thrombus formation that can lead to myocardial infarctions and strokes (Fuster et al., 2012).

The majority of mice strains are naturally resistant to lesion formation due to their high content of high-density lipoproteins and relative low levels of very-low-density (VLDL) and low-density lipoproteins (LDL). As a result, diet and genetic manipulation are the most effective mechanism for controlling atherosclerosis development in murine models (Getz and Reardon, 2006; Zaragoza et al., 2011).

- **Low-density Lipoprotein Receptor-deficient ($LDLR^{-/-}$)** – This model resembles

the human familial hypercholesterolemia (FH) syndrome caused by high levels of LDL molecules (cholesterol) and decreased levels of HDL molecules (cholesterol) in plasma. Lesion formation is induced through the feeding of a high-fat/cholesterol diet. LDLR$^{-/-}$ mice expressing the human apoB100 transgene [tg(*apoB*$^{+/+}$)] are commercially available presenting high LDL levels in plasma and atherosclerotic lesions on a low-fat diet (Ishibashi et al., 1993; Farese et al., 1996; Sanan et al., 1998)

- **Apolipoprotein E-deficient mouse model (ApoE$^{-/-}$)** – Animals deficient in the apoE gene exhibit atherosclerotic plaque formation that is widely distributed throughout the aorta. The lesion is proportional to the age and diet and resembles the process of atherosclerosis in humans. One of the downsides of the apoE$^{-/-}$ mice is that atherosclerosis develops with high levels of very low-density lipoproteins (VLDL) and intermediate-density lipoproteins (IDL) in plasma, in contrast to high LDL cholesterol molecules observed in humans. Instead, apoE$^{-/-}$ lipid profile resembles that of human type III hyperlipidaemia. Moreover, apoE$^{-/-}$ mice were demonstrated to have atheroprotective and anti-inflammatory properties, hence results must be carefully analysed for a good interpretation and translation (Farese et al., 1996; Sanan et al., 1998; Fuster et al., 2012; Zaragoza et al., 2011).

Both the LDLR$^{-/-}$ and the apoE$^{-/-}$ transgenic animals are commonly used to study atherosclerosis in humans, however, metabolic changes due to the animal genotype need to be considered when selecting the appropriate model. In bone marrow transplantation studies the LDLR$^{-/-}$ mice is preferred over apoE$^{-/-}$ animals owing to the production of apoE by donor bone-marrow macrophages. Instead, LDLR secretion by hematopoietic cells of a wild-type bone-marrow donor is irrelevant to the formation of the atheroma. Therefore, unless a bone marrow from an apoE$^{-/-}$ mouse is transplanted to the apoE-deficient animal, macrophage-derived apoE might induce an atheroprotective effect on the lesion (Bellosta et al., 1995; Fuster et al., 2012). This feature becomes extremely valuable in cell fate studies when the bone marrow of a reporter animal is transplanted in to the apoE-deficient recipient in order to trace the bone marrow-derived cells at the lesion site.

Models of in-stent restenosis – Neointima Hyperplasia (NIH) develops following percutaneous transluminal coronary angioplasty (PTCA) and stenting due to

endothelium damage that triggers a healing response. NIH is characterised by the accumulation of SMC-like cells and ECM molecules in the tunica intima resulting in the narrowing of the luminal area and thus vessel re-occlusion.

- **Models of blood-flow cessation -** Shear Stress is a biomechanical force that acts parallel to the endothelial lining of the vascular wall and is proportional in size to the magnitude of blood flow with a typical value of 10 to 20 dyn/cm^2. Laminar blood flow typically results in normal shear stress rates and is important for maintenance of vascular homeostasis. Disturbed non-laminar blood flow typically develops at vessel curvatures and bifurcation sites. Significant alterations to shear stress rates initiate vascular remodelling with a cascade of molecular and cellular processes activated in order to re-establish vascular haemostasis. Therefore, shear stress is implicated in the development of atherosclerosis and in-stent restenosis (Wang et al., 2018; Cunningham and Gotlieb, 2005; Korshunov and Berk, 2003).

  a. *Complete Carotid Artery Ligation* – Kumar and Lindner (1997) first proposed this model whereby net blood flow in the common carotid artery of a mouse was completely disrupted by knotting the vessel at the distal bifurcation and thus reducing shear stress rates. After 4 weeks ligation, the damaged vessel exhibited a decreased luminal area of approx. 80%, medial cell death, a 25% reduction in vessel circumference measured by the external elastic lamina (EEL), and increased thickness of the medial and intimal layers. The new intima was mostly found to be composed of SMC-like cells and some leukocytes. The endothelium was not denudated exerting a thrombus-free effect, however, thrombus formation was observed proximal to the ligation site (Kumar and Lindner, 1997; Wang et al., 2006). This model has been typically used when studying the genetic and molecular mechanisms involved in vascular remodelling and intima-media thickening.

  b. *Partial Carotid Artery Ligation* – In this model partial disruption of net blood flow is achieved by knotting the left internal and external carotid arteries leaving the occipital free of flow. The normal blood flow of carotid arteries is 0.5 ml/min with a reduction to 0.1 ml/min in the left carotid artery (LCA) and an increase to 1 ml/min in the right carotid artery (RCA) following ligation.

Shear stress drops to 4 dyn/cm^2 and rises to 32 dyn/cm^2 in the left and right carotid arteries, respectively. 4 weeks after partial ligation, the LCA shows a significant reduction in lumen diameter accompanied by an increase in the medial area, and intima thickening. Leukocytes are found in the adventitial, medial and intimal layers. The external and internal laminas are thin and break, allowing for cellular filtration and migration. It is noted that the endothelium remains intact creating a thrombogenic-preventive effect (Korshunov and Berk, 2003; Wang et al., 2006). This model is used when the primary end goal is to study genetics and molecular mechanisms involved in vascular remodelling and intima-media thickening owing to changes in shear stress caused by low blood flow.

The complete ligation technique is highly reproducible with an extensive vascular remodelling response. Although the degree of injury varies with murine strain, the main limitation of the complete ligation model is the slight damage caused to the endothelium that subsequently exerts a thrombogenic effect. This feature has been improved with the introduction of the partial carotid ligation technique that claims to be thrombus-free due to a subtle or none endothelial denudation. However, both models induce arterial lesions by oscillatory blood flow (Kumar and Lindner, 1997; Wang et al., 2018; 2006; Cunningham and Gotlieb, 2005; Korshunov and Berk, 2003).

- **Models of mechanical injury**
  a. *Wire injury of the murine carotid artery* – This model was first outlined by Lindner and colleagues (1993) with the aim of studying the mechanisms of atherosclerosis and vascular remodelling. This mouse injury model together with the variety of transgenic and knock-out/in mouse strains available at the time revolutionised the way vascular studies were conducted. In this model complete endothelial denudation was achieved using a flexible wire of 0.35mm in diameter. Briefly, the left external carotid artery was firstly ligated distal to the bifurcation, and a small incision between the ligature and the bifurcation was made to introduce a flexible wire into the vessel. Once in the common carotid artery, the wire was passed along the vessel in a rotational motion to denudate the endothelium. The wire was then removed from the vessel and a second suture was tied off on the left external carotid artery proximal to the

bifurcation. Platelets were seen to adhere to the internal lamina in areas of endothelial denudation. Evidence in the literature also suggested that there was little damage to the tunica media. SMC replication was observed in the media and intima reaching their highest rates of 9.5% and 66% at 5 and 8 days after injury, respectively. The endothelium was repaired within 3 weeks after wire injury, and a small intima thickening (2 or 3 cell layers) was detected in denuded places long the artery. Some leukocytes were found within the intima lesion (Lindner, Fingerle and Reidy, 1993; Wang et al., 2006).

b. *Wire injury of the murine femoral artery* – This model was developed by Sata *et al.* (2000) in order to induce abundant SMC apoptosis and proliferation, and thus neointima formation to mimic injury following PTCA. Complete endothelial denudation of the iliac artery was performed using a spring wire. This was achieved by first ligating the deep femoral artery (DFA) and a small incision made that served as an entry port for the wire. Following insertion, the wire was carefully moved to the common femoral artery (CFA) towards the iliac artery, and left in place for 1 min. The spring wire caused denudation of the endothelium by pushing the vessel open and thus mimicking the balloon angioplasty procedure. The wire was then removed from the vessel and a second suture was tied off on the DFA proximal to the bifurcation to enclose the opening. The procedure had a success rate of 95% with no rupture or extravasation of the femoral arteries. Complete endothelial removal was confirmed by the lack of CD31 positive stain. Vessel dilation was observed within the first 24 hr after wire injury remaining expanded till 8 days. The tunica media was drastically damaged with a significant number of apoptotic SMCs found within the first 6 hr after wire injury, and at 17 hr the cellular content of the medial layer was reduced to a few cells. At 1 week, SMC proliferation was observed in the media and intima. The endothelium was almost repaired within 4 weeks, and a large concentric intima thickening was detected long the artery. Immunostaining analysis showed that the neointima lesion was mainly composed of SMCs with no capillarisation. Occasionally, macrophages were found in the neointima, and thrombogenesis observed in injured vessels (Takayama et al., 2015; Sata et al., 2000; 2001; Wang et al., 2006).

These injury models offer an *in vivo* alternative to study the mechanisms of vascular remodelling triggered by PTCA resulting in the proliferation of medial SMCs, and the development of a neointima with a minimal immune response and thrombogenesis. Although the degree of injury varies depending on the genetic background of the animals, the main drawback of this model is its poor reproducibility, which is believed to be partially due to operator surgical skills. The absence of a significant intimal lesion caused by the wire-injury-of-the-murine-carotid-artery model was improved when Kumar and Lindner (1997), and Sata *et al.* (2000) introduced the complete-carotid-artery-ligation, and the wire-injury-of-murine-femoral-artery models, respectively. Nevertheless, results need to be consciously interpreted when being analysed as neointima hyperplasia in humans occurs in diseased vessels and not in the healthy arteries of animal models (Kumar and Lindner, 1997; Lindner, Fingerle and Reidy, 1993; Takayama et al., 2015; Sata et al., 2000; 2001; Wang et al., 2006).

Importantly, the injury models using the carotid artery address the role of vascular remodelling and intimal thickening associated with vessels containing SMCs of neuroectoderm embryological origin. These are known to be athero-prone regions of the vasculature and are suitable for disease modelling. In contract, the SMCs of the femoral artery following wire induced injury are of mesoderm embryological origin and are considered more athero-resistant (Bargehr et al., 2016).

1.5.1.2 The lineage tracing studies that have mostly contributed to our knowledge of SMC progeny in the murine neointima

Lineage tracing studies have emerged in recent years with the introduction of both constitutive and inducible Cre recombinase models in reporter mice and have revolutionized the ability to detect the origin of cells *in vivo* (Romagnani, Rinkevich and Dekel, 2015; Albarrán-Juárez et al., 2016).

The most popular inducible Cre recombinase system is the tamoxifen-inducible Cre recombinase, also known as Cre-ER^T recombinase. In this system, the Cre activity is under the control of a genetically modified human oestrogen receptor (ER^T) that binds to Tamoxifen (Tm) to translocate to the nucleus where recombination takes place. Reporter mice were initially introduced to confirm the efficiency of constitutive Cre recombination systems. These reporter strains consist of a marker gene such as the β-

galactosidase enzyme downstream of a loxP-flanked STOP sequence. Therefore, when the Cre-LoxP site-specific recombinase mouse is crossed with a reporter mouse their offspring (according to mendelian genetics) express the reporter gene under the control of a tissue-specific promoter. Reporter strains soon gained popularity especially after the development of the "Green Mouse", where an enhanced green fluorescent protein (eGFP) gene driven by the *cytomegalovirus* enhancer/chicken β-actin (CAG) promoter was inserted in the mouse genome. Since then, various fluorescent proteins have been genetically engineered, and introduced in the murine genome in order to create a wide range of reporter mice for different applications (Sauer and Henderson, 1988; Sauer, 1987; ORBAN, CHUI and MARTH, 1992; Doevendans, Daemen, de Muinck and Smits, 1998; Metzger and Chambon, 2001; Okabe et al., 1997; Abe and Fujimori, 2013) (The Jackson Laboratory, 2018).

Nowadays, the Cre-ER^T recombinase mouse in combination with a reporter mouse are powerful tools for the study of cell progeny during development, tissue regeneration and during pathological process. A major limitation of the single-coloured labelling technology is that tissue-specific cell subpopulations are not parsed, instead all cells belonging to one cell-type are visualised by one colour upon cre recombination. In 2007, Livet *et al.* introduced the Brainbow multicolour labelling approach making each tissue-specific cell be uniquely marked by the expression of one or combinational fluorescent proteins. This approach is especially important when addressing questions regarding the behaviour of individual cells within a subpopulation rather than that of an entire cell population (Livet et al., 2007; Weissman and Pan, 2015).

Despite the numerous lineage tracing studies performed up to date, the origin of the SMC-like cells in arteriosclerotic lesions remains controversial.

This following section highlights the seminal *in vivo* studies performed to date that address the origin of SMC-like cells in arteriosclerotic and atherosclerotic models.

Animal Models of Arteriosclerosis

Studies that support the putative role of differentiated medial SMCs and their progeny in contributing to intimal thickening following injury:

1. The Nemenoff *et al.* (2011) (Nemenoff et al., 2011) study –

Model animal: SM-MHC-CreER^{T2}/PTEN$^{flox\text{-}flox}$/Rosa26-LacZ (PTEN iKO), and SM-MHC-CreER^{T2}/Rosa26-LacZ (PTEN WT), UBI-eGFP mice
Animal age: Not specified
Tamoxifen (Tm) doses: 1 x 1mg for 5 days
Tm metabolism before injury: 4 days
Injury model: Wire-induced injury of the femoral artery (FA)
Duration of the injury: 3 weeks, unless otherwise specified

Briefly, the aim of this study was to investigate the role of SDF-1α in PTEN-deficient SMC transgenic animals and the contribution of i) mature vSMCs, and ii) bone marrow (BM)-derived cells to lesion intimal thickening in these animals. Intimal thickening was aggravated in the PTEN iKO transgenic mouse compared to the WT animals. Medial differentiated SM-MHC^{+} SMCs were indelibly marked in SM-MHC-CreER^{T2}/Rosa26-LacZ reporter mice before wire-induced injury. The majority of the cells populating the media and intima following injury were derived from resident differentiated vSMCs as they were indelibly labelled by β-galactosidase (β-gal), and most of them exhibited an apparent SMC phenotype by co-staining positive for α-actin (αSMA).

Secondly, chimera PTEN WT and iKO animals with eGFP-labelled BM were generated 6 weeks prior to Tm administration to study the role of bone marrow cells after FA injury. Accumulation of BM-derived (eGFP^{+}) cells wax evident in all the layers; however these cells were unable to express the SMC marker α-actin. Instead, the macrophage marker Mac3 was co-stained in these cells. (Nemenoff et al., 2011).

Overall, the study suggests that resident vSMCs were the major source of cells causing intimal thickening and that contribution of BM-derived macrophages to the lesion was correlated to the inflammatory response of the pathology rather than to the

cellularization event (Nemenoff et al., 2011).

2. The Herring *et al.* (2014) (Herring et al., 2014) study –

Model animal: SM-MHC-CreER^{T2}/Rosa26$^{flox\text{-}mT\text{-}stop\text{-}flox\text{-}mG}$ and α-actin-CreER^{T2}/Rosa26$^{flox\text{-}mT\text{-}stop\text{-}flox\text{-}mG}$ mice
Animal age: 5-6 weeks
Tamoxifen (Tm) doses: 1 x 1mg for 5 days
Tm metabolism before injury: 2 weeks
Injury model: Complete carotid artery ligation
Duration of the injury: 7, 14 and 28 days

The aim of the study was to re-evaluate whether pre-existing medial SMCs or resident vascular stem cells reported by Tang *et al.* (2012) (Tang et al., 2012) were a possible source of cell progenitor contributing to the lesional cells comprising the neointima. A dual-colour (mTmG) reporter mouse was crossed with either Myh11-CreER^{T2} or α-actin-CreER^{T2} to trace the vSMC progeny after carotid artery ligation injury. This technology facilitates the interpretation of the data by marking cells either green (meGFP**)** or tomato red (mTd) depending on the presence or absence of cre recombinase activity, respectively.

Once injury is performed on tamoxifen (Tm)-pre-treated animals, Myh11/α-actin-derived cells are identified by the expression of the eGFP protein, while Myh11^{+} or α-actin^{+} non-SMCs are positive for the mT protein. The majority of neointimal cells were derived from SM-MHC marked cells and α-actin cells, respectively, 28 days after injury as confirmed by the positive expression of the eGFP protein. Additionally, flow cytometry data revealed that no eGFP^{+} cells in the circulation at 7, 14 and 28 days post-surgery, suggesting that any eGFP^{+} cell found in the neointima originated locally. Interestingly, a large number of the mT^{+} cells were found to positively co-stain for either an endothelial marker CD31, or a monocytes/macrophage marker CD68 in immature lesions (14 days). In contrast, very few CD31^{+} and no CD68^{+} cells were present in mature lesions (28 days) (Herring et al., 2014).

Although the experiment could not rule out the contribution of other cell types to lesion

formation, the *in vivo* study provided convincing evidence that a large portion of the SMCs (approx. 80%) in neointimal lesions originated from contractile SMCs resident within the tunica media (Herring et al., 2014).

3. The Yang *et al.* (2016) (Yang et al., 2016) study –

Model animal: SM-MHC-CreER^{T2}/Rosa26-LacZ, Scl-CreER^{T2}/Rosa26-LacZ, and BM-EGFP mice
Animal age: 11 weeks
Tamoxifen (Tm) doses: 1 x 2.5mg for 10 days for both injury models
Tm metabolism before injury: 24 hours for the complete carotid artery ligation
Injury model: Complete carotid artery ligation (CCL) at the left common carotid artery bifurcation, and wire-induced injury of the femoral artery (FA).
Duration of the injury: 24, 38, and 59 days

The aim of the study was to specifically investigate the source of neointima cells in an adult animal (11 weeks old) as opposed to juvenile mice (younger than 6 weeks old) of previous studies (Herring et al., 2014). SM-MHC-CreER^{T2}/Rosa26-LacZ mice received daily I.P. injection of Tm (2.5mg) for 10 consecutive days, before CCL and FA injuries were performed 24 hours after the last Tm dose. The intimal lesions contained numerous-β-galactosidase^{+} marked cells with a subsequent loss of expression of SMC markers such as SM-MHC and alpha actin (α-SMA). Unexpectedly, some lesions (CCA and FA) exhibited high cellularisation but non-β-galactosidase (β-gal) staining, suggesting that certain lesions were formed from non-SMC-derived cells (Yang et al., 2016).

The group also studied the contribution of bone marrow cells (BMCs) to the intimal thickening after FA injury using chimeric mice with EGFP-labelled bone marrow. The data confirmed the presence of BMCs recruited at the lesion site; r similar to the Nemenoff study(Nemenoff et al., 2011). BMCs failed to express the SMC mature marker, SM-MHC within the neointima. Lastly, the use of Scl-CreER^{T2}/Rosa26-LacZ mice to mark and track endothelial cells (ECs) and their progeny identified a small fraction of EC-derived cell cells in the sub-endothelial region (Nemenoff et al., 2011;

Yang et al., 2016).

Overall, although mature vSMCs were in part responsible for the population of the neointima, the extent of their contribution was age- and animal-to-animal dependent. The average number of vSMC-derived cells within the neointima was less than 30% in both injury models in contrast to the Herring study. (Herring et al., 2014; Yang et al., 2016).

4. The Chappell *et al.* (2016) (Chappell et al., 2016) study –

Was conducted in two different injury models; however, herein the arteriosclerosis *in vivo* study is described.
Model animal: SM-MHC-CreER^{T2}/Rosa26-Confetti conditional mouse
Animal age: 6-8 weeks
Tamoxifen (Tm) doses: Low (1 x 0.1mg), medium (1 x 1mg), and high (10 x 1mg) for 2 weeks
Tm metabolism before injury: 1 week
Injury model: Complete carotid artery ligation at the left common carotid artery bifurcation
Duration of the injury: 28 days

The aim of the study was to investigate whether all, or a subset(s) of the vascular marked vSMC population in the tunica media of the carotid artery was capable of de-differentiation becoming migratory and proliferative, and thus contributing to the formation of the neointima. The SM-MHC^{+} cell populations were individually labelled using the SM-MHC-CreER^{T2}/Rosa26-Confetti animal, and a high dose of Tm for 2 weeks. 1 week after Tm administration, animals were injured for 28 days. In contrast to the control samples (right carotid arteries), the left ligated artery was composed of monochromatic patches within the lesion. Suggesting that neointimal cells derived from a discrete subpopulation of marked medial SMCs (Chappell et al., 2016)

5. The Majesky *et al.* (2017) (Majesky et al., 2017) study –

Model animal: SM-MHC-CreER^{T2}/Rosa26-YFP, Myh11-CreER^{T2}/Rosa26-LacZ, SM22α-Cre/Rosa26-YFP, and SM22α-Cre/Rosa26-YFP Klf4 SM-deficient Knockout mice
Animal age: 2 months
Tamoxifen (Tm) doses: 1 x 1mg for 5 days
Tm metabolism before injury: 10 days
Injury model: Complete ligation (CCL) of the left common carotid artery at the bifurcation, and wire-induced injury of the femoral artery (FA)
Duration of the injury: 4 weeks

The aim of this study was to primarily investigate the origin of the adventitia stem cell progenitors previously identified by the positive expression of the Sca-1 and CD34 markers (AdvSca-1), and their contribution to vascular remodelling (Hu et al., 2004; Majesky et al., 2017). In this context, two animal models were used to trace AvdSca1 cells back to the time of vascular development. 30 days postnatal, the carotid artery and aortic arch, descending aorta, and femoral artery of Myh11-CreER^{T2}/Rosa26-YFP mice were separately harvested and digested to detect Sca-1^{+}YFP^{+} double positive cells by flow cytometry analysis. Base-line results showed that approx. 8% of the entire Sca-1^{+} cell population within the three arteries were derived from SMCs. On the other hand, when using the constitutive SM22α-Cre/Rosa26-YFP animals the proportion of Sca-1^{+}YFP^{+} cells over the Sca-1^{+} population highly increased with approximate values of 60%, 41%, and 30% in the carotid artery and aortic arch, descending aorta, and femoral artery, respectively. Immunostaining analysis of common carotid arteries from 2 months old SM22α-Cre/Rosa26-YFP mice, visually confirmed the presence of αSMA^{-}Sca-1^{+}YFP^{+}, and αSMA^{-}CD34^{+}YFP^{+} cells within the tunica adventitia. Interestingly, flow cytometry analysis detected a positive expression of the pluripotency-associated transcription factor, Klf4, in both populations of YFP^{+}Sca-1^{+} and YFP^{-}Sca-1^{+} cells. Furthermore, chromatin immunoprecipitation (ChIP) assay was performed for the expression of the highly specific SMC chromatin mark, H3K4me2 in the SM-MHC and αSMA promoters of both isolated YFP^{+}Sca-1^{+} and YFP^{-}Sca-1^{+} cells. In contrast to the YFP^{-}Sca-1^{+} cells, isolated YFP^{+}Sca-1^{+}, aortic media tissue and mature SMC cells showed chromatin

enrichment of the H3K4Me2 mark in the SM-MHC and αSMA promoters. The data suggested that a subpopulation of AdvSca-1 was derived from mature SMCs.

The group also demonstrated that $YFP^{+}Sca\text{-}1^{+}$ cells were capable of transition to endothelial-like cells, macrophages and SMCs *in vivo*, and isolated $YFP^{+}Sca\text{-}1^{+}$ cells in culture were able to differentiate into adipocytes and chondrocytes. In order to evaluate the role of mature SMCs in adventitia remodelling after vascular injury, CCL surgery was performed in SM22α-Cre/Rosa26-YFP animals followed by immunohistochemistry analysis. 3 days post-operation, there was an increase in the numbers of $\alpha SMA^{-}YFP^{+}$ cells in the tunica adventitia, and their majority also co-stained positive for the Sca-1 protein. Moreover, the role of Kruppel-like transcription factor 4 (Klf4) in SMC de-differentiation towards the AvdSca-1 phenotype was studied *in vivo* and *in vitro*. The data demonstrated that Klf4 contributed to SMCs transition to a progenitor phenotype identified by the loss and gain expression of the αSMA, and Sca-1 markers, respectively.

Collectively, the data suggest that mature SMCs originate from a number of cell progenies by transitioning to a multipotent progenitor cell (AdvSca-1) that resides in the tunica adventitia of major and intermediate arteries. They hypothesised that mature SMCs would be activated during the first days after vascular injury contributing to generation of AdvSca-1 cell progenitors, which subsequently would participate in vascular remodelling and lesion formation (Majesky et al., 2017).

<u>Studies that support the putative role of resident vascular stem cells and their progeny in contributing to intimal thickening following injury:</u>

6. The Tang *et al.* (2012) (Tang et al., 2012) study –

Model animal: SM-MHC-Cre/LoxP-enhanced GFP mice and Sprague Dawley (SD) rats
Animal age: Not specified
Injury model: Wire-induced injury of the common carotid artery (CCA)
Duration of the injury: 5, 15, and 30 days

The aim of this study was to challenge the well-accepted theory that de-differentiation of resident vascular SMCs become migratory, and proliferative in a diseased condition contributing to vascular remodelling and neointima hyperplasia (Tang et al., 2012).

This work revealed for the first time the existence of a SM-MHC$^-$ cell type in the rat carotid artery wall, which comprised less than 10% of the medial cells. Using enzymatic digestion and explant methods, isolated SM-MHC$^-$ cells stained highly positive for the proliferation marker Ki67, and slightly expressed the early SMC marker α-actin. The same study was performed using the SM-MHC-Cre/Rosa26-eGFP mouse confirming that isolated eGFP$^-$ cells were the only survivors after 10 days in culture with DMEM/10% FBS. Characterisation studies also demonstrated that isolated rat SM-MHC$^-$ and murine eGFP$^-$ cells were positive for a repertoire of markers including SOX10, SOX17, S100β, and Nestin, but not for others attributed to MSC-like cells, and EC and/or EC progenitors as well as Sca-1 progenitors, and hematopoietic lineage cells. This new cell population gave rise to a variety of cell types *in vitro* and *in vivo*, and so adopted the name of *multipotent vascular stem cells,* MVSCs (Tang et al., 2012).

The role of different stimuli such as TGFβ1, and the Notch signalling pathway in driving MVSCs to a mature SMC phenotype was confirmed by *in vitro* studies. The data suggested that resident MVSCs are not derived from mature vSMCs although they have the potential to become SM-MHC$^+$ cells. The author also studied the possibility of a MVSC-MSC-SMC pathway by the spontaneous differentiation of rat MVSCs in DMEM/10%FBS. Results suggested that this differentiation pathway could explain the heterogeneity of vSMCs (Tang et al., 2012).

Overall, these results suggested the existence of a new progenitor cell present in the tunica media of blood vessels as a potential source of lesional cells contributing to intimal thickening. The study proposed for the first time that vascular diseases could be more a disease of resident stem cell (Tang et al., 2012).

7. The Yuan *et al.* (2017) (Yuan et al., 2017) study –

Model animal(s): SM-MHC-Cre/Rosa26-RFP, Tie2-Cre/Rosa26-RFP, SOX10-Cre/Rosa26-RFP, and SOX10-Cre/Rosa26-LacZ mice
Animal age: 2 months
Injury model: Wire-induced injury of common carotid artery (CCA) and the femoral artery (FA), and complete ligation of the left common carotid artery (CCL)
Duration of the injury: 2 weeks

The aim of this study was to clarify the cell progenitor(s) source of the heterogeneous populations contributing to intimal thickening and lesion formation after injury. Isolated cells from aortic tissue of SM-MHC-Cre/Rosa26-RFP animals were RFP^- cells and highly proliferative comparing to RFP^+ marked cells, and mostly expressed the neural crest marker, SOX10 (Yuan et al., 2017).

Using the SM-MHC-Cre/Rosa26-RFP mice and two injury models (CCA and CCL), the presence of two types of intimal lesion namely Type-I, and Type-II were revealed. Type-I neointima was characterised by high numbers of RFP^+ cells, and among them more than 90% co-stained positive for the SMC markers α-actin (α-act), calponin1 (CNN1), and smooth muscle myosin heavy chain (SM-MHC). In contrast, > 90% of RFP^- cells in type-II lesions were $\alpha\text{-actin}^+$, but only 25% of these cells were $CNN1^+$ and SM-SMC expression was hardly observed. $SOX10^+$ cells were found at low expression (~7%). The data suggests that type-I lesional cells originated predominantly from mature SMCs; however, the main cell progenitor in type-II neointima was uncertain. Using the SOX10-Cre/Rosa26-LacZ mouse and FA injury model, the data demonstrated significant stain of β-galactosidase (β-gal) with similar expression levels of the SMC markers to type-II lesion. Therefore, the latter lineage tracing model proposed $SOX10^+$ cells as a potential cell progenitor in type-II neointima hyperplasia (Yuan et al., 2017).

Lastly, using the Tie2-Cre/Rosa26-RFP mice to indelibly mark endothelial cells, a large number of RFP^+ cells were present within the lesion after 2 weeks. In contrast to previous studies(Cooley et al., 2014), most of lesional RFP^+ cells did not co-stained for α-act, but $CD31^+$, suggesting that injury-induced ECs did not transdifferentiate to a SMC phenotype (Cooley et al., 2014; Yuan et al., 2017).

Overall, the data demonstrated multiple cell progenitors (medial SMCs, $SOX10^+$ cells, and ECs) contributed to vascular remodelling and intima thickening after injury, which in part may explain the cellular diversity observed in neointima hyperplasia. Given the complexity of vascular diseases in humans, the progression and healing events of intima outgrowth may involve multiple cellular sources (Yuan et al., 2017).

Studies that support the putative role of circulating vascular stem cells and their progeny in contributing to intimal thickening following injury:

8. The Wan *et al.* (2012) (Wan et al., 2012) study –
Model animal(s): Nestin-Cre/Rosa26-EYFP
Animal age: Adult
Injury model: Wire-injured femoral artery (FA) in mice
Duration of the injury: 3 days to 2 weeks

This study aims to evaluate the contribution of bone marrow mesenchymal stem cells (MSCs) to vascular injury by mobilizing and recruiting them to the site of injury in respond to the migratory factors TGFβ. In this context, immunostaining analysis of the neointimal tissue sections demonstrated that NES^+ cells were only found in the luminal side of the neointima but not in the core of the lesion, which was positive for the αSMA marker. Nestin-Cre/Rosa26-EYFP mice revealed that 57 and 44.6% of the neointimal cells were $EYFP^+$ suggesting that upon vascular injury bone marrow ($NES^+Sca\text{-}1^+CD29^+CD11b^-CD45^-$) MSCs may be activated and released into the circulation to subsequently be recruited to the site of lesion thus contributing to neointima thickening and re-endothelialisation of the damaged vessel.

Furthermore, the involvement of TGFβ factors in the mobilisation and recruitment of bone marrow MSCs to the lesion after vascular injury was confirmed by a series of *in vivo* and *ex vitro* analysis.

Collectively, the data showed that bone marrow MSCs defined by the $NES^+Sca1^+CD29^+CD11b^-CD45^-$ protein profile was involved in neointima hyperplasia by contributing not only to the core SMC-like (αSMA^+) cells but also to

the endoluminal ($CD31^+$) cells in the lesion. Finally, the group demonstrated that bone marrow MSCs were mobilised and recruited to the lesional site by TGFβ factors (Wan et al., 2012).

9. The Chen *et al.* (2018) (Chen et al., 2018) study –

Model animal(s): Kit-CreER/Rosa26-RFP, and BM-eGFP mice
Animal age: Weeks
Tamoxifen (Tm) doses: 1 x 0.1-0.15 mg/g 4 times within a period of 2 weeks
Tm metabolism before injury: 2 weeks
Injury model: Wire-induced injury of the femoral artery (FA), and complete ligation of the left common carotid artery (CCL)
Duration of the injury: 2 and 4 weeks

The aim of this study was to investigate the role of c-kit^+ stem/progenitor cells previously reported to be resident of the aortic tunica adventitia by Hu *et al.* (2004) in sourcing the newly formed SMCs and ECs in the intima during vascular remodeling and neointima hyperplasia. Using Kit-CreER/Rosa26-RFP mice, there was little contribution of c-kit^+ cells to either SMCs or ECs within the newly formed neointima 2- and 4-weeks post-surgery as assessed by the lack of $RFP^+SM22\alpha^+$ and RFP^+CD31^+ co-staining expression, respectively. Interestingly, immunostaining analysis of FA cross-section at 2 weeks, showed that RFP^+ cells differentiated into myeloid cells including leukocytes (RFP^+CD45^+), monocytes/macrophage (RFP^+CD11b^+), and granulocytes ($RFP^+Gr\text{-}1^+$), which comprised ~10.5%, ~8.75%, and ~6.36% of the entire cell population, respectively (Hu et al., 2004; Chen et al., 2018).

As opposed to the sporadic RFP^+ cell population observed in the adventitial layer of healthy femoral and common carotid arteries, approx. 30% of the cells in bone marrow were RFP-labelled. Bone marrow transplantation studies revealed that BM-derived RFP^+ cells but not adventitial resident RFP^+ cells were the major source of the pro-inflammatory cell progeny found in the lesion (Chen et al., 2018).

Lastly, inhibition studies of c-kit^+ progenitor cells using the c-kit antagonist, ACK2

were conducted to analyze lesion progression *in vivo*. The data showed that the number of BM-derived and circulating RFP^+ cells decreased 10 days after FAI in the ACK2-treated animals as compared to the controls. Moreover, concomitant with a reduction in RFP^+ cells in the damaged artery, neointima hyperplasia declined by ~38% at week 4 (Chen et al., 2018).

Using two injury models, the study provided evidence *in vivo* that BM-derived RFP^+ cells rather than arterial resident RFP^+ cells were responsible for the inflammatory cell accumulation in the intima during vascular remodeling and neointima hyperplasia. ACK2 treatment demonstrated attenuation of neointima hyperplasia by reducing the number of RFP^+ and RFP^+-derived cells suggesting a potential target for treatment (Chen et al., 2018).

<u>Studies that support the putative role of resident endothelial cells and their progeny in contributing to intimal thickening following injury:</u>

10. The Cooley *et al.* (2014) (Cooley et al., 2014) study –

Model animal(s): Tie2-Cre/Rosa26-YFP ($Endotrack^{YFP}$), Tie2-Cre/Rosa26-LacZ ($Endotrack^{LacZ}$), Scl-$CreER^T$/Rosa26-YFP ($Ind.Endotrack^{YFP}$), SM22α-$CreER^{T2}$/Rosa26-YFP ($IndSM22\alpha Cre^T$) mice
Animal age: 4 weeks
Tamoxifen (Tm) doses: 2 rounds of 1x 1mg for 1 week with 1 week gap in-between
Tm metabolism before injury: Not specified
Injury model: Jugular vein was grafted to the femoral artery. Heparin was locally applied.
Duration of the injury: 7, 14, and 35 days

The aim of this study was to investigate the contribution of endothelial cells via the endothelial-to-mesenchymal transition (EndoMT) to neointima hyperplasia caused by venous grafting. Furthermore, the role of the SMAD-dependent transforming growth factor-β (TGF-β) signalling pathway was investigated in mediating EndoMT.

In naive (untouched) $Endotrack^{YFP}$ and $Ind.Endotrack^{YFP}$ jugular vein cross-sections,

approx. 98.5%, and 52% of the cells were marked by the endogenous YFP, respectively. These cells were associated with the endothelium as confirmed by co-expression of the endothelial marker CD31. 35 days after grafting, YFP^+ cells represented ~52%, and ~28% over the entire lesional cell population for $Endotrack^{YFP}$ and $Ind.Endotrack^{YFP}$ veins, respectively.

YFP^+ cells of $Endotrack^{YFP}$ grafts were analysed for different endothelial (CD31, VE-cadherin, and endoglin) and smooth muscle cell markers (αSMA SM22α, calponin, smoothelin, and SM-MHC) at different time points, 0, 7, 14, and 35 days. The data showed that the number of non-luminal neointimal YFP^+ cells expressing the endothelial markers decreased over time, and no co-staining was detected at day 35. In parallel, expression of αSMA (approx. 85%), and SM22α in neointimal YFP^+ cells increased with time. Intermediate SMC markers such as calponin and smoothelin were slightly increased, while protein levels of SM-MHC were not detectable 35 days after grafting. Interestingly, YFP^- cells within the venous neointima highly co-stained for all the SMC markers. SMC lineage tracing studies using the $Ind.SM22\alpha Cre^T$ mouse suggested that 16% of the lesional cells were originated from resident vSMCs 35 days after graft implantation.

Moreover, the TGFβ signalling pathway was investigated due to its known implications in vascular remodelling, and EndMT in development. Phosphorylated SMAD2/3 (pSMAD2/3) was observed in YFP^+ cells of $Endotrack^{YFP}$ grafts at days 3 and 7, however its activation gradually declined with no detectable levels at day 35. Contrariety, phosphorylated Smad1/5/8 (p-Smad1/5/8) in YFP^+ cells was initially observed at days 3 and remained activate throughout the entire experimental time length. Using a TGFβ neutralizing antibody (TGFβ NeuAb) and a IgG control to treat $Endotrack^{YFP}$ venous grafts *ex vivo* before implantation to recipient mice, demonstrated decreased levels of p-SMAD2/3 in YFP^+ cells at day 7, and reduced neointima hyperplasia 35 days post-surgery comparing to the IgG control samples.

The data suggested that endothelial cells contributed to the cellularization of the neointima caused by vein graft procedure via Endothelial-Mesenchymal Transition, which is in part mediated by the TGFβ signalling pathway (Cooley et al., 2014).

Animal Models of Atherosclerosis

Studies that support the putative role of medial differentiated SMCs and their progeny in contributing to intimal thickening in atherosclerotic mice fed on a western diet:

1. The Shankman *et al.* (2015) (Shankman et al., 2015) study –

Model animal: SM-MHC-Cre^{T2}/Rosa26-eYFP/ApoE$^{-/-}$, and SM-MHC-Cre^{T2}/Rosa26-eYFP/Klf4$^{\Delta/\Delta}$/ApoE$^{-/-}$ mice
Animal age: 6-8 weeks
Tamoxifen (Tm) doses: 1 x 1mg for 10 days
Tm metabolism before injury: 0 days
Injury model: Western diet (21% milk fat and 0.15% cholesterol)
Duration of the injury: 18 weeks

The aim of this study was to determine that mature SMCs or macrophages were the major source of lesional cells contributing to atherosclerotic plaque formation, and whether SMC phenotypic switching in the adult organism could be regulated by the Klf4 transcriptional factor (Shankman et al., 2015).

Cross-sections of brachiocephalic arteries (BCA) were analysed for synthetic SMCs 18 weeks after western diet. Results exhibited that approx. 80% of atherosclerotic cells were derived from mature SMCs as shown by their YFP$^+$α-actin$^-$ (co)expression. Co-staining studies revealed that phenotypically modulated SMCs (YFP$^+$) contributed to other cell types within the lesion such as macrophage-like cells (YFP$^+$α-actin$^-$ LGALS3$^+$), mesenchymal-like cells (YFP$^+$α-actin$^-$ Sca-1$^+$), and others. *In situ* hybridisation proximity ligation assay (ISH-PLA) was performed on human atherosclerotic coronary artery sections to detect the Myh11 H3K4me2 (PLA) epigenetic signature on CD68$^+$ cells. Results showed that 18% of CD68$^+$ cells were doubled positive (PLA$^+$CD68$^+$) meaning that this macrophage-like cell population were SMC-derived (Shankman et al., 2015).

Conditional klf4-deficiency SMC/ApoE$^{-/-}$ mice were generated to study the pluripotency role of Klf4 in regulating the phenotypic switch of mature SMCs within atherosclerotic lesions. Although, the mean percentage of YFP$^+$ cells was not affected

in the Klf4-knockdown mouse comparing to the Klf4-WT, the outcomes were more associated to reduction of the lesional area (about 50%), and increased plaque stability. The number of α-actin^{+} cells increased in the fibrous cap, albeit were not associated to a SMC origin (YFP^{-}). Interestingly, SMC-derived macrophage-like cells declined in numbers within the atheroma. I*n vitro* studies on cultured SMCs loaded with cholesterol showed Klf4-dependent SMCs transition to macrophage and mesenchymal phenotypes as well as increased phagocytosis (Shankman et al., 2015).

The data suggested that mature SMCs were the major cell progenitor contributing to the cellularisation of atherosclerotic plaques by transitioning to multiple cell phenotypes associated to macrophage, mesenchymal cells, and others. Compellingly, although the loss of Klf4 in SMCs did not affect their capability to originate other cell phenotypes, it limited their transition to macrophage-like cells within the lesion. Most notably, Klf4-deficient SMCs had an overall anti-atherosclerosis effect shown by reduction of the lesional area, and plaque stability (Shankman et al., 2015).

2. The Albarran-Juarez *et al.* (2016) (Albarrán-Juárez et al., 2016) study –

Model animal: SM-MHC-Cre^{T2}/ Rosa26$^{flox\text{-}mT\text{-}stop\text{-}flox\text{-}mG}$ ApoE$^{-/-}$ and LysM-Cre/Rosa26$^{flox\text{-}mT\text{-}stop\text{-}flox\text{-}mG}$ ApoE$^{-/-}$ mice
Animal age: 6-8 weeks
Tamoxifen (Tm) doses: 1 x 1mg for 5 days
Tm metabolism before injury: 5 days
Injury model: Western diet (21% butter fat and 1.5% cholesterol)
Duration of the injury: 5 days (basal analysis) and 16 weeks

The aim of this study was to identify the source of vascular smooth muscle cells and macrophages within atherosclerotic lesions. Using SM-MHC-Cre^{T2}/ Rosa26$^{flox\text{-}mT\text{-}stop\text{-}flox\text{-}mG}$ ApoE$^{-/-}$, it was observed that a large proportion of the SMCs within the medial layer underlying the atherosclerotic plaques were EGFP^{-} implying that these cells were not SMC-derived. In detail, 61% and 35% of these EGFP^{-} cells were positive for antibodies staining for SM-MHC and CD68, respectively. In order to examine if EGFP^{-} cells underlying the plaques were originated from myeloid cells, aortic cross-

section of LysM-Cre/Rosa26$^{flox\text{-}mT\text{-}stop\text{-}flox\text{-}mG}$ ApoE$^{-/-}$ mice were co-stained for the macrophage marker CD68. Results showed that neither SM-MHC^{+} nor CD68^{+} non-SMC-derived cells were derived from macrophages (CD69^{-}) or myeloid (EGFP^{-}) (Albarrán-Juárez et al., 2016).

On the other hand, it was interesting to note that more than 70% of EGFP^{+} cells within the core of the atheromatic lesion were αSMA^{-} whereas αSMA^{+} SMC-derived cells were primarily observed within the fibrous cap. Approx. 31% of αSMA^{+} lesional cells were found to be EGFP^{-} and therefore analysis using cross-sections from LysM-Cre/Rosa26$^{flox\text{-}mT\text{-}stop\text{-}flox\text{-}mG}$ ApoE$^{-/-}$ mice revealed that 17% of αSMA^{+} non-SMC-derived cells were originated from myeloid cells (EGFP^{+}) (Albarrán-Juárez et al., 2016).

Overall, the study suggested that that vascular smooth muscle cells within the atheroma had a great level of plasticity, becoming rapidly de-differentiated by downregulation of SM markers such as αSMA. De-differentiated SMCs were able to adapt a macrophage-like phenotype, and strongly contributed to matrix changes and inflammation in the plaque. Nevertheless, cells present within the atheromatic media originated from a cell population other than vascular SMCs or myeloid cells, and yet a population of non-SMC/myeloid-derived cells were found within the atheromatic lesion (Albarrán-Juárez et al., 2016).

<u>Studies that support the putative role of resident adventitial stem cells and their progeny in contributing to intimal thickening in atherosclerotic mice fed on a western diet:</u>

3. The Hu *et al.* (2004) (Hu et al., 2004) study –

Model animal: SM22-Rosa26-LacZ/ApoE$^{-/}$
Animal age: 3 months
Injury model: The vena cava was grafted to the right common carotid artery in an end-to-end anastomoses using cuffs
Duration of the injury: 2 and 4 weeks

The aim of this study was to investigate the presence of a stem/progenitor cell resident of the vessel adventitia contributing to vascular remodelling and atheroma formation as opposed to previously reported bone marrow cells (Sata et al., 2002; Hu et al., 2004). Using the Rosa26-LacZ/ApoE$^{-/-}$ mouse, a population of Sca-1^{+} cells (21%) was found in the adventitia but not in the media and intima of the aorta. These progenitor cells were isolated and characterised *in vitro* showing a unique protein profile (c-kit^{+}Lin^{-} Sca-1^{+}) distinctive from bone marrow progenitors. Differentiation studies on Sca-1^{+} cells isolated from the Rosa26-LacZ/ApoE$^{-/-}$ and SM22-Rosa26-LacZ mice towards the smooth muscle cell phenotype were carried out by PDGF-BB stimulation for 3 days. Results suggested that Sca-1^{+} cells have the potential to become mature SMCs by upregulation of the SMC cell markers, α-actin, SM22, calponin, and SM-MHC (Hu et al., 2004).

Aortic cross-section of chimeric mice with β-gal-labelled bone marrow showed the sporadic presence of bone marrow cells in the adventitia layer by X-gal staining, and CD45 co-expression. Despite of this, adventitial explants demonstrated that the cells emerging from the tissues were β-gal^{-} cells. Moreover, cultured adventitial cells using SM-LacZ chimeric mice with WT bone marrow showed β-gal^{+} expression 3 days after PDGF-BB treatment. The data suggested that a cell progenitor resided in the adventitial layer and was not originated from bone marrow cells. In order to evaluate the role of Sca-1 cell progenitors *in vivo*, cultured Sca-1^{+}β-gal^{+} cells from Rosa26-LacZ/ApoE$^{-/-}$ animals was transferred into irradiated ApoE$^{-/-}$ vena cava iso-grafted to the right carotid artery. 4 weeks after grafting, approx. 21% of the lesional cells were β-gal^{+}. In a paralleled experiment to study Sca-1^{+} cells transition to a SMC phenotype, isolated Sca-1^{+}β-gal^{-} cells from SM22-Rosa26-LacZ/ApoE$^{-/-}$ animals were applied onto irradiated ApoE$^{-/-}$ vena cava iso-grafted to the right carotid artery. Results showed that Sca-1^{+}β-gal^{-} cells acquired β-gal staining 2 and 4 weeks after grafting (Hu et al., 2004).

The data demonstrated that a Sca-1^{+} cell progenitor resident of the arterial adventitia did not derive from bone marrow cells and was involved in vascular remodelling and atherosclerosis by contributing to lesional SMCs (Hu et al., 2004).

Despite the great advances that transgenic animals have contributed to the molecular

mechanisms of neointima hyperplasia and vascular remodelling, the source of SMC stem/progenitor cells in the adult organism, it is still a conflicting area that remains under investigation.

1.6 Aim of this Study

The major aim of this study was to determine whether a S100β^{+}/Sca1^{+} resident vascular stem cell population within discrete embryological regions of athero-prone (neuroectoderm) versus athero-resistant (mesoderm) vessels contribute to intimal thickening following flow restriction -induced vascular injury.

In order to achieve this goal, the following specific aims were addressed:

- To determine the presence of a S100β^{+}/Sca-1^{+} vascular stem cell population within intimal lesions as a potential source of the SMC-like cells contributing to intimal thickening after vascular injury.
- To determine the origin of cells that accumulate within intimal lesions using lineage tracing analysis of an S100β^{+}/Sca-1^{+} vascular stem cell population following carotid ligation.
- To isolate and characterize S100β^{+}/Sca-1^{+} vascular stem cells isolated from discrete embryological regions of mouse aorta, namely aortic arch (athero-prone-neuroectoderm) vs thoracic aorta (athero-resistant- mesoderm).
- To examine differences in the embryological origin of the S100β^{+}/Sca-1^{+} vascular stem cells isolated from discrete embryological regions of athero-prone (neuroectoderm) vs athero-resistant (mesoderm) vessels of the murine aorta namely the aortic arch (athero-prone) and the thoracic aorta (athero-resistant).
- To determine whether S100β^{+}/Sca-1^{+} resident vascular stem cells isolated from discrete embryological regions of athero-prone (neuroectoderm) vs athero-resistant (mesoderm) vessels of the murine aorta undergo myogenic differentiation in response to various stimuli known to contribute to vascular lesion *in vivo,* including transforming growth factor-β1 (TGFβ1), Jagged1-activated Notch, Wnt4 and sonic hedgehog (Shh).

Chapter 2

Materials & Methods

2.1 Biological Materials

2.1.1 Commercial Cell Lines & Tissue-derived Cells

Table 2-1. Cells used during the course of study.

Cells	Cell Type	Morphology	Tissue of Origin	Description
mC3H/10T1/2, Clone 8 (ATCC® CRL-226™)	Embryonic Cells	Fibroblast	Sarcoma	C3H/10T1/2, Clone 8 derived mouse C3H embryo's sarcoma by Reznikoff, C., Brankow, D., and Heidelberger, C.
mNE-4C (ATCC® CRL-2925™)	Neuroectodermal Stem Cell	Neuroepithelial	Neural ectoderm or Neural plate	NE-4C cells derived from the cerebral vesicle of a 9-day old mouse embryo with knocked-out p53 gene.
MOVAS (ATCC® CRL-2797™)	Vascular Aortic Smooth Muscle Cells	Spindle-shaped	Aorta	MOVAS were isolated by collagenase-elastase digestion, and immortalised with retrovirus
Tissue Cells	**Cell Type**	**Morphology**	**Cell Origin**	**Description**
mAA-vSCs mTA-vSCs	Vascular Aortic Stem Cells	Neural-like	Neuroectodermal	mAA-vSCs and mTA-vSCs isolated from the vessel wall of murine aortic arch and thoracic aorta, respectively, using an altered enzymatic dispersion

2.1.2 Antibodies

Table 2-2. Antibodies and their corresponding dilutions used in immunocytochemistry.

Antibodies were diluted in antibody solution [2.5% BSA, 0.3M Glycine and 1% Tween in Dulbecco's Phosphate Buffered Saline (DPBS)].

Antibody/Product Name	Supplier/Product Number	Dilutions
Mouse anti-mouse/rat nestin [Rat-401]	Abcam (ab11306)	1/200
Rabbit anti-mouse Calponin [EP798Y]	Abcam (ab46794)	1/200
Goat anti-mouse/rat/human smooth muscle Myosin heavy chain	Santa Cruz (sc-79079)	1/200
Mouse anti-human/rat SOX10	R&D System (MAB2864)	1/100
Mouse anti-human SOX17	R&D System (MAB1924)	1/100
Rabbit Anti-S100β	Merck Millipore (ABN59)	1/100
Rabbit Anti-mouse/rat S100 beta [EP1576Y]	Abcam (ab52642)	1/100
Rabbit anti-mouse/rat Sca1	Millipore (AB4336)	1/100
Alexa Fluor® 488 Goat anti-mouse IgG	Invitrogen (A-11001)	1/1000
Alexa Fluor® 488 Goat anti-rabbit IgG	Invitrogen (A-11008)	1/1000
Alexa Fluor® 488 Donkey anti-goat IgG	Invitrogen (A-11055)	1/1000

Table 2-3. Antibodies and their corresponding dilutions used in immunohistochemistry.

Antibodies were diluted in blocking buffer (5% BSA, 0.3M Glycine, and 1% Tween in DPBS).

Antibody/Product Name	Supplier/Product Number	Dilutions
Rat anti-mouse Sca1 / Ly6A/E antibody [D7] (FITC) antibody	Abcam (ab25031)	1/200

Rabbit anti-mouse/rat alpha smooth muscle cell Actin antibody	Abcam (ab5694)	1/200
Chicken anti-GFP antibody	Abcam (ab13970)	1/1000
Rabbit Anti-RFP/tdT antibody	Abcam (ab62341)	1/1000

Table 2-4. Antibodies and their corresponding dilutions used in Chromatin Immunoprecipitation (ChIP).

Antibody/Product Name	Supplier/Product Number
Rabbit anti-mouse Tri-Methyl-Histone H3 (Lys27) [C36B11]	Cell Signalling Technology (9733S)
Rabbit anti-mouse Di-Methyl-Histone H3 (Lys4) [C64G9]	Cell Signalling Technology (9725S)
Rabbit anti-mouse Tet2	Abcam (ab94580)
Normal Rabbit IgG (ChIP graded)	Cell Signalling Technology (2729)

Table 2-5. Antibodies and their corresponding dilutions used in Flow Cytometry.

Antibody/Product Name	Supplier/Product Number	Dilutions
Rat anti-mouse Sca1 (Ly-6A/E) [E13-161.7]	STEMCELL Technology (60032)	1/100
Rat anti-mouse IgG2a, kappa Isotype [RTK2758]	STEMCELL Technology (60076)	1/100
Rabbit Anti-mouse/rat S100 beta [EP1576Y]	Abcam (ab52642)	1/100
Normal Rabbit IgG (F graded)	Cell Signalling Technology (2729)	1/100

2.1.3 Primers used in this study

Table 2-6. Customised primers used in this study from Integrity DNA Technology (IDT).

Customised primer		Sequences
Mm_Sm-mhc	Forward	5' - GCA GTG AGC TCT CAG TCA TC - 3’
	Reverse	5' - CAA TGC CTC CTC TGA CAA GT - 3'
Mm_Cnn1	Forward	5’ - GCT TGT CTG CTG AAG TAA AGA AC - 3'
	Reverse	5’ - TCC ATG AAG TTG TTC CCG ATG - 3'
Mm_Hey1	Forward	5'- GTA CCC AGT GCC TTT GAG AA -3'
	Reverse	5'- ACT CCG ATA GTC CAT AGC CA -3'
Mm_Teashit3	Forward	5' - GAG AAG GAA CTC AGC AAG GC - 3'
	Reverse	5' - CTC CAG GCT ATC AGA CAC GA - 3'
Mm_Gli1	Forward	5' - TTG GAT TGA ACA TGG CGT CT - 3'
	Reverse	5' - CCT TTC TTG AGG TTG GGA TGA - 3'
Mm_Hprt	Forward	5’ - GGC TAT AAG TTC TTT GCT GAC CTG C - 3'
	Reverse	5’ - GCT TGC AAC CTT AAC CAT TTT GGG - 3'
Mm_Gaphd	Forward	5’ - GCC TCC AAG GAG TAA GAA AC - 3'
	Reverse	5’ - GCC TCC AAG GAG TAA GAA AC - 3'
Mm_Sm-mhc (for ChIP PCR)	Forward	5’ - CCC TCC CTT TGC TAA ACA CA - 3'
	Reverse	5’ - CCA GAT CCT GGG TCC TTA CA - 3'

Table 2-7. Primers used in this study from QIAGEN.

Primer	Product Name	Product Code
Hprt	Mm_Hprt_1_SG QuantiTect Primer Assay	QT00166768
S100β	Mm_S100b_1_SG QuantiTect Primer Assay	QT00151536

Sox10	Mm_Sox10_1_SG QuantiTect Primer Assay	QT00295204
Nestin	Mm_Nes_1_SG QuantiTect Primer Assay	QT00316799
Gapdh	Mm_Gapdh_3_SG QuantiTect Primer Assay	QT01658692
Pax6	Mm_Pax6_1_SG QuantiTect Primer Assay	QT01052786
Pax1	Mm_Pax1_1_SG QuantiTect Primer Assay	QT01052779
Nkx2-5	Mm_Nkx2-5_1_SG QuantiTect Primer Assay	QT00124810
Kdr	Mm_Kdr_1_SG QuantiTect Primer Assay	QT00097020
Tbx6	Mm_Tbx6_1_SG QuantiTect Primer Assay	QT00098861
Collagen type III, alpha 1	Mm_Col3a1_1_SG QuantiTect Primer Assay	QT01055516
Jagged1	Mm_Jag1_1_SG QuantiTect Primer Assay	QT00115703
Bcl2l11	Mm_Bcl2l11_1_SG QuantiTect Primer Assay	QT00132979

2.1.4 Chemical and Biological agents used in this study

Table 2-8. Chemical and Biological Agents used in this study.

Supplier	Product and Catalogue No
Seralab	Chick Embryo Extract (CE-650-J)
R&D System	Recombinant Mouse TGF-beta 1 Protein, CF (7666-MB-005/CF), Recombinant Mouse FGF basic Protein (3139-FB-025), Mouse Sonic Hedgehog/Shh N-Terminus Antibody (MAB4641), Recombinant Rat PDGF-BB Protein (520-BB-050), Recombinant Rat Jagged 1 Fc Chimera Protein, CF (599-JG-100), Recombinant Human IgG1 Fc, CF (110-HG-100)
PeproTech	Recombinant Murine PDGF-BB (315-18), Recombinant Murine FGF-basic (450-33), Recombinant Murine Sonic Hedgehog (315-22)
BioLegend	Recombinant Mouse TGF-β1 (carrier-free) (763102)

MSC	SensiFast™ SYBR® No-ROX One-Step Kit (BIO-72005), SensiMix™ SYBR® No-ROX Kit (QT650-05)
Promega	ReliaPrep™ RNA Cell Miniprep System (Z6012)
Merck Millipore	Ultra-Pure filtered water delivered from Milli-Q® Advantage A10 or a Milli-Q® Integral
QIAGEN	RNase-Free DNase I (79254), Rotor-Gene SYBR® Green RT-PCR Kit (204174),
Thermo Scientific	RNase away spray (10666421), Thermo Scientific™ Nalgene™ Rapid-Flow™ Sterile Disposable Filter Units with PES Membrane (10411791)
Gibco	B-27® Supplement (50X) serum free (17504044), 2-Mercaptoethanol (50 mM)(31350010), CTS™ (Cell Therapy Systems) N-2 Supplement (A1370701), TrypLE™ Select Enzyme (1X) no phenol red (12563029), MEM α nucleosides GlutaMAX™ Supplement (32571036), Fungizone® Antimycotic (20mL) (15290018), DEPC treated water (750024), OPTI-MEM reduced serum medium (111058021)
Invitrogen	AlamarBlue® Cell Viability Reagent (DAL1100), PageRuler™ Plus Prestained Protein Ladder, 10 to 250 kDa (26619), CTS™ CELLstart™ Substrate (A1014201), TRIzol® RNA Isolation Reagents (15596026), UltraPure™ DEPC-Treated Water (750023)
Bio-Rad	Bio-Rad Protein Assay (500-0006)
StemCell Technology	ClonaCell™-TCS Medium (03814)
Sigma-Aldrich	DAPT (D5942), Water (W4502), Sodium bicarbonate solution (S8761), Sodium pyruvate solution (S8636), Minimum Essential Medium (56416C), 2-mercaptoethanol (M-7154), Collagenase (C6885), DMEM (D5796), DMSO (C6164), Elastase from porcine pancreastype III (E0127), Bovine Serum Albumin (A4503), Glycine (G8898), L-Glutamine Solution (G7513),

	Penicillin-Streptomycin (P4333), Poly-L-Lysine (P9155), Retinoic acid (100nM) (R2656), Soybean Trypsin inhibitor (10109886001, Roche), Triton X-100 (T8787), Trypan Blue (T8154), Trypsin (T4174), TWEEN® 20 (P1379), Minimum Essential Medium Eagle (M0644), Fluoromount™ Aqueous Mounting Medium (F4680), Trizma® base (T1503), Cyclopamine hydrate (C4116), Chloroform (650498 Riedel-de Haën), 2-Propanol (I9516), heat inactivated FBS (F9665), Sterile Dulbecco's Phosphate Buffered Saline (DPBS) without Calcium and Magnesium (D8537), Hank's Balanced Salt solution (H6648), Formaldehyde (F8775), Ethanol (E7023), Glutaraldehyde in H_20 (G5882), Fluoroshield™ with DAPI (F6057), Proteinase K from *Tritirachium album* (P2308)
ATCC	Fetal Bovine Serum, ES Cell Qualified (ATCC® SCRR-30-2020™),
MyBio	ChIP-IT Express® HT from Active Motif (53018)
Abcam	Chromatin Extraction Kit (ab223876)

2.2 RNA Manipulation

2.2.1 RNA Storage

RNA samples were stored in DEPC-Treated Water at -80°C. RNA was placed on ice outside the -80°C freezer. RNA samples received DNase I treatment before storage.

2.2.2 Total RNA Extraction from tissue and cultured cell samples

Total RNA extraction from tissue and cultured cell samples were processed using the ReliaPrep™ RNA Cell Miniprep System kit from Promega. The protocol provided by the kit was followed in detail for both sample types. Lysates from tissue were prepared differently when compared to cell samples due to the need to first homogenise the specimens. In order to do so, tissues were weighed and pulverised by snap-freezing in liquid nitrogen and crushed using a clean pestle and mortar. Cells were harvested, counted and washed in Hank's balanced salt solution (HBSS) twice to remove any

trace of growth medium. A cell pellet was obtained by centrifuging the cell suspension at 300 x g for 5 min at room temperature and lysis buffer (1:100 1-thioglycerol:BL buffer) was added to samples. The volume of lysis buffer was dependent on the number of cells and the weight of the tissue. The subsequent lysate was mixed by vortexing and/or pipetting. 100% Isopropanol was added to the samples according to the volume of lysis buffer and vortexed to homogenize the solution. Samples were left to rest on the bench for 2 min, and volumes were then transferred to pre-assembled filtered minicolumns. Samples were centrifugated at 12,000 – 14,000 x g for 30 sec at room temperature. The flow-throughs were discarded from the collection tubes and 500 µl of RNA wash buffer was added to the minicolumns. Samples were centrifugated at 12,000 – 14,000 x g for 30 sec at room temperature. The flow-throughs were discarded from the collection tubes, and 30 µl of DNase I solution was added to the minicolumns followed by 15 min incubation. 200 µl of column wash solution was added to each minicolumn and tubes were centrifuged at 12,000 – 14,000 x g for 15 sec at room temperature. Two more washes in RNA wash buffer were carried out before eluting the purified RNA. The filtered minicolumns were placed in nuclease-free tubes and nuclease-free water was added. The volume of nuclease-free water added to elute the RNA from the filter membrane depended on the cell/tissue input. Samples were centrifuged twice using the same flow-through at 12,000 – 14,000 x g for 1 min at room temperature. RNA concentration was determined using the NanoDrop® ND-1000 Spectrophotometer (Thermo Scientific). Samples were aliquoted in small volumes and stored at -80°C.

Products provided by ReliaPrep™ RNA Cell Miniprep System Kit (Z6012, Promega):

- ReliaPrep™ Minicolumns
- Collection Tubes
- Elution Tubes
- BL Buffer
- Column Wash Solution (CWS)
- DNase I
- MnCl2, 0.09M
- Yellow Core Buffer
- RNA Wash Solution (RWS)

- 1-Thioglycerol
- Nuclease-Free Water

2.2.3 RNA Measurements

The concentrations of isolated nucleic acid samples were determined spectrophotometrically using the NanoDrop® ND-1000 Spectrophotometer (Thermo Scientific). This technology is capable of reading RNA concentration of 1 µl samples with high accuracy and reproducibility. The optics of the apparatus consists of 2 fibre optic cables (the receiving and the source fibres), which are separated by a controlled gap of 1 mm and 0.2 mm paths. When 1 µl sample is loaded onto the end of the receiving fibre, the 2 fibres become bridged by the liquid and a xenon light lamp flashes light to the sample. The light passing through the sample is measured by the detector as *Intensity of Light*, which it is then converted to *Absorbance* by applying the -log of such intensity. Results are translated into a user friendly table and graphed by the manufacturer's software. The maximum concentration capacity of the instrument is approx. 3000 ng/µl (RNA) and 3700 ng/µl (dsDNA) and it can measure samples 50X more concentrated than a regular spectrophotometer without diluting them. In order to measure concentration of RNA or/and dsDNA, the software applies a modified version of the Beer-Lambert equation below:

$$\mathbf{c = (A * e) / b;}$$

Where, **c:** Concentration of RNA or dsDNA[ng/µl], **A:** Absorbance [AU], **e:** wavelength-dependent extinction coefficient [ng-cm/µl] for RNA: 40 ng-cm/µl and for dsDNA: 50ng-cm/µl. **b:** path length [cm] (In our instrument, b: 1cm).

Moreover, the absorbance of a sample is measured by the instrument at the optimal wavelength, which it is 260 nm in the case of RNA, but also dsDNA. To measure the absorbance of pure RNA or dsDNA, a blank sample must be used to subtract the intensity value of components but RNA or dsDNA. The blank is typically the solvent used to resuspend the RNA or dsDNA pellet in.

$$\mathbf{Absorbance = -log\ (Intensity_{sample} / Intensity_{blank})}$$

Therefore, pure RNA at 40 ng/µl in aqueous solution has an A_{260} of 1, while 40 ng/µl of pure dsDNA has an absorbance reading of 1 at this wavelength.

The instrument can also be used as a measure of dsDNA and RNA purity as a ratio of absorbance at 260 and 280 nm. A ratio of approx. 2.0, and of 1.8 is an indication of an acceptable purity for RNA and dsDNA, respectively. Lower values are usually due to protein and phenol contamination. A second measurement of purity is the A_{260}/A_{230} ratio, which indicates the presence of co-purified substance if lower than the acceptable A_{260}/A_{230}ratio value. For nucleic acids the acceptable A_{260}/A_{230} ratio varies between 1.8 and 2.2 (NanoDrop Technology, Inc., 2007).

2.3 Real Time Reverse-Transcriptase Polymerase Reaction Chain

Real Time RT-PCR was performed to study relative changes in gene expression under different treatment conditions. In order to carry out this analysis, a reference gene commonly known as housekeeping gene was selected to ensure that changes in the gene of interest were due to a treatment and not secondary to other changes within the cells owing to the environmental stimulus. Housekeeping genes are usually involved in metabolic activities, therefore, they are constitutively expressed as they seem fundamental to cell survival (Fairfax and Salimnia, 2010). According to the cell/tissue type one of the following two housekeeping genes were used to carry out real time RT-PCR in this Thesis:

Hypoxanthine Phosphoribosyltransferase (HPRT) – used as housekeeping gene in mouse vascular stem cells, mSMCs, mNE-4Cs and mC3H cells.

Glyceraldehyde-3-phosphate dehydrogenase (GAPDH) – used as housekeeping gene in mouse vascular aortic stem cells, mSMCs, mNE-4Cs, mC3H cells and mouse aortic tissue without tunica adventitia.

Regarding the choice of real time PCR chemistry to detect changes in gene expression, either Rotor-Gene SYBR Green RT-PCR (QIAGEN) or The SensiMix™ SYBR® No-ROX (BioLine) protocols were used to carry out *Real TimeOne-Step RT-PCR* using the Real Time Rotor-GeneRG-3000™ light cycler from Corbett Research. The

advantage of one-step PCR over the two-step RT-PCR protocol includes less manipulation of the sample as all reagents are added to a single tube, and the minus reverse transcriptase (-RT) sample is also ran per primer set in order to identify genomic DNA contamination present in our RNA samples.

The principle behind this method is that the fluorescence emitted by the SYBR Green Dye-cDNA complex in the reaction tube is directly proportional to the start amount of gene-specific mRNA in the desired cells. Hence, the higher the fluorescence the greater the expression of gene-specific mRNA in the cell type of interest. In order to amplify the desired mRNA targets, gene-specific primer sets (Forward and Reverse Primers) are needed. These primers are not included in the above kits, and therefore, they need to be bought separately (see section 2.1.3, Table 2-7 for primers used in this study).

2.3.1 Real Time One-Step RT-PCR by QIAGEN

The kit used in this study to perform QIAGEN Real Time One-Step RT-PCR was Rotor-Gene SYBR® Green RT-PCR Kit (QIAGEN, 204174). This kit includes all the necessary components (Table 2-9) except for the gene-specific primers and the RNA samples. The protocol used was obtained from the Rotor-Gene SYBR Green Handbook by QIAGEN. Table 2-10 for preparation of reaction tubes, and Table 2-11 for how to set up the cycling conditions of the Real Time Rotor-GeneRG-3000™ Lightcycler.

Table 2-9. Components supplied in the Rotor-Gene SYBR® Green RT-PCR Kit.

Components	Description
2x Rotor-Gene SYBR Green RT-PCR Master Mix	*HotStarTaq Plus DNA Polymerase (DNA poly)* - new version of the QIAGEN HotStarTaq DNA Polymerase, which has been modified to reduce the hot activation time. It is activated by an incubation step of 5 min at 95°C, avoiding any activity while sitting in the reaction tube, and during reverse transcription reaction
	Rotor-Gene SYBR Green RT-PCR Buffer - contains a novel additive known as Q-Bond®, that increases the affinity of the HotStarTaq

	Plus DNA Polymerase to single-stranded DNA oligonucleotides. Additionally, a unique balanced combination of KCl and $(NH_4)_2SO_4$ salts are present in the buffer as well as $MgCl_2$ in order to increase the ratio of specific to non-specific primer binding during annealing step. This buffer is designed to shorten cycle times (denaturation, annealing of primers and extension)
	dNTPmix - dATP, dCTP, dGTP, dTTP
Rotor-Gene RT Mix	An optimal blend of two reverse transcriptase enzymes capable of transcribing through secondary structures, and a wide range of RNA amounts present in the samples: • Omniscript® reverse Transcriptase - RNA amounts ≥ 50 ng; • Sensiscript® reverse Transcriptase - RNA amounts < 50 ng
Fluorescent Dye	*SYBR Green I* - the dye binds to double-stranded DNA during extension step. The dye has a maximum excitation wavelength of 494 nm, and its emission wavelength is optimally detected at 521 nm. These requirements are compatible with the optic system of the Real Time Rotor-GeneRG-3000TMlightcycler from Corbett Research used in this study.
RNase-Free Water	PCR-grade

Table 2-10. Preparation of a single Reaction Tubes.

Components	Volume	Final Concentration
2x Rotor-Gene SYBR Green RT-PCR Master Mix	12.5 µl	1X
Forward Primer*	2.5 µl	1 µM
Reverse Primer*	2.5 µl	1 µM
Rotor-Gene RT Mix	0.25 µl	
Template RNA (2ng/µl)**	5 µl	
RNase-Free Water or DEPC water	2.25 µl	
Total reaction volume	**25 µl**	

*For this study QuantiTect Primer Assays were used (see section 2.1.3, Table 2-7). QIAGEN primer sets were supplied in separate or single tubes at a concentration of 25 µM. **NanoDropped RNA samples were equally brought to the same concentration before use.

Table 2-11. Cycling Condition Setup.

Step	Time	Temperature	Cycles
Reverse Transcription	10 min	55°C	1 cycles
PCR Activation Step	5 min	95°C	1 cycles
Cycling Steps			35-40 cycles
Denaturation	5 sec	95°C	
Annealing and Extension	10 sec	60°C	

2.3.3 Real Time One-Step RT-PCR by BioLine

The kit used in this study to perform Real Time One-Step RT-PCR was SensiFAST™ SYBR® No-ROX One-Step Kit (BioLine, BIO-72001). This kit provided all the necessary components (Table 2-12) except for the gene-specific primers and the RNA samples.

The Protocol used was obtained from in the SensiFAST™ SYBR® No-ROX One-Step Kit (BioLine, BIO-72001). Table 2-13 for preparation of reaction tubes, and Table 2-14 for how to set up the cycling conditions of the Real Time Rotor-Gene RG-3000™ Lightcycler.

Table 2-12. Components supplied in the SensiFAST™ SYBR® No-ROX One-Step Kit.

Components	Description
2x SensiFAST™ SYBR® No-ROX One-Step mix	*HotStar DNA Polymerase (DNA poly)* - Modification of the enzyme was achieved by antibody, and thus a shorter activation time is needed comparing to chemically-modified DNA poly. It does not become activated till its PCR initiation step at 95°C, avoiding any activity during reverse transcription and amplification steps.
	SYBR Green I and *dNTP mix* (dATP, dCTP, dGTP, dTTP)
RiboSafeRNase Inhibitor	A cocktail of recombinant RNases (A,B and C). They inhibit any RNase present in the reaction mix, and thus preventing any RNA degradation. Do not inhibit DNA polymerase and Reverse Transcriptase activities.
Reverse transcriptase	
DEPC-Water	PCR-grade

Table 2-13. Preparation of a single Reaction Tubes.

Components	Volume	Final Concentration
2x SensiFAST™ SYBR® No-ROX One-Step mix	10 µl	1X
10 µM Forward Primer*	0.8 µl	400 nM
10 µM Reverse Primer*	0.8 µl	400 nM
Reverse Transcriptase	0.2 µl	
RiboSafe RNase Inhibitor	0.4 µl	
Template RNA (4ng/µl)**	4 µl	
RNase-Free Water or DEPC water	3.8 µl	
Total reaction volume	**20 µl**	

*For this study IDT Primer were used (see section 2.1.3, Table 2-6). IDT primer sets were supplied in separate tubes at a concentration of 50 µM. The volume used in preparation of the reaction tubes was previously optimized in our lab. The efficiency of the primers were tested by RT-PCR. **NanoDropped RNA samples were equally brought to the same concentration before use.

Table 2-14. Cycling Condition Setup.

Step	Time	Temperature	Cycles
Reverse Transcription	10 min	45°C	1 cycle
PCR Activation Step	2 min	95°C	1 cycle
Cycling Steps			35-40 cycles
Denaturation	5 sec	95°C	
Annealing	10 sec	60°C	
Extension	5 sec	72°C	

2.3.4 Relative expression ratio analysis by the REST© tool

In order to calculate relative changes in the expression of the target gene of interest an improvement of the $2^{-\Delta\Delta CT}$ method was used in this study. The Comparative C_t method ($\Delta\Delta C_t$) described by Livak and Schmittgen (2001) is one of the most used to calculate relative mRNA expressions of target genes between target and reference (control) samples. In this method, the difference in cycle number (C_t) values between target and reference genes in a control sample ($\Delta C_{tcontrol}$) is then subtracted from the difference of C_t values between the same target and reference genes in the target sample ($\Delta C_{ttarget}$), resulting in the $\Delta\Delta C_t$($\Delta C_{ttarget}$ - $\Delta C_{tcontrol}$). However, in order to compare these values with each other, an amplification efficiency of 100% is assumed across the different genes and samples. This assumption is practical but it does not reflect the real situation. Amplification efficiency varies due to the nature of the components present in the reaction tubes, for instance, presence of PCR inhibitor, RNA extraction (operator handling differences), different SYBR Green Mix, primers, probes, and enzymes. Therefore, PCR amplification efficiency needs to be determined to correct for this assumption (Bustin*et al*, 2009) (Pfaffl, 2000). In this study, a software tool known as the REST© (relative expression software tool) Tool, is used to calculate relative gene expression ratios within a sample group (different target samples against the control) including the PCR implication efficiency. This software utilised a mathematical model including the PCR amplification efficiency (E) developed by Pfaffl (Pfaffl *et al*, 2002)

Pfaffl, M.W. developed a mathematical model where the PCR amplification efficiency (E) was included in the calculation of relative gene expression ratios. This mathematical model applies *the 10-fold serial dilution curve* method to calculate gene-specific amplification efficiencies, which consists of generating a serial dilution curve for each gene of interest plus an appropriately selected reference gene. The A serial dilution curve is performed using a high quality sample keeping all the other components constant (Primers, SYBR mix, RT enzyme, and additives). Subsequently, for each gene of interest, the C_t values of each diluted sample is plotted in a curve, C_t versus $\log_{10}$ (diluted samples concentration). Finally, the amplification efficiency (E) for each gene is then calculated by *the 10-fold serial dilution method,* where the negative slope of the linear portion of the curve is used in the calculation (Bustin *et al*, 2009) (Pfaffl *et al*, 2002).

$$\mathbf{E_{target\ or\ reference} = 10^{-(1/slope)} - 1}$$

Where, **E:** gene-specific amplification efficiency, and **Slope**: the linear portion of a C_t versus $\log_{10}$ (diluted samples) curve.

In a PCR amplification efficiency 100% the E = 2, meaning that the $E_{target} = E_{ref} = 2$, and thus the slope of the linear portion of the curve is -3.33 (Pfaffl, 2000). The final formula developed by Pfaffl, M.W was able to calculate the gene expression ratio between two samples (Control versus Sample):

$$\mathbf{Ratio = (E_{target})^{\Delta C_{ttarget\ (control\ -\ sample)}} / (E_{reference})^{\Delta C_{treference\ (control\ -\ sample)}}}$$

Moreover, the same author (2002) once more contributed to the PCR analysis world by publishing the REST© tool which is still in use, and it is able to calculate gene relative gene expression ratios between sample groups using C_t values and including the PCR implication efficiency.

Real time PCR amplification efficiencies were not calculated by QIAGEN RT-PCR reactions, as the company guaranteed a PCR amplification efficiency of 2 for every primer. Therefore, when no PCR amplification efficiency was calculated REST© tool assumed an E = 2. Instead, a serial dilution curve was calculated by each IDT primers, and C_t values were inserted into the REST© tool, so the efficiencies could be calculated and included in the relative gene expression within a sample group.

2.4 Chromatin Immunoprecipitation (ChIP) followed by Polymerase Chain Reaction (PCR)

Chromatin Immunoprecipitation followed by Polymerase Chain Reaction (ChIP-PCR) was carried out using three different kits for chromatin extraction, immunoprecipitation and PCR. The protocols provided by the kits were followed and any variation from the protocol was noted as outline below.

2.4.1 Chromatin Extraction

Chromatin extraction was carried out using the Chromatin Extraction Kit from Abcam. The provided protocol was divided into the different steps as follow:

Staring material preparation – Adherent cells were detached and pelleted down as described in Section 2.8.2 of this Chapter. Cell pellets were washed once in cold Hank's balanced salt solution (HBSS) and resuspended in cold HBSS (1 ml per 2-5 x 10^6 cells). Each 1 ml was transferred into a RNA/DNA-free 1.5 ml tube and centrifuged at 200 x g and 4°C for 5 min. Supernatant was discarded and pellets were ready for fixation. Aortas were harvested from the animals and cleaned as described in Section 2.8.1 (Figure 2.1) of this Chapter. Tissues were weighed and cut into small pieces. Approx. 20 mg of tissues was transferred into RNA/DNA-free 1.5 ml tubes.

Cross-linking – Cell pellets (2-5 x 10^6 cells/pellet) or tissue pieces (20 mg) were resuspended in 1 ml of 1% formaldehyde for 10 min at room temperature with mixing on a seesaw platform. Samples were centrifuged at 1000 x g and 4°C for 3 min. Supernatant was discarded and samples resuspended in 1 ml of 1X Formaldehyde Quenching Solution in phosphate basic solution (PBS). Samples were incubated for 5 min at room temperature with mixing on a seesaw platform followed by a centrifugation step at 1000 x g and 4°C for 3 min. Supernatant was discarded and samples were washed twice in 1 ml of cold PBS. Centrifugations were carried out at 1000 x g and 4°C for 3 min. After the last centrifugation, PBS was removed and samples were stored at -80°C for next step.

Chromatin extraction – frozen samples were always used for this step to minimize any variability between the usage of fresh or frozen material. The volume of lysis buffer (LB) was prepared according to the number of cells and quantity of tissue samples to be processed. 1 ml of LB: 5 µl of 200X protease inhibitor cocktail (PIC) + 995 µl of extraction and lysis buffer (ELB).

Fixed cell samples (2-5 x 10^6 cells) or tissue pieces (20 mg) were resuspended in 500 µl or 300 µl of LB, respectively and incubated at room temperature for 30 min with mixing on a rotator wheel. Tissue pieces were homogenized using a Dounce tissue homogenizer prior to incubation. Cell samples were then centrifuged at 1000 x g and

room temperature for 3 min and supernatant discarded. The pellets were resuspended in 300 µl of fresh LB. Samples were ready for sonication.

Sonication step – shearing chromatin was performed at 0°C (ice water). The power of the sonicator and time was adjusted according to each sample type:

- Cell samples containing 3 x 10^6 cells –
    - mAA-vSCs and mTA-vSCs: 5 cycles (10 sec ON – 10 sec OFF) at 15 mAmp
    - mESCs: 7 cycles (10 sec ON – 10 sec OFF) at 15 mAmp
- 20 mg of tissue samples – 3 min in a water-bath sonicator followed by 9 cycles (10 sec ON – 10 sec OFF) at 40 mAmp

After DNA fragmentation, 10 µl of IP Buffer Concentrate was added to every 100 µl of sonicated chromatin. DNA concentration was measured using the NanoDrop® ND-1000 Spectrophotometer (Thermo Scientific). Samples were stored at -80°C for next step.

Products provided by Chromatin Extraction Kit (ab223876, Abcam):

- Extraction and Lysis Buffer
- Formaldehyde Quenching Solution (10X)
- IP Buffer Concentrate (11X)
- Protease Inhibitor Cocktail

2.4.2 Chromatin Immunoprecipitation (ChIP)

Chromatin Immunoprecipitation (ChIP) assay was performed using the ChIP-IT Express® HT kit from Active Motif. The protocol provided by the kit was followed in detail and any deviation was specified as outlined below:

Chromatin lysates were thawed and their the concentration of the chromatin was adjusted to the limiting sample in order to work with the same concentration in all samples

10 µl of each sample was transferred to a clean 0.2 ml tube and labelled as the *Input*

Table 2-15. ChIP reaction components.

Reagent	Volumes (µl)
Protein G Magnetic Beads	25
ChIP Buffer 1	20
Sheared Chromatin	100
Protease Inhibitor Cocktail (PIC)	2
RNA/DNA-free H_2O	50
Antibody	3
Total Volume	200

DNA. Input samples are stored at -20°C and use later in the Reverse Cross-linking step.

The immunoprecipitation reaction was set up according to the company recommendation in 0.2 ml tubes (Table 2-15). For 100 µl of sheared chromatin, 3 µl of antibody was added to the reaction (Table 2-4). Incubation was carried out on end-to-end rotator overnight at 4°C. On the following day, samples were briefly spun down, and placed on a magnetic stand to pellet the beads. The supernatant was carefully removed avoiding disturbance to the pellet.

It is important to note that beads must be kept hydrated at all times to ensure the beads do not become damaged or degraded. The beads were washed three times with 200 µl of ChIP Buffer 1 were performed followed by two more washes with 200 µl of ChIP Buffer 2. After the final wash the supernatant was discarded and resuspended in 50 µl of Elution Buffer AM2. Samples were allowed to incubate on an end-to-end rotator for 15 min. Samples were briefly spun down proceeded by reverse cross-linking step.

50 µl of the Reverse Cross-Linking Buffer was added to each 50 µl of eluted chromatin sample (IP samples) and mixed by pipetting. Tubes were placed on a magnetic stand to pellet the beads. The supernatants containing the eluted chromatin were carefully transferred to clean 0.2 ml tubes. The 10 µl Input samples saved at the beginning of

the protocol were thawed and the following reagents were added 88 µl of ChIP buffer 2 and 2 µl of 5M NaCl. All the samples (IP and Input) were incubated at 65°C for 2.5 hours. Samples were briefly spun down and allowed to reach room temperature before the addition of 2 µl of Proteinase K. Samples were mixed and incubated at 37°C for 1 hour. Samples were briefly spun down and returned to room temperature before the addition of 2µL of Proteinase K Stop Solution. DNA concentration was measured using the NanoDrop® ND-1000 Spectrophotometer (Thermo Scientific), and stored at -20°C.

Products provided by Express® HT kit (53018, Active Motif):

- 5M NaCl
- Proteinase K (0.5 µg/µl)
- Proteinase K Stop Solution
- Protease Inhibitor Cocktail (PIC)
- ChIP Buffer 1
- ChIP Buffer 2
- Elution Buffer AM2
- Reverse Cross-linking Buffer
- LSV Protein G Magnetic Beads

2.4.3 Real Time Polymerase Chain Reaction (PCR)

Real Time Polymerase Chain reaction (PCR) was performed using the SensiMix™ SYBR® No-ROX Kit from BioLine (QT650-05). The gene-specific primers for this PCR was adopted from Gomez *et al.* (Table 2-6) (Gomez et al., 2013). Optimization of the PCR cycling conditions was carried out for the specific pair of primers.

Table 2-16. Preparation of a single Reaction Tubes.

Components	Volume	Final Concentration
2x SensiMix™ SYBR® No-ROX	12.5 µl	1X
25 µM Forward Primer	0.2 µl	200 nM
25 µM Reverse Primer	0.2 µl	200 nM
Template (IP or Input)	12.1 µl	
Total reaction volume	**25 µl**	

Table 2-17. Cycling Condition Setup.

Step	Time	Temperature	Cycles
Polymerase Activation	10 min	95°C	1 cycle
Cycling Steps			40 cycles
Denaturation	15 sec	95°C	
Annealing	15 sec	52°C	
Extension	45 sec	72°C	

2.5 Immunocytochemistry

Unless otherwise specified, cells were seeded at a density of 1000 cells/well for immunocytochemistry in order to allow for clear visualisation of the cells. Cells were seeded onto 6-well plates containing sterile coverslips. Coverslips were sterilized in 70% ethanol for 30 min and washed up to 5 times in sterile water to remove any trace of alcohol. Before the seeding steps, the 6-well plates containing the coverslips were placed under UV light for 30 min to ensure sterile conditions. Fluorochrome-conjugated antibody control samples were prepared to optimise the imagining parameters thus excluding false positive readouts due to secondary antibody non-

specific binding. Hence, one control sample was prepared per type used during the experiment (Goat, mouse and rabbit).

The protocol was divided in different steps as follow:

Fixation and Permeabilization – 3 to 4 days after seeding, cells were washed with HBSS to remove all trace of growth medium followed by the either fixation or fixation/permeabilization step. For extracellular staining, fixation was carried out using a 3.7-4% Formaldehyde solution for 15 min at room temperature. For intracellular staining, cells were also permeabilised with a 3.7-4% Formaldehyde/0.1% Triton X-100 solution and incubated for 15 min at room temperature. Cells were washed 3 times in DPBS.

Blocking – Samples were blocked for non-specific binding sites using blocking buffer for 1 hr at room temperature with gentle agitation. The blocking solution consisted of 5% BSA, 0.3M Glycine and 1% Tween-20 in DPBS solution. Cells were washed 3 times in DPBS.

Immunolabelling – Antibodies were diluted at a desired concentration in antibody solution, which consisted of 2.5% BSA, 0.3M Glycine and 1% Tween-20 in DPBS (Section 2.1.2, Table 2-2). The primary antibody (1° Ab) dilution was added to the coverslips. Cells were then allowed to incubate overnight at 4°C. From now on, all steps were carried out in darkened conditions to protect samples from the light. On the proceeding day, washing steps were carried out followed by incubation of the corresponding fluorochrome-conjugated antibody known as the secondary antibody (2° Ab) for 1-2 hour at room temperature with gentle agitation. Cells were washed 3 times in DPBS. Lastly, cells were incubated in a DAPI dilution (1:1000 in 1 % Tween-20 DPBS) for 15 min at room temperature in order to stain the nuclei. For preparation of the 2° Ab controls, cells were subjected to the entire immunolabelling protocol except for the primary antibody incubation step. Instead, antibody solution was used to replace the primary antibody dilution.

Mounting – Coverslips were mounted onto microscope slides for fluorescent microscopy analysis. 40 µl of a water-based mounting medium was added on to each glass slide. The coverslips were carefully placed (tissue-face down) onto the mounting

medium-containing slide avoiding the formation of bubbles. The samples were cured overnight at 4°C protected in the dark to allow the mounting media to solidify.

Analysis – All images were taken and compiled using Olympus BX51 Fluorescence Microscope and Cell^F Multi-fluorescence and Imaging Software. 5 images were taken per sample at 20X for counting analysis and 60X for visualisation purposes. The fraction of DAPI stained cells that were positive for a given marker were counted and calculated using the image-analysis software (Schneider, Rasband and Eliceiri, 2012), and Microsoft Office Excel 2011, respectively (Section 2.10).

Cell Number Analysis

Cell Number analysis of immunolabelled cell samples was calculated based on the number of cells per high power field on control versus treated samples. All images taken and compiled using Olympus BX51 Fluorescence Microscope and Cell^F Multi-fluorescence and Imaging Software were used to calculate cell count of the corresponding immunocytochemistry experiment.

Briefly, DAPI stained cells (blue dots) were counted per region using ImageJ, an image-analysis software (Schneider, Rasband and Eliceiri, 2012) and entered in an excel file (Microsoft Office Excel 2011). Each cell number was then calculated per regions of view, in order to provide the average cell number per μm^2 using the known area per region of view. The average cell number per μm^2 of the samples were compared to each other in order to determine the cell count.

2.6 Flow Cytometry

Flow Cytometry is a method used in biotechnology and other industries to count and sort cells. FACS (Fluorescent Activated Cell Sorting) is a type of flow cytometry whereby cell samples flow through the cytometer in a single cell fluid suspension. Cell samples are treated with fluorescent particles in preparation for this method of analysis. Particles which can be used include Annexin V and Alexa Fluor 488/647 for example. The cytometer contains a laser which analyses the particles as they pass by. This laser measures the forward scatter and side scatter of the cells analysing the size

of the cell and granularity of the cell respectively. The laser measures these parameters based on fluorescence of each individual cell as it passes a certain point. The fluorescent particles are excited at a certain wavelength and then emit at another wavelength depending on each individual particle. For example Alexa Fluor 488 excites at 499 nm and emits and 519 nm. There are filters in front of the detectors in the cytometer that restrict the light that reaches the detector to a specific range of wavelengths.

Flow cytometry was used to screen isolated murine vascular stem cells for different markers representing stem cell phenotypes. Samples were prepared in a series of steps as follow:

Fixation/Permeabilization – the kit used was BD Bioscience Cytofix/Cytoperm™ and the protocol provided was used. Briefly, 500,000 cells were used per sample (equal cell number). After the cells were pelleted they were fixed (if appropriate for the antigen) using BD cytoperm solution for 20 minutes at 4°C.

Immunolabelling – Following two brief wash steps the appropriate primary antibody was added at a final concentration of 1µg per sample. The cells were incubated at 4°C for 30 minutes. The cells were washed again and incubated with appropriate secondary antibody (Alexa Fluor 647) for 30 minutes at 4°C.

Data acquisition – Cells were analysed using BD FACSAria™ using the corresponding detector according to the secondary fluorescent probe used *(Figure 2.9)*.

Data analysis – was performed using FlowJo and De Novo software FCS Express 4 Flow Cytometry.

2.7 Scanning Electron Microscopy (S.E.M.)

In order to analyse the morphology and structure of the external laminar in aortas after the removal of the adventitia layer scanning electron microscopy (S.E.M) was performed. Samples were prepared in a series of steps as follow:

Tissue extraction – Aortas were gently harvested from mice avoiding damage of the tissue. Following extraction the adventitia layer was removed by incubating the tissues in a collagenase solution (detailed protocol in Section 2.8.1).

Fixation – Tissues were placed in sterile 60 mm petri dishes and fixed in 2% Glutaraldehyde in 1X DPBS at room temperature overnight. Samples were then washed in 10 ml of distilled water 3 times for 5 min.

Dehydration – Samples were exposed to a series of ethanol dilutions for 15 min each (35%, 50%, 70%, 95%, and 2 x 100%) at room temperature.

Finally, samples were immersed in hexamethyldisilazane (HDMS) for 1 min, and placed in a clean 60mm petri dish to allow the HDMS to evaporate in the fume hood overnight. Samples were mounted on SEM stubs and stored in a desiccator till imaged.

Imaging – Mounted aortas were coated using the Edwards Pirani 501 Scancoat Gold Sputtering Coater (Edwards Laboratories, USA). All images were taken and compiled using EVO LS15 Scanning Electron Microscope (Zeiss, Germany).

2.8 Cell Culture Methods

All cell culturing techniques were aseptically carried out using a Biosciences Air 2000 Mac laminar flow cabinet. Cells were maintained in a HERA water jacketed cell culture incubator at 37°C and 5% CO_2. Cells were visualised using a Nikon Eclipse TS100 phase-contrast microscope.

2.8.1 Cell lines

Mouse Embryonic Cells (mC3Hs)

Mouse embryonic cells (mC3H/10T1/2 [Clone 8] or mC3Hs, ATCC® CRL-226™) were maintained in medium as recommended by ATCC®. The basal salt medium Minimum Essential Medium Eagle (EMEM) was pre-made. 1 L of EMEM was made up of 9.61 g of EMEM Powder which contained an initial 2 mM L-Glutamine, 20 ml of Sodium Bicarbonate, 10 ml of Sodium Pyruvate, and 970 ml of Ultra-Pure Water

(Merck Millipore). The basal medium at pH 7 was filtered using a sterile 1L filter unit under sterile conditions. The complete medium was composed of EMEM supplemented with heat-inactivated embryonic qualified FBS to a final concentration of 10%, 1% penicillin/streptomycin, and extra 2mM L-Glutamine (final concentration of L-Glutamine = 4 mM).

Mouse Neuroectodermal Stem Cells (mNE-4Cs)

Mouse neuroectodermal stem cells (mNE-4Cs, ATCC® CRL-2925™) were maintained in medium as recommended by ATCC®. The basal salt medium Minimum Essential Medium Eagle (EMEM) was pre-made. 1 L of EMEM was made up of 9.61 g of EMEM Powder which contained an initial 2 mM L-Glutamine, 20 ml of Sodium Bicarbonate, 10 ml of Sodium Pyruvate, and 970 mL of Ultra-Pure Water (Merck Millipore). The basal medium at pH 7 was filtered using a sterile 1L filter unit under sterile conditions. The complete medium was composed of EMEM supplemented with 10% embryonic qualified FBS, 1% penicillin/streptomycin, and extra 2mM L-Glutamine (final concentration of L-Glutamine = 4 mM). Before NE-4C cells were seeded onto plates/dishes, the surface of the culture vessel was pre-coated with 15µg/ml Poly-L-Lysine. The plates were pre-coated and left to dry for 5 minutes. Afterwards wells were washed briefly with sterile water and left to dry for at least 2 hours before the cells were seeded.

Mouse Aortic Smooth Muscle Cells (mSMCs)

Mouse aortic smooth muscle cells (mSMCs or MOVAS, ATCC® CRL-2797™) were cultured in DMEM supplemented with 10% Sigma-Aldrich FBS, and 1% of Penicillin and Streptomycin.

Isolation and culture of rat/mouse vascular stem cells (vSCs) by explants and enzymatic dispersion

The protocols for isolation of vascular stem cells (vSCs) from the tunica media of the aortic arch and thoracic aorta were performed as previously described, with some minor modifications (Tang et al., 2012). Isolated aortic vSCs were cultured in DMEM medium for the maintenance of neuroectodermal-derived cells (NE-MM) as described by Tang and colleagues (Tang et al., 2012). Please see Table 2-18.

Table 2-18. Neuroectodermal Maintenance Medium (NE-MM).

Stock Solutions/Powders	Final Concentrations or Percentage	Volumes in 50 ml
Dulbecco's Modified Eagle's Medium (DMEM)		46.48 ml
Chick Embryo Extract (CEE)	2%	1 ml
FBS embryonic qualified (ATCC®)	1%	500 µl
B-27® Supplement, serum free (50X)	1X	1 ml
CTS™ (Cell Therapy Systems) N-2 Supplement (100X)	1X	500 µl
Recombinant Mouse FGF basic Protein (100 µg/mL)	0.02 µg/mL	10 µl
Penicillin-Streptomycin (10000 units-10 mg / ml)	1%	500 µl
1:20 diluted 2-Mercaptoethanol*	50 nM	5 µl
1:10 diluted Retinoic Acid**	100 nM	5 µl

* 1 in 20 dilution of 2-Mercaptoethanol (50 mM)

DMEM	95 µl
2-Mercaptoethanol (50 mM)	5 µl

** 1 in10 dilution of Retinoic Acid (100 mM)

DMEM	95 µl
Retinoic Acid (100 mM)	5 µl

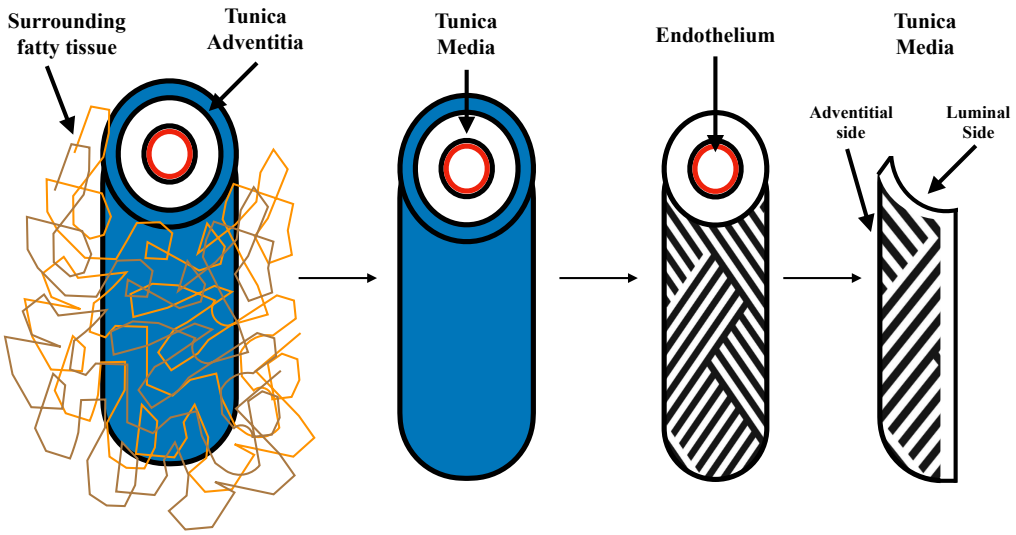

Figure 2.1. Obtaining the tunica media by following a series of steps.

Removal of the adventitial layer

The use of animals in this study was carried out according to the EU legislation (Directive 2010/63/EU) for the protection of animals used in research. Sprague Dawley rats or C3Hs/HuJ mice were anesthetised with an overdose of pentobarbital sodium (0.1mg/g) and death by exsanguination was confirmed by an authorised professional. The ribcage was cut open at the front of the animal to expose internal organs. These were removed so the back of the ribcage was in view. The aorta was carefully excised using a tweezers and a scissors. The tweezers were carefully run along the side of the aorta to loosen it from the backbone. The aorta tissue was harvested from the heart collecting it along the spine to the abdominal area. The tissue was placed in cold Hank's solution and adipose tissue removed using two tweezers. A 2 ml syringe and a needle were used to wash the lumen area of the vessel and remove any trace of blood. The adventitia was then enzymatically removed by incubation of the tissue in 0.7 mg/ml Collagenase solution (Table 2-19) for approx. 10-20 min at 37°C. Once the adventitia became lose, it was carefully removed using forceps under a dissecting microscope as an intact layer (Figure 2.1).

Table 2-19. Collagenase Solution.

2 ml of Collagenase was prepared to loosen the adventitia of 2 rat aortas or 4 mouse aortas. The final solution was filtered using a 0.2 µm syringe end filter under sterile conditions

Stock Solutions/Powders	Final Concentrations	Volumes/Weights in 2ml
MEM α nucleosides GlutaMAX™ Supplement		2 ml
Soybean Trypsin inhibitor (50 mg/ml)	0.4 mg/ml	16 µl
Bovine Serum Albumin	1 mg/ml	2 mg
Collagenase type 1A (125 Units/mg)	0.7mg/ml	1.4 mg

Tissue explant method

The aorta was divided into aortic arch (AA) and thoracic aorta (TA). Each tissue section was cut into 1 mm-sized pieces with a sterile blade and placed in wells of a 6-well plate pre-coated with CELLstart™ Dilution (Invitrogen) (Table 2-20).

Approximately 5-6 pieces of tissues were added per well (Figure 2.2). The small pieces were left to air-dry for approx. 30 min before the neuroectodermal maintenance medium (NE-MM) (Table 2-18) was carefully added to each well. About 500 µl of MM was firstly added to each well trying to avoid tissue detachment and placed in the incubator at 37°C, 5% CO_2. Four hours after incubation, each well was filled with another 500 µl of MM and left to incubate for 7 days in a humidified incubator at 37°C, 5% CO_2.

After 7 days, explants were checked for cells avoiding disruption of the tissues. Once cells began to explant out of the tissue, the tissue pieces were removed. Each well was washed briefly with sterile Hank's and warm fresh NE-MM was added. Cells were fed every 2-3 days and passaged every 3-4 days depending on how confluent they were (usually around 70%). The cells had a very low adherence rate after being detached

with 0.5X TripLE, therefore the first feeding was performed 48 hr after passage.

Enzymatic Dispersion

The aorta was cut into small tissue pieces with a sterile blade and placed in a 0.7 mg/ml Collagenase Type 1A and 0.25 mg/ml Elastase type III (Collagenase/Elastase) solution (Table 2-21) at 37°C. The tissues were vortexed every 15 min for approx. 2 ½ hours or until the tissue was completely digested. Dispersed cells were centrifuged and washed twice in warm NE-MM and seeded on wells of a CELLstart™ pre-coated 6-well plate with 2mL of NE-MM (Figure 2.3). Cells were incubated at 37°C, 5% CO_2 for 1 week with minimal disturbance.

Table 2-20. CellStart Dilution for a 6-well plate.

Stock Solutions	Final Concentrations	Volumes 5 ml (750 µl/well)
Dulbecco's Phosphate Buffered Saline with calcium and magnesium	1X	4410 µl
CTS™ CELLstart™ Substrate	1:50	90 µl

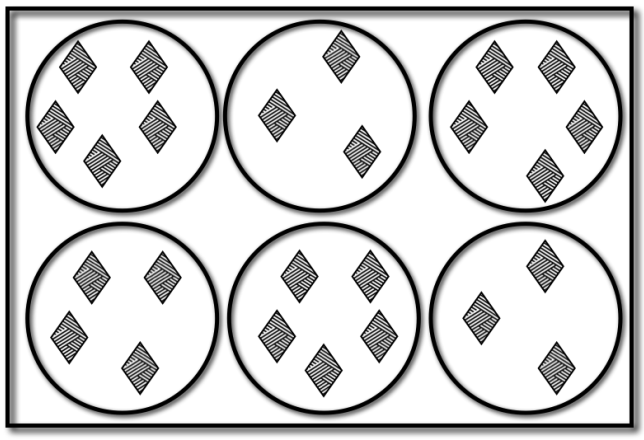

Figure 2.2. Tissue pieces on a CellStart pre-coated 6-well plate.

The striped pattern indicates adventitial side facing upwards, while the luminal side of the layer is in contact with the well surface.

Table 2-21. Collagenase/Elastase Solution.

2 ml of Collagenase/Elastase was prepared to digest the aortic tissues of 2 rats or 4 mice. The final solution was filtered using a 0.2 µm syringe end filter under sterile conditions.

Stock Solutions/Powders	Final Concentrations	Volumes/Weights in 2ml
MEM α nucleosides GlutaMAX™ Supplement		2 ml
Soybean Trypsin inhibitor (50 mg/ml)	0.4 mg/ml	16 µl
Bovine Serum Albumin	1 mg/ml	2 mg
Collagenase type 1A (125 Units/mg)	0.7 mg/ml	1.4 mg
Elastase Type III	0.25 mg/ml	0.5 mg

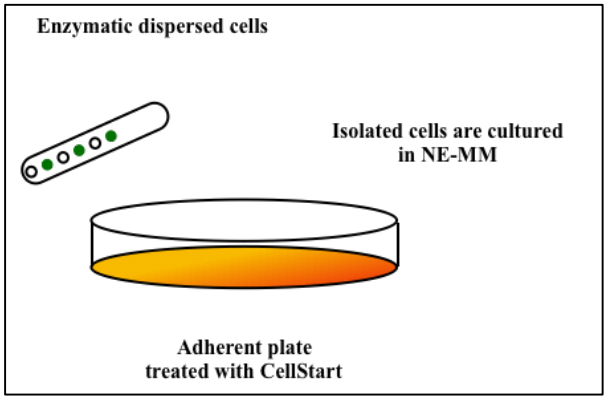

Figure 2.3. Schematic illustration of the seeding step on a CellStart pre-coated 6-well plate after cell enzymatic dissociation.

Modified Enzymatic Dispersion

The aorta was cut into small tissue pieces as above and digested with Elastase type III (Appendix) at 37°C. Dispersed cells were centrifuged and washed in warm NE-MM twice and seeded (1st seeding) in a well of a non-adherent 6-well plate with 3 ml of

NE-MM. At 48 hrs, suspension cells were transferred (2nd seeding) in to a well of a CELLstart™ pre-coated 6-well plate with an extra 2 ml of fresh NE-MM. 4 mL of NE-MM was added to the remaining cells in the non-adherent surface well (Figure 2.4). Cells were incubated at 37°C, 5% CO_2 for 1 week with minimal disturbance.

All steps were carried out under aseptic conditions in a laminal flow hood. Surgical tools and a surgical platform were sterilised by autoclave. Solutions and culture vessels were all of cell-culture grade. See Table 2-8. Cells were passaged using Hank's balanced salt solution (HBSS) and 0.5 x TrypLE select. There was no need for CELLstart™ precoated vessels after P1, hence cells were maintained in adherent cell-culture graded plates/flasks. Cells were healthy and proliferative when seeded at a cell density of 1 x 10^4 cells per cm^2 or higher. Feeding was carried out every 3-4 days.

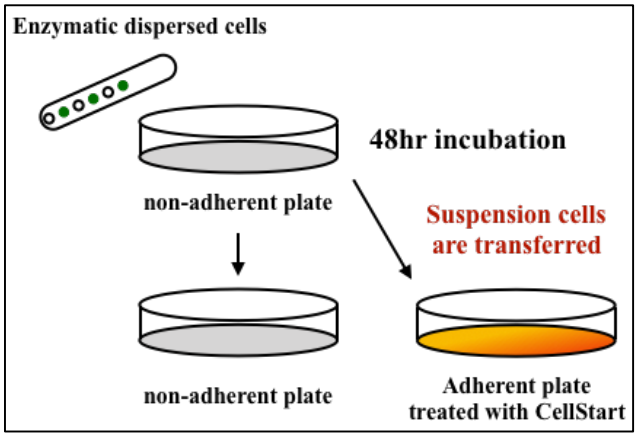

Figure 2.4. Schematic illustration of the seeding steps of the modified enzymatic dispersion protocol.

2.8.2 Cell Subculture and Expansion

All cell lines used were adherent therefore detachment from their surface was required for cell subculture. Cells were sub-cultured using either 1X Trypsin (for mouse aortic smooth muscle cells, mSMCs) or 0.5X TrypLE select (for stem cells). Once they reached approx. 70-80% confluency, the cell growth medium was removed from the flasks/culture dishes and washed twice in Hank's balanced salt solution (HBSS).

Detachment solution was added to the culture vessel just to cover the surface area and cells were incubated at 37°C for 2-5 minutes (depending on cell type). Warm fresh maintenance medium was added to neutralise the detaching agent. Cells were pelleted by centrifugation at 300 *x g* for 5 minutes at room temperature. Cells were re-suspended in the appropriate volume of maintenance medium and counted using a haemocytometer (Section 2.8.3). Cells were split at a cell density of 1-4 x 10^4 cells per cm^2 according to the specifications of individual cell lines.

Important:

- Rat/mouse isolated vascular stem cells (vSCs) were sub-cultured in non-CELLstart™ precoated vessels after P1. Only regular adherent cell-culture grade plates/flasks were used to maintain the cells in culture. vSCs had a very low adherence rate after being detached with 0.5X TripLE, therefore the first feeding was always performed after 48 hr from subculture.
- Mouse neuroectodermal cells (mNE-4Cs) required pre-coated culture vessels with 15 µg/ml of Poly-L-Lysine (as outlined above).

2.8.3 Cell Counting

A 20 µl cell suspension was mixed gently at 1:1 with 20µl of Trypan Blue. Following this a 20 µl aliquot was added to the haemocytometer through the sample introduction point (Figure 2.5). Trypan blue will stain non-viable cells due to their leaky membrane. Viable healthy cells do not take up the dye and will appear bright under the microscope in comparison to the dead cells. Four chambers or primary squares were counted excluding any cells, which touched the line indicating the left side of the square and the topside of the square.

The cell number was calculated using the formula:

(Cell Number)/4 * (Dilution Factor) * 1x10^4(area under cover slip mm) = Number of viable cells/ml

Dilution factor = 2 as the cell suspension was diluted by an half with Trypan Blue

2.8.4 Cryogenic Preservation and Recovery of Cells

Cells were stored in cryovials suspended in Liquid Nitrogen at -196°C for long-term storage. Briefly, cells were detached and pelleted down as outlined in Section 2.8.2; however, re-suspension was carried out using a cryofreezing medium in place of the maintenance medium. Cryofreezing medium was composed of regular growth medium (cell-type dependent) supplemented with 15% (v/v) FBS and 10% (v/v) DMSO. 1 ml of cryofreezing medium was used to resuspend 1 x 10^6 cells and transferred to a sterile cryogenic vial. Samples were placed in a Mr Frosty™ cryofreezing container, and stored in a -80°C freezer overnight, where the cells slowly freeze down at the rate of –1°C/minute. The cryovials were then transferred to the liquid nitrogen on the next day.

When required for use, vials containing the desired frozen cells were rapidly thawed in a water bath at 37°C followed by one wash with 5 ml of cold fresh maintenance medium (cell-type dependent) and a second wash in warm fresh maintenance medium. Cells were pelleted down by centrifugation at 300 *x g* for 5 min at room temperature. Once washed, cells were resuspended in a final 5 ml of warm fresh maintenance medium and transferred to a T25 flask where they were incubated at 37°C, 5% CO_2 and 95% humidity.

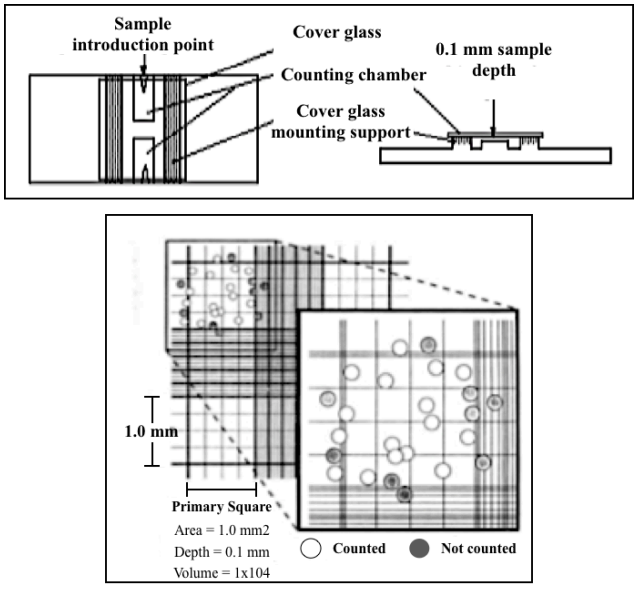

Figure 2.5. Schematic of a haemocytometer cell counting (Provost & Wallert Research, 2015).

2.9 Animal Work

Animal work was conducted by Liu W under the supervision of Prof Eileen Redmond in the University of Rochester Medical Centre, United States. Protocols were approved and carried out according to their institutional guidelines.

2.9.1 Animal Models

Tamoxifen-inducible S100β-EGFP/cre-ER^{T2}/ROSA26R^{tdTomato} animal model

The R26-loxP-tdT reporter [*Gt(ROSA)26Sor$^{tm9(CAG\text{-}tdTomato)Hze}$*/J, Stock numbers 007905] and S100β-GCE [Tg(S100β-EGFP/cre-ER^{T2})22Amc, Stock number 014160] transgenic mice were bought from The Jackson Laboratory.

The R26-loxP-tdT reporter strain consists of the red fluorescent marker gene, tdTomato upstream of a loxP-flanked stop sequence that prevents the transcription of the maker gene. This cassette (loxP-tdT) is driven by the constitutive CAG promoter and inserted into the Rosa26 loci within the animal genome (Figure 2.6, a). When bred with mice that express Cre recombinase enzyme under the control of a tissue-specific promoter, the offspring will express the red fluorescent protein owing to the deletion of the loxP-flanked stop sequence by the Cre recombinase enzyme, and thus indelibly marking the tissue-specific cells and their progeny (Figure 2.6, c). Therefore, the Cre-loxP technology has widely been used to carry out *in vivo* tracing studies (The Jackson Laboratory, 2018).

The S100β-GCE transgenic strain expresses the enhanced green fluorescent protein (EGFP) and Cre recombinase under the control of the S100 calcium binding protein β (S100β) promoter. Positive expression of the EGFP protein is only detected in cells with active S100β promoter, thus marking those cells currently expressing the S100β protein. Similarly, Cre recombinase transgene is transcribed and translated in cells with an active S100β promoter. Because Cre recombinase protein is fused to the tamoxifen-inducible oestrogen receptor (ER^{T2}), Cre-ER^{T2} protein is localised in the cellular cytoplasm and it does not translocate to the nucleus unless tamoxifen binds to the oestrogen receptor (Figure 2.6, b). If tamoxifen is present within the cell, it binds to the Cre-ER^{T2} protein resulting in its translocation to the nucleus, where Cre

mediated recombination takes place at loxP sites (Figure 2.7). Tamoxifen-inducible animals allow researchers to control gene activity in a special temporal manner. Therefore, the S100β-GCE transgenic strain does not only facilitate the study of constitute S100β^{+} cells by the detection of the EGFP protein but also it has the potential to trace the S100β cell progeny when bred with a reporter animal (The Jackson Laboratory, 2018).

Consequently, the Rosa26-loxP-tdTomato mice and the S100β-GCE transgenic strain were bred to obtain offspring with the follow final genotype, S100β-EGFP/cre-ER^{T2}/Rosa26t^{dTomato} (Figure 2.6, c). The animals facilitate the study of S100β-expressing cells by detecting the expression of the EGFP protein as well as indelibly marking the S100β cell progeny in a special and temporal manner owing to the administration of tamoxifen (Figure 2.7) (Metzger and Chambon, 2001) (Barker N. et al., 2007) (Kretzschmar K., and Watt F.M., 2012). Therefore, these animals allowed us to calculate the ratio of cells expressing the S100β protein within the lesions 21 days after injury (Section 2.9.1). Moreover, these animals provided clear evidence of the S100β cell progeny within the affected vessels versus controls 21-day post-surgery in order to investigate the source of lesional cells.

Although, new CreER constructs were developed to reduce sensitivity of the CreER protein to endogenous oestrogen, and thus to prevent unspecific Cre-loxP recombination from occurring, leakiness is still a common downfall of inducible CreER/loxP transgenic animals (Kretzschmar K., and Watt F.M., 2012). As a result, two groups of transgenic animals were created in order to control for non-specific Cre recombination:

i. Tamoxifen treated animals (experimental samples) – mice within this group were given an intra-peritoneal (I.P.) injection of Tamoxifen (1 mg/kg of body weight) per day for 5 consecutive days in order to induce Cre-loxP recombination and thus mark the S100β^{+} cells with the red fluorescent protein (dtTomato) (Figure 2.7).
ii. Vehicle treated animals (drug control samples) – mice within this group were given an intra-peritoneal (I.P.) injection of Corn oil per day for 5 consecutive

days. Corn oil was utilised as the vehicle to dissolve tamoxifen and so was used as a tamoxifen control to assess tdTomato protein by leakiness.

Following tamoxifen/corn oil administration, animals were left to recover for 2 or 4 weeks to allow for the elimination of tamoxifen (Reinert et al., 2012). Animals were monitored multiple times every day for signs of side effects during recovery. Tamoxifen/corn oil treated animals were then subjected to complete carotid artery ligation for 21 days post tamoxifen withdrawal. The protocol is detailed in section 2.9.1.

Herein, the tamoxifen-inducible Cre animals were used to delete the loxP-flanked stop sequence within the reporter cassette at the Rosa26 loci in order to activate transcription of the fluorescent protein (tdTomato) and thus indelibly mark the S100β-positive cell progeny. Because the Cre recombinase enzyme activity varies according to different factors such as type of tissue, animal age and tamoxifen dose, recombination efficiency must be calculated to determine the actual number of cells that would express the fluorescent protein if efficiency were of 100%. To do so, nerve bundles, known to positively express the glial cell marker S100β, were harvested from animals that were subjected to tamoxifen administration followed by 21 day-injury. The fractions of $EGFP^+$ or tdT^+ cells over DAPI were counted and calculated using ImageJ™, an image-analysis software (Schneider, Rasband and Eliceiri, 2012), and Microsoft Office Excel 2011, respectively (Section 2.10). Because EGFP protein is expressed in S100β-activated promoter, the ratio of $EGFP^+$ cells over DAPI was considered to be 100% efficiency and tdT^+ over DAPI fraction was compared to the EGFP sample.

The results showed that the efficiency of Cre-recombination, in the Cre-LoxP system used for the tracing *in vivo* studies, was $98.18 \pm 2.95\%$ compared to the control sample (100%). The fraction of $S100\beta^+$ cells over the total number of cells (DAPI) was 0.998 ± 0.006 and 0.980 ± 0.0289 calculated from the EGFP and tdT images, respectively (Figure 2.8, A and B). The Mann-Whitney test (non-parametric t-test) showed no significant difference between the two samples, therefore it was concluded that recombination occurred at its maximum efficiency (100%).

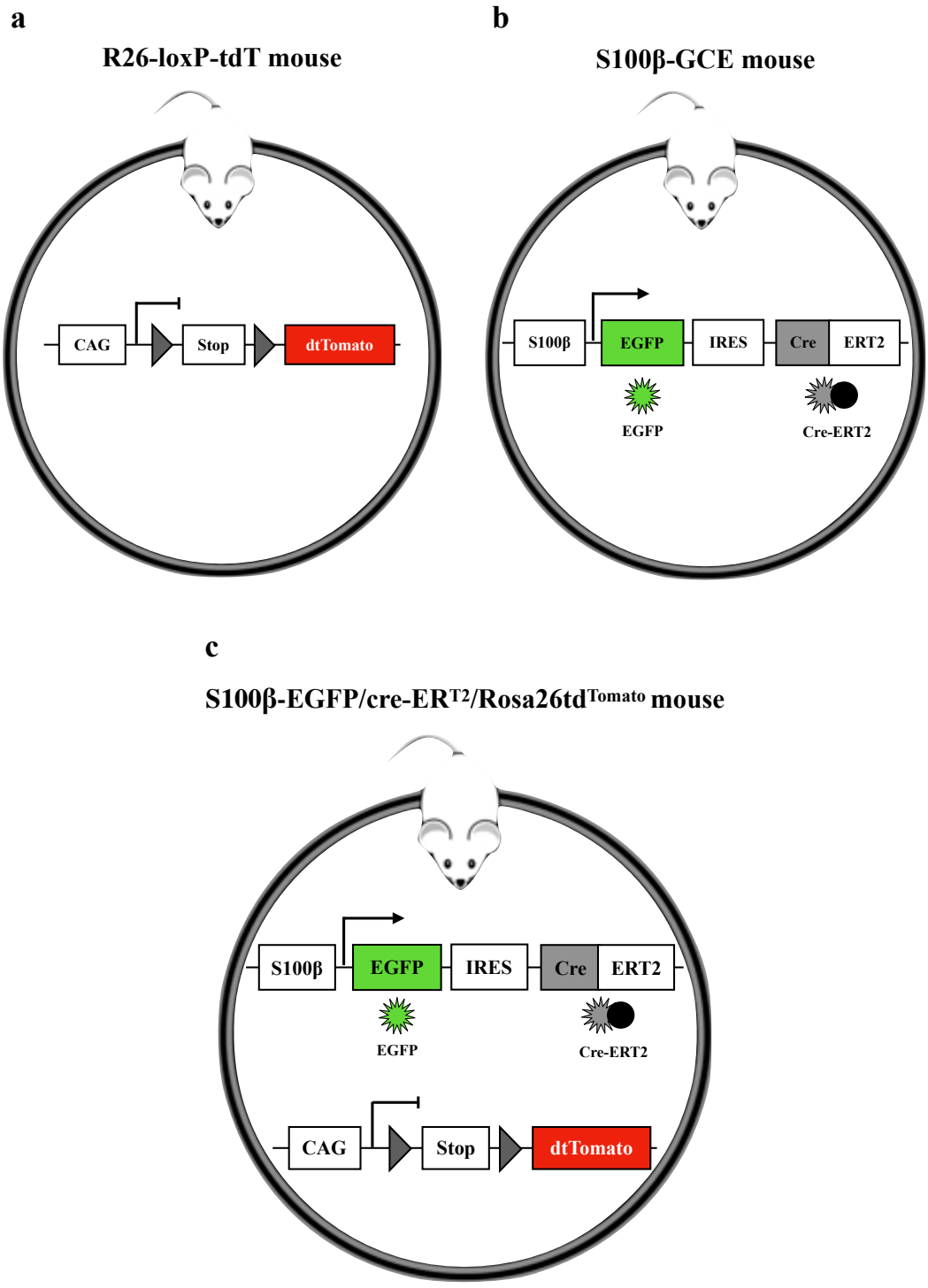

Figure 2.6. Genetics of the S100β-EGFP/cre-ER^{T2}/Rosa26td^{Tomato} animals used in the *in vivo* tracing study.

Genetics of (**a**) the reporter mice (R26-loxP-tdT) and (**b**) the S100β-CreER^{T2} strain. Both animal strains were bred together in order to generate offspring with the desired genetics **(c)** for the *in vivo* tracing study.

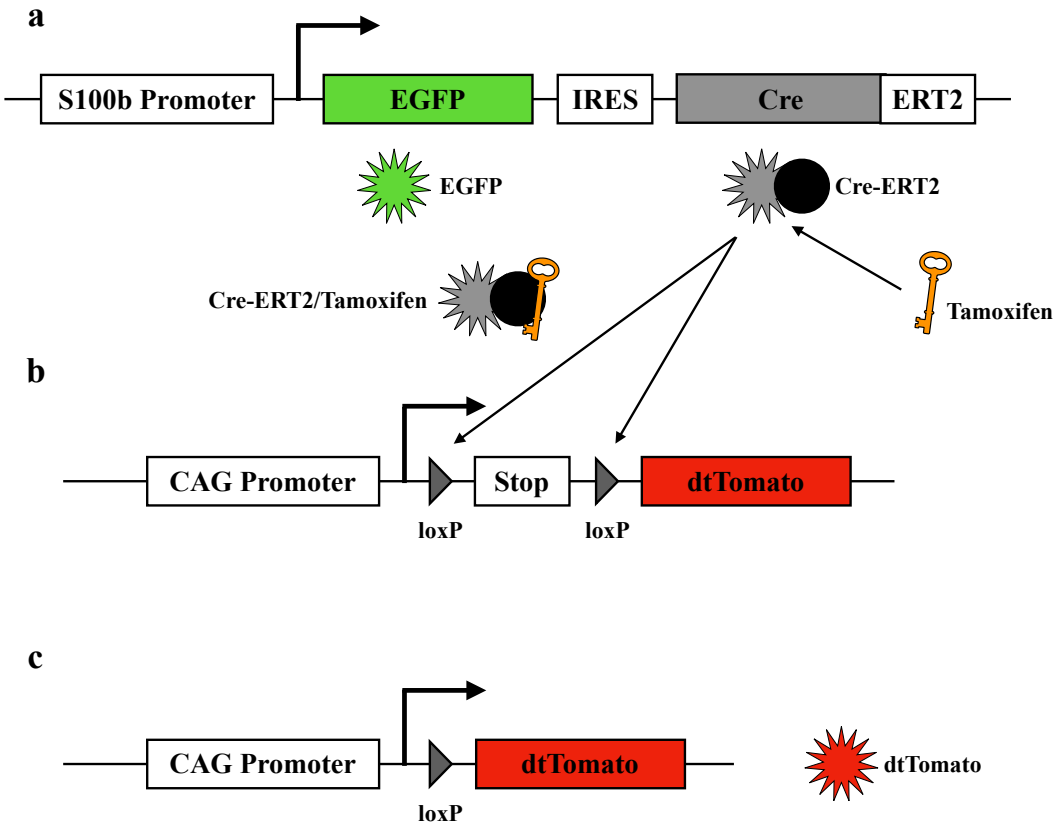

Figure 2.7. Tamoxifen-inducible Cre-loxP technology.

S100β^{+} cells conjunctively express **a)** the EGFP protein and the Cre-ER^{T2} protein, confirming transcription and translation of the Cre-ER^{T2} protein under the activity of the S100β promoter. **b,c)** Animals treated with tamoxifen, an anti-oestrogen drug induce Cre recombination at the loxP sites, allowing for the expression of the red fluorescent protein, tdTomato. Cre-loxP recombination is not reversible even when cells do not express the S100β protein, and thus cells are indelibly marked by the expression of the tdTomato protein regardless of their fate. Cre-loxP recombination does not occur in corn oil treated animals, which is confirmed by the absence of tdTomato protein expression (control vehicle samples).

(A)

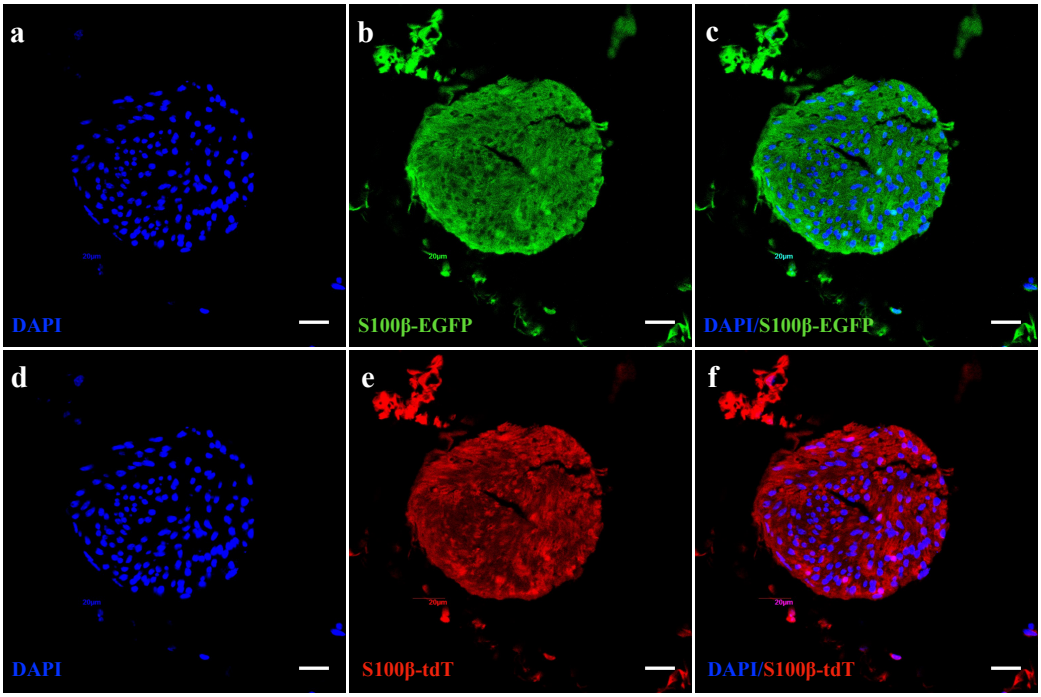

Figure 2.8. Cre-recombination Efficiency.

Animals were treated with Tamoxifen for 5 consecutive days followed by 2-week recovery before injury as described in this Section. 21 days post-surgery, the sinus nerves were harvested and prepared for imaging.

(A) Representative images of **(a, d)** DAPI nuclear staining, **(b)** S100β-EGFP expression, **(e)** S100β-tdTomato (S100β-tdT) expression and **(e, f)** merged images. Scale bars, 20µm.

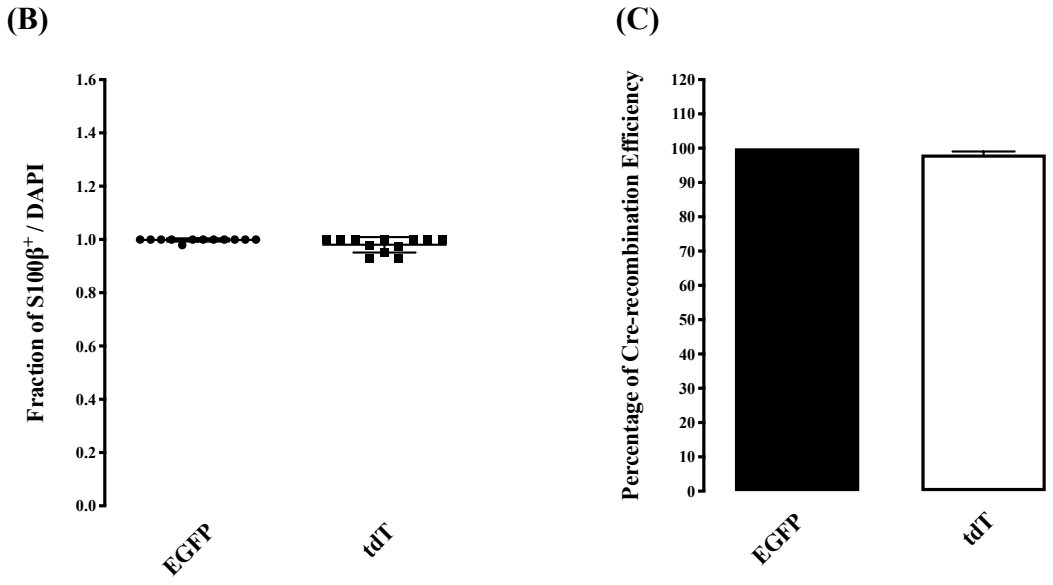

Figure 2.8. Cre-recombination Efficiency.

Animals were treated with Tamoxifen for 5 consecutive days followed by 2-week recovery before injury as described in this Section. 21 days post-surgery, the vagus nerves were harvested and prepared for imaging.

(B) Using immune-fluorescent images of the sinus nerves as shown in **A**, the average fractions of S100β-EGFP$^+$ and S100β-tdT$^+$ cells over the total number of cells (DAPI) were calculated and compared. Data are presented as average ± S.D. (n = 2). Mann-Whitney test with significance value of $P \leq 0.05$.

(C) The data compared the efficiency percentage of the cre-recombination in the tdT nerves versus the EGFP (control, 100%). The average ratio of S100β-EGFP$^+$ / DAPI and S100β-tdT$^+$ / DAPI were normalised against the S100β-EGFP$^+$ / DAPI ratio as the EGFP sample was the control. The rations were then multiplied by 100% to calculate the percentage of Cre recombination efficiency based on the tdT$^+$ expression. Data are average ± S.D. (n = 2). Mann-Whitney test with significance value of $P \leq 0.05$.

Sca-1-EGFP animal model

Tg(Ly6a-EGFP)G5Dzk/J transgenic mice commercially obtained from The Jackson Laboratory (Stock number 012643) express the enhance green fluorescent protein (eGFP) under the control of the murine lymphocyte antigen 6 complex (ly6a)

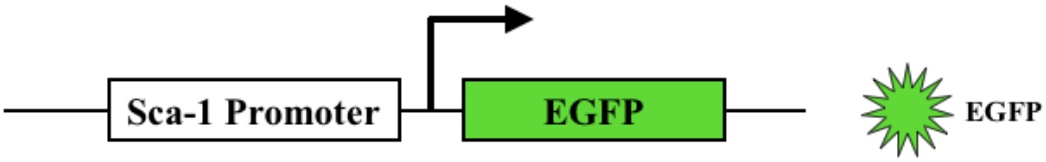

Figure 2.9. Representation of the Sca-1-EGFP transgene. Expression of the EGFP protein is driven by the Sca-1 promoter when active.

promoter also known as the Sca-1 promoter (Figure 2.8). The Sca-1-EGFP mice were utilised to visualise constitutive Sca-1-EGFP^{+} cells in healthy versus diseased vessels. Animals were subjected to partial carotid artery ligation (Section 2.9.1) and interrogated for Sca1-EGFP expression after 14 days (Section 2.9.3, Method 1).

2.9.2 Injury Models

Complete or Partial Carotid Artery Ligation – Background and Protocol

Aseptic techniques and conditions were strictly adhered to throughout the surgical procedure in order to preserve the animals' welfare and to enhance their recovery, minimizing post-operative traumas and infections potentially affecting the experimental results. All surgical instruments, cue tips, gauze and ligation silk were previously sterilised (autoclave 121°C for 15 minutes). The surgical station was covered with sterile drapes and all the surgical surfaces and instruments sprayed with 70% ethyl alcohol. A heating pad was placed under the sterilized surgical stage and allowed to heat up prior to continue with procedure. The animal was quickly anesthetized under inhaled isoflurane/oxygen anaesthesia (4 % / 2 L/min) in an enclosed chamber. After induction of anaesthesia, the animal was positioned on the prepared clean surgical stage, and surgical plane of anaesthesia was maintained under 1.7 - 3 % isoflurane 1 L/min oxygen for the duration of the protocol. Subsequently, the mouse was injected with an analgesic (0.075 mg/kg buprenorphine) via intraperitoneal administration (IP) and an ophthalmic solution was applied for ocular protection prior to securement to the surgical stage in the supine position using surgical tape. The mouse was then covered in sterile drape excluding the zone of surgery, face, neck and a foot. Hair was removed from the surgery site (neck) using a hair removal cream followed by sanitation using Betadine solution and alcohol with sterile gauzes.

The surgical plane of anaesthesia was assessed by checking toe pinch reflex immediately prior to surgery and every 5 minutes thereafter. A midline cervical incision of 1-2 cm in length was made 2 cm from the rodent's submental (Figure 2.9). The salivary glands were then opened to either side, and the trachea and muscles exposed (Figure 2.10). With the aid of dissecting microscope and fine forceps, the muscles were carefully loosened away and drew back with sterile retractors. The left common carotid artery was then identified in a triangular space known as the carotid space (Figure 2.10), which boundaries are between the superior belly of omohyoid muscle, the posterior belly of digastric muscle, and the sternocleidomastoid muscle.

The common carotid arteries are contained in a sheath known as the carotid sheath, where the jugular vein and the vague nerve are also enclosed (Figure 2.8). Consequently, the carotid sheath was meticulously opened to prevent any traumas to the vein and nerve. The separation was made along the left common carotid artery to the bifurcation where it branches into an external and an internal carotid artery, leaving the zone cleaned to be ligated (Figure 2.10). For complete carotid artery ligation, the artery was tied off at the carotid artery bifurcation using a 6-0 silk suture. For partial carotid ligation, the external and internal arteries were separately tied off using a 6-0 silk suture. The external artery was ligated above the occipital vessel thus creating a reduced blood-flow injury model.

Following ligation, all disturbed tissue was readjusted back into place and the neck incision (2 layers, muscle and skin) was closed with a non-continuous suture using 6-0 coated vicryl. Once completed, iodine was applied to the site to sanitise the area. The mouse was then given an IP injection of 500 μL saline 0.9 % NaCl and buprenorphine every 6 - 12 hours as necessary. The mouse was then placed in a clean cage under a heating lamp and observed every 1-2 hr post-surgery until recovered enough to return to the housing facility.

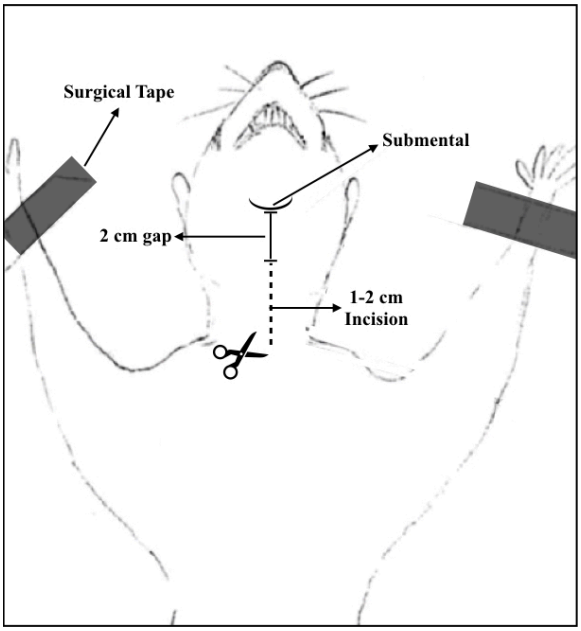

Figure 2.10. Supine position and Surgical incision.

The head and neck are accessible. An incision of 1-2 cm is made ending 2 cm below the mouse's submental.

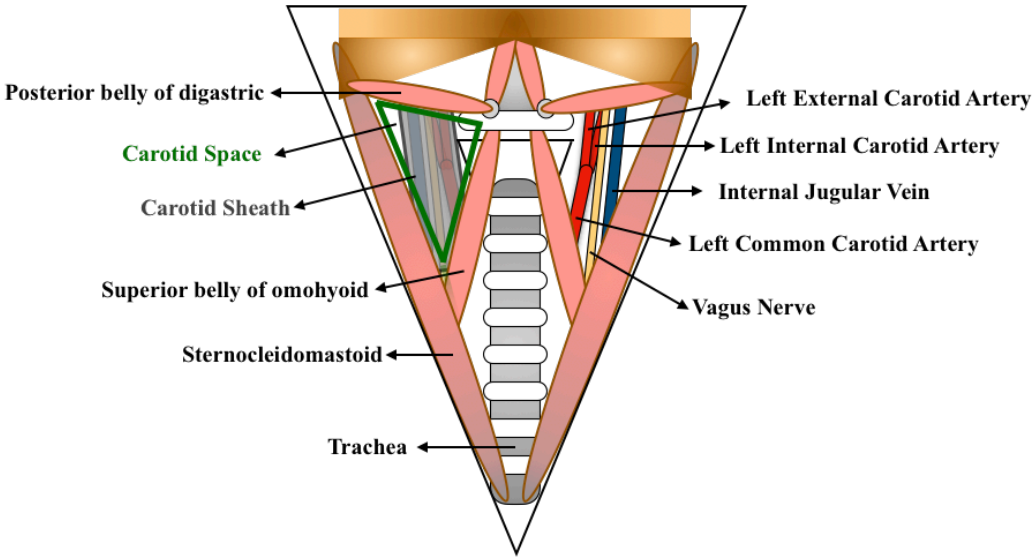

Figure 2.11. Schematic representation of the Neck and Carotid Triangle.

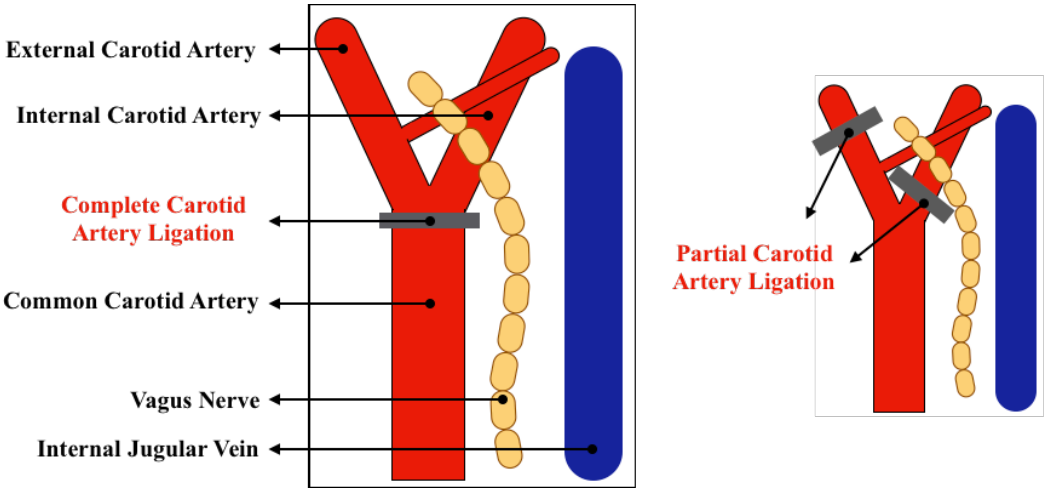

Figure 2.12. Schematic representation of Complete and Partial Carotid Artery Ligation.

The left common carotid artery was either completely or partially ligated using a 6-0 silk suture.

2.9.3 Immunohistochemistry

Immunohistochemistry technique was performed during the *in vivo* studies presented in Chapter 3 as well as in Chapter 4 for cell examination after enzymatic adventitia removal.

Tissues donated from our collaborators in the University of Rochester, United States were processed according to method 1, and tissues prepared in Dublin City University were processed according to method 2.

2.9.3.1 Method 1

Tissue Harvest and Paraffin Preservation

Twenty one or fourteen days post-surgery, the right and left common carotid arteries were perfused and fixed before they were harvested for paraffin embedding. Briefly, animals were anaesthetised using an IP anaesthesia (100 mg/kg Ketamine/ 16 mg/kg Xylazine), and surgical plane of anaesthesia was assessed by checking toe pinch reflex. Immediately after, heart perfusion was performed with 1x phosphate-buffered saline

(PBS) solution. Tissue was dissected from the animal and gently cleaned in a sterile petri-dish containing sterile 1x PBS under a dissection microscope using fine forceps. The tissue was briskly submerged in histology dye rinsing off any excess with 1x PBS. Consequently, the tissue was transferred into 10% neutral buffered formalin (estimated 20 - 30 times the volume of the tissue), and incubated at 4°C overnight. The sample was finally handed to pathology for paraffin embedding and sectioning using a microtome.

Preparation of Tissue Cross-sections for Confocal Analysis

Paraffin-preserved tissues from both animal models (Sections 2.9.1) required preparation before imaging. The protocol was divided in different steps as follow:

- *Tissue Rehydration* – It was conducted at room temperature by immersing the slides in xylene for 20 min followed by a gradients of ethanol for 5 minutes respectively: 100 %, 90 %, 70 % and 50 % ethanol. Afterwards, the slides were rinsed in distilled H_2O, and incubated once in 1x PBS for 10 minutes. The slides were kept moist in 1x PBS for cell nuclei staining.
- *Cell Nuclei Staining* – Staining was carried out using a DAPI : PBS (dilution 1:1000) solution at room temperature for 15 min. Finally, the samples were mounted using a water-based mounting medium, and gently covered with a coverslip avoiding the formation of bubbles. All the images were taken and compiled using Olympus FluoView™ FV1000 confocal microscope and FV10-ASW 4.2 Viewer software. All results are representative of experiments that were repeated with $n \geq 3$. Images were analysed with ImageJ software (Section 2.10).

Tissue samples subjected to co-localization studies were processed differently as outlined below.

Immunolabeling Protocol of Tissue Cross-sections

Paraffin-preserved tissues from S100β-EGFP/cre-ER^{T2}/$ROSA26R^{tdTomato}$ mice (Sections 2.9.1) were subjected to co-localisation studies to evaluate the expression of the SCA-1 and αSMA proteins in the lesion 21 days post-injury. The protocol was divided in different steps as follow:

- *Tissue Rehydration* – as outlined above. The slides were kept moist in 1x PBS for immunolabelling.
- *Antigen Retrieval* – It was necessary to recover protein antigens before immunolabelling. The slides were heated at 80 – 100°C for 20 min in antigen retrieval buffer (ARB – 10 mM sodium citrate, 0.05 % Tween 20, pH 6.0).
- *Immunolabelling* – all samples were incubated in blocking buffer (5 % BSA, 0.3 M Glycine, 1% Tween PBS) at 4°C overnight in order to prevent unspecific binding of antibodies. Primary antibodies marking the desired protein antigens were prepared in blocking buffer at the recommended dilution (Table 2-3). Tissues were left to incubated in diluted primary antibody at 4°C overnight. The slides were washed twice with 1x PBS to remove any unbound primary antibody. The secondary antibody was added to the tissues at the correct dilution previously prepared in blocking buffer (Table 2-3) and allowed to incubate at 4°C overnight. The fluorophore-conjugated secondary antibody bound to the constant fragment of the primary antibody resulted in the fluorescent detection of the desired protein antigen marked by the primary antibody. Subsequently, the slides were washed twice with 1x PBS to remove any unbound secondary antibody followed by a nuclear staining step using DAPI solution (dilution 1:1000 in DPBS) at room temperature for 15 min. Finally, the samples were mounted using a water-based mounting medium, and gently covered with a coverslip avoiding the formation of bubbles. All the images were taken and compiled using Olympus FluoView™ FV1000 confocal microscope and FV10- ASW 4.2 Viewer software. In order to set up the zero-fluorescent value establishing the negative control, each secondary antibody used in immunolabelling required its control sample. This involved the preparation of a tissue subjected to the entire protocol except for the primary antibody incubation step. Instead, blocking buffer was used to replace the primary antibody dilution. This secondary control sample set up the fluorescent threshold value for imaging preventing false positive results. All results are representative of experiments that were repeated with $n \geq 3$. Images were analysed with ImageJ software (Section 2.10).

2.9.3.2 Method 2

Tissue Harvest and Paraffin Preservation

Animals were anaesthetised using an IP anaesthesia (100 mg/kg Ketamine/16 mg/kg Xylazine), and surgical plane of anaesthesia was assessed by checking toe pinch reflex. Aortas were gently harvested from the animal and carefully cleaned in a sterile petri-dish containing sterile Hank's balanced salt solution (HBSS) under a dissection microscope using fine forceps. Thereafter, the adventitia layer was removed as outline in Section 2.8.1 (Figure 2.1). Subsequently, the tissues were subjected to immunohistochemistry technique, and the protocol was divided in different steps as follow:

- *Tissue Fixation* – aortas were transferred into 3.7 - 4% Formaldehyde (estimated 20 - 30 times the volume of the tissue) and incubated at 4°C overnight.
- *Tissue Dehydration* – conducted at room temperature. Samples were exposed to increasing concentrations of ethanol dilutions (35%, 50%, 70%, 95% and 100%) for 30 min each followed by 2 x 15 min incubations with Xylene before paraffin embedding.
- *Tissue Paraffin Embedding* – Paraffin was allowed to melt at 60°C. Tissues were immersed in liquid paraffin and incubated in an oven at 60°C for approx. 3 hours to allow a good infiltration of the paraffin into the tissue. Subsequently, the tissues were embedded in clean paraffin making sure of the correct orientation (up-right). The oven was turned off and the tissues were kept in it to gradually cool down overnight.
- *Tissue sectioning* – The Leica RM 2235 Microtome used in this step was kindly provided by Prof. Caitriona Lally in The University of Dublin. Paraffin blocks were cooled down on an ice block before sectioning. The blocks were then placed into the microtome chuck, so the wax block faced the blade and was aligned in the vertical plane. The dial was set to cut 5 µm sections along the fixed vessels. Paraffin-embedded tissue ribbons were transferred to 37ºC water bath and subsequently onto the surface of clean superfrost glass slides. Slides were allowed to dry before the hydration step.

- *Tissue Hydration* – conducted at room temperature. Paraffin-embedded tissues were exposed to 2 x 10 min incubations with Xylene followed by decreasing concentrations of ethanol dilutions (100%, 95%, 90% and 70%) for 10 min each. Thereafter, tissues were washed 3x HBSS for 10 min.
- *Antigen Retrieval* – The slides were heated at 80 – 100 °C for 20 minutes in antigen retrieval buffer (ARB – 10 mM sodium citrate, 0.05 % Tween 20, pH 6.0).
- *Mounting and Cell Nuclei Staining* – Using a DAPI-fortified mounting medium, tissues were mounted and stained at the same time. Mounting medium was added drop-wise on to the tissue avoiding disturbance. A coverslip was carefully placed on to the tissue ensuring that no bubbles were formed within the tissue between the two glass surfaces. The mounting medium was allowed to solidify at room temperature and the samples were analysed using the Olympus BX51 Fluorescence Microscope and Cell^{F} Multi-fluorescence and Imaging Software.

2.9.4 Morphometric Analysis

Morphometric analysis was conducted to compare the physical changes such as area and volume of adventitial, medial and luminal layers between healthy (Sham) and injured (Ligated) vessels of the S100β-EGFP and Sca-1-EGFP animals. The areas of each carotid artery layers including the adventitia, media, and (neo)intima, were measured using ImageJ, an image-analysis software (Schneider, Rasband and Eliceiri, 2012) and their volumes were calculated using the method outlined by Korshunov and Berk (2003). Briefly, 20X S100β-EGFP and Sca-1-EGFP images were used to determine the area of each arterial layer. The following trace readings were used: the circumference of endothelium was used to calculate the luminal area; the intimal area was delimited by the internal elastic lamina and the single-cell endothelium; the neointima area was defined by the internal elastic lamina and the luminal area; the internal elastic lamina and external elastic lamina were used to determine the medial area; and the external elastic lamina and the outer edge was used to confine the adventitial area (Figure 2.10). Morphometric variability along the carotid artery has been previously reported by Korshunov and Berk (2003) and is possibly due to differences in vessel hemodynamics. Therefore, they described a method for calculating the compartment volumes over the entire vessel length and thus generating a more accurate morphometric analysis of the vessel under investigation. Herein,

morphometry analysis was conducted in accordance to the Korshunov and Berk's method. Concisely, three to four 4 μm sections were used every 200 μm over the entire length of 2 mm vessel carotid artery. The mean area was calculated for each of 10 divisions, and then multiplied by 200 mm length. Finally, the volume of each division was added up and the volume of the entire vessel was obtained. This method evaluates remodelling taking into account changes in the whole vessel volume rather than a small section where it could result in an inaccurate approximate (see formula 1).

$$Volume = \sum_{i=8} (Area_i * 200),\ \mu m^3$$

Vessel Volume by Korshunov and Berk's method

Where v*olume* is the area volume of a 1600 μm length of vessel; $Area_i$ is the area at one division and 200 is the length between divisions. A minimum of four animals per group was assessed and results expressed as mean ± SD. Differences between groups were assessed by one-way ANOVA and a reading of $p \leq 0.05$ was considered significant.

2.10 Data Analysis

Results are expressed as mean ± S.E.M or S.D. Experimental points were performed in triplicate with a minimum of three independent runs. Data were assessed for normal distribution and analysis using GraphPad 6 Prism™ (GraphPad software, La Jalla, California, USA). For normal distribution of data, a parametric unpaired student t-test or two-way ANOVA followed by Tukey corrections was performed for comparison of two or ≥ 3 groups, respectively. For non-parametric data, a Mann-Whitney test or a Krustal-Wallis with Dunn's multiple comparisons test (One-way ANOVA non parametric test) were performed for comparison of two or ≥ 3 groups, respectively. The corresponding statistical test is described in each figure, a value of $p \leq 0.05$ was considered significant. The PCR data was analysed and fold changes calculated using the Comparative C_T method ($\Delta\Delta C_T$) with Microsoft Office Excel 2011. Morphometry, immunocytochemistry and immunohistochemistry images were analysed using ImageJ, an image-analysis software (Schneider, Rasband and Eliceiri, 2012). For

morphometry, the areas of the artery layers, measured by the software, served to calculate the volume changes (Section 2.9.4). For immunocytochemistry and immunohistochemistry, the software was used to calculate the fraction of DAPI stained cells that were positive for a given marker.

Chapter 3

S100β^{+} and Sca-1^{+} cells contribute to the neointimal formation and arteriosclerotic lesions *in vivo*

3.1 Introduction

Intimal thickening due to the accumulation of SMC-like cells is a key event leading to atherosclerotic-prone lesions and an important marker of subclinical disease, yet the fundamental aspects of vascular cell accumulation, proliferation and the early phenotypic changes within the vessel wall remain unresolved. Lineage tracing analysis has provided conflicting evidence for the involvement of 'reprogrammed' de-differentiated SMC, resident stem cell-derived progeny and SMCs derived from endothelial-mesenchymal-transition (EndMT) in progressing subclinical atherosclerosis (Chapter 1, Section 1.5.1.2). However, the factors that dictate phenotypic changes, reprogramming and/or differentiation of these discrete cell populations and their progeny remain unknown.

Numerous pathologic observations from human vessels confirm that smooth muscle cell (SMC)-rich early 'transitional' lesions are present in atherosclerotic-prone regions of arteries before the retention of lipid and the appearance of a developed plaque (Sakamoto et al., 2018). These lesions represent an important therapeutic target and are successfully modelled *in vivo* using wildtype mice with flow restriction due to carotid artery ligation (Korshunov and Berk, 2003). Plaque formation is further facilitated when ApoE gene-deficient mice are concurrently placed on a western diet (Liu et al., 2011)

Many efforts have also focused on reducing the incidence rates of intimal thickening due to in-stent restenosis (ISR) following percutaneous transluminal coronary angioplasty (PTCA) and stenting for the treatment of atheromas (Aoki and De Gregorio, 2018). The introduction of the first-generation and second-generation drug-eluting stents (DES) has significantly reduced re-occlusion rates of vessels when compared to their bare-metal stent (BMS) equivalents. However, ISR remains a major concern in the DES era, with re-occurrence rates of up to 15% witness within the first year following intervention (MD et al., 2018).

In-stent restenosis also known as *clinical restenosis or neointima hyperplasia (NIH)* is mainly characterised by extensive proliferation and migration of vascular smooth muscle-like cells into the intimal space of the stented artery resulting in the formation of a new (neo) intima (Indolfi et al., 2003). This neointima formation may ultimately

result in the re-occlusion of the stented vessel. The source of smooth muscle-like cells contributing to NIH is a topic of much controversy. Different schools of thought within the literature, debate the cellular origin of these SMC-like cells in the neointima including i) contractile vSMCs (SM-MHC^{+}) residents of the tunica media, ii) circulating bone-marrow progenitor cells (HSCs and MSCs), iii) resident vascular adventitial (Sca-1^{+}) and medial stem cells (S100β Sox10 Nestin^{+}), and iv) endothelial cell progenitors (CD31 VE-cadherin^{+}**)** (Indolfi et al., 2003; Hu et al., 2004; Saiura et al., 2001; Sata et al., 2002; Sata, 2003; Shimizu et al., 2001; Shi et al., 1996; Li et al., 2000; Sartore et al., 2001; Cooley et al., 2014).

The use of animal models has been the foundation of basic and preclinical research into the study of cardiovascular syndromes (Chen, Shannon and Shen, 2013; Breckenridge, 2013; Konstantinov and Jankovic, 2013). Since the development of the Cre-LoxP system, and reporter mice, transgenic animals have revolutionised the study of physiological and pathological mechanisms of vascular disease (Sauer, 1987; Sauer and Henderson, 1988; Doevendans et al., 1998; Metzger and Chambon, 2001; Abe and Fujimori, 2013; Okabe et al., 1997) (Sauer, 1987; Orban, Chui and Marth, 1992). Intensive *in vivo* work has been focused on addressing the conflicting data about the source of SMC-like cells contributing to neointima formation; for instance, the use of transgenic mice in combination with injury models of neointima hyperplasia such as carotid artery ligation and femoral artery wire-induced injury, have shown that vSMCs were in part responsible for the lesional cells comprising the new intima. Using cell fate mapping, these lineage tracing studies employed tamoxifen-inducible SM-MHC-creER$^{(T2)-/+}$/mTmG$^{-/+}$ mice, and tamoxifen-inducible SM-MHC-creER$^{(T2)-/+}$/ROSA26-LacZ mice (Herring et al., 2014; Nemenoff et al., 2011; Yang et al., 2016). On the other hand, animal models used for the study of graft vasculopathy and neointima formation, such as heterotopic/orthotopic cardiac/bone marrow transplantations, as well as transluminal injury of the femoral artery and aortic transplantation, have all shown that circulating bone-marrow derived SMC progenitors from the recipient subjects were responsible for neointima hyperplasia and atherosclerosis (Saiura et al., 2001; Sata et al., 2002; Sata, 2003; Shimizu et al., 2001). Moreover, *in vivo* studies using injury models of neointima hyperplasia in combination with different lineage tracing strategies employing Tie2-Cre/ROSA26-stop-YFP/LacZ and Tie-CreER^{T}/ROSA26-stop-YFP/LacZ transgenic mice to mark and track endothelial cells

have revealed that endothelial cell progenitors were also an important source of SMC-like cells populating the new intima (Cooley et al., 2014; Wang et al., 2015). Several other studies have reported the presence of adventitial cell progenitors (Sca-1$^+$) (Hu et al., 2004; Passman et al., 2008) and medial cell progenitors (S100β, Sox10, Nestin$^+$) (Tang et al., 2012), (Yuan et al., 2017), (Wan et al., 2012) that also contribute to neointimal formation following injury. *Ex vivo* and *in vivo* work has provided compelling evidence that these progenitors are capable of undergoing SMC transition, and thus contributing to neointima growth in vascular lesions (Wang et al., 2015).

In spite of the great advances that transgenic animals have provided in understanding the molecular cues and mechanisms responsible for neointima hyperplasia and vascular remodelling, the source of SMC stem/progenitor cells within the adult vasculature is still an active area of research that remains under investigation. Given the extensive list of possible SMC progenitor cells, we sought to determine the presence and putative role of S100β$^+$ and Sca-1$^+$ stem cells within the vasculature of a healthy vessel and how these cells might contribute to neointimal formation following carotid artery induced injury *in vivo*. We further used lineage tracing analysis to indelibly mark and track S100β progenitor cells within the vessel wall and examined their co-localisation with SMC-like cells and Sca-1$^+$ progenitors following injury.

3.2 Strategy

The main objective of this thesis was to definitively determine whether resident vascular stem cells (vSCs) within the vessel wall are a source of SMC-like cells following injury, and secondly could the embryological origin of these progenitor cells dictate their fate towards a SMC lineage in the process of neointimal formation and vascular remodelling. In order to address these questions, it was necessary to first design an *in vivo* experiment that:

i) Determines the presence of S100β^{+} and Sca-1^{+} vSCs in healthy and injured vessels and evaluates the morphometric changes following vascular remodelling.
ii) Evaluates the origin of SMC-like (αSMA^{+}) cells within the neointima of injured arteries by cell fate mapping S100β progenitor cells and their progeny using lineage tracing following vascular injury.
iii) Assesses the co-localisation of S100β cells and their progeny with one or more vSCs within the neointima.

In order to address these objectives, the preferred injury model chosen to reproduce the compliance mismatch (Colombo et al., 2013) and neointimal hyperplasia typical of in-stent restenosis (ISR) was the carotid artery ligation model. This model is characterised by the accumulation of SMC-like cells within the neointima and the radial expansion of the tunica intima (Peterson, Liaw and Lindner, 2016; Kumar and Lindner, 1997).

3.2.1 Determine the presence of vSCs in healthy and diseased vessels using Sca-1-EGFP and S100β-EGFP transgenic mice

The aim of this *in vivo* study was to investigate the presence of Sca-1 and S100β progenitor cells within healthy and injured vessels following carotid artery-induced vascular injury and neointimal formation. To do this we employed two different transgenic animal models (i) B6.Cg-Tg(Ly6a-EGFP)G5Dzk/J (Sca-1-EGFP) mice (The Jackson Laboratories: JAX stock #012643) as Ly6a-GFP transgenic mice have an enhanced green fluorescent protein (EGFP) under the control of murine lymphocyte antigen 6 complex locus A (Ly6a/(Sca-1) promoter and (ii) B6;DBA-Tg(S100β-EGFP/cre/ERT2)22Amc/J (S100β-EGFP) transgenic mice (The Jackson Laboratories:

JAX stock #014160) as these mice express the EGFP/cre-ER^{T2} (Enhanced Green Fluorescent Protein and cre/ESR1) fusion gene under the direction of the mouse S100β neural promoter. In this context, the Sca-1-EGFP mice (Section 2.10.2) were selected to visualise Sca-1^{+} stem cells due to their abundance and SMC myogenic differentiation potential (Hu et al., 2004; Passman et al., 2008) whereas the S100β-EGFP/cre-ER^{T2} mice (Section 2.10.1) were selected to visualise S100β1^{+} cells due to their presence within the vessel wall (Tang et al., 2012) and their SMC myogenic differentiation potential (Kennedy et al., 2014). Both cell populations could be visualised through EGFP fluorescence staining in situ.

3.2.2 Perform cell fate mapping of S100β cells within the vessel wall following vascular injury

Here, the aim was to track the cell progeny of vascular stem cells within the vessel wall after injury and determine their contribution to neointima hyperplasia and vascular remodelling, thereby elucidating a possible source of the SMC-like cells during disease progression. Because there was neither a constitutive nor inducible commercial Sca-1/cre animal model available at the time of experimentation, it was only possible to conduct S100β lineage tracing studies. In this context, S100β-EGFP/cre-ER^{T2} mice were mated with Gt(ROSA)26Sor$^{tm9(CAG\text{-}tdTomato)Hze}$ mice, which were commercially obtained from The Jackson Laboratories to generate the tamoxifen-inducible S100β-EGFP/cre-ER^{T2}/ROSA26R^{tdTomato} animals, and thus to track vSC-derived (S100β-tdT^{+}) cell progeny following injury induced vascular remodelling (Section 2.10.3).

3.2.3 Determine whether or not the S100β progeny, S100β-tdT^{+} within the neointima are also Sca-1^{+}

The progeny from both an adventitial Sca-1^{+} and a medial S100β^{+} resident vascular stem cell population have been proposed to contribute to the SMC-cell like cells in the neointima (Hu et al., 2004; Passman et al., 2008; Tang et al., 2012). In this context, tissue sections indelibly marked for the S100β marker (S100β-tdT^{+}) were also interrogated for Sca-1^{+} expression using an anti-Sca-1 antibody to reveal the presence of a unique resident vascular stem cell population contributing to the source of lesional cells.

3.2.4 Methodology

In order to facilitate the clear understanding of the proceeding results, a brief summary of the steps taken within the *in vivo* study are presented below. Full protocols are detailed in Materials and Methods, Chapter 2 Section 2.10.

i. Our collaborators at the Department of Surgery, University of Rochester, Rochester NY, USA performed all the surgical interventions on the transgenic animals. Both tamoxifen-inducible S100β-EGFP/cre-ER^{T2}/$ROSA26R^{tdTomato}$ and Sca-1-EGFP animals were used at the age of 6-8-week-old to investigate the presence of a stem/progenitor cell in the vasculature and their role in neointima hyperplasia. Two injury models of neointima thickening were selected to carry out these experiments: i) tamoxifen-inducible S100β-EGFP/cre-ER^{T2}/$ROSA26R^{tdTomato}$ mice were subjected to complete carotid artery ligation for a length of 21 days and ii) Sca-1-EGFP strain were subjected to a partial carotid artery ligation for 14 days. Co-localisation studies were carried out on the S100β animals' tissue sections using anti-EGFP antibody and anti-tdTomato. Further to this, mouse anti-Sca-1 and anti-αSMA antibodies were used to immunolabel the the tissue samples. There was no need to immunolabeling the Sca-1-EGFP tissue sections with anti-EGFP, so these sections were ready to image after DAPI staining. All the images were taken and compiled using Olympus FluoView™ FV1000 confocal microscope and FV10- ASW 4.2 Viewer software. Images were subsequently analysed at the Vascular Biology and Therapeutics laboratories at DCU for expression and morphometric analysis.
ii. Morphometry was performed to observe the physical changes in sham (control) versus ligated vessels. ImageJ™, an image-analysis software was used to calculate the volumes and areas of the three carotid artery layers: adventitia, media, and (neo)intima (Schneider, Rasband and Eliceiri, 2012).

Overall, we hypothesise that activation of resident vascular stem cells in ligated stenotic vessels accounts for the extensive proliferation, migration and accumulation of neointimal cells in injured vessels. We believe that this complex healing response culminates in vSC proliferation, asymmetric division and partial myogenic differentiation to a SMC-like phenotype following expression of SMC differentiation markers, smooth muscle α-actin (SMA), smooth muscle myosin heavy chain 11 (SM-

MHC) and Calponin 1 (Cnn1) and thus contributes to the occlusion and narrowing of the vessel lumen (Rensen, Doevendans and van Eys, 2007)

3.3 Results

3.3.1 Morphometric analysis of sham and ligated vessels reveals vascular remodelling concomitant with an increase in the number of S100β-EGFP$^+$ and Sca-1-EGFP$^+$ cells within the media and neointima of injured vessels

3.3.1.1 Morphometric analysis of the left carotid artery (LCA) and right carotid artery (RCA) in sham and ligated vessel 21 days post ligation

Morphometry was carried out in accordance to Korshunov and Berk's method explained in Chapter 2, Materials & Methods, Section 2.9.4.

No significant changes were observed in the adventitial, medial, intimal or luminal volumes of the right carotid (RCA) of sham and ligated animals 21 days post ligation (Figure 3.1). In contrast, there was a significant increase in the intimal volume observed in the ligated LCA ($8.24 \pm 4.68 \times 10^8$ μm^3) concomitant with a reduction in the luminal volume ($2.01 \pm 1.53 \times 10^8$ μm^3) when compared to the sham LCA control vessels (1.13 ± 0.44 and $9.09 \pm 5.57 \times 10^8$ μm^3, respectively) (Figure 3.2).

3.3.1.2 Increased number of S100β-eGFP and Sca-1-EGFP cells within injured vessels post ligation

Qualitative and quantitative analyses was carried out on tissue sections from sham and ligated RCA and LCA carotid arteries of S100β-eGFP and Sca-1-EGFP animals, respectively. These comparisons controlled for pre- and post-operative protocols as well as vascular remodelling due to the surgery.

The data is presented as follows: i) sham right carotid artery (RCA) versus ligated RCA and ii) sham left carotid (LCA) arteries versus the ligated LCA (Section 2.9.2).

In both sham and ligated S100β-eGFP transgenic animals, there was no significant presence of S100β$^+$ cells in the medial or intimal layers of RCA vessels (Figure 3.3A,

B). In contrast, a significant number of S100β$^+$ cells were present in the adventitial layers of both sham and ligated vessels and a significantly greater number of S100β$^+$ cells present in the adventitial layer of ligated RCA vessels (0.21 ± 0.20 cell fraction), when compared to the RCA sham controls (0.03 ± 0.06 cell fraction), after 21 days post ligation (Figure 3.3, B).

There was also no significant presence of S100β$^+$ cells in the medial or intimal layers of sham LCA vessels after 21 days (Figure 3.4, A and B). Similar to the sham RCA vessels, a small fraction of S100β$^+$ cells were present in the adventitial layer of the sham LCA vessels (0.04 ± 0.07 cell fraction) (Figure 3.4, B). However, there was a marked significant increase in the number of S100β$^+$ cells present in the medial (0.24 ± 0.16) and intimal (0.49 ± 0.17) layers of ligated LCA vessels when compared to the LCA sham controls (0.008 ± 0.02 and 0 ± 0, respectively) 21 days post ligation (Figure 3.4, B).

In Sca-1-EGFP transgenic animals, there was no significant presence of Sca-1-EGFP$^+$ cells in the medial layer of sham LCA. However, there was a significant presence of Sca-1-EGFP$^+$ in both the adventitial (0.11 ± 0.09 cell fraction) and intimal (0.20 ± 0.11 cell fraction) layers of sham LCA vessels (Figure 3.5, A and B). Moreover, there was a marked significant increase in the number of Sca-1-EGFP$^+$ in the adventitial (0.34 ± 0.11), medial (0.18 ± 0.19), and intimal (0.62 ± 0.25), layers of the ligated LCA when compared to the sham LCA controls 21 days post ligation (Figure 3.5, A and B).

No significant changes in volume are observed for each carotid layer when comparing the cross-sections of the right sham carotid arteries against the right carotid arteries of the ligated animals. Values are given as average ± S.D. with 2 to 4 sections analysed per animal (Sham n = 2 and Ligated n = 6). All layer comparisons made to corresponding Sham layer. Unpaired or/and Mann-Whitney t-test with significance value of $P \leq 0.05$ were carried out.

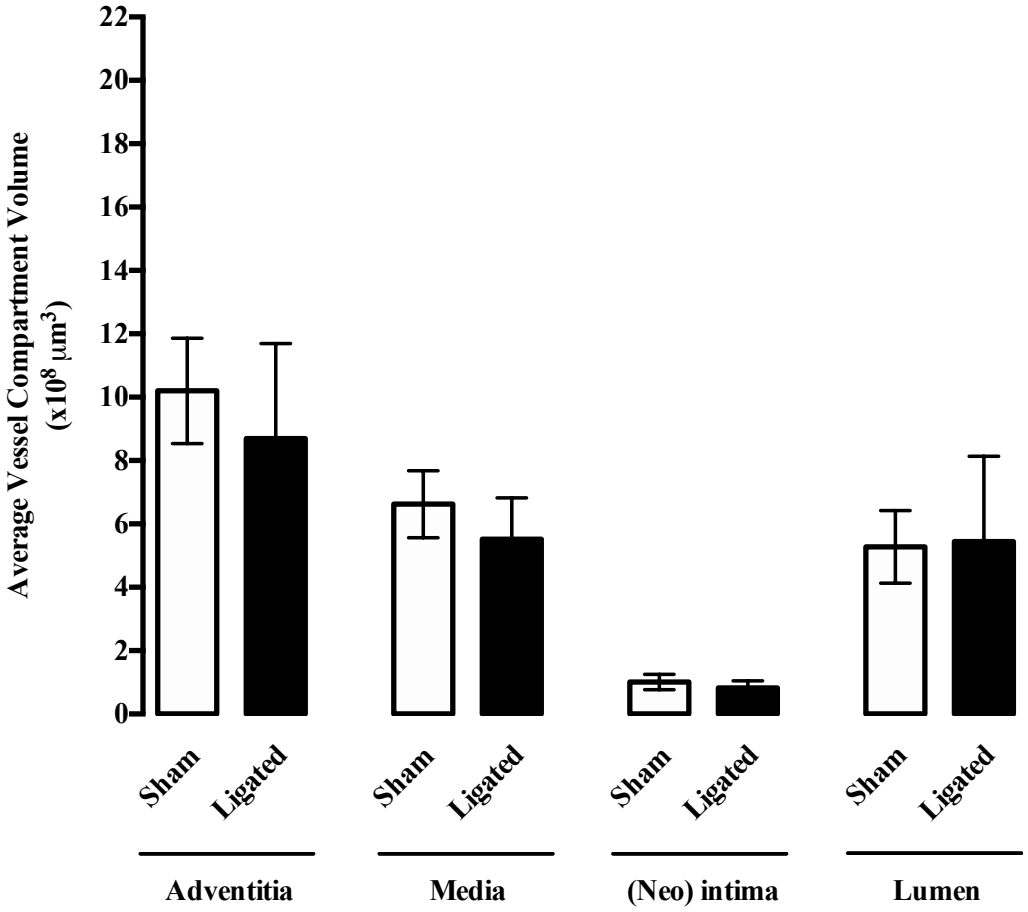

Figure 3.1. Morphometric analysis of adventitial medial, intimal and luminal volumes in RCA vessels from S100β-EGFP/cre/ERT2/ROSA26RtdTomato transgenic mice 21 days post ligation.

No significant changes in volume are observed for each carotid layer when comparing the cross-sections of the right sham carotid arteries against the right carotid arteries of the ligated animals. Values are given as average ± S.D. with 2 to 4 sections analysed per animal (Sham n = 2 and Ligated n = 6). All layer comparisons made to corresponding Sham layer. Unpaired t-test with significance value of $P \leq 0.05$.

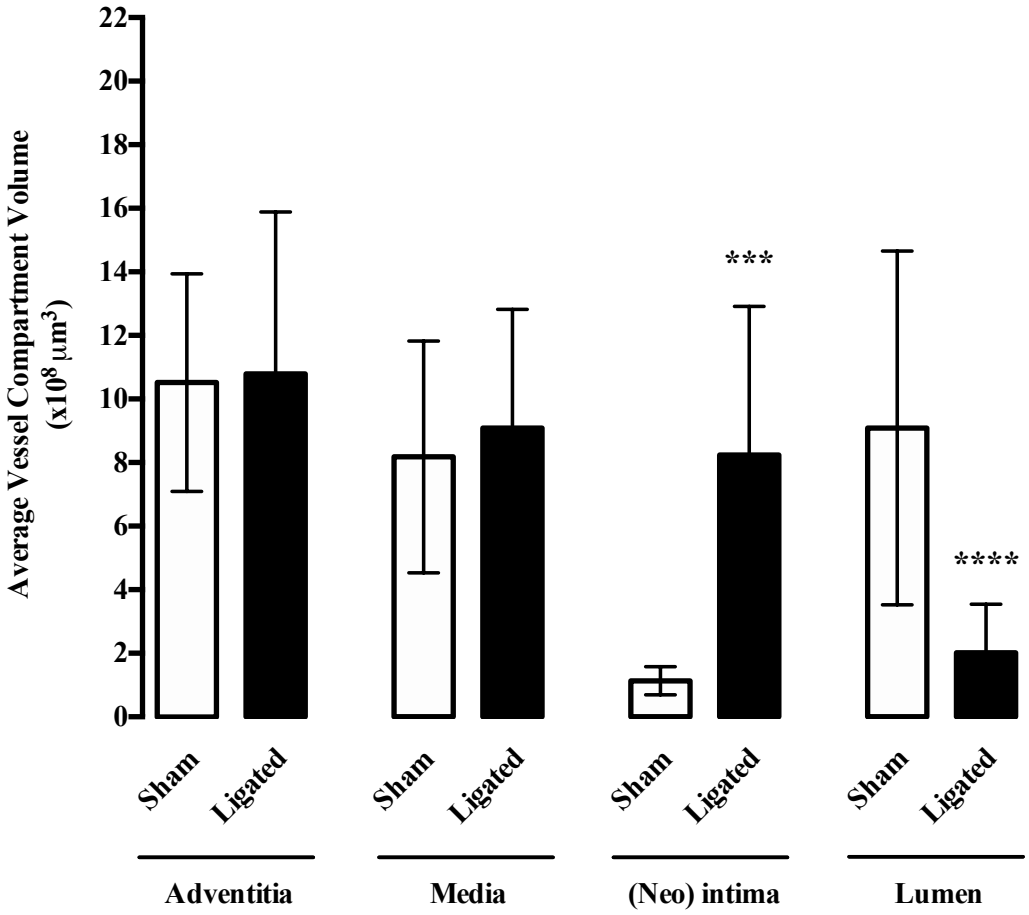

Figure 3.2. Morphometric analysis of adventitial medial, intimal and luminal volumes in LCA vessels from S100β EGFP/cre/ERT2/ROSA26RtdTomato transgenic mice 21 days post ligation.

There is an increase in neointima volume (Unpaired t-test) accompanied with a decrease in luminal area (Mann-Whitney t-test) in the ligated LCA when compared to the sham LCA. The adventitia and media exhibit no significant changes 21 days after complete carotid artery ligation. Values are given as average ± S.D. with 2 to 4 sections analysed per animal (Sham n = 2 and Ligated n = 6). All layer comparisons made to corresponding Sham layer. Unpaired and Mann-Whitney t-test with significance value of $P \leq 0.05$. Results: *** $p<0.001$ and **** $p<0.0001$.

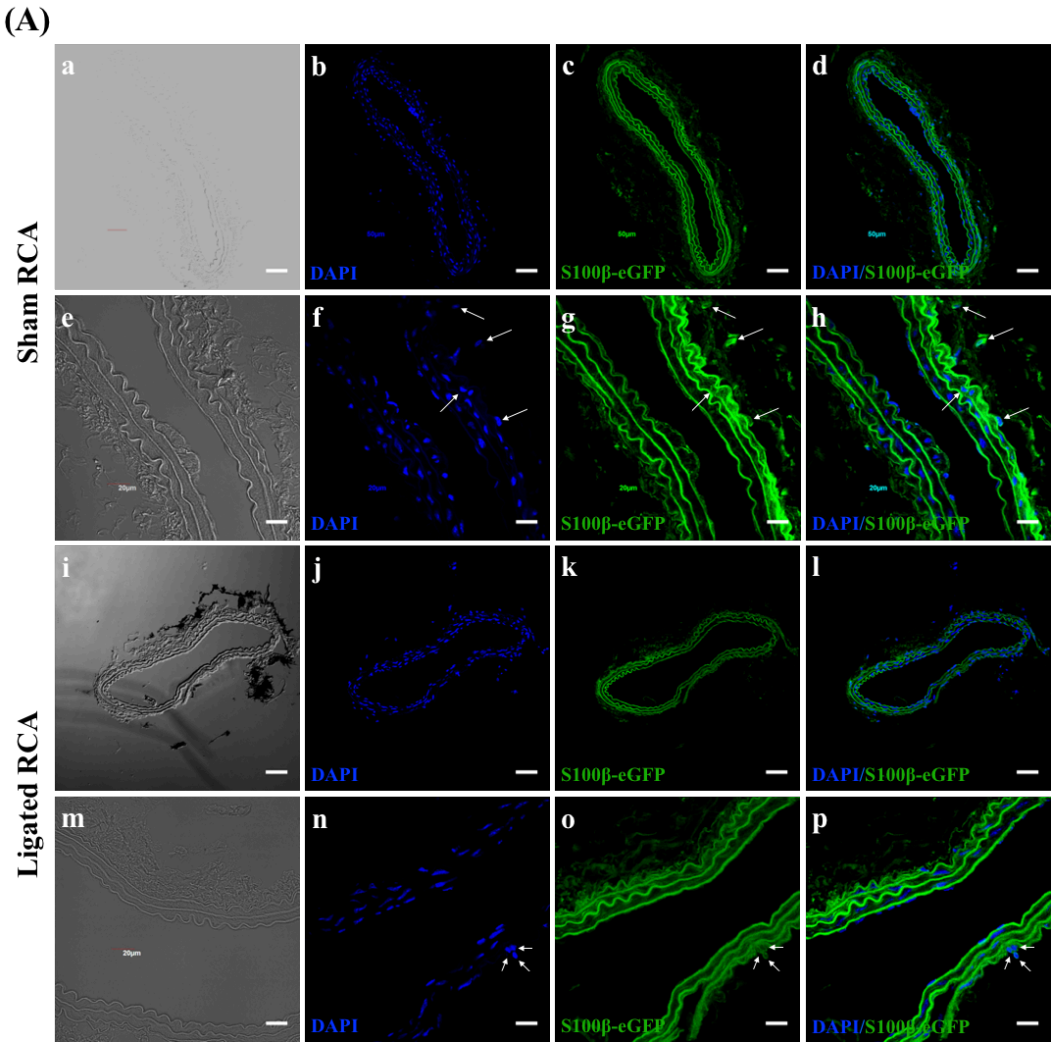

Figure 3.3. S100β-GFP expression in sham and ligated RCA from S100β-EGFP/cre/ERT2/ROSA26RtdTomato transgenic mice.

(A) Cross-sections of right sham and ligated LCA prepared 21 days post ligation. Representative images of Sham RCA at low and high magnifications **(a-d)** 20X and **(e-h)** 60X, and the ligated RCA at **(i-l)** 20X and **(m-p)** 60X. Representative images of **(a, e, i, m)** cross-section bright field **(b, f, j, n)** DAPI nuclear staining **(c, g, k, o)** S100β-GFP expression and **(d, h, l, p)** composite merged images. Scale bars, 20 μm.

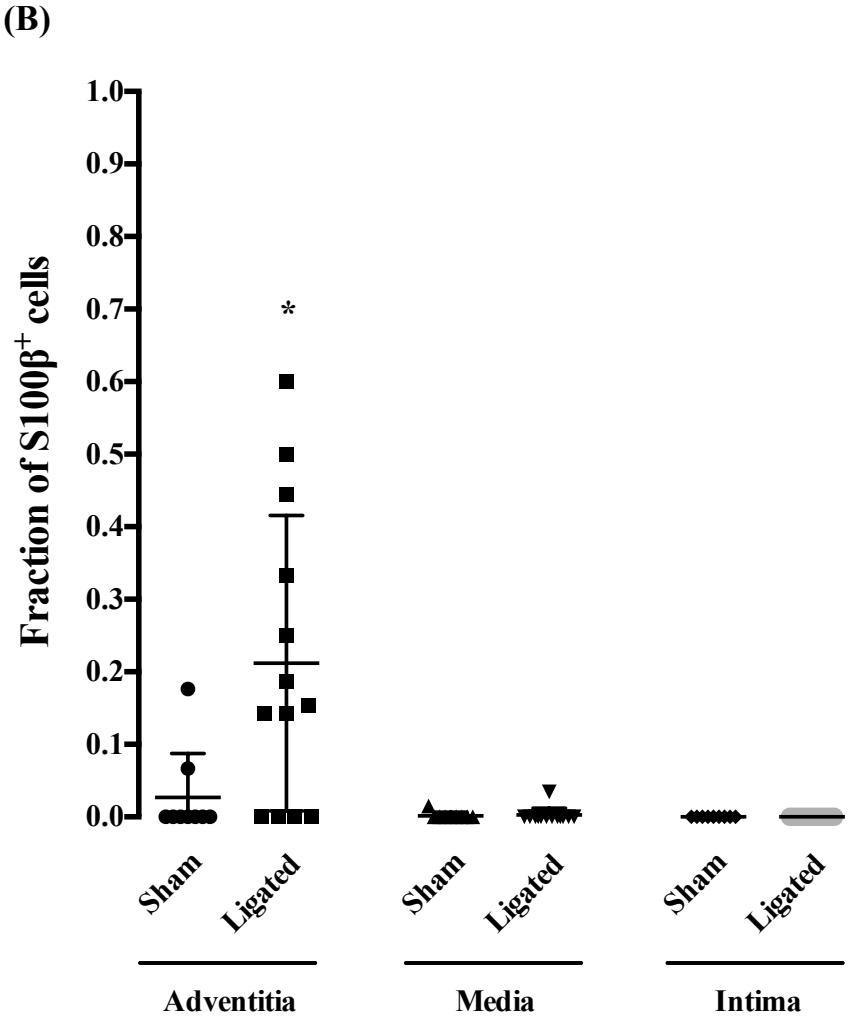

Figure 3.3. S100β-GFP expression in sham and ligated RCA from S100β-EGFP/cre/ERT2/ROSA26R^{tdTomato} transgenic mice.

(B) Fraction of S100β-eGFP^{+} cells in each layer: Adventitia (A), Media (M) and Intima (I). The data compared the fraction of eGFP^{+} cells in sham versus the ligated vessels in each group as an average ± S.D. (Sham n = 2 and Ligated n = 6). All layer comparisons made to corresponding Sham layer. Mann-Whitney t-test with significance value of P≤0.05. Results: * p=0.0155.

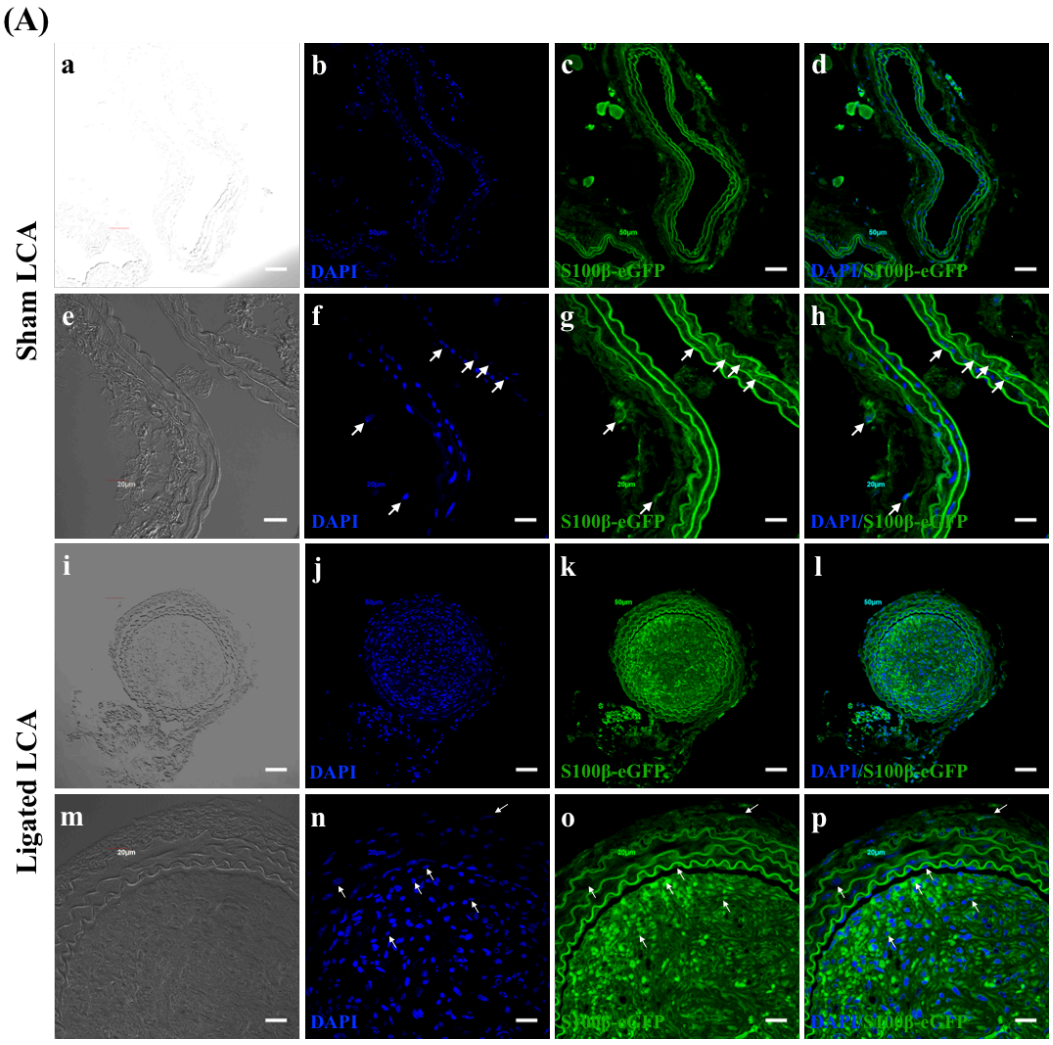

Figure 3.4. S100β-GFP expression in sham and ligated LCA from S100β-EGFP/cre/ERT2/ROSA26RtdTomato transgenic mice.

(A) Cross-sections of left sham and ligated LCA prepared 21 days post ligation. Representative images of Sham LCA at low and high magnifications **(a-d)** 20X and **(e-h)** 60X, and the ligated LCA at **(i-l)** 20X and **(m-p)** 60X. Representative images of **(a, e, i, m)** cross-section bright field **(b, f, j, n)** DAPI nuclear staining **(c, g, k, o)** S100β-GFP expression and **(d, h, l, p)** composite merged images. Scale bars, 20 µm.

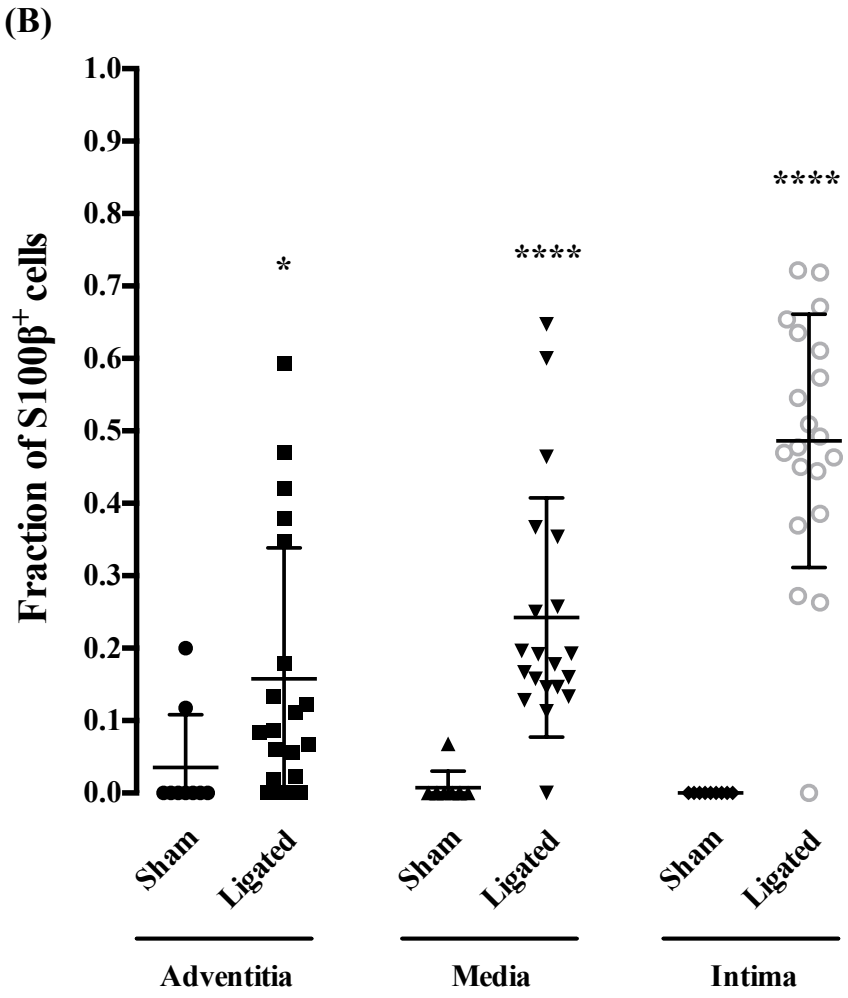

Figure 3.4. S100β-GFP expression in sham and ligated LCA from S100β-EGFP/cre/ERT2/ROSA26R^{tdTomato} transgenic mice.

(B) Fraction of S100β-eGFP^{+} cells in each layer: Adventitia (A), Media (M) and Intima (I). The data compared the fraction of eGFP^{+} cells in sham versus the ligated vessels in each group as an average ± S.D. (Sham n = 2 and Ligated n = 6). All layer comparisons made to corresponding Sham layer. Mann-Whitney t-test with significance value of P≤0.05. Results: * p=0.0168 and **** p<0.0001.

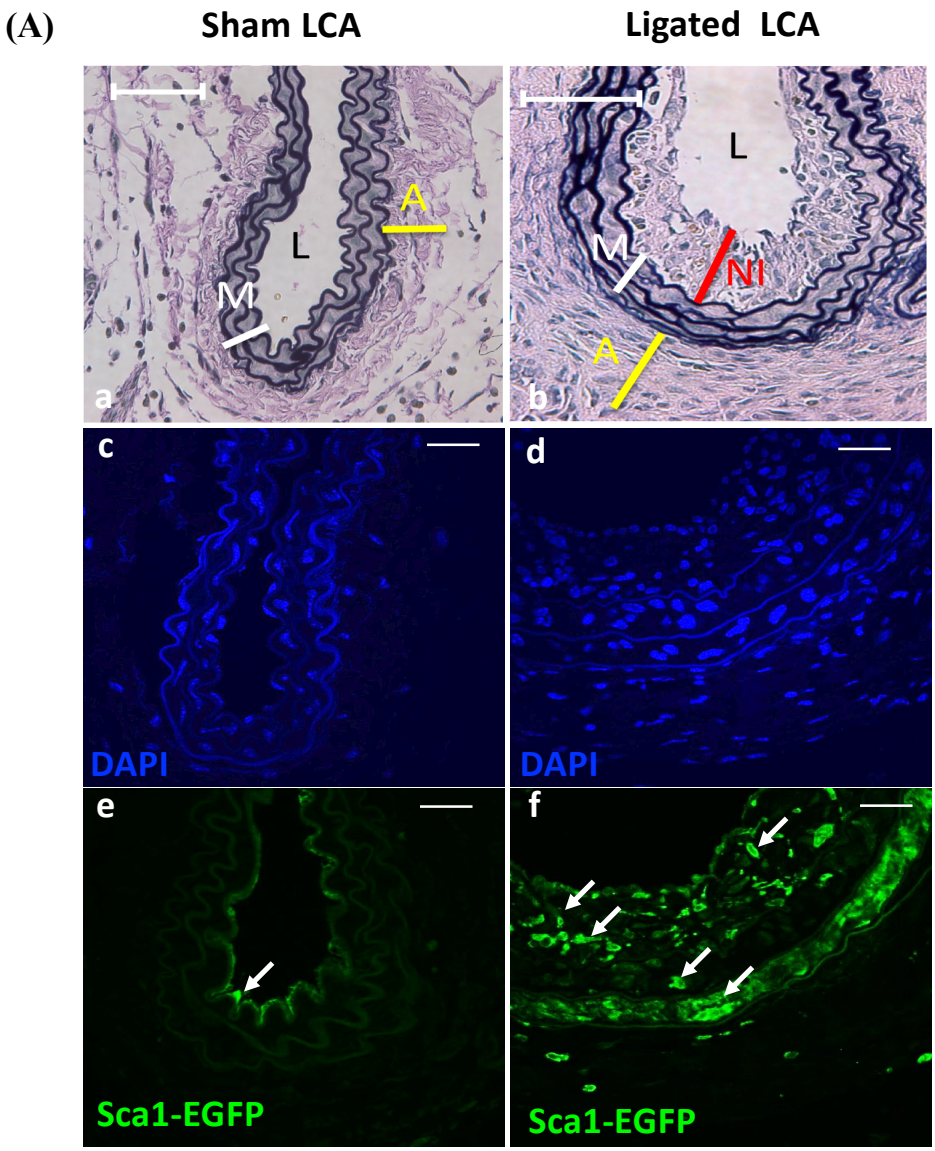

Figure 3.5. Sca-1-EGFP expression in sham and ligated LCA from the Sca-1-EGFP transgenic mice 14 days after partial carotid artery ligation.

(A) Cross-sections of LCA were prepared 14 days post-ligation. Representative images of sham LCA at **(a, c, e)** 60X and ligated LCA **(b, d, f)** 60X. Representative images of **(a, b)** cross-section bright field, **(c, d)** DAPI nuclear staining, **(e, f)** Sca-1-EGFP expression. White arrows indicate Sca-1^{+} cells.

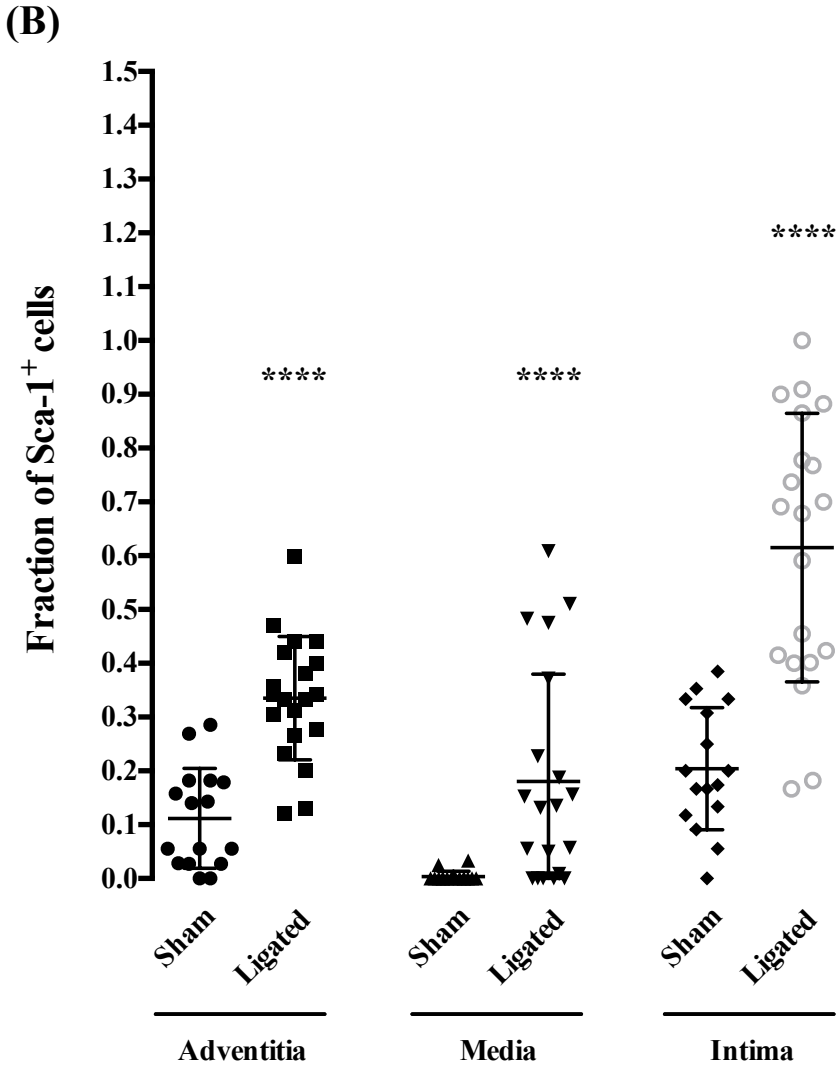

Figure 3.5. Sca-1-EGFP expression in sham and ligated LCA from the Sca-1-EGFP transgenic mice 14 days after partial carotid artery ligation.

(B) Fraction of Sca-1-EGFP$^+$ cells in each layer: Adventitia (A) (Unpaired t-test), Media (M) (Mann-Whitney) and Intima (I) (Unpaired t-test). The data compared the fraction of EGFP$^+$ cells in sham versus the ligated vessels in each group as an average ± S.D. ($n \geq 3$). All layer comparisons made to corresponding Sham layer. Unpaired and Mann-Whitney t-test with significance value of $P \leq 0.05$. Results: **** $p < 0.0001$.

3.3.2 Lineage tracing analysis using tamoxifen-inducible S100β-EGFP/cre /ERT2/ROSA26RtdTomato animals reveals the presence of S100β-derived cells (S100β-tdT+) in the neointimal and medial layers of ligated vessels 21 days post-ligation.

Qualitative and quantitative analyses were carried out on tissue sections from sham and ligated tamoxifen-inducible S100β-EGFP/cre/ERT2/ROSA26R^{tdTomato} transgenic mice. The data is presented as follow: i) sham RCA versus ligated RCA and ii) sham LCA versus ligated LCA, Corn oil was administered to control for drug specificity ruling out any possible Cre-loxP recombination in the absence of tamoxifen (Section 2.9.1).

In S100β-EGFP/cre/ERT2/ROSA26R^{tdTomato} transgenic mice treated with corn oil for 5 consecutive days prior to ligation, there was no S100β-tdT^{+} cells present within the sham or ligated LCA after 21 days post ligation (Figure 3.6). This suggests that no S100β cells are marked with tdTomato in the absence of administration of tamoxifen.

In the RCA vessels from both sham and ligated S100β-EGFP/cre/ERT2/ROSA26R^{tdTomato} transgenic animals treated with tamoxifen to mark S100β-tdT^{+}, there was no significant presence of S100β-tdT^{+} cells in the medial or intimal layers (Figure 3.7). In contrast, a significant number of S100β-tdT^{+} cells were present in the adventitial layer of both sham and ligated RCA vessels and a significantly greater number of S100β-tdT^{+} cells present in the adventitial layer of ligated RCA vessels (0.21 ± 0.20 cell fraction), when compared to the RCA sham controls (0.03 ± 0.06 cell fraction) after 21 days post ligation (Figure 3.7, B).

In the LCA vessels from sham S100β EGFP/cre/ERT2/ROSA26R^{tdTomato} transgenic animals treated with tamoxifen to mark S100β-tdT^{+}, there was no significant presence of S100β tdT^{+} cells in the intimal layers of LCA vessels after 21 days (Figure 3.8, A and B). A few S100β-tdT^{+} cells were observed in the medial layer of the sham LCA vessels and a significant number of S100β-tdT^{+} cells were present in the adventitial layer of sham LCA vessels (0.04 ± 0.07 cell fraction) (Figure 3.8, A and B). In contrast, there was a marked significant increase in the number of S100β-tdT^{+} cells present in the adventitial (0.13 ± 0.12), medial (0.14 ± 0.09), and intimal (0.54 ± 0.18), layers of ligated LCA vessels when compared to the LCA sham controls 21 days post ligation (Figure 3.8, A and B).

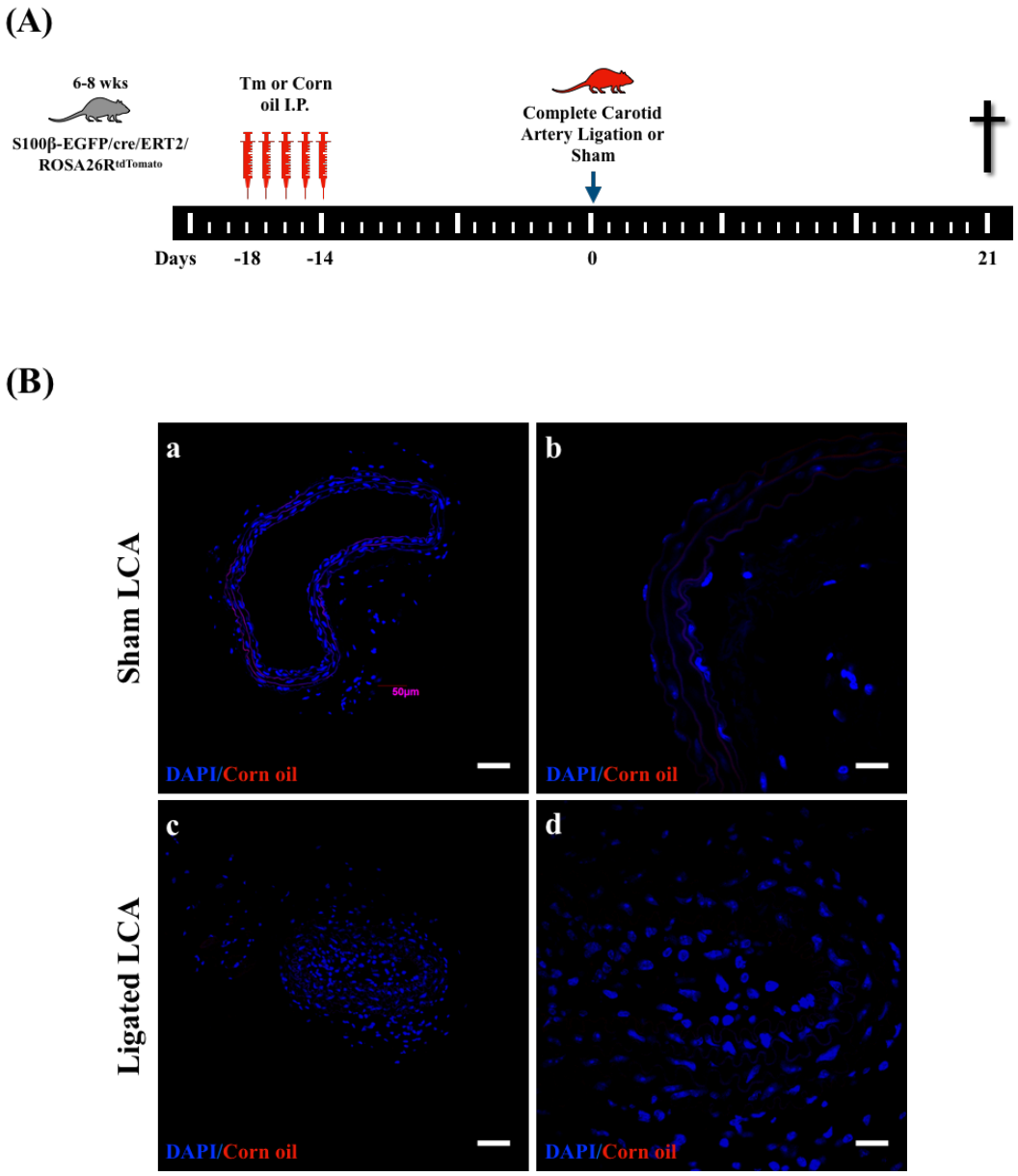

Figure 3.6. S100β-tdTomato expression in sham and ligated LCA of S100β-EGFP/cre/ERT2/ROSA26R^{tdTomato} transgenic mice after 21 days that were pre-treated with corn oil for 5 days prior to ligation after 2 weeks.

(A) Timeline strategy: 1x 1 mg/kg of Tamoxifen (Tm)/Corn Oil was daily administered to 6-8 weeks (wks) old animals by intraperitoneal (I.P.) injection for 5 consecutive days. Sham or ligation-induced injury was conducted 2 weeks after the last corn oil injection. Analysis was carried out 21 days post-ligation.

(B) Representation images from **(a, b)** sham LCA and **(c, d)** ligated LCA are shown at **(a, c)** low (20X) and **(b, d)** high (60X) magnification. Scale bar 20 μm.

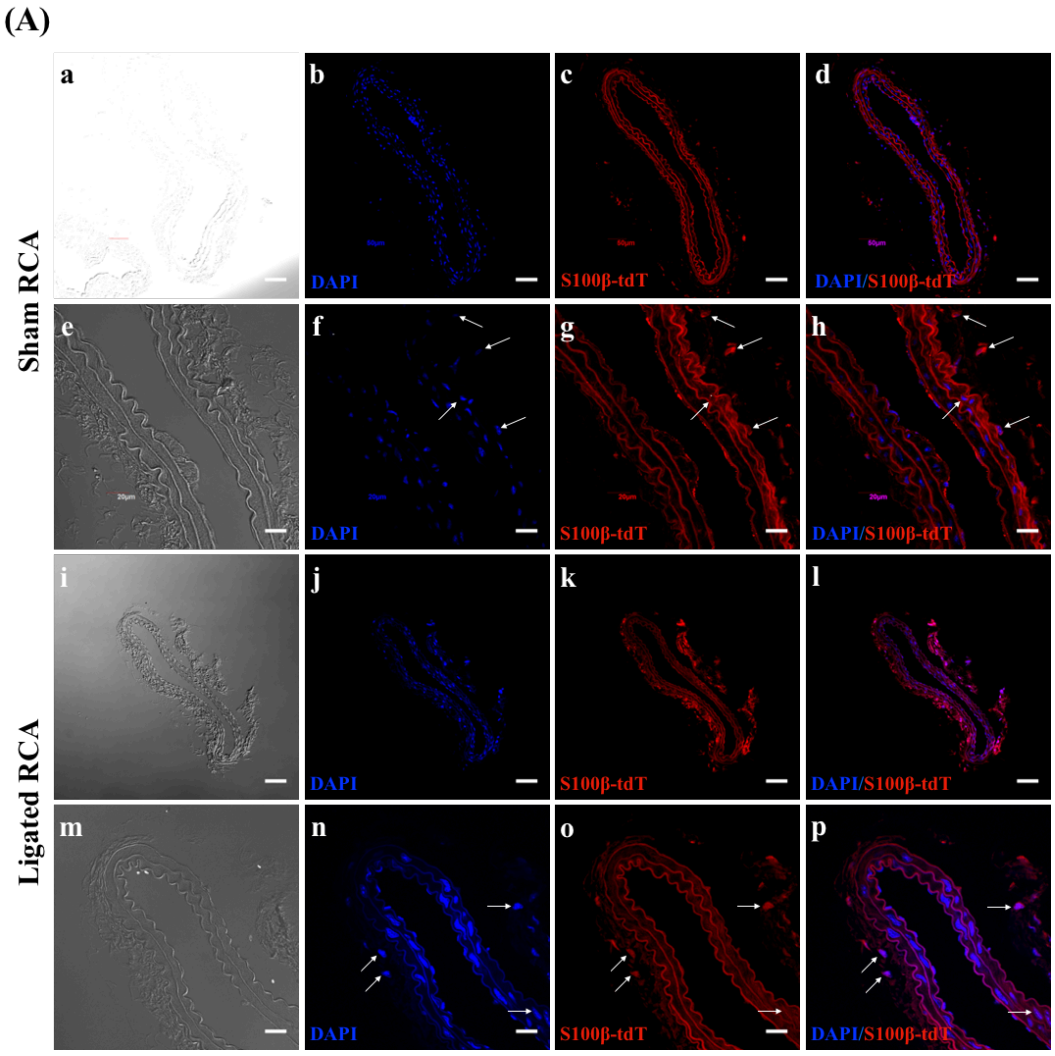

Figure 3.7. S100β-tdTomato expression in sham and ligated RCA of S100β-EGFP/cre/ERT2/ROSA26R^{tdTomato} transgenic mice 21 days that were pre-treated with tamoxifen for 5 days prior to ligation after 2 weeks.

(A) Animals were treated with Tamoxifen for 5 consecutive days followed by 2-week recovery before injury. Cross-sections of sham and ligated RCA were prepared 21 days post-surgery, and images were taken at **(a-d, i-l)** low 20X and **(e-h, m-p)** high 60X magnification. Representative images of **(a, e, i, m)** cross-section bright field **(b, f, j, n)** DAPI nuclear staining **(c, g, k, o)** S100β-tdTomato expression and **(d, h, l, p)** composite merged images. Scale bars, 20 μm.

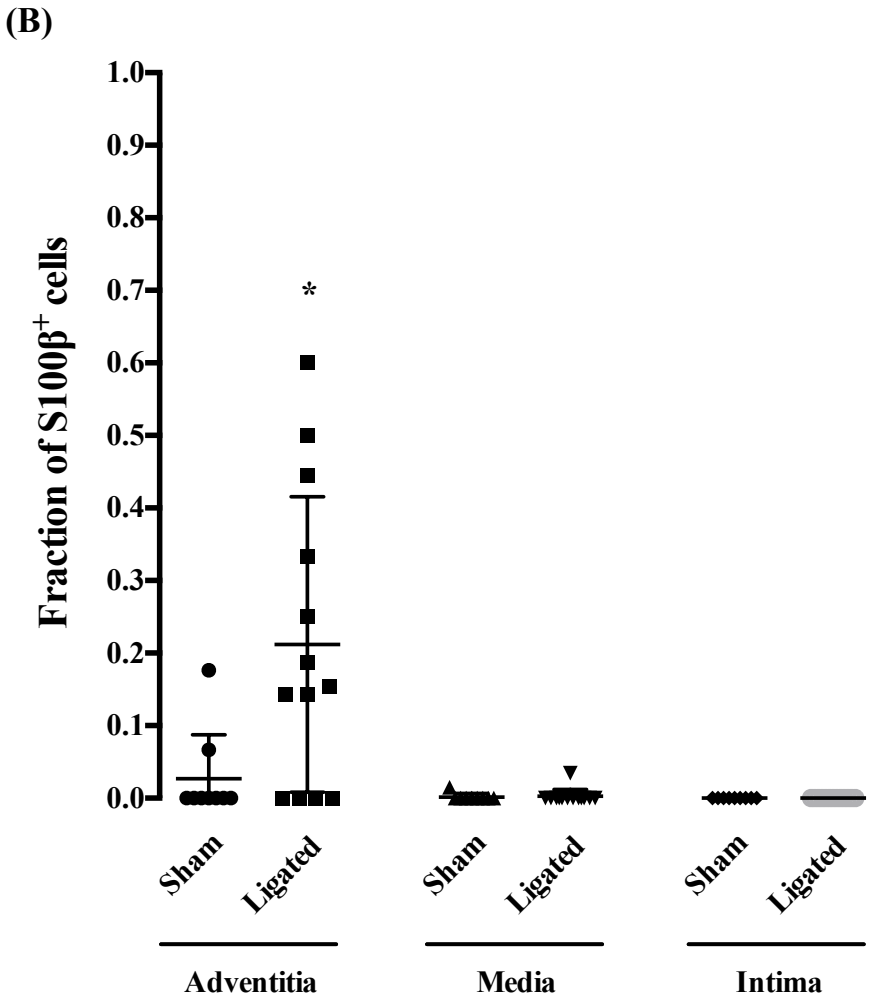

Figure 3.7. S100β-tdTomato expression in sham and ligated RCA of S100β-EGFP/cre/ERT2/ROSA26R^{tdTomato} transgenic mice 21 days that were pre-treated with tamoxifen for 5 days prior to ligation after 2 weeks.

(B) Fraction of S100β-tdT^{+} cells in each layer: Adventitia (A), Media (M) and Intima (I). The data compared the fraction of S100β-tdT^{+} cells in sham versus the ligated RCA vessels in each group as an average ± S.D. (Sham n = 2 and Ligated n = 6). All layer comparisons made to corresponding Sham layer. Mann-Whitney t-test with significance value of P≤0.05. Results: * p=0.0155.

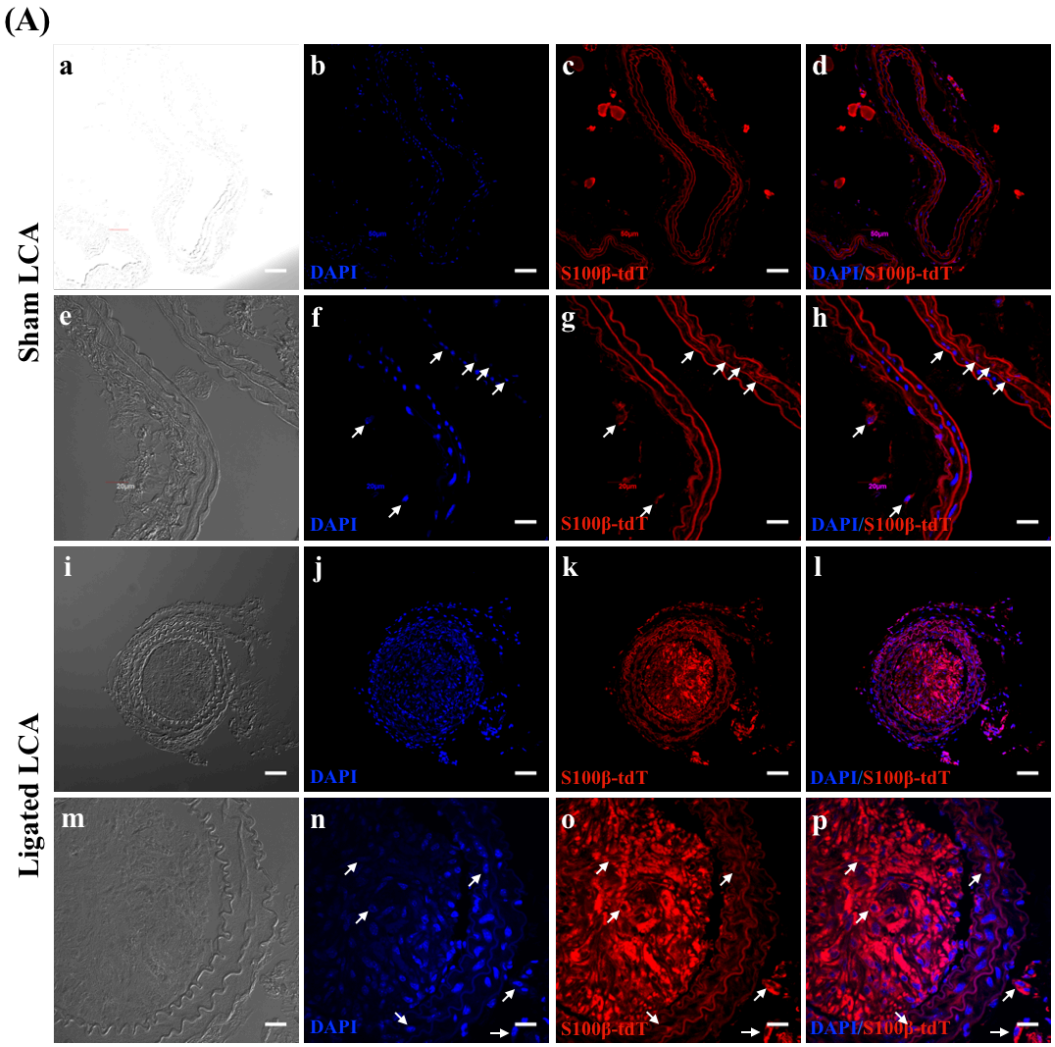

Figure 3.8. S100β-tdTomato expression in sham and ligated LCA of S100β-EGFP/cre/ERT2/ROSA26R^{tdTomato} transgenic mice after 21 days that were pre-treated with tamoxifen for 5 days prior to ligation after 2 weeks.

(A) Animals were treated with Tamoxifen for 5 consecutive days followed by 2-week recovery before injury. Cross-sections of sham and ligated LCA were prepared 21 days post-surgery and images were taken at **(a-d, i-l)** low 20X and **(e-h, m-p)** high 60X magnification. Representative images of **(a, e, i, m)** cross-section bright field **(b, f, j, n)** DAPI nuclear staining **(c, g, k, o)** S100β-tdTomato expression and **(d, h, l, p)** composite merged images. Scale bars, 20 μm.

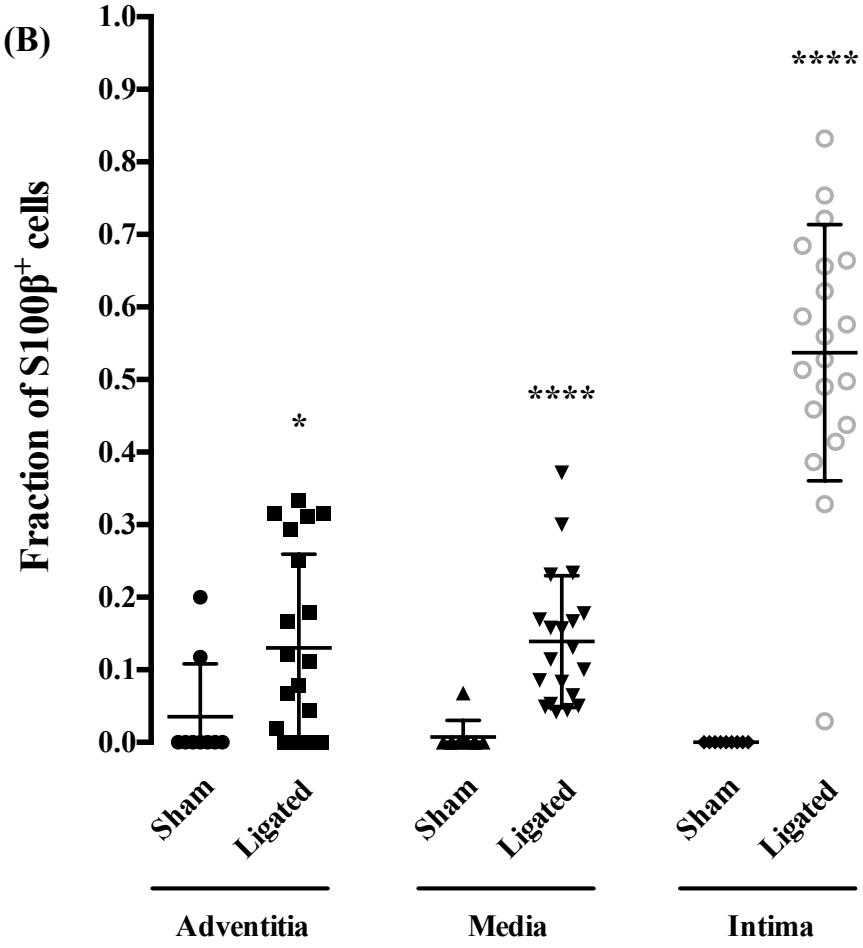

Figure 3.8. S100β-tdTomato expression in sham and ligated LCA of S100β-EGFP/cre/ERT2/ROSA26R^{tdTomato} transgenic after 21 days that were pre-treated with tamoxifen for 5 days prior to ligation after 2 weeks

(B) Fraction of S100β-tdTomato^{+} cells in each tunica layer namely Adventitia (A), Media (M) and Intima (I). The data compared the fraction of S100β-tdT^{+} in the LCA of sham versus the ligated vessels in each group as average ± S.D. (Sham n = 2 and Ligated n = 6). All layer comparisons made to corresponding Sham layer. Mann-Whitney t-test with significance value of P≤0.05. Results: *p=0.029 and **** p<0.0001.

3.3.3 Co-localisation of a Sca-1$^+$ cell population with S100β-tdT$^+$ cells in the neointima and media of ligated vessels after injury

3.3.3.1 Lineage tracing studies reveal the presence of S100β-derived Sca-1$^+$ cells (S100β-tdT$^+$ Sca-1-white$^+$) in the neointima of ligated vessels after 21 days post ligation

Since a significant number of marked and tracked S100β-tdT$^+$ cells are present in the intima after injury (Figure 3.8, A and B) concomitant with a large number of transiently expressing Sca-1$^+$-EGFP cells (Figure 3.5, A and B), and S100β-EGFP cells (Figure 3.4, A and B) after injury, the co-localisation of Sca-1$^+$ cells with S100β-tdT$^+$ cells were assessed in the LCA from S100β-EGFP/cre/ERT2/ROSA26R^{tdTomato} transgenic mice after 21 days ligation when compared to the contralateral RCA controls.

The S100β-tdT$^+$ cells were co-stained with a monoclonal anti-Sca-1 antibody (Sca-1-white) and the images were analysed to determine the fraction of S100β-tdT$^+$ cells that were Sca-1-white$^+$ cells (Section 2.9.3.1).

The data in this section examined the fraction of S100β-tdT$^+$ cells in the RCA (control) versus the LCA (injured) of the ligated animal and the fraction of S100β-tdT$^+$ cells that were Sca-1$^+$ in the RCA (control) versus the LCA (injured) of the ligated animal.

There was a significant increase in the number of S100β-tdT$^+$ cells in the LCA from ligated animals when compared to the RCA of the same animal (Figure 3.9, A and B). In particular there was a significant increase in the number of S100β-tdT$^+$ cells in the medial (0.14 ± 0.9 cell fraction) and intimal (0.54 ± 0.18 cell fraction) layers when compared to the contralateral RCA controls (0.002 ± 0.009 and 0 ± 0, respectively). (Figure 3.9, A and B).

There was also a significant increase in the number of Sca-1$^+$ cells in the LCA from ligated animals when compared to the RCA of the same animal (Figure 3.10, A and B). In particular there was a significant increase in the fraction of DAPI nuclei that were Sca-1$^+$ cells in the medial (0.08 ± 0.04) and intimal (0.50 ± 0.20) layers when

compared to the contralateral RCA controls (0.006 ± 0.01 and 0.18 ± 0.12, respectively) (Figure 3.10, A and B).

This co-localisation of Sca-1$^+$ cells and S100β-tdT$^+$ cells was confirmed in ligated LCA (Figure 3.11, A) when compared to RCA vessels with a significant increase in the fraction of DAPI nuclei that were S100β-tdT$^+$ cells and Sca-1$^+$ in the medial (0.08 ± 0.04) and intimal (0.40 ± 0.18) layers compared to the contralateral RCA controls when co-stained with an anti-Sca-1 antibody (0.006 ± 0.01 and 0 ± 0, respectively) (Figure 3.11, B).

Finally, the fraction of S100β-tdT$^+$ cells that were Sca-1$^+$ was significantly higher in the adventitia, medial and intimal layers of LCA vessels when compared to the contralateral RCA controls.

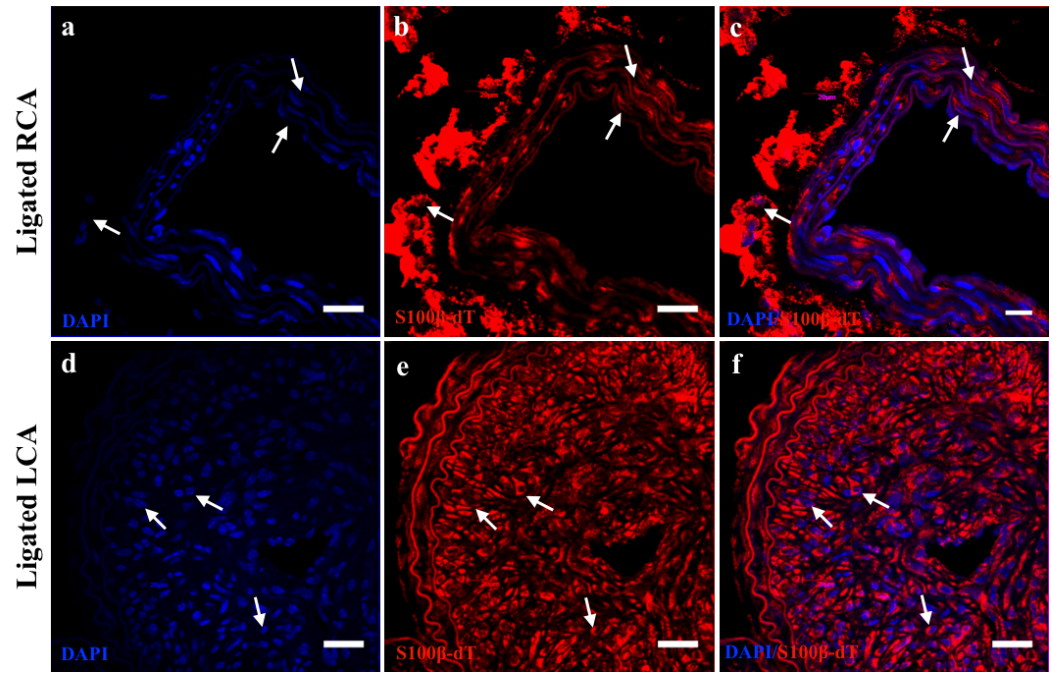

Figure 3.9. S100β-tdTomato expression in RCA and LCA of ligated S100β-EGFP/cre/ERT2/ROSA26RtdTomato transgenic mice after 21 days that were pre-treated with tamoxifen for 5 days prior to ligation after 2 weeks.

Animals were subjected to complete ligation of the left carotid artery, and analysis was carried out 21 days post-intervention.

(A) Cross-sections of **(a-c)** RCA (control) and **(d-f)** LCA. Representative images of **(a, d)** DAPI nuclear staining, **(b, e)** S100β-tdTomato (S100β-tdT) expression and **(c, f)** composite merged images. White arrows indicate S100β^{+} cells. Scale bars, 20 μm.

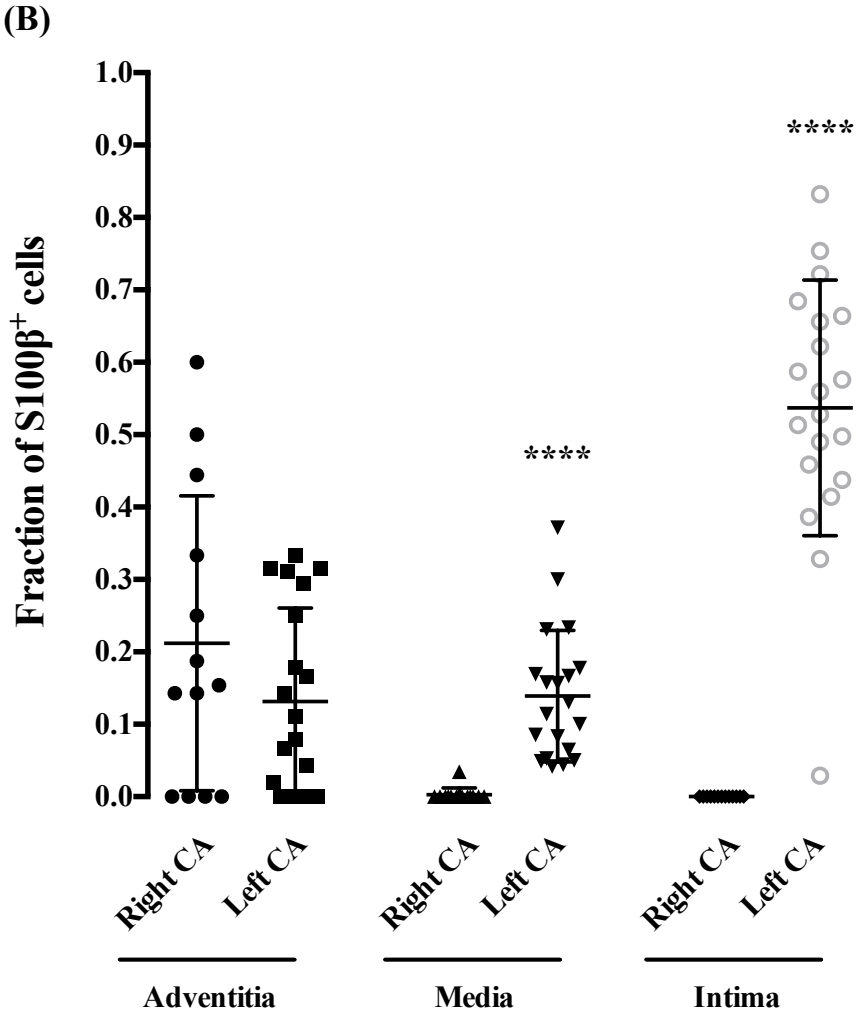

Figure 3.9. S100β-tdTomato expression in RCA and LCA of ligated S100β-EGFP/cre/ERT2/ROSA26R^{tdTomato} transgenic mice after 21 days that were pre-treated with tamoxifen for 5 days prior to ligation after 2 weeks.

(B) Fraction of S100β-tdT^{+} cells in each layer. Adventitia (A), Media (M) and Intima (I). The data compared the fraction of S100β-tdT^{+} cells in the right carotid artery (Right CA) and left carotid artery (Left CA) of the same ligated animal in each group as average ± S.D. (RCA n = 2 and LCA n = 3). All layer comparisons made to corresponding Right CA layer. Mann-Whitney t-test with significance value of P≤0.05. Results: **** p<0.0001.

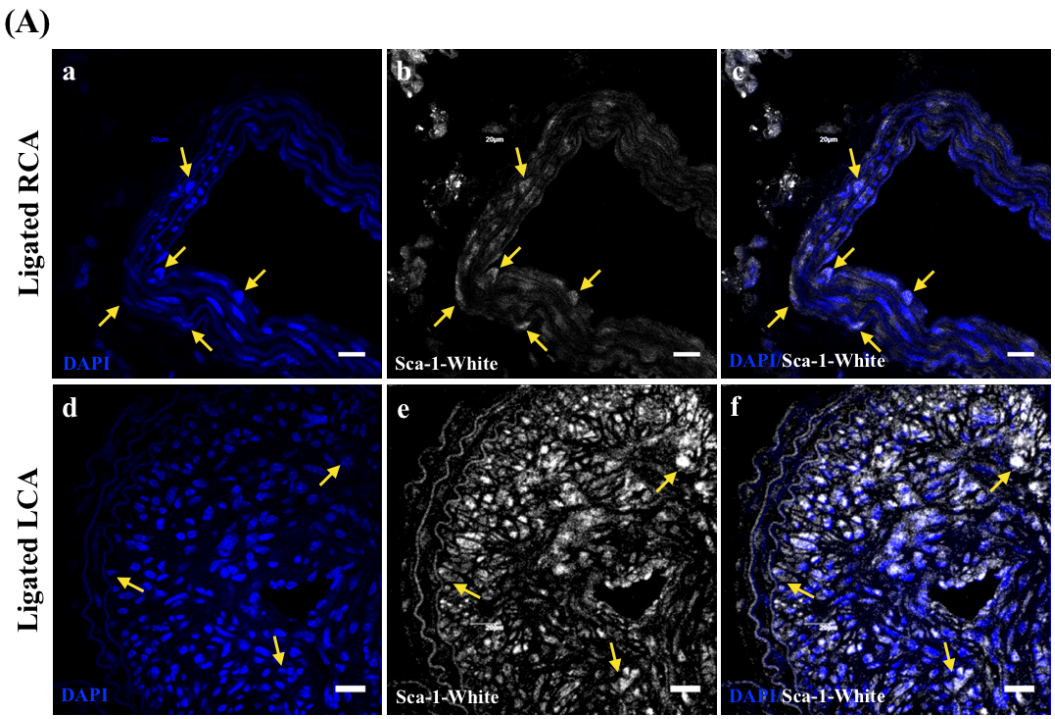

Figure 3.10. Profile of Sca-1+ cells in RCA and LCA of ligated S100β-EGFP/cre/ERT2/ROSA26RtdTomato transgenic mice after 21 days that were pre-treated with tamoxifen for 5 days prior to ligation after 2 weeks.

Animals were subjected to complete ligation of the LCA and analysis was carried out 21 days post-ligation.

(A) Cross-sections of (**a-c)** RCA (control) and (**d-f)** LCA were immuno-stained with an anti-Sca-1 antibody (white). Representative images of **(a, d)** DAPI nuclear staining **(d, e)** Sca-1-white expression and **(c, f)** composite merged images. Yellow arrows indicate Sca-1^{+} cells. Scale bars, 20 μm.

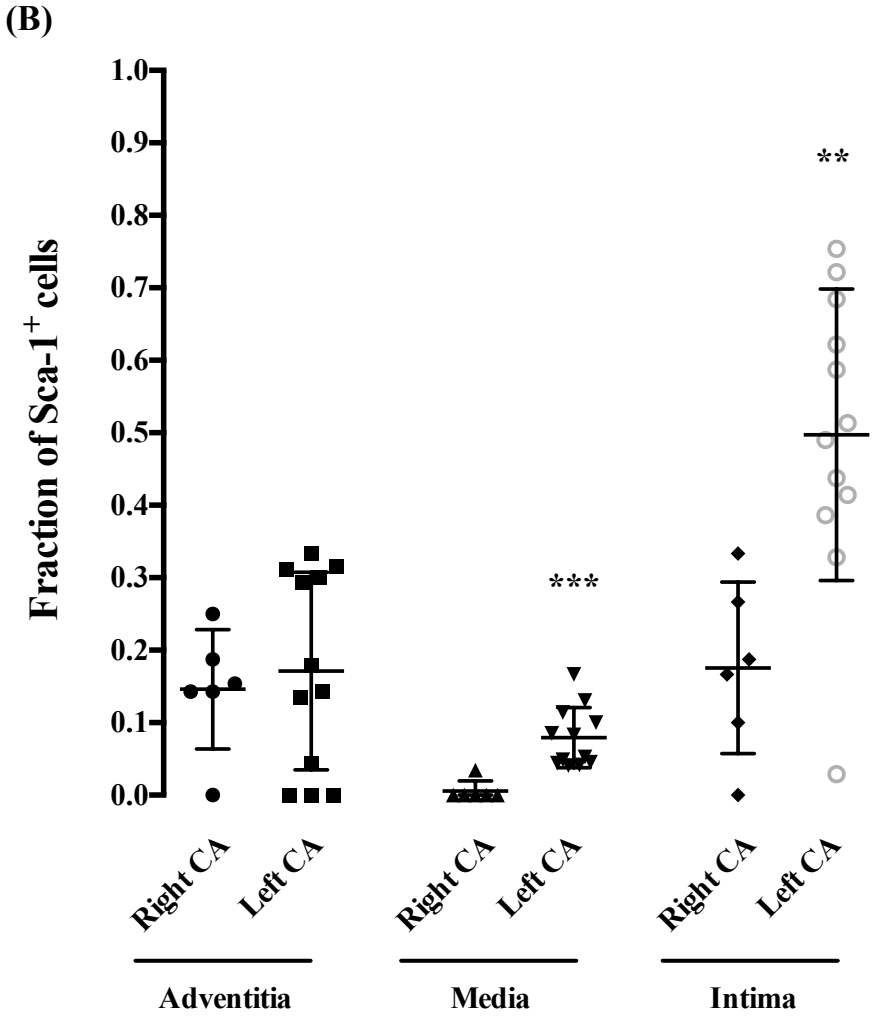

Figure 3.10. Profile of Sca-1$^+$ cells in RCA and LCA of ligated S100β-EGFP/cre/ERT2/ROSA26R^{tdTomato} transgenic mice after 21 days that were pre-treated with tamoxifen for 5 days prior to ligation after 2 weeks.

(B) Fraction of Sca-1$^+$ cells (white) in each layer. Adventitia (A), Media (M) and Intima (I). The data compared he fraction of Sca-1$^+$ cells (white) in the right carotid artery (Right CA) and left carotid artery (Left CA) of the same ligated animals in each group as average ± S.D. (RCA n = 2 and LCA n = 3). All layer comparisons made to corresponding Right CA layer. Mann-Whitney t-test with significance value of P≤0.05. Results: ** p<0.001 and *** p=0.0001.

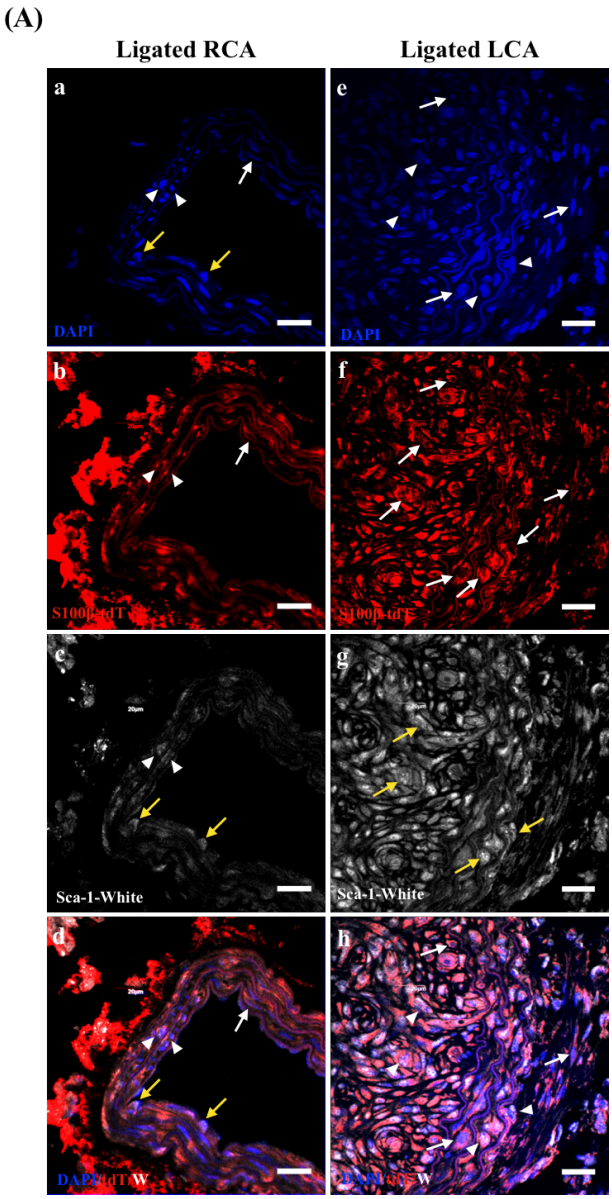

Figure 3.11. Co-localisation of S100β-tdT+ and Sca-1+ cells in RCA and LCA of ligated S100β-EGFP/cre/ERT2/ROSA26RtdTomato transgenic mice after 21 days that were pre-treated with tamoxifen for 5 days prior to ligation after 2 weeks.

Animals were subjected to complete ligation of the LCA and analysis was carried out 21 days post-ligation. **(A)** Cross-sections of **(a-d)** right carotid artery (RCA, control) and **(e-h)** left carotid artery (LCA) of ligated animals. Representative images after immunohistochemical analysis of vessels with anti-Sca-1 antibody (white) and anti-tdT antibodies. Representative images of **(a, e)** DAPI nuclear staining, **(b, f)** S100β-tdTomato (tdT) expression, **(c, g)** Sca-1-white expression (W) expression and **(d, h)** composite merged mages. White or yellow arrows indicate S100β^{+} or Sca-1^{+} cells, respectively. Arrowheads indicate double-positive (Sca-1^{+}/S100β^{+}) cells. Scale bars, 20μm.

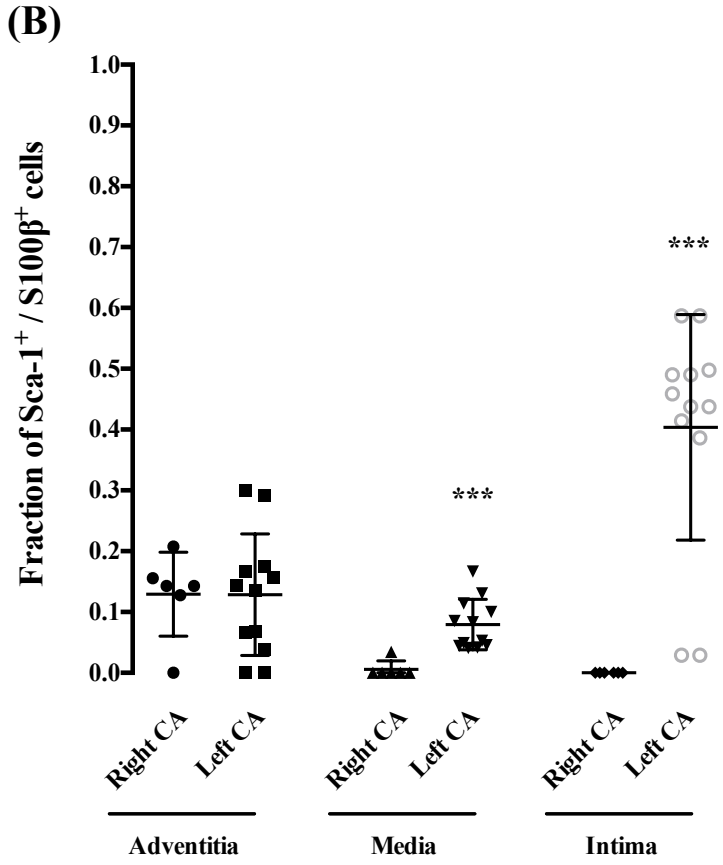

Figure 3.11. Co-localisation of S100β-tdT+ and Sca-1+ cells in RCA and LCA of ligated S100β-EGFP/cre/ERT2/ROSA26RtdTomato transgenic mice after 21 days that were pre-treated with tamoxifen for 5 days prior to ligation after 2 weeks.

Animals were subjected to complete ligation of the LCA and analysis was carried out 21 days post-ligation. **(B)** Fraction of DAPI nuclei that were Sca-1$^+$/ S100β$^+$ positive cells. The data compared the right carotid artery (Right CA) and left carotid artery (Left CA) of the same ligated animals in each group as average ± S.D. (RCA n = 2 and LCA n = 3). All layer comparisons made to corresponding Right CA layer. Mann-Whitney t-test with significance value of P≤0.05. Results: *** p=0.0001.

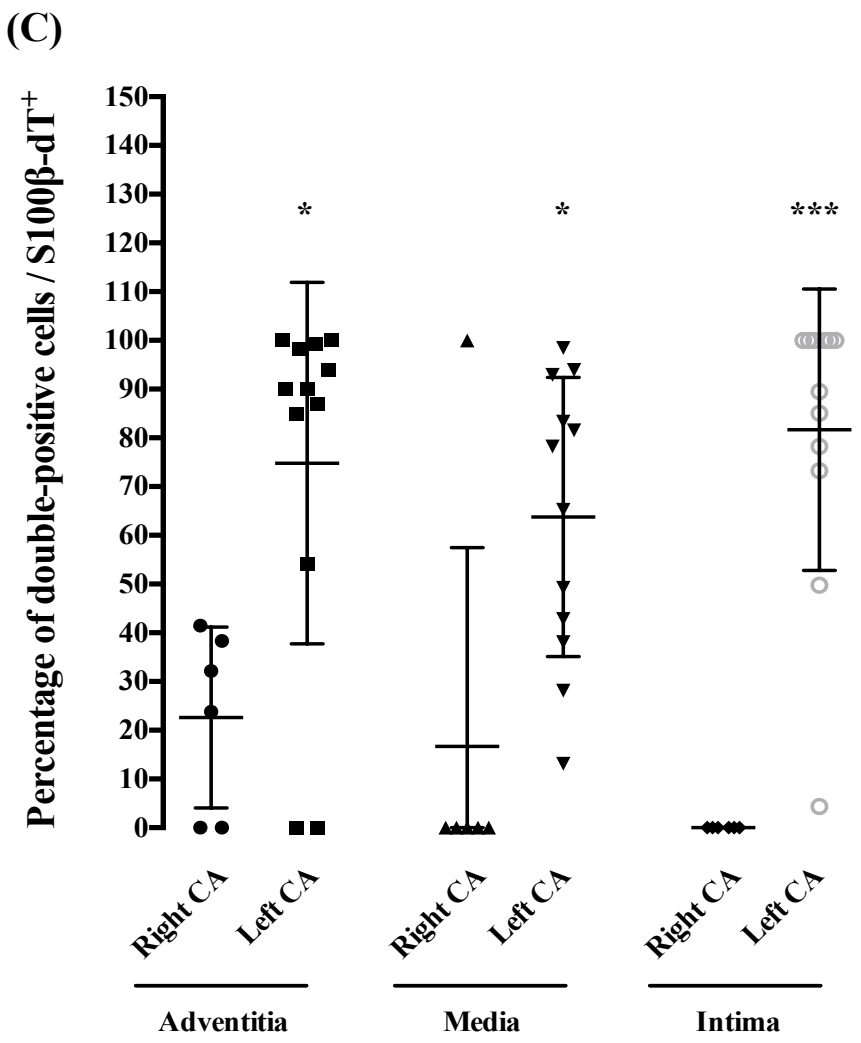

Figure 3.11. Co-localisation of S100β-tdT+ and Sca-1+ cells in RCA and LCA of ligated S100β-EGFP/cre/ERT2/ROSA26RtdTomato transgenic mice after 21 days that were pre-treated with tamoxifen for 5 days prior to ligation after 2 weeks.

Animals were subjected to complete ligation of the LCA and analysis was carried out 21 days post-ligation. **(C)** Percentage of S100β$^+$ cells that were double-positive for S100β$^+$ and Sca-1$^+$ in each layer. Adventitia (A), Media (M) and Intima (I). The data compared the right carotid artery (Right CA) and left carotid artery (Left CA) of the same ligated animals in each group as average ± S.D. (RCA n = 2 and LCA n = 3). All layer comparisons made to corresponding Right CA layer. Mann-Whitney t-test with significance value of P≤0.05. Results: *p<0.05 and ***p=0.0001.

3.3.4 Co-localisation of a αSMA$^+$ cell population with S100β-tdT$^+$ cells in the neointima and media of ligated vessels after injury.

In order to assess whether the fraction of S100β-tdT$^+$ cells from the RCA and LCA in ligated animals were also smooth muscle alpha-actin (alpha-SMA, αSMA) positive, cross sections were co-stained with a monoclonal anti-αSMA antibody (αSMA-white) and images were analysed to determine the fraction of i) DAPI nuclei that were S100β-tdT$^+$, ii) the fraction of DAPI nuclei that were αSMA-white$^+$ cells and iii) the fraction of DAPI nuclei that were αSMA-white$^+$ S100β-tdT$^+$ cells (Section 2.9.3).

The data was assessed in the LCA and the contralateral RCA control of the ligated animals. As before, there was a significant increase in the number of S100β-tdT$^+$ cells in the medial (0.14 ± 0.9 cell fraction) and intimal (0.54 ± 0.18 cell fraction) layers of the LCA of ligated animals when compared to the contralateral RCA control (0.002 ± 0.009 and 0 ± 0, respectively) (Figure 3.12, A and B).

There was no significant change in the fraction of DAPI nuclei that were SMA$^+$ in the LCA when compared to the contralateral RCA control (Figure 3.12, A and C). There were few cells in the media (0.03 ± 0.03) and intima (0.01 ± 0.01) of the LCA that were S100β-tdT$^+$/αSMA$^+$ double stained cells when compared to the contralateral RCA controls (0 ± 0) (Figure 3.12, A and B).

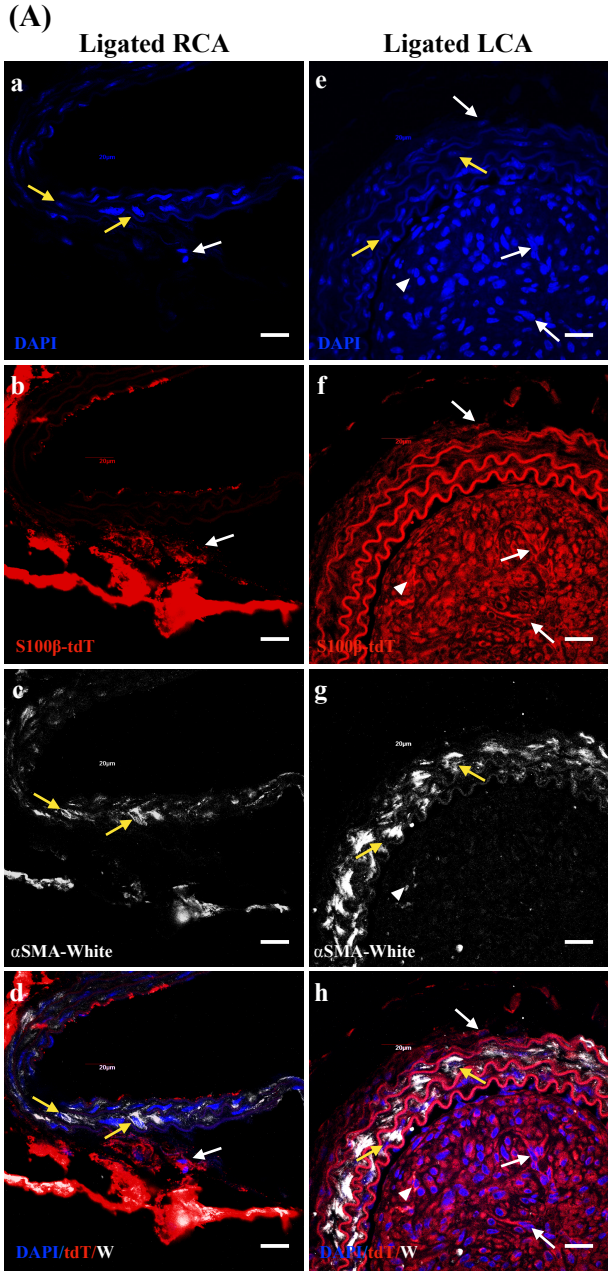

Figure 3.12. Co-localisation of S100β-tdT+ and alpha-SMA+ cells in RCA and LCA of ligated S100β-EGFP/cre/ERT2/ROSA26RtdTomato transgenic mice after 21 days that were pre-treated with tamoxifen for 5 days prior to ligation after 2 weeks.

Animals were subjected to complete ligation of LCA and analysis was carried out 21 days post-ligation. **(A)** Cross-sections of **(a-d)** RCA (control) and **(e-h)** LCA of ligated animals were immuno-stained with anti-αSMA. Representative images of **(a, e)** DAPI nuclear staining, **(b, f)** S100β-tdTomato (tdT) expression, **(c, g)** αSMA-White (W) and **(d, h)** composite merged images. White or yellow arrows indicate $S100\beta^{+}$ or αSMA^{+} cells, respectively. Arrowheads indicate double-positive ($\alpha SMA^{+}/S100\beta^{+}$) cells. Scale bars, 20µm.

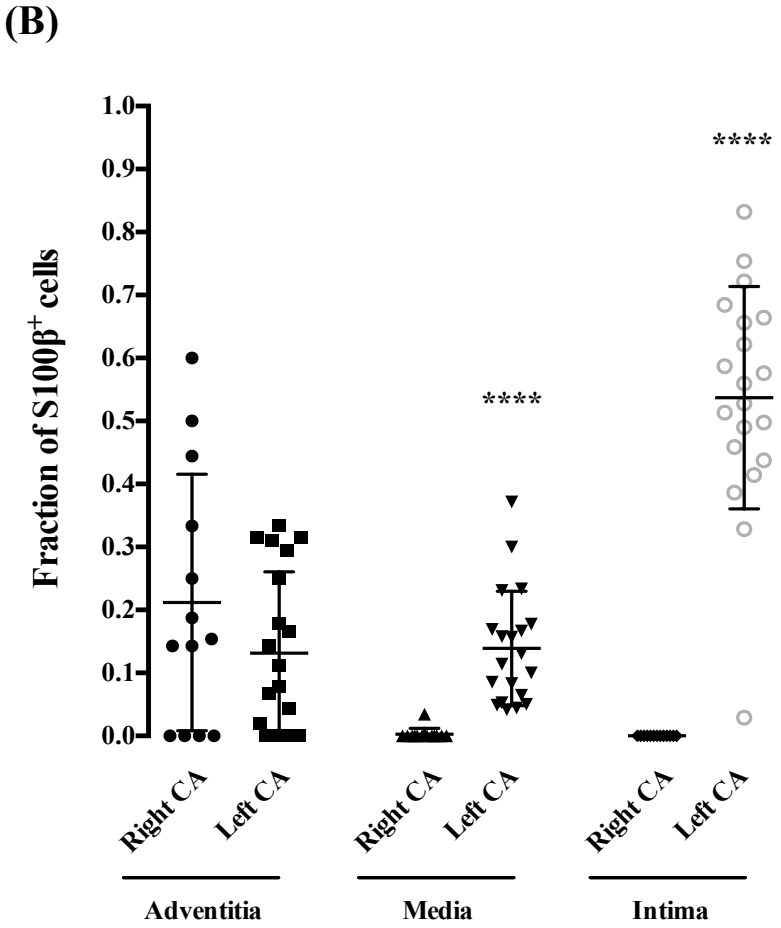

Figure 3.12. Co-localisation of S100β-tdT+ and alpha-SMA+ cells in RCA and LCA of ligated S100β-EGFP/cre/ERT2/ROSA26RtdTomato transgenic mice after 21 days that were pre-treated with tamoxifen for 5 days prior to ligation after 2 weeks.

Animals were subjected to complete ligation of LCA and analysis was carried out 21 days post-ligation. **(B)** Fraction of DAPI nuclei that were S100β-tdT$^+$ in each layer. Adventitia (A), Media (M) and Intima (I). The data compared right carotid artery (Right CA) and left carotid artery (Left CA) of the same ligated animals in each group as average ± S.D. (RCA n = 2 and LCA n = 3). All layer comparisons made to corresponding Right CA layer. All layer comparisons made to corresponding Right CA layer. Mann-Whitney t-test with significance value of P≤0.05. Results: **** p<0.0001.

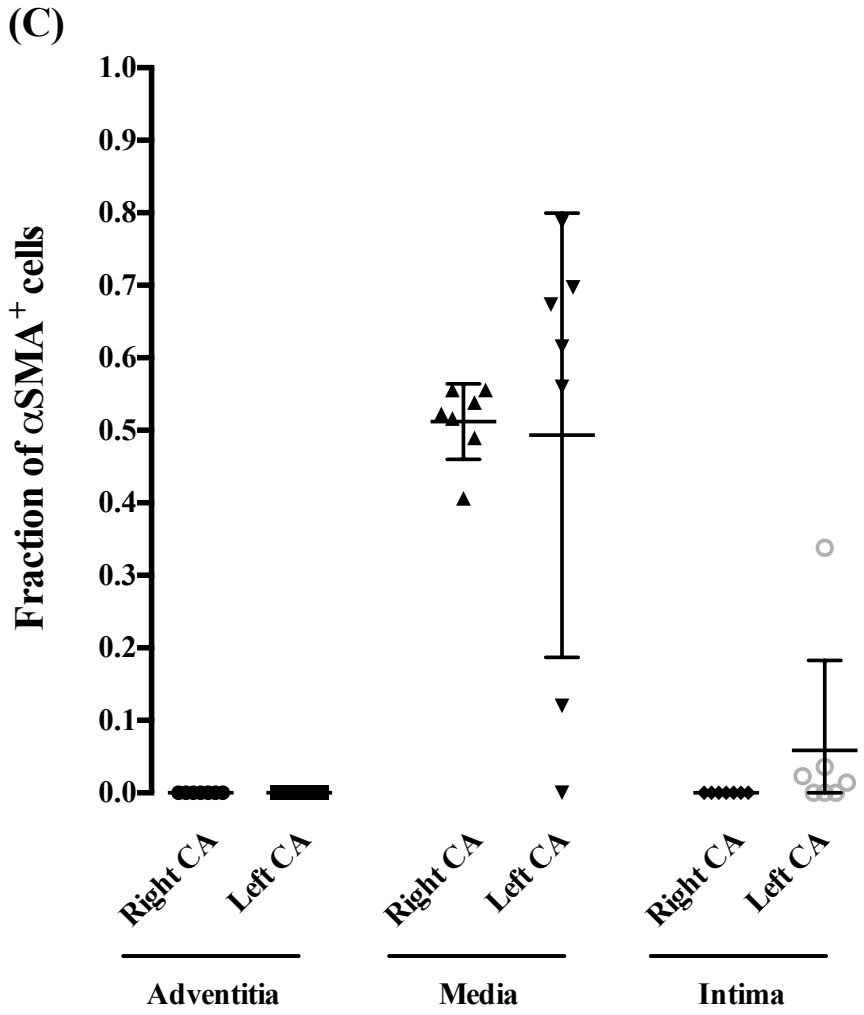

Figure 3.12. Co-localisation of S100β-tdT+ and alpha-SMA+ cells in RCA and LCA of ligated S100β-EGFP/cre/ERT2/ROSA26RtdTomato transgenic mice after 21 days that were pre-treated with tamoxifen for 5 days prior to ligation after 2 weeks.

Animals were subjected to complete ligation of LCA and analysis was carried out 21 days post-ligation. **(C)** Fraction of DAPI nuclei that were αSMA^+ in each layer. Adventitia (A), Media (M) and Intima (I). The data compared right carotid artery (Right CA) and left carotid artery (Left CA) of the same ligated animals in each group as average ± S.D. (RCA n = 2 and LCA n = 2). All layer comparisons made to corresponding Right CA layer. Mann-Whitney t-test with significance value of $P \leq 0.05$. Results: * $p<0.05$.

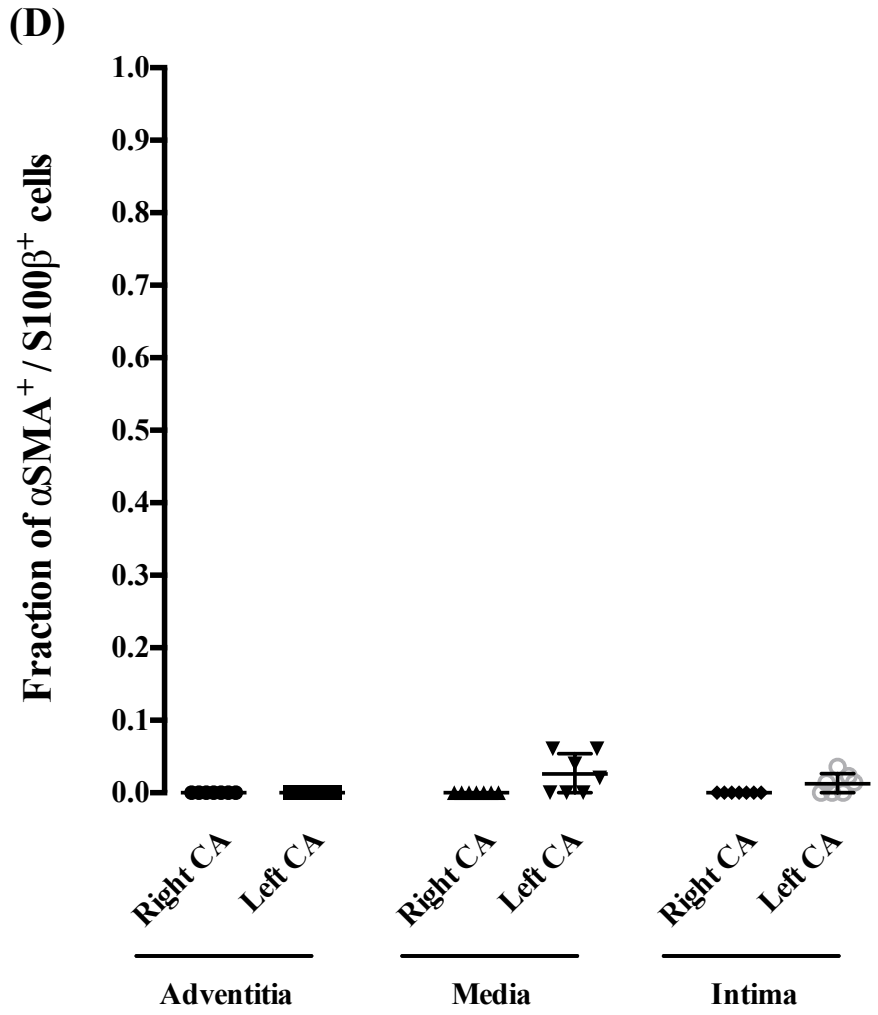

Figure 3.12. Co-localisation of S100β-tdT+ and alpha-SMA+ cells in RCA and LCA of ligated S100β-EGFP/cre/ERT2/ROSA26RtdTomato transgenic mice after 21 days that were pre-treated with tamoxifen for 5 days prior to ligation after 2 weeks.

Animals were subjected to complete ligation of LCA and analysis was carried out 21 days post-ligation. **(D)** Fraction of DAPI nuclei that were S100β-tdT$^+$/αSMA$^+$ in each layer Adventitia (A), Media (M) and Intima (I). The data compared right carotid artery (Right CA) and left carotid artery (Left CA) of the same ligated animals in each group as average ± S.D. (RCA n = 2 and LCA n = 2). All layer comparisons made to corresponding Right CA layer. Mann-Whitney t-test with significance value of P≤0.05.

3.3.5 Summary

- Sca-1-EGFP$^+$ and S100β-EGFP$^+$ cells were predominantly found within the adventitial layer of sham animals RCA and LCA. Only a few S100β-EGFP$^+$ cells were present in the tunica media and 10-20% Sca-1-EGFP$^+$ cells were present in the intima (endothelium). However, Sca-1-EGFP$^+$ and S100β-EGFP$^+$ cells were abundantly present in the neointima of LCA vessels when compared to sham and the contralateral RCA control.
- Lineage tracing analysis of marked S100β-tdT$^+$ cells confirmed that >50% of neointimal cells in the LCA were derived from a S100β-tdT$^+$ cell and that the majority of these cells were S100β (S100β-EGFP$^+$) and Sca1 (Sca-1-EGFP$^+$) positive. Therefore, S100β$^+$ stem cells were a modest population within the vessel wall before injury, primarily within the adventitia, but then rapidly expanded after injury becoming a major source of neointimal cells.
- The fraction of S100β-tdT$^+$ cells that were Sca-1$^+$ was significantly higher in the adventitia, medial and intimal layers of LCA vessels when compared to the contralateral RCA controls.
- While there was a large number of double positive (S100β-tdT$^+$Sca-1$^+$) cells within the neointima at 21 days post-ligation, the S100β stem cell population were not the only source of Sca-1$^+$ cells found in the lesion ruling out the possibility of a single stem cell progenitor contributing to the heterogenous neointima.
- There was no significant change in the fraction of DAPI nuclei that were SMA$^+$ in the LCA when compared to the contralateral RCA control. The majority of medial cells in the sham LCA and RCA were SMA$^+$ but S100β negative and the fraction of S100β/SMA$^+$ cells in the ligated LCA did not increase after injury.
- There were few cells in the adventitia, media and intima of medial of both the LCA and RCA that were S100β-tdT$^+$/SMA$^+$ double stained cells. Despite this, there was an increase in the fraction of DAPI nuclei that were S100β-tdT$^+$/SMA$^+$ in the LCA when compared to the contralateral RCA control.

3.4 Discussion

Multiple *in vivo* studies have focused on investigating the source of SMCs during vascular remodelling and neointima hyperplasia; however, the data does not always support each other, and thus making it a controversial topic. For many years, it was accepted that mature vascular SMCs were responsible for the SMC-like cells present within vascular lesions. Using fate mapping animal models in combination with the latest injury models of neointima hyperplasia, different authors have supported this paradigm (Section 1.1.12) (Nemenoff et al., 2011; Chappell et al., 2016; Yang et al., 2016; Herring et al., 2014; Shankman et al., 2015; Albarrán-Juárez et al., 2016). Other groups demonstrated the presence of stem/progenitor cells within the arterial wall following injury and concluded that these cells were in part responsible for the cellularisation of the lesion during vascular remodelling and neointima hyperplasia. Tang *et al.* (2012) and others reported the presence of a SM-MHC negative cell in tunica media of carotid arteries *in vivo*. These groups also demonstrated that these cells were capable of undergoing smooth muscle cell transition *in vitro* (Yuan et al., 2017; Tang et al., 2012; Sainz et al., 2006). A Sca-1^{+} stem/progenitor cell was also identified in the adventitial layer of large and medium-sized arteries (Aortic root, and femoral artery) and shown to adopt a SMC, and EC phenotype, *ex vitro* (Hu et al., 2004; Passman et al., 2008). The latter finding was recently expanded by an *in vivo* study that traced the origin of adventitial Sca-1 (AdvSca-1) progenitors. The group reported that a subpopulation of AvdSca-1 cells are derived from vascular smooth muscle cells (Majesky et al., 2017). Endothelial progenitors, bone marrow cells and adventitial mesenchymal stem cells (MSC-likes) have also been reported to be involved in atherosclerosis and neointima thickening (Sata et al., 2002; Cooley, 2004; Chen et al., 2018; Kramann et al., 2016).

The aim of this study was to interrogate normal and injured carotid arteries for the presence of S100β and Sca-1 vascular stem/progenitor cells within the vessel wall and assess their involvement in vascular remodelling and neointima hyperplasia. To achieve this, two transgenic murine models of neointimal formation were employed, namely the inducible S100β-EGFP/cre/ERT2/ROSA26R^{tdTomato} and the Sca-1-EGFP mice and were used in combination with the complete and partial carotid ligation blood-flow cessation injury model, respectively.

Morphometric analysis of normal and injured vessels revealed that carotid arteries undergo vascular remodelling following ligation. Analysis of the cross sections of LCA and RCA and estimation of the volume of adventitial, medial and intimal compartments revealed significant remodelling within the neointima of injured vessels. No significant volumetric changes were observed in the adventitial and medial layers of the ligated arteries, although there was a notable trend towards increased volumes in both compartments. Previous studies from both our group and other researchers confirmed that partial and/or complete carotid artery ligation results in significant intimal, medial and adventitial thickening (Fitzpatrick et al., 2017). One possible reason for this discrepancy may be the reliance on DAPI stained cross sections for this study instead of the more reliable Verhoeff-van Gieson staining of the lamina employed by previous studies. Nevertheless, it is clear from these studies that significant accumulation of neointimal cells prevails following carotid artery ligation leading to increased intimal and decreased luminal volume in these vessels.

The presence of S100β-positive (S100β^{+}) and Sca-1-positive (Sca-1^{+}) cells in normal carotid arteries was confirmed by examining the LCA of sham animals and the contralateral RCA of ligated animals for expression of the EGFP protein using S100β-EGFP/cre/ERT2/ROSA26R^{tdTomato} (in the absence of tamoxifen) and the B6.Cg-Tg(Ly6a-EGFP)G5Dzk/J Sca-1-EGFP transgenic mice. This data clearly demonstrates that S100β^{+} and Sca-1^{+} cells are present predominantly in the adventitial layer of the RCA and LCA prior to injury. Although not significant, it is noted that a few S100β-EGFP-positive (S100β-EGFP^{+}) cell were also present in the medial layer of sham/RCA vessels. This suggests that if S100β cells are present in the medial layer of normal vessels, there are very few and may have been missed due to the sectioning protocol employed. No Sca-1^{+} cells were observed in the medial layer of normal vessels. However, in agreement with previously reported results showing the expression of the Sca-1 marker in intimal endothelial cells of the murine vasculature (Luna, Paez and Cardier, 2004; Pratumvinit et al., 2013; Yu, Song, Wang and Zeng, 2016; Xu et al., 2018), a significant amount of Sca-1-EGFP-positive (Sca-1-EGFP^{+}) cells were present in the intimal endothelium layer of both the RCA and LCA of sham animals (~ 10%).

In injured carotid arteries of S100β-EGFP/cre/ERT2/ROSA26R^{tdTomato} transgenic

mice, the number of S100β-EGFP$^+$ cells increased significantly in all three layers post ligation and this number was highly pronounced in the newly formed intima representing ~ 48% of the entire neointimal cell population. The mean percentage of S100β-EGFP$^+$ cells calculated for the adventitial and medial compartments were also increased at 15.8% and 24.2%, respectively. In parallel studies using B6.Cg-Tg(Ly6a-EGFP)G5Dzk/J Sca-1-EGFP transgenic mice, the number of Sca-1-EGFP$^+$ cells in the neointima of injured vessels was ~ 60%. Moreover, on average 33.5% and 18% of the adventitial and medial cells were Sca-1-EGFP$^+$.

In order to identify the origin of these medial and neointimal S100β$^+$ and Sca-1$^+$ cells in injured vessels, lineage tracing analysis was performed on S100β-EGFP/cre/ERT2/ ROSA26R^{tdTomato} transgenic mice treated with tamoxifen (1x 1 mg/kg) or corn oil (vehicle) for 5 consecutive days prior to ligation to mark the S100β$^+$ and track these cells and their progeny. Cross-sections of RCA and LCA vessels from corn oil treated animals confirmed that no S100β-tdT-positive cells (S100β-tdT$^+$) were present in absence of tamoxifen, indicating that cre-loxp recombination activity was specific to tamoxifen administration ruling out the chance of false positives. Moreover, analysis of the number of S100β-tdT$^+$ cells in the carotid sinus of these animals confirmed that the level of recombination was >90% as all S100β$^+$ cells in the neurons were marked following tamoxifen treatment for 5 days. Similarly, the level of recombination was high in sham LCA and ligated RCA vessels since the percentage of adventitial S100β cells that were marked as S100β-tdT$^+$ was a comparable percentage to the adventitial S100β-EGFP$^+$ cells.

Lineage tracing analysis revealed that ~ 50% of the neointimal cells in ligated vessels were S100β-tdT$^+$, indicating that these cells were derived from a pre-existing S100β population. Moreover, as no medial SM-MHC$^+$ SMCs were marked in sham LCA prior to ligation, it can be assumed that these S100β-tdT$^+$ marked neointimal cells did not originate from medial SMCs. In contrast to the neointima, the number of S100β-tdT$^+$ cells present in the media and adventitia comprised ~ 13% of the total cell population. Although it may not appear to be a large increment, it is a significant value when compared to that of the sham LCA and ligated contralateral RCA vessels, suggesting

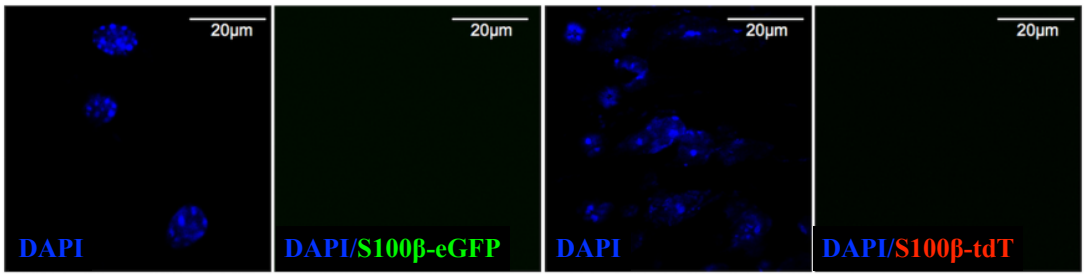

Figure 3.13. S100β-EGFP and S100β-tdTomato expression in bone-marrow.

Bone marrow smears from S100β-EGFP/cre/ERT2/ROSA26R^{tdTomato} transgenic mice treated with tamoxifen for 5 days.

that a small population of marked S100β-tdT+ cells in healthy vessels are responsible for the migrative and proliferative accumulation of cells during disease progression.

Notably, a significant number of double-positive cells for S100β-tdT and S100β-EGFP were present within the lesions suggesting that a large portion of the S100β-EGFP$^+$ cells were derived from a parent S100β-tdT$^+$ cell population. Furthermore, the proportion of S100β-tdT$^+$ cells (~ 50%) was comparable to the number of S100β-EGFP$^+$ cells (~ 48%), suggesting that most S100β-derived cells in the neointima were still expressing S100β and had not yet differentiated to a SMC-like cell. In support of this contention, co-localisation of S100β-tdT$^+$ with αSMA$^+$ cells were low indicating that at least in this model, these cells had not yet become SMC-like cells after 21 days post ligation. Subsequent studies performed at the University of Rochester confirmed that these S100β-tdT$^+$ cells were unlikely to be derived from bone-marrow since no S100β-tdT$^+$ cells were marked in bone-marrow smears (Figure 3.13).

Previous studies have highlighted the putative role of an adventitial Sca-1$^+$ cell population in contributing to the intimal medial thickening after vascular injury (Hu et al., 2004; Passman et al., 2008). These adventitial Sca-1$^+$ cells were capable of undergoing myogenic (SMC) and vasculogenic (EC) differentiation *in vitro* and *in vivo* (Torsney and Xu, 2011). On the other hand, Sainz *et al.* (2006) reported the existence of a small population of Sca-1$^+$ cells present with the tunica media of arteries (~ 6%) and also capable of undergoing myogenic and vasculogenic differentiation *in vitro*

(Sainz et al., 2006). Additionally, Tang *et al.* (2012) provided circumstantial evidence from lineage tracing studies of SM-MHC Cre-LoxP marked SMC cells that neointimal cells of injured vessels were the progeny of a medial SM-MHC^{-}, S100β^{+} vascular cell progenitor capable of myogenic differentiation *in vitro* (Tang et al., 2012). In this study, we revealed the presence of a sparse population of both S100β^{+} and Sca-1^{+} cells within the vessel wall that appear to migrate, proliferate and expand after vascular injury contributing to neointimal formation. In order to investigate whether these two stem cell populations were derived from a single parent population, cross-sections of LCA from injured vessels marked with S100β-tdT^{+} cells were co-stained with an anti-Sca-1-antibody (white) and anti-tdTomato (red). Approximately 88.5% of the Sca-1^{+} (Sca-1-white) cells within the adventitial layer of the RCA contralateral control vessel were positively stained for tdTomato (red) and comprised ~ 22.6% of the entire S100β-tdT^{+} population. These data suggest that the adventitial S100β^{+} and Sca-1^{+} populations are most likely derived from the same population. Isolation and characterisation of these populations *in vitro* should clarify this assumption.

In contrast, ~ 18% of intimal endothelial cells co-stained positive for the Sca-1 marker, in normal vessels but no double-positive (Sca-1^{+}S100β^{+}) cells were observed in the endothelium of normal vessels (RCA of ligated vessels) suggesting that the endothelial Sca-1^{+}/S100β^{-} cells are distinct from the adventitial Sca-1^{+}/S100β^{+} population. In injured vessels, the percentage of DAPI nuclei that were double positive for Sca-1^{+}/S100β-tdT^{+} cells across the tunica layers was calculated as 12.7% in the adventitia, 8% in the media and 40.4% in the intima. With the exception of the tunica media where all of the Sca-1^{+} cells were also S100β^{+}, we found that the proportion of Sca-1^{+}/S100β-tdT^{+} cells over the S100β-tdT^{+} cell population was 74.8% and 81.7% in the adventitia and neointima, respectively. Collectively, these results suggest the presence of a Sca-1^{+}/S100β-tdT^{+} stem cell population residing within the tunica adventitia gives rise to a significant number of neointimal cells.

A recent study by Majesky *et al.* (2017) using SM22α-cre/Rosa26-YFP to indelibly mark SMCs reported that ~ 60% of the AdvSca-1^{+} cells in the aortic arch and carotid arteries were derived SMCs (Majesky et al., 2017) (Section 1.1.12). Data from our study indicates that an additional ~ 12% of the adventitial cells following injury were derived from a parent S100β^{+} stem cell population and the majority of these cells were

positive for Sca-1 suggesting that in addition to SMC derived-progeny, adventitial Sca-1$^+$ cells are also derived from a non-SMC parent. Furthermore, recent studies using multicolour lineage tracing of marked SM-MHC$^+$ SMC cells suggest that the majority of neointimal cells following carotid injury are derived from contractile SMCs as a result of the dedifferentiation of a subpopulation of medial mature SMCs (Chappell et al., 2016). Our data would suggest that in addition to these SMC-derived neointimal lesional cells, a significant proportion of neointimal cells are derived from a non-SMC, S100β$^+$ parent population that resides predominantly in the adventitia but also in the media.

Lastly, cross sections of LCA and RCA from S100β-EGFP/cre/ERT2/ ROSA26R^{tdTomato} transgenic mice were also interrogated for the early smooth muscle cell marker alpha actin (αSMA) using an anti-αSMA-white antibody. In control vessels, the percent of αSMA$^+$ cells in the tunica media was ~ 50% of the entire cell population while ~ 3% of the lesional cells were αSMA$^+$ in the injured vessel. This was unexpected as the number of αSMA$^+$ cells in the medial layer of any vessel in non-transgenic mice is usually near 100%. The data from literature along with findings from our research group have repeatedly reported that the majority of neointima cells are SMC-like αSMA$^+$ cells after vascular injury (Fitzpatrick et al., 2017). Hence, we contend that the immune-staining protocol for the anti-αSMA antibody may have been unsuccessful due to intensive tissue manipulation and/or the majority of neointimal S100β-tdT$^+$ marked cells had not yet undergone myogenic differentiation.

Collectively, using transgenic animal models Sca-1-EGFP and S100β-EGFP and fate-mapping S100β$^+$ cells using S100β-EGFP/cre/ERT2/ROSA26R^{tdTomato} transgenic mice following tamoxifen treatment combined with immunohistochemical analysis of Sca-1 and αSMA, our data supports the hypothesis that a S100β parent resident stem cell population significantly contribute to neointima formation in an injury model of arteriosclerotic disease. Indeed, a large proportion of the S100β-derived cells stained positive for the Sca-1 in both control and ligated vessels. However non-S100β-derived Sca-1$^+$ cells were also found within the various layers, suggesting that the cellular composition of vascular lesions is heterogeneous and different progenitors may contribute to the formation of the neointima.

Chapter 4

S100β^{+} vascular stem/progenitor cells reside in the vessel wall of the aortic arch (athero-susceptible) and thoracic aorta (athero-resistant)

4.1 Introduction

For many years, it was believed that blood vessels were composed of a single smooth muscle cell (SMC) layer embedded within extracellular matrix proteins such as elastin and collagen produced by intramural fibroblasts. In 1979, *in vivo* studies suggested that SMCs possessed two possible phenotypes according to their function, namely contractile and synthetic, but these phenotypes were interchangeable (phenotypic switching) allowing the cells to adopt to variations in the microenvironment (Chung, Schwartz and Murry, 1998). The hypothesis that SMC de-differentiation and phenotypic switching during vascular remodelling and arteriosclerosis has been long considered, the embryological origin of these cells were never questioned as possible predictors to specific vascular pathologies (Owens, 2007)., For instance, during vascular injury such as atherosclerosis, SMC phenotypic switching was predicted to occur within regions of turbulent and pulsatile blood flow such as the aortic arch, whereas aneurism formation was more frequently observed within the aortic abdominal stretch where laminar flow is encountered (Wasilewski, Głowacki and Poloński, 2013). Discrete vascular lesions were then proposed to be site-specific due in part to local vessel haemodynamics, which affect the endothelium structure triggering the expression of modulatory genes responsible for the maintenance of vascular homeostasis in normal physiological vessels (for more information refer to Section 1.1.6/7) (Majesky, 2007; 2003; Sinha, Iyer and Granata, 2014; Rensen, Doevendans and van Eys, 2007; Gammill and Bronner-Fraser, 2003; Chamley-Campbell, Campbell and Ross, 1979; Parameswaran and Tam, 1995; Hao, Gabbiani and Bochaton-Piallat, 2003).

Nowadays, vascular smooth muscle cells (vSMCs) are known to be embryologically diverse. The novel clinical observation by deBakey and Glaeser demonstrated that recurrence of atherosclerosis and survival in different arterial beds including the coronary artery, the branch of the aorta, the abdominal visceral artery and the terminal abdominal aorta is distinctive in response to the same risk factors (e.g. age, diabetes, hypertension, cholesterol) (Debakey et al, 1985). Moreover, an *in vivo* study carried out by Haimovici and Maier suggested that disease development was intrinsic to tissue origin rather than haemodynamic conditions (Haimovici and Maier, 1964). More recently, Trigueros-Motos *et al.* reported a higher expression profile of a range of

Homeobox genes in paraxial mesodermal (PM)-derived SMCs from aortic athero-resistant region (thoracic aorta) than neuroectodermal (NE)-derived SMCs isolated from the susceptible region (aortic arch) (Trigueros-Motos et al., 2013). Trigueros-Motos *et al.* also identified a possible feedback loop between the NF-κB and the HoxA9, where NF-κB DNA-binding activity was significantly higher in the aortic arch and NE-SMCs than in thoracic aorta and PM-SMCs, repressing the expression of HoxA9 (See Section 1.1.7) (Trigueros-Motos et al., 2013). *In vitro* experiments showed that HoxA9 and NF-κB inhibited one another in NE- and PM-SMCs (Section 1.1.7) (Bennett, Sinha and Owens, 2016; Cheung et al., 2012; DeBakey and Glaeser, 2000; Sinha, Iyer and Granata, 2014; Haimovici and Maier, 1964; Trigueros-Motos et al., 2013)

There is considerable evidence suggesting that the embryological origin of cells in vascular pathology may have a significant impact on the way in which they respond to the equivalent stimuli. The data from the lineage tracing analysis outlined in Chapter 3 demonstrated the putative role of S100β^{+} progenitors in contributing to vascular remodelling and intimal thickening after carotid artery ligation. Although, very few S100β^{+} cells were present within the tunica media as previously reported by Tang *et al.* (2012) (Tang et al., 2012), these cells were readily observed within the adventitia. Importantly, lineage tracing analysis of Sox10^{+} cells and their progeny in Sox10-Cre/Rosa26-LacZ transgenic mice revealed the presence of Sox10^{+} cells within the femoral artery before endothelial denudation vascular injury and remodelling (Yuan et al., 2017). Moreover, when aortic vascular cells marked with SM-MHC using Cre-LoxP were isolated by enzymatic digestion and cultured for two weeks, a large number of non-SMC derived proliferating cells stained positive Sox10 (Tang et al., 2012; Yuan et al., 2017; Sainz et al., 2006). This data strongly suggests that vSMCs in culture may be derived from a non-SMC parent cell in low abundance within the vascular media (Yuan et al., 2017). Moreover, previous studies have suggested that SMCs in culture and neointimal cells in vascular lesions *in vivo* retain the histone mark at the SM-MHC locus, namely histone 3 lysine 4 di-methylation (H3K4me2) that is present in aortic SMCs but remains stable following phenotypic switching and de-differentiation of vSMCs *in vitro* (Gomez et al., 2013).

Given these findings we sought to isolate a resident non-SMC S100β^{+} vascular stem

cell population from the medial layer of athero-susceptible and athero-resistant aortic regions by both explant culture and enzymatic digestion with preferential plating. Subsequently, immunocytochemistry, real-time RT-qPCR and Chromatin Immunoprecipitation (ChIP) analysis on stem cell, germline markers and SMC differentiation markers were carried out to characterise these cells and thus compare their developmental embryological origin to that of fresh aortic SMCs. Finally, as some investigators have questioned the protocols for isolating stem cells from medial segments of aortic tissue (Tang, Wang, Wang and Li, 2013; Nguyen et al., 2013), we assessed the efficiency of the enzymatic removal of the adventitia prior to isolation of vascular stem cells by performing immunohistochemistry and scanning electron microscopy (SEM) of the adventitial medial boundary to examine the presence of residual cells on the lamina.

4.2 Strategy

In order to identify a vascular S100β$^+$ stem cell population the following strategy was adopted. Murine vascular cells were isolated from the tunica media of the aortic arch (disease-prone) and the thoracic aorta (disease-resistant) using an enzymatic dispersion protocol adapted from Tang *et al.* (2012) (Tang et al., 2012).

The main objectives of chapter 4 are as follows:

i) To isolate vascular stem cells from murine tunica media of athero-susceptible (aortic arch; neuroectoderm) and athero-resistant (thoracic aorta; paraxial mesoderm) regions using an altered enzymatic dispersion protocol.

ii) To characterize the isolated vascular stem cells (vSCs) from both neuroectodermal (NE), and the paraxial mesodermal (PM) regions of the aorta by immunocytochemistry, real-time RT-qPCR of stem and SMC differentiation markers and Chromatin Immunoprecipitation (ChIP) analysis of stable histone marks.

iii) To determine and compare the embryological origin of the isolated vSCs from both neuroectodermal (NE), and the paraxial mesodermal (PM) regions of the aorta.

iv) To clarify the vessel compartment (adventitial vs medial) where vascular stem cells reside within the athero-susceptible and athero-resistant aortic regions.

4.2.1 Isolate vascular stem cells from the tunica media of murine aortic tissue using an altered enzymatic dispersion protocol

The two isolation protocols (explant and enzymatic dispersion) as described previously (Tang et al., 2012; Kennedy et al., 2014) were adopted as our main techniques. Our group has previously identified and characterized multipotent vascular stem cells (MVSCs) in the medial layer of rat thoracic aortas using explant techniques (Kennedy et al., 2014). It is noted that the same protocol was trialed for adult mice with little success. Therefore, an altered enzymatic dispersion protocol was adapted from previous published work (Zaniboni et al., 2015) and optimized for the isolation of murine stem cells from the athero-susceptible (aortic arch; neuroectoderm) and athero-resistant (thoracic aorta; paraxial mesoderm) aortic region by preferential

plating following enzymatic digestion of aortic medial cells.

4.2.2 Characterize the isolated vascular stem cells (vSCs) from both neuroectodermal (NE), and the paraxial mesodermal (PM) regions of the murine aorta

In order to gain insight into the properties of vascular stem cells (vSCs) derived from mouse aortic tissue, different characterisation methods were utilised to elucidate their stemness and embryonic origin, which may in part dictate their lineage-specific response to common stimuli during disease. In this context, vSCs were interrogated to identify their cell phenotype by examining specific markers associated to stem cells and vascular smooth muscle cells, respectively. Stem cell markers included S100 calcium bind protein β (S100β; glial cell marker), SRY-box 10 (Sox10; neural stem cell marker), SRY-box 17 (Sox17; endodermal and hematopoietic cell marker) and Nestin (NES; neuroectoderm marker) (Tang et al., 2012). Smooth muscle cell markers included smooth muscle myosin heavy chain (SM-MHC; mature smooth muscle cell marker) and Calponin1 (Cnn1; intermediate smooth muscle cell marker) (Campbell et al., 1979).

The likelihood that mAA-vSC and mTA-vSCs are derived from a parent SMC was addressed by determining the stable histone mark, H3K4me2 at the SM-MHC locus as this is known as an exclusive epigenetic signature of SMCs and is maintained even after phenotypic switching (Gomez et al., 2013). Therefore, the origin of vSCs was assessed by determining the levels of both H3K4me2 and the trimethylation of lysine 27 on histone 3 (H3K27me3) mark on the SM-MHC promoter in isolated vSCs and compared to fresh aortic SMC and SMCs in culture.

4.2.3 Compare the embryological origin of the isolated vSCs to that of the resident tissue

Mouse aortic arch and thoracic aortic vascular stem cells (mAA-vSCs and mTA-vSCs respectively) were analysed for their transcript expression levels of markers associated to germ layer specification (neuroectodermal [NE] versus mesodermal [M]) in order to determine their embryological origin. Aortic arch and thoracic aorta tissues as well as commercially available murine established cell lines such as smooth muscle cells

(mSMCs or MOVAS), embryonic cells (mC3Hs), and neuroectodermal stem cells (mNE-4Cs) were used as controls for the specific developmental markers (Section 2.8.1). Markers used included Pair box 6 (Pax6; neural crest marker), T-box transcription factor 6 (Tbx6; paraxial mesodermal marker), Pair box 1 (Pax1; paraxial mesodermal marker), Kinase insert domain receptor (KDR also known as VEGFR2; lateral plate mesodermal marker) and NK2 Homeobox 5 (Nkx2-5; lateral plate mesodermal marker) (Cheung et al., 2012).

4.2.4 Identification of the vascular stem cell niche in the aorta – "tunica media versus tunica adventitia"

According to the results obtained in Chapter 3 of this thesis, few S100β$^+$ or Sca-1$^+$ cells were present within the medial layer of arteries in sham animals (Figure 3.3, Figure 3.4 and Figure 3.5). However, the presence of S100β$^+$ and Sca-1$^+$ cells in the vessel was more frequently observed within the adventitial layer (Figure 3.3, Figure 3.4 and Figure 3.5). Furthermore, investigators have questioned the protocols for isolating stem cells from medial segments of aortic tissue suggesting that they may in fact be derived from the adventitial layer (Tang et al., 2013; Nguyen et al., 2013). Given this finding, whole aortas were harvested, and the adventitial layer removed intact using a collagenase solution (Section 2.8.1, Table 2-19). Aortic tissues were prepared for i) histochemical analysis and nuclear staining only (DAPI) (Section 2.9.3.2) and ii) scanning electron microscopy (S.E.M.) interrogation (Section 2.7) of the external lamina in order to determine whether adventitial cells remain within the medial/adventitial boundary at the external elastic lamina.

4.2.5 Methodology

In order to facilitate a clear understanding of the proceeding results, a brief summary of the steps taken within this study is presented below. Briefly, cells were analysed for stem cell markers, SMC markers and enrichment of stable histone marks, (histone 3 lysine 4 di-methylation - H3K4me2) for SMCs (Gomez et al., 2013), (histone 3 lysine 27 tri-methylation - H3K27me3) for stem cells (Gaydos et al., 2014) and the DNA binding of (Tet methylcytosine dioxygenase 2 - TET-2), a de-methylase strongly associated with SMC differentiation (Liu et al., 2013) at the SM-MHC locus by ChIP-PCR analysis. For full protocols refer to Materials and Methods Section, Chapter 2, as

referenced below.

i) *Isolation of vascular non-SMC stem cell progenitors (Section 2.8.1)* – A modified Enzymatic Dissociation Method was used to isolate vascular non-SMC stem cells.

ii) *Expansion and maintenance of isolated stem cells (Section 2.8.1 & 2.8.2)* – isolated cells were cultured and expanded in a neuroectodermal maintenance medium (NE-MM) published previously (Tang et al., 2012). Cells were healthy and proliferative when seeded at a cell density of 1 x 10^4 cells per cm^2 or higher, otherwise their replication rate was slow and, in some cases, they stopped growing. Feeding was carried out every 3-4 days. The seeding efficiency was ~ 15-20%.

iii) *Usage of commercial cell lines (Section 2.9.1) and aortic tissues* – Commercial cell lines were grown and maintained as per the manufacturer's recommendations. Mouse neuroectodermal cells (mNE-4Cs) and embryonic mesenchymal fibroblast cells (mC3H-10T1/2) were chosen to control for the expression of neuroectodermal and mesodermal specific genes, respectively. The murine smooth muscle cell line and the aortic tissue samples represented negative controls for all the stem cell genes but positive for the smooth muscle cell transcripts.

iv) *Immunocytochemical analysis of stem cell and SMC markers (Section 2.5)* –1° Abs were used to interrogate vSCs against the following phenotypic markers S100β, SOX10, SOX17, NES, SCA-1, SM-MHC, and CNN1 to determine the levels of stem cell and SMC specific markers, respectively. All images were taken and compiled using Olympus BX51 Fluorescence Microscope and Cell^F Multi-fluorescence and Imaging Software.

v) *Chromatin Immunoprecipitation (ChIP) followed by real time PCR (ChIP-PCR) (Section 2.4)* – DNA samples were immunoprecipitated with anti-H3K4me2, H3K27me3 and TET-2 before real-time PCR was performed using a primer pair specific for the CpG island regions of the smooth muscle myosin heavy chain (SM-MHC) promoter. Fold enrichment of the histone modifications and TET-2 binding at the SM-MHC gene was calculated using Ct values obtained from PCR analysis.

vi) *Gene expression analysis by real time RT-qPCR (Section 2.3)* – Relative quantification of mRNA expression was performed on vSCs using specific primers for the following transcripts, S100β, Sox10, NES, Pax6, Tbx6, Pax1, Nkx2.5, KDR, Cnn1, and SM-MHC to determine the levels of stem cell and SMC specific

markers.

vii) *Immunohistochemistry (IHC) (Section 2.9.3.2)* – Briefly, tissues were sectioned at 5 μm using a microtome and placed on SuperFrost™ glass slides for analysis and interrogated for the presence of cells on the external elastic lamina using the Olympus BX51 Fluorescence Microscope and Cell^{F} Multi-fluorescence and Imaging Software.

viii) *Scanning Electron Microscopy (S.E.M.) (Section 2.7)* – Briefly, mouse aortas without adventitia were fixed, dehydrated and immersed in HDMS followed by mounting on S.E.M. stubs and gold coated using the Edwards Pirani 501 Scancoat Sputtering Coater (Edwards Laboratories, USA). The specimens were subsequently examined for the presence of cells on the external elastic lamina. All images were taken and compiled using EVO LS15 Scanning Electron Microscope (Zeiss, Germany).

Overall, this chapter will determine existence of a non-SMC cell progenitor within the vessel wall of the aortic artery *in vitro*. As demonstrated in Chapter 3 of this thesis by fate-cell mapping, a large number of the lesional cells were derived from a S100β^{+} stem cell present in the vessel wall thus contributing to neointima hyperplasia. We believe that a complete understanding of the molecular mechanisms and protein and mRNA expression profiles is key in the treatment of this stem cell disease.

4.3 Results

4.3.1 Isolation of vascular stem cells from the tunica media of murine aortic tissue

Using an optimised enzymatic cell dissociation technique (Section 2.8.1), vSCs from both disease-susceptible (aortic arch - neuroectodermal, NE), and disease-resistant (thoracic aorta - paraxial mesodermal, PM) regions of the murine aorta were successfully isolated (full protocol in Section 2.9.4) using preferential seeding on adherent and non-adherent plates adapted from previous protocols (Tang et al., 2012).

Isolated cells from both NE and PM regions were cultured in NE-MM, expanded following dissociation and routinely passaged several times. The stem cells exhibited a uniform neural-like morphology in low density culture adopting a dendritic-like tree shape and retaining their morphological characteristics at low density throughout repeated passage (Figure 4.1).

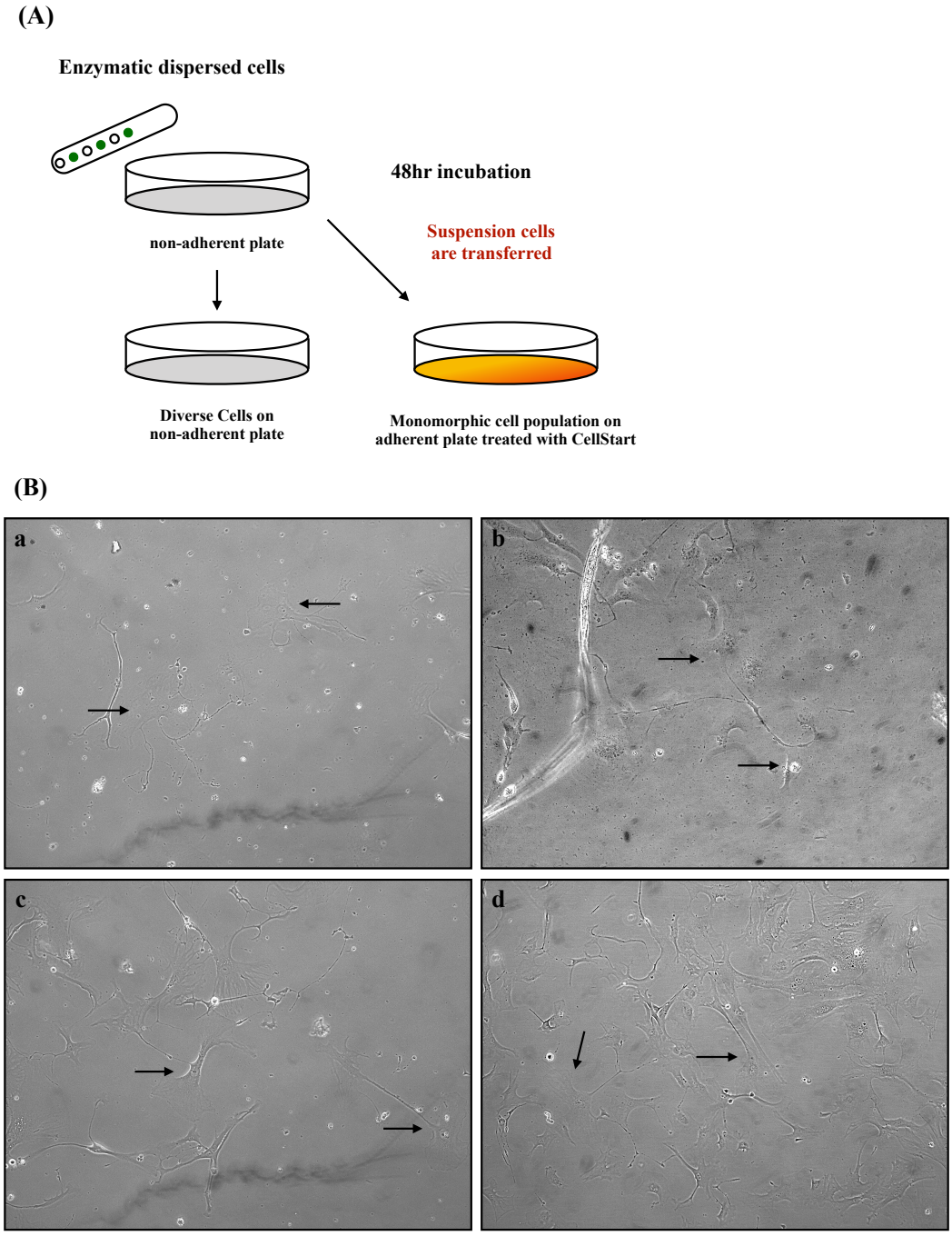

Figure 4.1. Enzymatic dissociation and expansion of murine vascular stem cells (vSCs) isolated from aortic arch and thoracic aorta.

(A) Schematic illustration of modified protocol for enzymatic dissociation and expansion of vSCs (Section 2.8). **(B)** Primary vascular stem cells isolated from the tunica media of aortic arch **(a, c)** and thoracic aorta **(b, d)** and grown in NE-MM after one week **(a, b)** and two weeks **(c, d)** in culture. Arrows indicates a neuron-like morphology.

4.3.2 Characterization of isolated stem cells from the tunica media of murine aortic tissue

Mouse vascular stem cells (vSCs) from the tunica media of the aortic neuroectodermal (NE) and paraxial mesodermal (PM) regions were isolated by the modified enzymatic dissociation technique as described in Section 2.8.1.

Firstly, vSCs isolated from aortic arch (mAA-vSCs) and thoracic aorta (mTA-vSCs) were evaluated for their S100β and Sca-1 expression by Flow cytometry (FACS). Both vSCs showed positive expression of the S100β and Sca-1 markers when compared to endogenous control samples (IgG isotype controls) (Figure 4.2, c-f). In order to test the positive expression of S100β and Sca-1 markers, mouse neuroectodermal stem cells (mNE-4Cs) (Figure 4.2, a) and mouse embryonic stem cells (mC3Hs) (Figure 4.2, b) were used as they are known for the expression of the markers, respectively.

The murine vSCs were analysed for the presence of stem/progenitor markers (S100β, NES, SOX10, SOX17, and Sca-1) and smooth muscle cell differentiation markers (CNN1 and SM-MHC) by fluorescent immunocytochemistry as described in Section 2.5. Control experiments were performed with secondary fluorescent IgG antibodies alone and demonstrated minimal background staining (data no shown).

Immunocytochemical analysis for stem cell markers revealed that SOX10 staining was predominantly nuclear whereas the staining pattern for S100β, NES, SOX17, and Sca-1 was predominantly cytoplasmic (Figure 4.3 and 4.4). The majority of murine vSCs from the aortic arch were positive for the stem cell markers S100β, NES, SOX10, SOX17, and Sca-1 but negative for SMC differentiation markers, CNN1 and SM-MHC (Figure 4.4). Similarly, murine vSCs from the thoracic aorta were positive for the stem cell markers S100β, NES, SOX10, SOX17, and Sca-1 but negative for SMC differentiation markers, CNN1 and SM-MHC (Figure 4.3).

Murine vSCs were also examined for enrichment of specific histone marks on the SM-MHC promoter and compared to those of fresh aortic tissue, mouse smooth muscle cells (mSMCs) and murine embryonic stem cells (mESCs). The origin of the vSCs was determined by examining the stable histone mark, H3K4me2 for SMCs (Gomez et al.,

2013), H3K27me3 for stem cells (Gaydos et al., 2014) and the DNA binding of TET-2, a de-methylase strongly associated with SMC differentiation (Liu et al., 2013) at the SM-MHC locus by ChIP analysis.

Freshly isolated vascular SMCs and murine SMCs in culture were enriched for the stable histone mark, H3K4me2 at the SM-MHC locus concomitant with significant DNA binding of the de-methylase TET-2 to the SM-MHC promoter (Figure 4.5, a and b). However, there was a small enrichment of H3K27me3 at the SM-MHC promoter (Figure 4.5, c and d). In contrast, mESCs and murine vSCs isolated from the aortic arch were enriched for the histone mark, H3K27me3 but not H3K4me2 at the SM-MHC locus while exhibiting little DNA binding of the de-methylase TET-2 to the SM-MHC promoter (Figure 4.5, e and f).

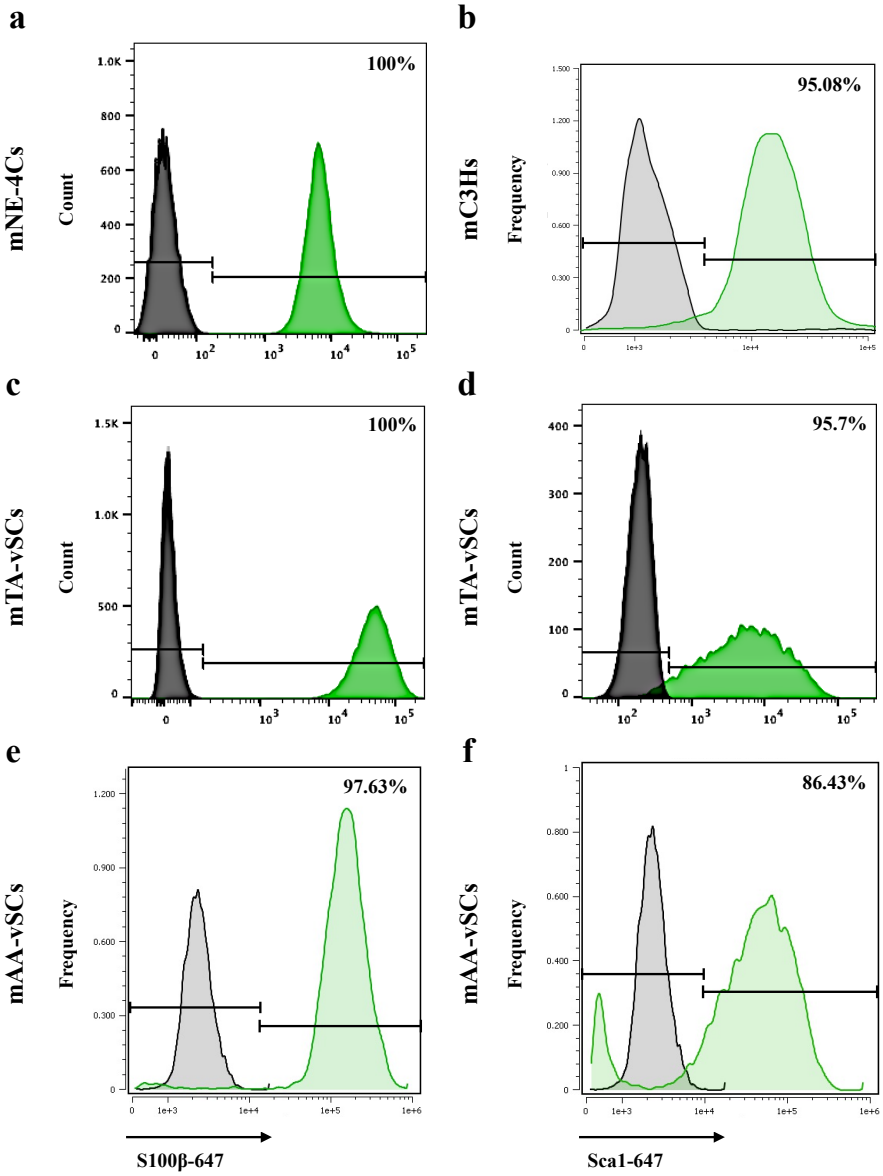

Figure 4.2. Flow Cytometry analysis of murine vSCs isolated from aortic arch (mAA-vSCs) and thoracic aorta (mTA-vSCs).

Flow Cytometry analysis of **(a)** mouse neuroectodermal stem cells (mNE-4C), **(b)** mouse embryonic stem cells (mC3Hs), **(c, d)** mTA-vSCs and **(e, f)** mAA-vSCs cultured in their corresponding maintenance medium was carried out with antibodies against **(a, c, e)** S100β and **(b, d, f)** Sca-1. mNE-4C and mC3Hs samples were prepared as positive controls for S100β and Sca-1 markers, respectively. Samples were probed with their corresponding AlexaFluor-647 secondary antibody. Grey picks are IgG controls whereas Green picks are either anti-S100β or anti-Sca-1. The data in charts **a, c and d** were analysed using FlowJo and it is presented as Counts versus Fluorescence intensity. The data in charts **b, e and f** were analysed by CellStream Sofware and it is presented as Frequency against Fluorescence intensity. The experiment was performed once.

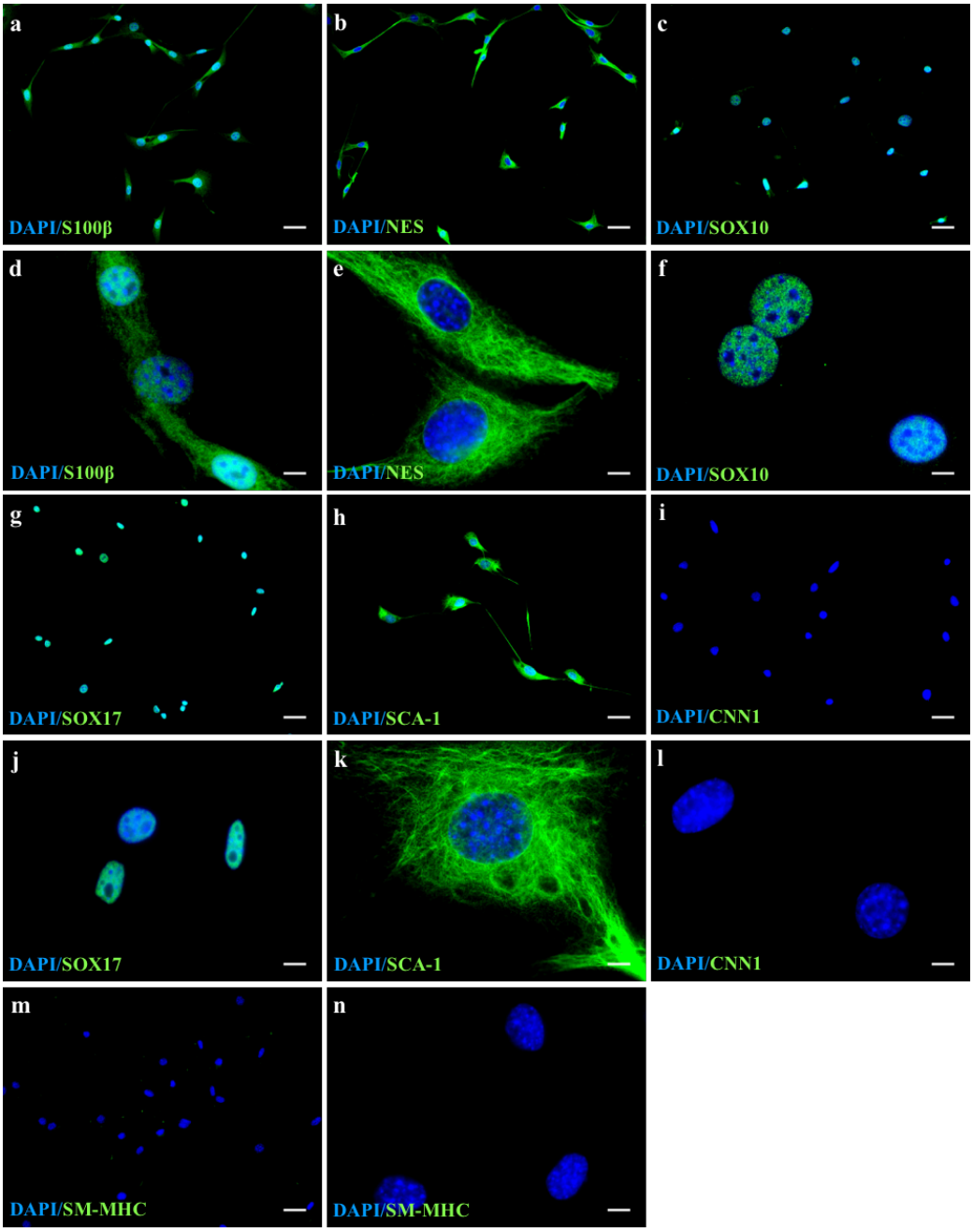

Figure 4.3. Immunocytochemical analysis of murine vSCs isolated from the medial layer of thoracic aorta.

All vSCs were seeded on cover-slips at low density (~1,000cells/well) and cultured in NE-MM for ~3 days. Immunocytochemical analysis was performed as descried in Section 2.5. Representative images of S100β (**a, d**), Nestin (NES) (**b, e**), SOX10 (**c, f**), SOX17 (**g, j**), Sca-1 (**h, k**), Calponin 1 (CNN1) (**I, l**), and smooth muscle myosin heavy chain (SM-MHC) **(m, n)**. Samples were probed with their corresponding AlexaFluor-488 secondary antibody. All images are representative of $n \geq 5$. Scale bars, 20μm.

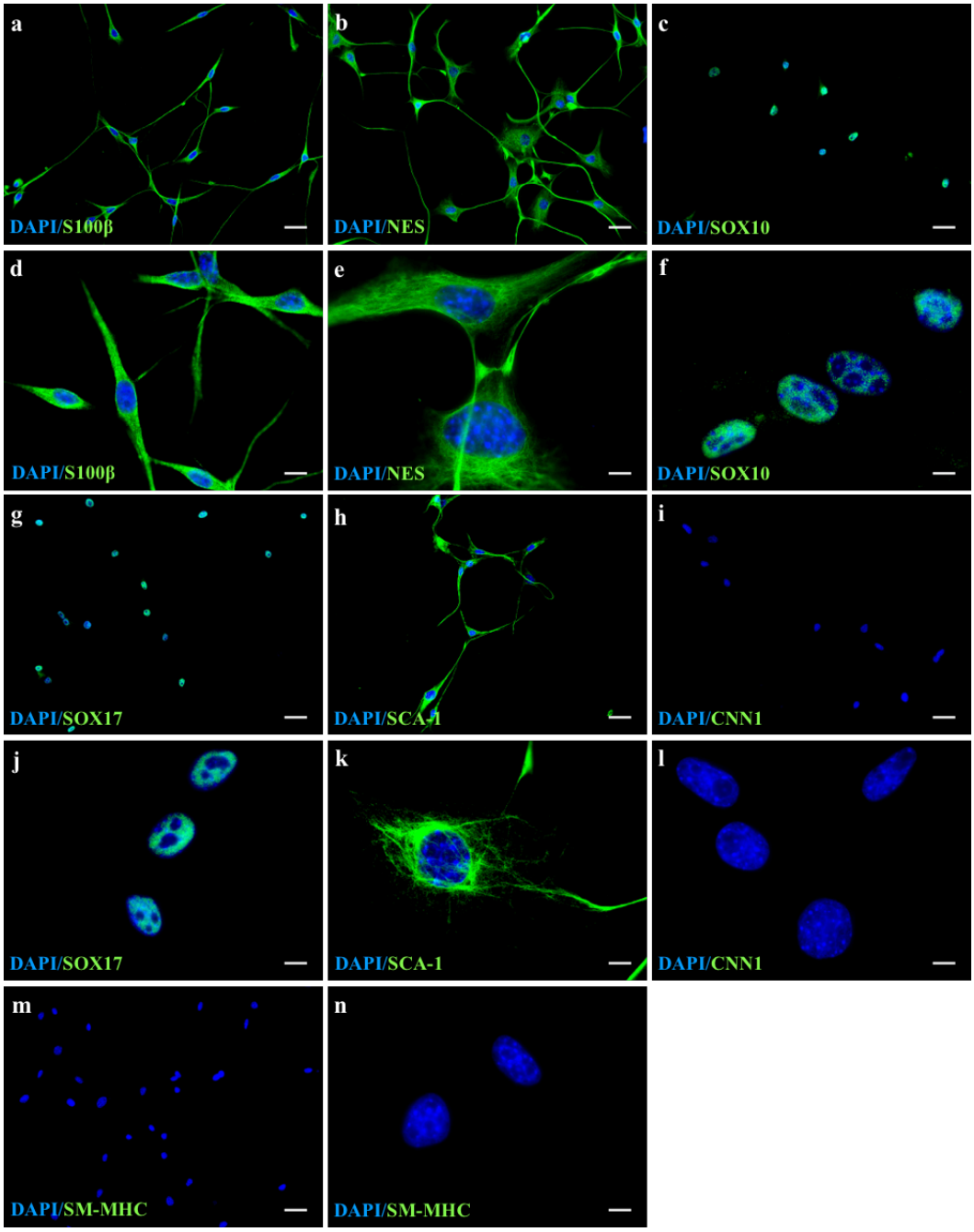

Figure 4.4. Immunocytochemical analysis of murine vSCs isolated from the medial layer aortic arch.

All vSCs were seeded on cover-slips at low density (~1,000cells/well) and cultured in NE-MM for ~3 days. Immunocytochemical analysis was performed as descried in Section 2.5. Representative images of S100β (**a, d)** Nestin (NES) **(b, e),** SOX10 **(c, f)**, SOX17 **(g, j),** Sca-1 (**h, k)** Calponin 1 (CNN1) (**I, l)** and smooth muscle myosin heavy chain (SM-MHC) **(m, n)**. Samples were probed with their corresponding AlexaFluor-488 secondary antibody. All images are representative of $n \geq 5$. Scale bars, 20µm.

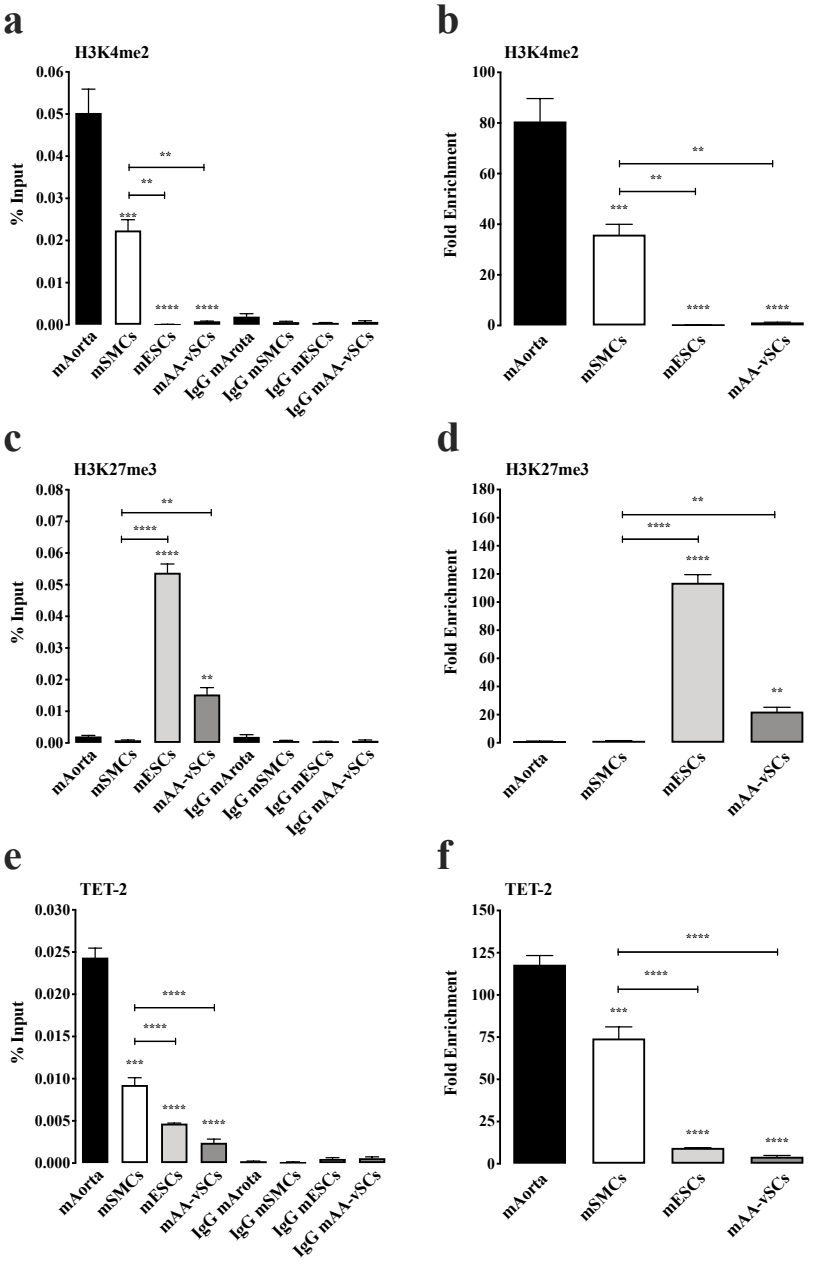

Figure 4.5. ChIP-PCR analysis of mAA-vSCs on H3K4me2, H3K27me27 histone modifications and TET-2 binding at the SM-MHC promoter.

(a, c, e) The % Input and **(b, c, f)** fold enrichment of **(a, b)** dimethylation of lysine 4 on histone 3 (H3K4me2), **(c, d)** trimethylation of lysine 27 on histone 3 (H3K27me3) and **(e, f)** TET-binding in mAA-vSCs at the SM-MHC locus. The experiments were performed in triplicate and are representative of three independent experiments. The experiments were performed in triplicate and are representative of three independent experiments. Data are mean ± S.E.M. (n=3). One-way ANOVA with significance value of P≤0.05. Results: ****p<0.0001. Turkey's test for multiple comparisons with significance value of P≤0.05. Results: ***p<0.001 and ****p<0.0001. Significance are against the control sample (mAorta) unless indicated by a capped line.

4.3.3 Murine stem cells from the tunica media of the aortic arch and thoracic aorta are of a neuroectodermal origin

Murine vSCs from the tunica media of the aortic neuroectodermal (NE) and paraxial mesodermal (PM) regions of the mouse aorta were isolated and characterised as described in Section 4.2.1 and Section 4.2.2. Since the embryological origin of a progenitor cell may be linked to the lineage-specific progeny that drives disease pathology, vSCs from neuroectodermal NE (athero-prone) and paraxial mesodermal PM (athero-resistant aortic regions) were analysed for the relative expression of specific developmental markers of embryological origin (Trigueros-Motos et al., 2013; Bennett, Sinha and Owens, 2016).

During embryogenesis, specification of lateral plate mesoderm and paraxial mesoderm follows a posterior-anterior BMP gradient along the primitive streak (Rivera-Pérez and Hadjantonakis, 2014). We therefore examined vSCs isolated from aortic arch and thoracic aorta for (i) lateral plate markers, KDR and Nkx2-5, (ii) paraxial mesoderm markers; Pax1, TbX6 and (iii) neuroectoderm markers, S100β, Nestin, and Sox 10 by real time RT-qPCR (Cheung et al., 2012). Murine aortic arch and thoracic aorta tissues as well as mouse smooth muscle cells (mSMCs), embryonic mesenchymal fibroblast cells (mC3H/10T1/2), and neuroectodermal stem cells (mNE-4Cs) were used as controls for each comparison (Section 2.8).

The experimental results are presented as follow:

- Mouse aortic arch vascular stem cells - mAA-vSCs,
- Mouse thoracic aortic vascular stem cells - mTA-vSCs,
- Mouse aortic arch tissue - mAA,
- Mouse thoracic aortic tissue - mTA,
- Mouse smooth muscle cells - mSMCs,
- Mouse embryonic mesenchymal fibroblast cells - mC3Hs,
- Mouse neuroectodermal stem cells - mNE-4Cs.

Murine vSCs from both aortic regions were significantly enriched for neuroectodermal markers S100β, Nestin, and Sox 10, respectively when compared to murine thoracic aortic SMCs in culture (Figure 4.6, 4.7 and 4.8). In contrast, vSCs from both regions were not enriched for SMC marker genes, Sm-mhc or Cnn1 unlike the enriched freshly isolated mSMCs from aortic arch (AA) and mSMCs in culture (Figure 4.9 and 4.10).

Murine vSCs from both aortic regions were significantly enriched for the neuroectodermal marker, Pax6 (Figure 4.13) but not for paraxial mesoderm (Pax1, TbX6) and parallel plate mesoderm (KDR and Nkx2-5) markers, respectively when compared to neuroectoderm (mNE-4Cs) and mesoderm (mC3H/10T1/2) cells, respectively (Figure 4.11, 4.12, 4.14 and 4.15).

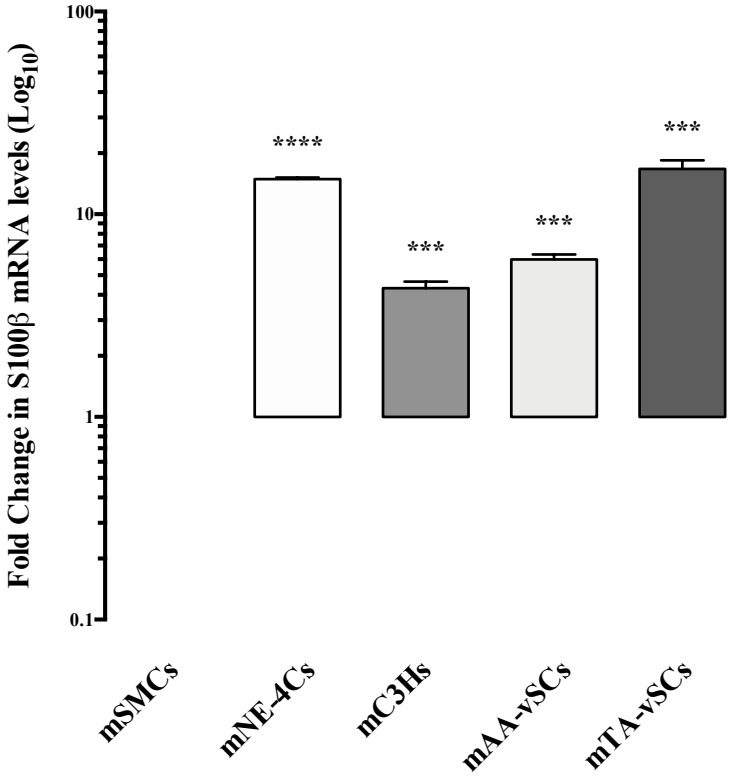

Figure 4.6. Relative S100β mRNA expression levels in mAA-vSCs and mTA-vSCs compared to SMC controls.

RNA samples were prepared using Mini-Columns, and concentrations were measured by NanoDrop instrument. Relative mRNA expression levels of *S100β* was calculated using the Comparative C_T method ($\Delta\Delta C_T$). The data was normalized against the endogenous gene HPRT. Mouse smooth muscle cells (mSMCs), mouse neuroectodermal cells (mNE-4Cs), mouse embryonic cells (mC3Hs), mouse aortic arch tissue (mAA), mouse thoracic aorta tissue (mTA), mouse aortic arch vascular stem cells (mAA-vSCs), and mouse thoracic aortic vascular stem cells (mTA-vSCs). The experiments were performed in triplicate, charts are representatives of three independent experiments. Data are mean ± S.E.M (n=3). One-way ANOVA with significance value of $P \leq 0.05$. Results: ****$p<0.0001$.

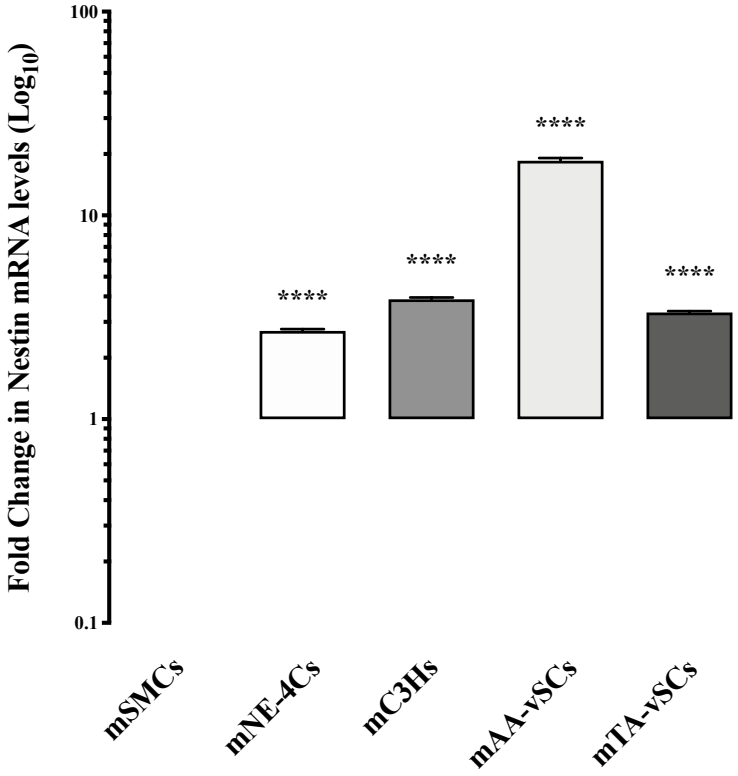

Figure 4.7. Relative Nestin mRNA expression levels in mAA-vSCs and mTA-vSCs compared to SMC controls.

RNA samples were prepared using Mini-Columns, and concentrations were measured by NanoDrop instrument. Relative mRNA expression levels of *S100β* was calculated using the Comparative C_T method ($\Delta\Delta C_T$). The data was normalized against the endogenous gene HPRT. Mouse smooth muscle cells (mSMCs), mouse neuroectodermal cells (mNE-4Cs), mouse embryonic cells (mC3Hs), mouse aortic arch tissue (mAA), mouse thoracic aorta tissue (mTA), mouse aortic arch vascular stem cells (mAA-vSCs), and mouse thoracic aortic vascular stem cells (mTA-vSCs). The experiments were performed in triplicate, charts are representatives of three independent experiments. Data are mean ± S.E.M (n=3). One-way ANOVA with significance value of $P \leq 0.05$. Results: ****$p<0.0001$.

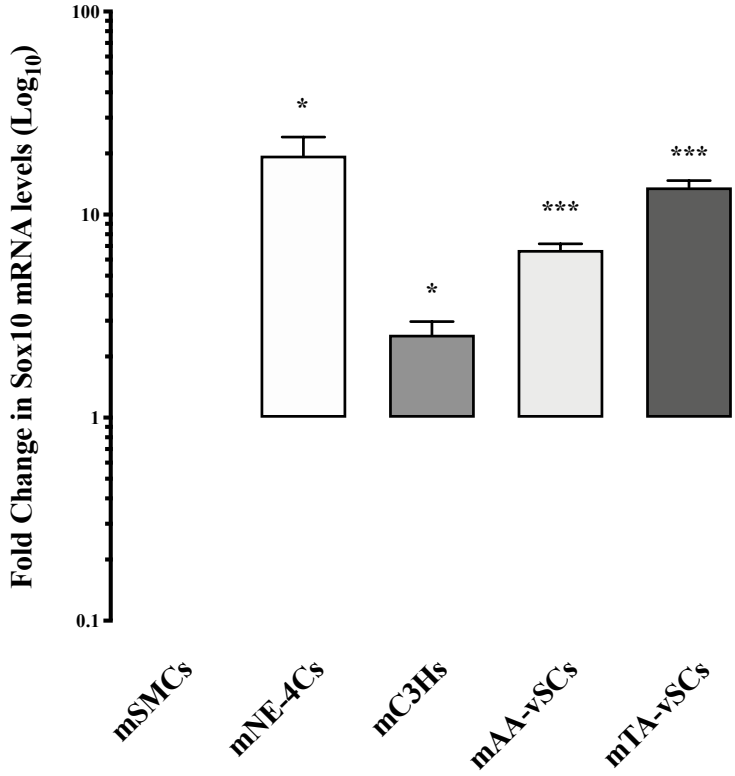

Figure 4.8. Relative Sox10 mRNA expression levels in mAA-vSCs and mTA-vSCs compared to SMC controls.

RNA samples were prepared using Mini-Columns, and concentrations were measured by NanoDrop instrument. Relative mRNA expression levels of *S100β* was calculated using the Comparative C_T method ($\Delta\Delta C_T$). The data was normalized against the endogenous gene HPRT. Mouse smooth muscle cells (mSMCs), mouse neuroectodermal cells (mNE-4Cs), mouse embryonic cells (mC3Hs), mouse aortic arch tissue (mAA), mouse thoracic aorta tissue (mTA), mouse aortic arch vascular stem cells (mAA-vSCs), and mouse thoracic aortic vascular stem cells (mTA-vSCs). The experiments were performed in triplicate, charts are representatives of three independent experiments. Data are mean ± S.E.M (n=3). One-way ANOVA with significance value of $P \leq 0.05$. Results: *$p<0.05$ and ***$p<0.001$.

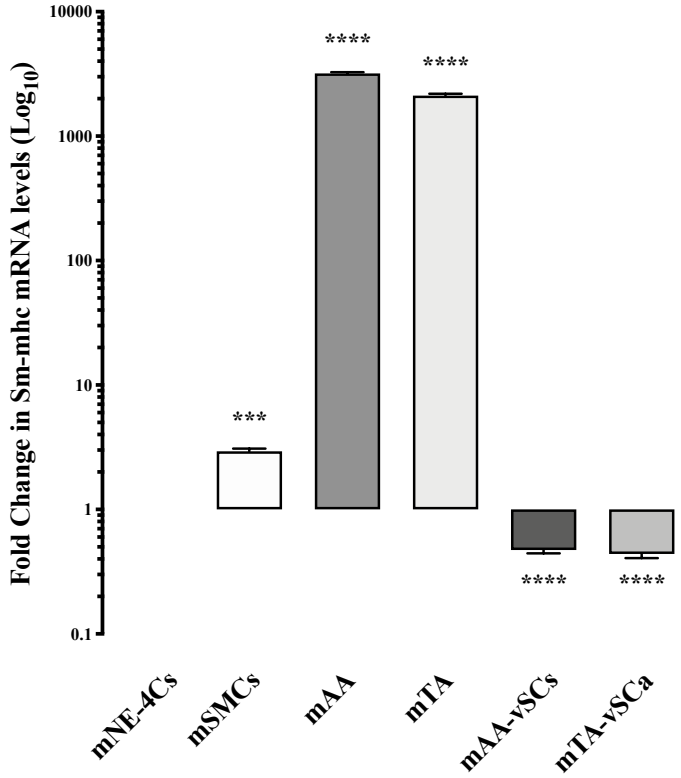

Figure 4.9. Relative SM-MHC mRNA expression levels in mAA-vSCs and mTA-vSCs compared to neural stem cell mNE-4C controls.

RNA samples were prepared using Mini-Columns, and concentrations were measured by NanoDrop instrument. Relative mRNA expression levels of *SM-MHC* were calculated using the Comparative C_T method ($\Delta\Delta C_T$). The data was normalized against the endogenous gene GAPDH. Mouse smooth muscle cells (mSMCs), mouse neuroectodermal cells (mNE-4Cs), mouse embryonic cells (mC3Hs), mouse aortic arch tissue (mAA), mouse thoracic aorta tissue (mTA), mouse aortic arch vascular stem cells (mAA-vSCs), and mouse thoracic aortic vascular stem cells (mTA-vSCs). The experiments were performed in triplicate, charts are representatives of three independent experiments. Data are mean ± S.E.M (n=3). One-way ANOVA with significance value of $P \leq 0.05$. Results: ***$p<0.001$ and ****$p<0.0001$.

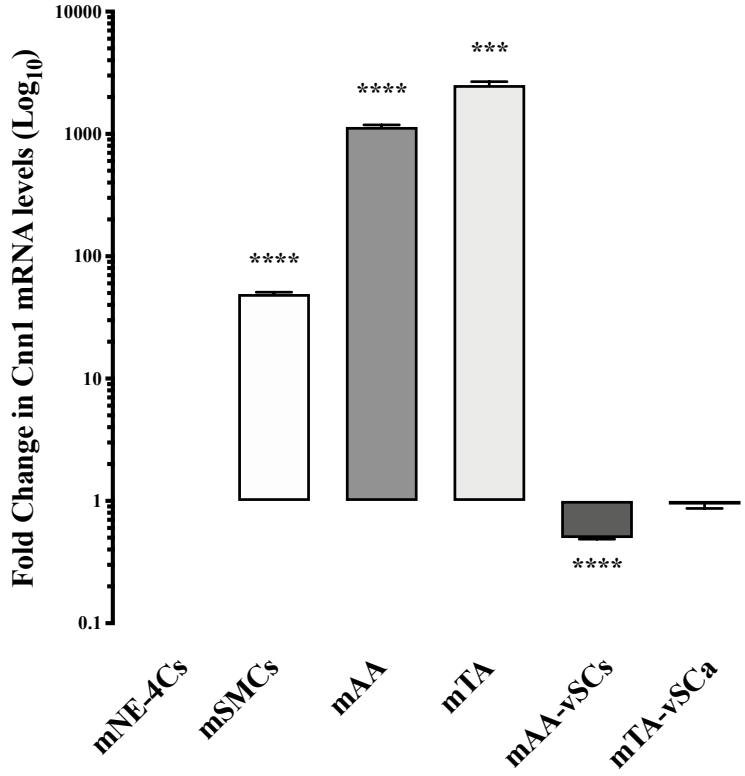

Figure 4.10. Relative CNN1 mRNA expression levels in mAA-vSCs and mTA-vSCs compared to neural stem cell mNE-4C controls.

RNA samples were prepared using Mini-Columns, and concentrations were measured by NanoDrop instrument. Relative mRNA expression levels of *Cnn1* was calculated using the Comparative C_T method ($\Delta\Delta C_T$). The data was normalized against the endogenous gene GAPDH. Mouse smooth muscle cells (mSMCs), mouse neuroectodermal cells (mNE-4Cs), mouse embryonic cells (mC3Hs), mouse aortic arch tissue (mAA), mouse thoracic aorta tissue (mTA), mouse aortic arch vascular stem cells (mAA-vSCs), and mouse thoracic aortic vascular stem cells (mTA-vSCs). The experiments were performed in triplicate, charts are representatives of three independent experiments. Data are mean ± S.E.M. One-way ANOVA with significance value of $P \leq 0.05$. Results: ***$p<0.001$ and ****$p<0.0001$.

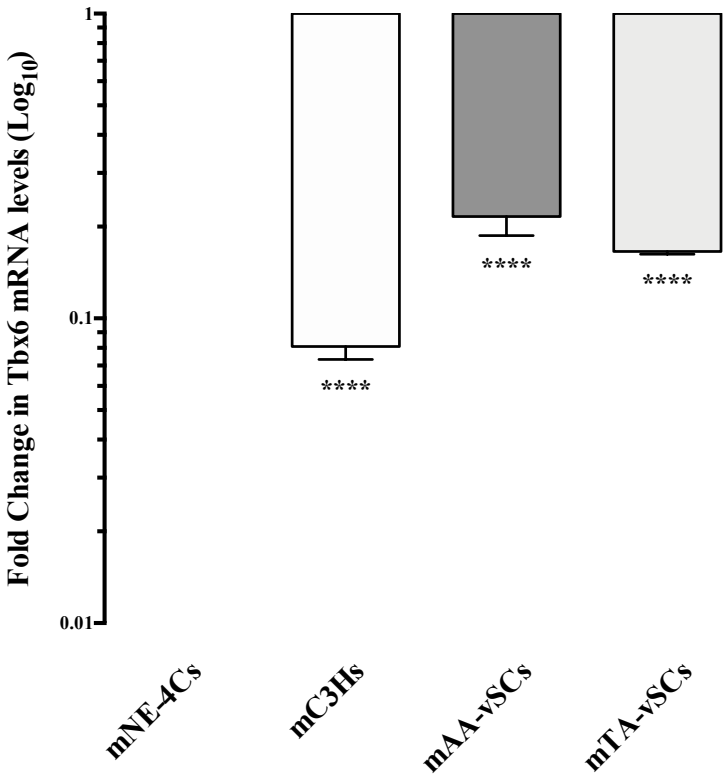

Figure 4.11. Relative Tbx6 mRNA expression levels in mAA-vSCs and mTA-vSCs compared to mNE-4C controls.

RNA samples were prepared using Mini-Columns, and concentrations were measured by NanoDrop instrument. Relative mRNA expression levels of *Tbx6* were calculated using the Comparative C_T method ($\Delta\Delta C_T$). The data was normalized against the endogenous gene HPRT. Mouse neuroectodermal cells (mNE-4Cs), mouse embryonic cells (mC3Hs), mouse aortic arch vascular stem cells (mAA-vSCs), and mouse thoracic aortic vascular stem cells (mTA-vSCs). The experiments were performed once. Data are mean ± S.E.M (n=3). Unpaired t-test with significance value of $P \leq 0.05$. Results: ****$p<0.0001$.

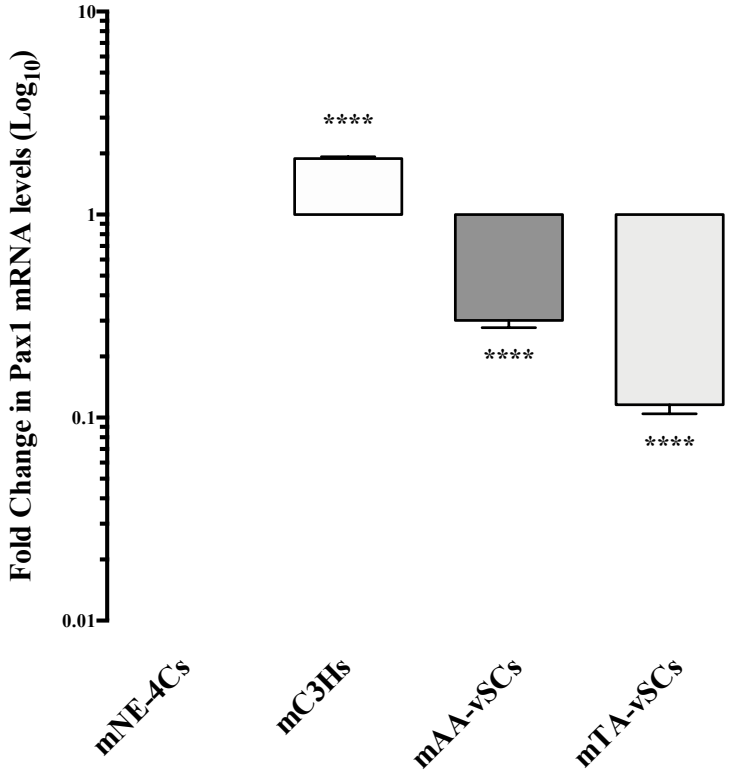

Figure 4.12. Relative Pax1 mRNA expression levels in mAA-vSCs and mTA-vSCs compared to mNE-4C controls.

RNA samples were prepared using Mini-Columns, and concentrations were measured by NanoDrop instrument. Relative mRNA expression levels of *Pax1* were calculated using the Comparative C_T method ($\Delta\Delta C_T$). The data was normalized against the endogenous gene HPRT. Mouse neuroectodermal cells (mNE-4Cs), mouse embryonic cells (mC3Hs), mouse aortic arch vascular stem cells (mAA-vSCs), and mouse thoracic aortic vascular stem cells (mTA-vSCs). The experiments were performed once. Data are mean ± S.E.M (n=3). Unpaired t-test with significance value of $P \leq 0.05$. Results: ****$p<0.0001$.

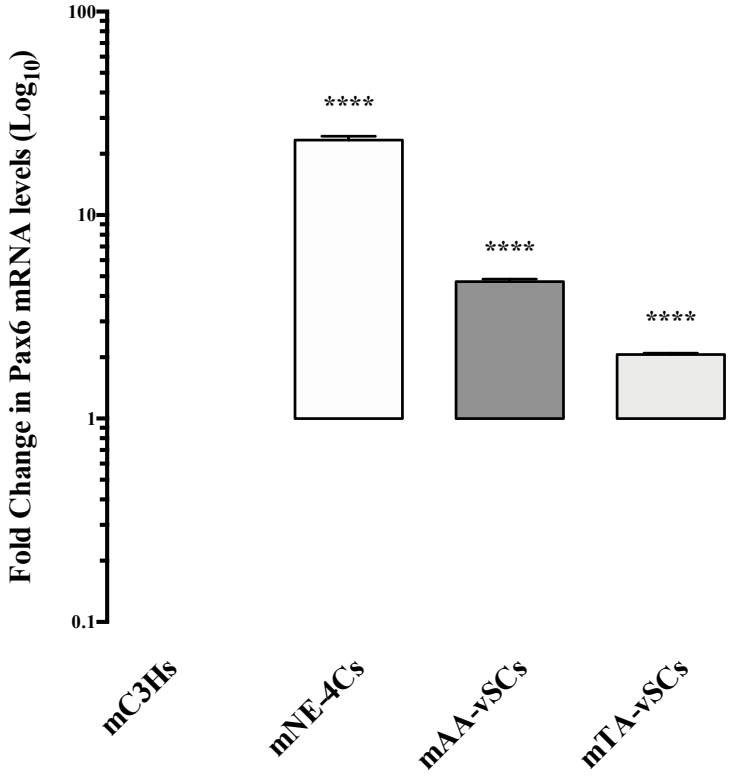

Figure 4.13. Relative Pax6 mRNA expression levels in mAA-vSCs and mTA-vSCs compared to mC3H-10T1/2 controls.

RNA samples were prepared using Mini-Columns, and concentrations were measured by NanoDrop instrument. Relative mRNA expression levels of *Pax6* were calculated using the Comparative C_T method ($\Delta\Delta C_T$). The data was normalized against the endogenous gene HPRT. Mouse neuroectodermal cells (mNE-4Cs), mouse embryonic cells (mC3Hs), mouse aortic arch vascular stem cells (mAA-vSCs), and mouse thoracic aortic vascular stem cells (mTA-vSCs). The experiments were performed once. Data are mean ± S.E.M (n=3). Unpaired t-test with significance value of $P \leq 0.05$. Results: ****$p<0.0001$.

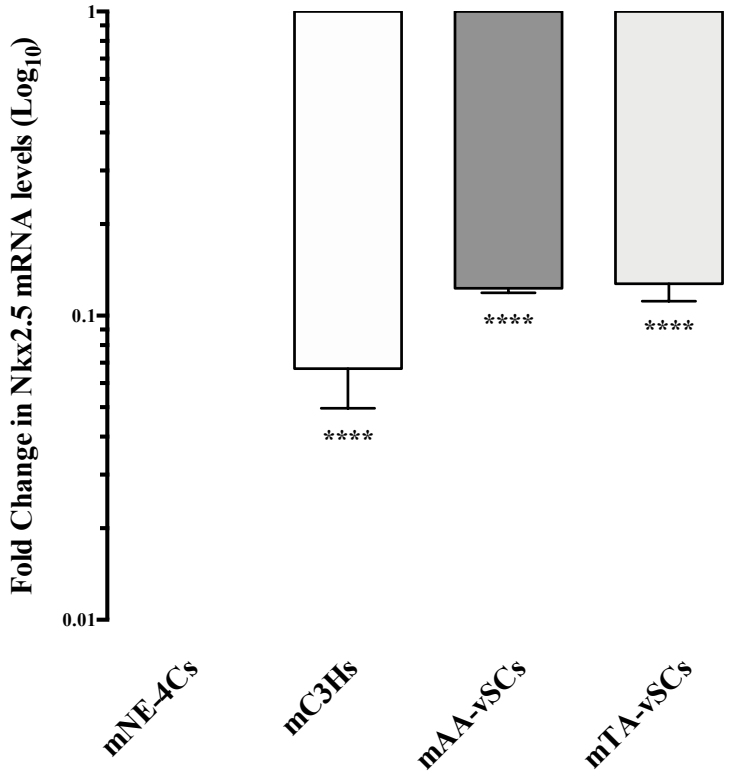

Figure 4.14. Relative Nkx2.5 mRNA expression levels in mAA-vSCs and mTA-vSCs compared to mNE-4C controls.

RNA samples were prepared using Mini-Columns, and concentrations were measured by NanoDrop instrument. Relative mRNA expression levels of *Nkx2.5* were calculated using the Comparative C_T method ($\Delta\Delta C_T$). The data was normalized against the endogenous gene HPRT. Mouse neuroectodermal cells (mNE-4Cs), mouse embryonic cells (mC3Hs), mouse aortic arch vascular stem cells (mAA-vSCs), and mouse thoracic aortic vascular stem cells (mTA-vSCs). The experiments were performed once. Data are mean ± S.E.M (n=3). Unpaired t-test with significance value of $P \leq 0.05$. Results: ****$p<0.0001$.

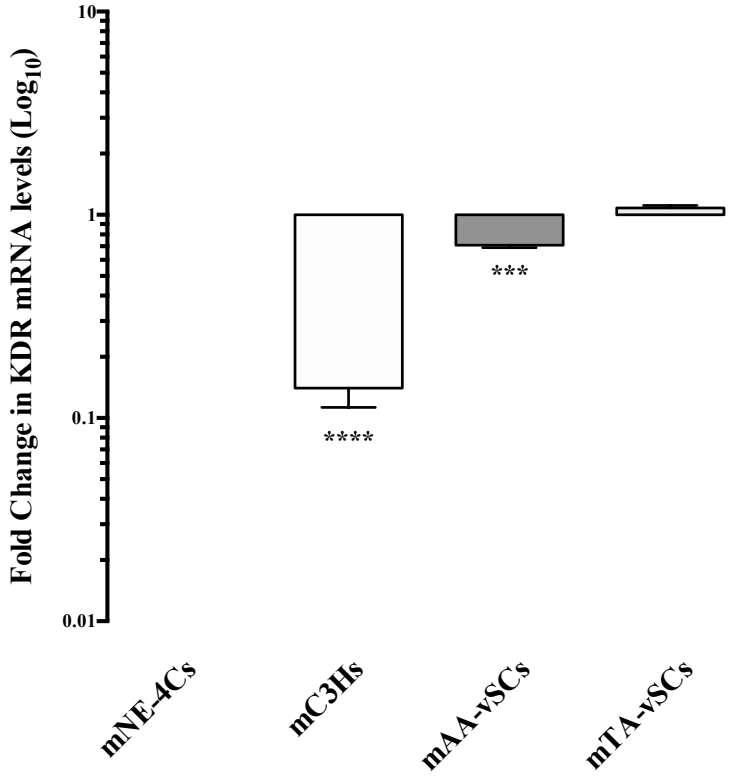

Figure 4.15. Relative KDR mRNA expression levels in mAA-vSCs and mTA-vSCs compared to mNE-4C controls.

RNA samples were prepared using Mini-Columns, and concentrations were measured by NanoDrop instrument. Relative mRNA expression levels of *KDR* were calculated using the Comparative C_T method ($\Delta\Delta C_T$). The data was normalized against the endogenous gene HPRT. Mouse neuroectodermal cells (mNE-4Cs), mouse embryonic cells (mC3Hs), mouse aortic arch vascular stem cells (mAA-vSCs), and mouse thoracic aortic vascular stem cells (mTA-vSCs). The experiments were performed once. Data are mean ± S.E.M (n=3). Unpaired t-test with significance value of $P \leq 0.05$. Results: ***p<0.001 and ****p<0.0001.

4.3.4 Identification of the location of vascular stem cells

4.3.4.1 Histochemical analysis for the presence of cells on the external lamina of the adventitial medial boundary following removal of the adventitia

Whole mouse aortas were harvested, and the adventitial layer removed intact using a collagenase treatment as described in Section 2.8.1 (Table 2-19). Tissue cross-sections were prepared, and nuclei stained with a DAPI nuclear stain (Section 2.9.3.2). The percentage of DAPI nuclei remaining after adventitial removal on the external lamina was determined using Olympus BX51 Fluorescence Microscope and Cell^{F} Multi-fluorescence and Imaging Software.

Several cells remained at the external elastic lamina following removal of the intact adventitial layer since several DAPI nuclei were observed on the adventitial side of the external laminar (marked by a white broken line) (Figure 4.16).

4.3.4.2 Scanning Electron Microscopy (SEM) analysis for the presence of cells on the external lamina of the adventitial medial boundary after enzymatic removal of the adventitia

Whole mouse aortas were harvested, and the adventitial layer removed using a collagenase digestion as described in Section 2.8.1 (Table 2-19). The tissues were longitudinally opened and prepared for scanning electron microscopy (S.E.M.) (Section 2.7). All images were taken and compiled using EVO LS15 Scanning Electron Microscope (Zeiss, Germany).

Representative SEM images demonstrate the presence of cells/tissue on the external lamina at the adventitial boundary after enzymatic adventitial removal. The data indicate that the removal of the adventitia was not 100% efficient and the external lamina may harbor residual cells/tissue (Figure 4.17).

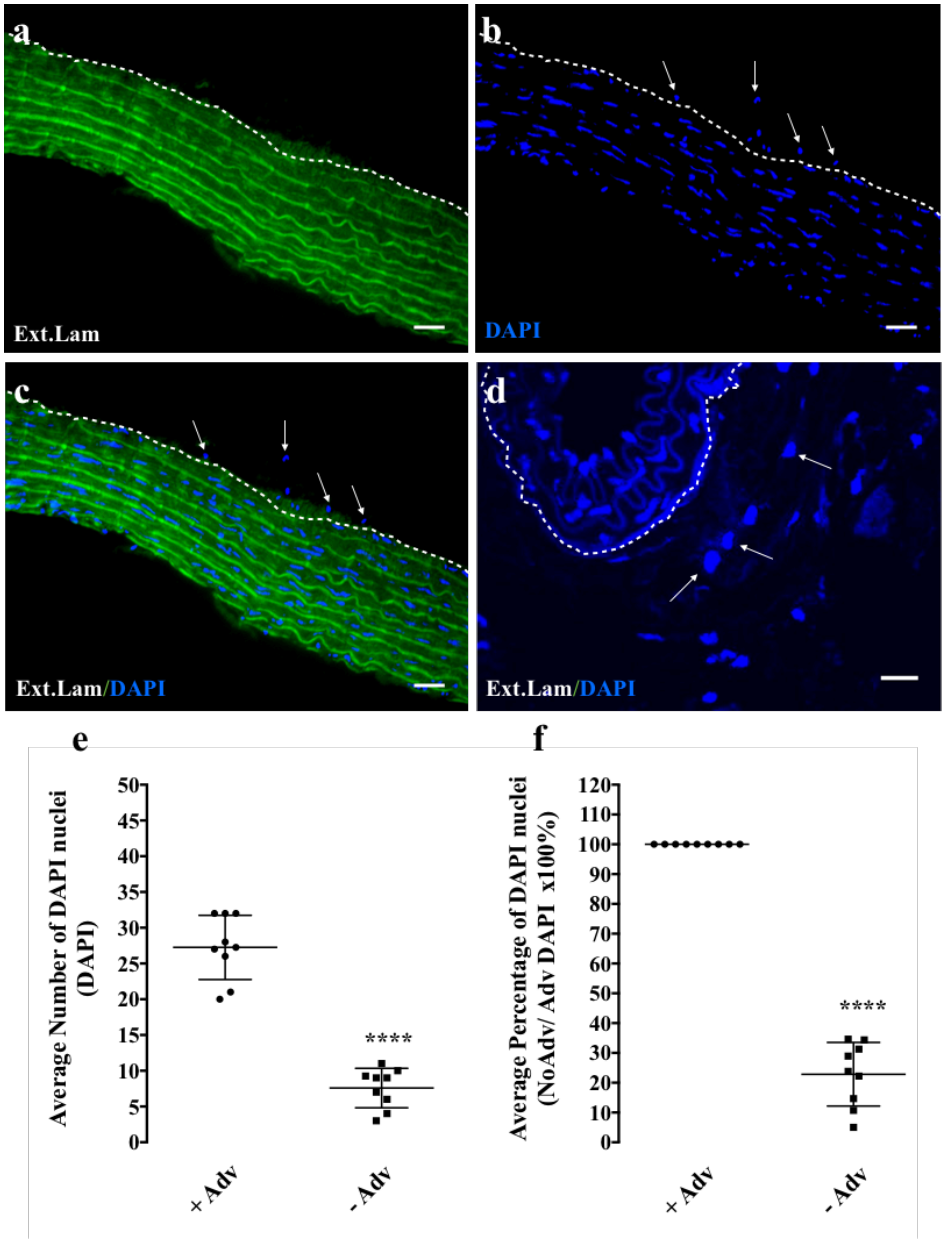

Figure 4.16. Cells are still present on the adventitia-side external laminar after enzymatic adventitia removal.

Aortic tissue was harvested, and the intact adventitia layer enzymatically removed using a dissecting microscope. Tissue cross-sections were processed, and cell nuclei evaluated using DAPI nuclear staining as described in Section 2.10.5/6. Representative images (**a)** bright collagen fibres and (**b)** DAPI nuclei and (**c)** merged composite images. (**d)** White arrows indicate cells on the external laminar at the adventitia side. ImageJ was used to (**e)** count the number of cells in vessels with adventitia (+Adv) and without adventitia (-Adv) and (**f)** plot the percentage of -Adv cells over +Adv cells. Images are representative of n ≥ 5. Scale bars, 20 mm. Data are mean ± S.D (n=10). Unpaired t-test with significance value of P≤0.05. Results: ****p<0.0001.

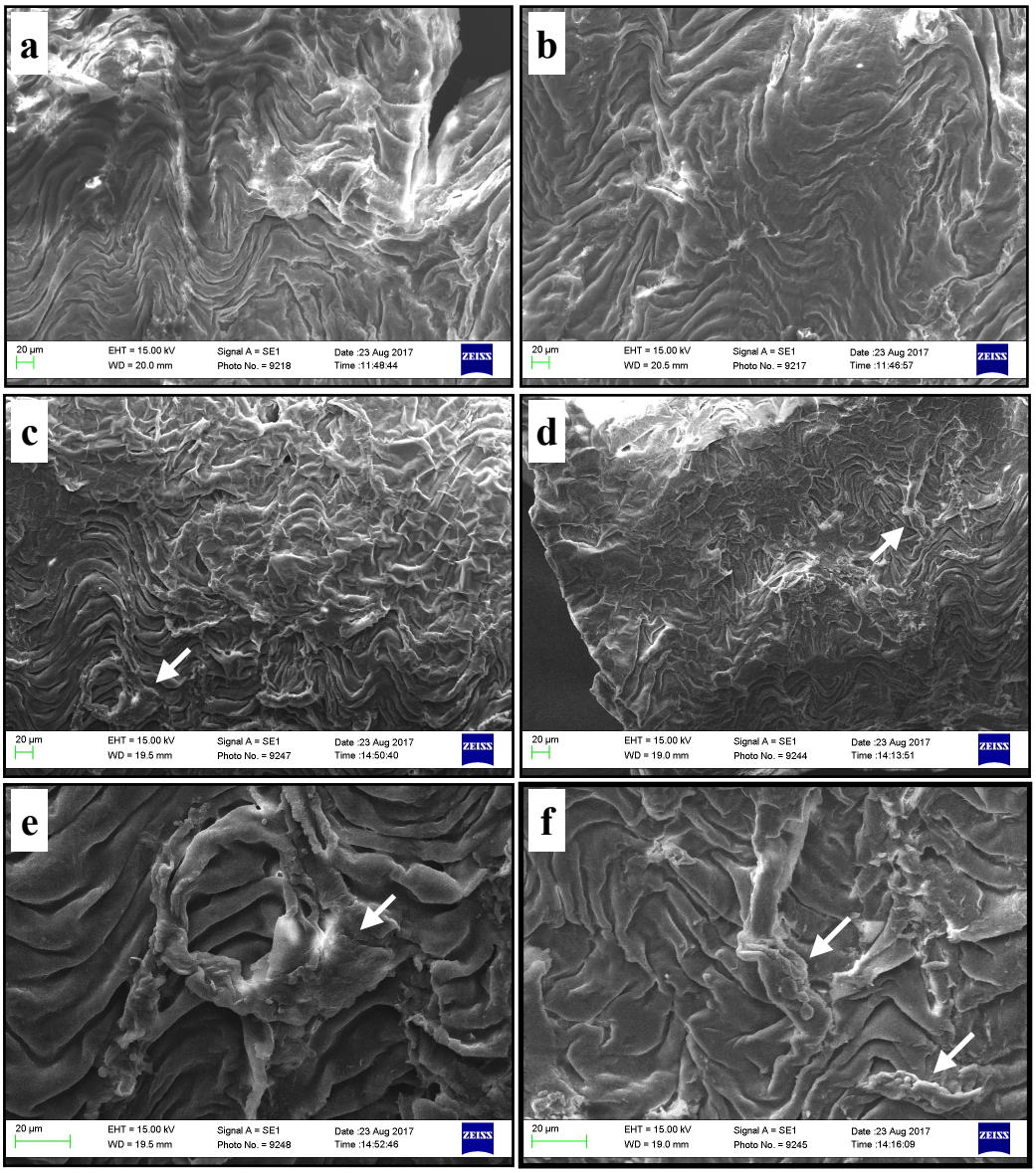

Figure 4.17. Adventitial tissue/cells are still present on the external lamina after enzymatic removal of the adventitial layer.

Aortic tissue was harvested, and the adventitia layer was enzymatically removed. Tissue samples were processed for SEM. as described in Section 2.7. Representative SEM images across the external lamina of **(a, b)** clean (no cells) and **(c, d)** residual tissue/cell after enzymatic adventitia removal. Representative images in **(e, f)** are magnifications of **c and d**, respectively, showing the presence of tissue/cells at a closer angle. White arrows indicate tissue/cells on the external laminar Images are representative of $n \geq 5$. Scale bars, 20 µm.

4.3.5 Summary

- Murine stem cells from the tunica media of the aortic arch (mAA-vSCs) and thoracic aorta (mTA-vSCs) were successfully isolated using a modified enzymatic dispersion protocol
- Flow cytometry analysis confirmed that these isolated cells were positive for both S100β and Sca-1 proteins as observed in the *in vivo* model presented in Chapter 3.
- Immunocytochemical analysis confirmed that stem cells derived from mAA-vSCs and mTA-vSCs were S100β, Nestin, SOX10, SOX17 and SCA-1 positive but negative for SMC differentiation markers (SM-MHC and CNN1).
- Transcriptional analysis confirmed that stem cells derived from mAA-vSCs and mTA-vSCs were S100β, Nestin, Sox10, Sox17 and Sca-1 positive but negative for SMC differentiation markers (Sm-mhc and Cnn1).
- Transcriptional analysis also confirmed that mAA-vSCs and mTA-vSCs had a neuroectodermal embryological origin by the positive expression of the neuroectodermal transcript, Pax6. Cells were all negative for the mesodermal genes, Pax1, Tbx6, KDR, and Nkx2.5.
- Histochemical and SEM analysis revealed the presence of residue adventitial cells/tissue after enzymatic removal thus qualifying the source of medial vascular stem cells.

4.4 Discussion

Previous work published by our group and others (Yuan et al., 2017; Tang et al., 2012; Sainz et al., 2006; Kennedy et al., 2014) demonstrated the presence of a stem/progenitor cell in the tunica media of rat/mouse aorta *in vitro.* Additionally, studies presented in Chapter 3 of this thesis demonstrated the presence of a S100β-positive ($S100\beta^+$) stem cell progenitor resident within arterial wall. These $S100\beta^+$ cells were predominantly resident in the adventitial layer, but a few cells were also present in the medial layer in sham or RCA control vessels. Moreover, we report that these cells and their progeny are involved in neointimal formation after vascular injury. Previous studies have confirmed the presence of $SOX10^+$ cells within the media layer, albeit at very low density (Yuan et al. 2017), and while these cells were not specifically stained for S100β *in situ*, the likelihood that they are $S100\beta^+$ is high as these same $SOX10/S100\beta^+$ multipotent stem cells have been isolated from arterial medial sections or rat, mouse and human vessels (Tang et al., 2012).

Specific-disease susceptibility is known to occur within different sections of the aorta that are athero-prone (aortic arch region), or athero-resistant (thoracic aorta). Some authors suggested this phenomenon is due to local vessel hemodynamics (Majesky, 2007; Rensen, Doevendans and van Eys, 2007; Hao, Gabbiani and Bochaton-Piallat, 2003; Majesky, 2003), while others reported that the embryological origin of the tissue/cells dictates their susceptibility to discrete vascular lesions (Trigueros-Motos et al., 2013; Haimovici and Maier, 1964; Sinha, Iyer and Granata, 2014; Cheung et al., 2014; Bennett, Sinha and Owens, 2016; DeBakey and Glaeser, 2000). Herein, this *in vitro* study aimed to isolate and characterise a stem/progenitor population from the tunica media of the two embryological-derived aortic regions, the aortic arch athero-prone (neuroectodermal, NE) and the thoracic aorta, athero-resistant (paraxial mesodermal, PM) followed by comparisons of their embryological origin.

The isolation of mouse vascular stem cells from the medial layer of the aortic arch (mAA-vSC) and thoracic aorta (mTA-vSCs) was carried out using a modified version of the enzymatic dispersion protocol, as previously described (Tang et al., 2012). The isolation protocol had a success rate of ~ 20% for aortic arch tissue, while cells isolated from thoracic aorta has a higher success rate ~ 50%. The cells from both aortic regions

exhibited a uniform neural-like morphology and were positive for S100β, Nestin, SOX10 and SOX17 proteins but negative for the smooth muscle cell markers CNN1 and SM-MHC. Moreover, both mAA-vSC and mTA-vSCs were positive for the stem cell marker SCA-1. This was in contrast to previous studies that reported medial S100β^{+} stem cells were SCA-1 negative (Tang et al., 2012). This discrepancy is most likely due to the differentiation media (DMEM supplemented with FCS) used for determining SCA-1 immunoreactivity in these studies. In our hands, vSCs grown in neuroectodermal maintenance medium (NE-MM) showed positive expression of S100β and SCA-1 markers that was confirmed by Flow cytometry analysis. Flow cytometry studies confirmed that the cells observed within the vessel wall of control tissue sections in Chapter 3 and that subsequently shown to be involved in neointima hyperplasia after injury were successfully isolated.

The likelihood that mAA-vSC and mTA-vSCs are derived from a parent SMC was addressed by determining the presence of the stable histone mark (H3K4me2) in these cells. The enrichment of the SMC histone signature on the SM-MHC gene was significant in fresh aortic tissue and de-differentiated mSMCs in culture but absent in embryonic stem cells (mESCs), as previously described (Gomez et al., 2013). Notably, the enrichment of the SMC histone signature was also absent in mAA-vSC cells strongly suggesting that mAA-vSC cells were not derived from SMCs that may have de-differentiated in culture. In support of this conclusion, parallel analysis of TET-2 binding to the SM-MHC, which is indicate of SMCs, was also reduced in both mAA-vSC and mESCs when compared to fresh aortic SMC and mSMCs in culture. Finally, the enrichment of H3K27me3 in both mAA-vSC and mESCs but not in fresh aortic SMC and mSMCs in culture further supports the conclusion that mAA-vSC are stem cells that are not derived from medial SMCs.

The likelihood that mAA-vSC and mTA-vSCs are derived from a similar embryological origin was also addressed by determining the transcriptomic profile of these cells. The C3H/10T1/2 cells were originally established from mouse embryonic mesoderm as an *in vitro* model to study SMC differentiation (Xie et al., 2011). The murine neuroectodermal stem cell line (mNE-4C) has been routinely used to generate neural cells (Demeter, Zádori, Agoston and Madarász, 2005). Therefore, we used these cell line as mesodermal and neuroectodermal lineage controls. The relative expression

of Cnn1 and Sm-mhc transcripts in mAA-vSC and mTA-vSCs and mNE-4Cs was negligible but high in fresh aortic SMCs and mSMCs in culture. In contrast, mAA-vSC and mTA-vSCs were enriched for neuroectodermal transcripts (S100β, Sox10, Nestin and Pax6) but not for paraxial mesoderm and lateral plate mesoderm (Tbx6, KDR, Nkx2-5 and Pax1).

Several investigators have questioned the protocols for isolating these medial stem cells from aortic tissue suggesting that they make be in fact derived from the adventitial layer (Tang et al., 2013; Nguyen et al., 2013). Given this finding, whole aortas were harvested, and the adventitial layer removed intact using collagenase before histochemical analysis of DAPI stained nuclei and scanning electron microscopy (SEM) analysis was performed in order to examine the efficiency of the removal step during isolation of cells. Notably, the presence of cells on the tunica adventitial side of the external lamina was demonstrated with 23.84 ± 10.68 % of adventitial cells remaining compared to tissues with a tunica adventitial layer. Moreover, SEM analysis confirmed the presence of residual tissue/cells. The data suggests that residual tissue may possibly harbour cells, which may be the source of isolated vSCs thought to be medial progenitors. Indeed, marked S100β-tdT^{+} cells in our lineage tracing studies confirm the predominant adventitial source of these cells with very few S100β^{+} cells marked in the medial layer.

Collectively, the data suggested the presence of a single non-SMC neuroectodermal-derived stem/progenitor cell (vSC) within the vessel wall of both athero-susceptible and athero-resistant aortic regions. Although, the lineage tracing study presented in Section 3 of this thesis showed the presence of few cells within the tunica media of sham RCA tissue sections, both the SEM and lineage tracing studies strongly suggested that vSCs are predominantly present in the adventitial layer at the adventitial medial boundary. Whether or not mAA-vSC and mTA-vSCs respond in a similar manner to various inductive differentiation stimuli that we and others have shown are recapitulated during disease progression in the adult organism remains unknown (Redmond et al., 2013; 2014). The answer will be important in determining how committed/limited these stem cells are by their microenvironment.

Chapter 5

Jagged1/Notch stimulates myogenic differentiation of resident vascular S100β^{+} stem/progenitor cells

5.1 Introduction

Intimal thickening is an important early process in the development of an arteriosclerotic disease. Numerous pathologic observations in human vessels confirm that smooth muscle cell (SMC)-rich early adaptive 'transitional' lesions are present in atherosclerotic-prone regions of arteries before the retention of lipid and the appearance of a developed plaque (Sakamoto et al., 2018). These transitional lesions are the result of deleterious changes in blood flow/pressure or compliance mismatch following stent deployment causing endothelial dysfunction (Nakagawa and Nakashima, 2018). They represent an important therapeutic target and are successfully modelled in vivo using wildtype mice with flow restriction due to carotid artery ligation, as previously outlined. The process of restenosis is mainly described by the extensive proliferation and migration of vascular smooth muscle-like cells (vSMCs) into the intimal space of the stented artery resulting in the formation of a new (neo) intima (Indolfi et al., 2003). Due to this, there has been a huge interest in elucidating the molecular mechanisms implicated in vascular remodelling and neointima hyperplasia during in-stent restenosis. Various *in vivo* studies have shown the participation of various signalling pathways during vascular remodelling and neointimal formation, including Transforming Growth Factor-β (TGF-β), Notch, Hedgehog (Hh) and Wnt/β-catenin signalling.

The TGF-β1 signalling is an important mechanism of SMC differentiation and maintenance of stem cells and adult contractile vSMCs, respectively (Wang et al., 2015). TGF-β1 treatment of progenitors cells from the tunica adventitia (Sca-1^+ cells) and media (S100β^+ cells) was shown to induce myogenic differentiation *in vitro* (Hu et al., 2004; Tang et al., 2012). The SMAD/TGF-β signalling has also been reported to be activated in endothelial cells after vein grafting *in vivo*. However, when vein grafts were pre-treated with a pan-TGF-β neutralising antibody prior to implantation, a reduction in the neointimal area was achieved (Cooley, 2005). *In vivo* studies and targeted mutagenesis have revealed a specific role for Notch1 and Jagged1 during development and during vascular remodelling (Morrow et al., 2008b). Notch1-knockout mice resulted in early embryonic lethality owing to arteriovenous malformations and defects in the endothelial cells. The transcription levels of Notch1 receptor and Jagged1 ligand mRNAs were observed to be upregulated within lesions

after vascular injury (Gridley, 2007). *In vitro* studies using human and rat vascular smooth muscle cells exposed to cyclic mechanical strain demonstrated a reduction in the expression of Notch1 receptor protein and mRNA concomitantly with increased expression of alpha actin (αSMA), calponin (CNN) and smooth muscle myosin heavy chain (SM-MHC). The effect of cyclic mechanical strain was able to be restored by overexpression of Notch1 intracellular domain in vSMCs (Morrow, Cullen, Cahill and Redmond, 2007a). Wnt signalling has also been shown to induce cell proliferation of vascular smooth muscle cells *in vitro* (Ezan et al., 2004). *In vivo studies* demonstrated that Wnt4 was upregulated in vascular lesions after balloon-wire injury and complete ligation of the carotid arteries (Tsaousi et al., 2011; Hua et al., 2014). Additionally, microarray analysis performed on PDGF-BB-treated vSMCs showed elevated expression levels of Wnt4 mRNA compared to quiescent vSMCs (Tsaousi et al., 2011). According to data published by our research group, Sonic Hedgehog (Shh) induced myogenic differentiation in purified Sca-1^+ cells from murine adventitial layer, an effect that was reduced by treatment with ethanol. *In vivo* studies performed using Sca-1-EGFP transgenic mice, showed the presence of Sca-1-$EGFP^+$ cells within the intimal lesion on day 14 post partial carotid ligation. Immunolabelling studies on Sca-1-EGFP cross-sections revealed that the Hh receptor Patched 1 (Ptch1) and the Shh target gene Gli2 were markedly expressed in injured carotid arteries compared to sham-operated vessels, and some Sca-1-$EGFP^+$ cells were also positive for the Shh markers. Daily moderate ethanol treatment resulted in significant reduction in neointimal lesion with attenuation of Shh signalling as confirmed by decreased expression of Patch and Gli2 proteins (Fitzpatrick et al., 2017). Moreover, Shh-activated Hh signalling was shown to stimulate cell proliferation and survival of vascular SMCs *in vitro*. Additionally, ectopic expression of Shh demonstrated to activate the Notch signalling pathway by increasing the expression of the Notch target genes. The Shh-induced effect was attenuated by treating the cells with an Notch inhibitor (Morrow et al., 2009).

Overall, convincing evidence have shown that these factors recapitulate during disease conditions activating the proliferation and migration of lesional and thus contributing to vascular remodelling and neointima hyperplasia.

As previously mentioned in this thesis (Section 4.1) a new line of inquiry has emerged

into the embryological origin of the cells and tissue as a possible factor in driving certain vascular pathologies irrespectively of the environmental cues (Bennett, Sinha and Owens, 2016; Cheung et al., 2012; DeBakey and Glaeser, 2000; Sinha, Iyer and Granata, 2014; Haimovici and Maier, 1964; Trigueros-Motos et al., 2013). In particular, as vascular beds display differential disease susceptibility, it is likely that their embryological origin (neuroectoderm [NE] vs paraxial mesoderm [PM]) in addition to endothelial dysfunction may influence disease localisation and progression (Cheung et al., 2012). The results presented in this report, see Chapter 4, demonstrated that mouse vascular stem/progenitor cells (vSCs) isolated from the aortic tunica media of both athero-susceptible (aortic arch; mAA-vSCs) and athero-resistant aortic (thoracic aorta; mTA-vSCs) regions shared a common neuroectodermal origin regardless of the region of the tissue they reside. The lineage tracing study carried out in Chapter 3, revealed the presence of a neuroectoderm S100β^{+} cell progenitor within the vessel wall of the common carotid arteries, and their contribution to vascular remodelling and neointima hyperplasia after injury.

Given these findings, we proposed to investigate how isolated mAA-vSCs and mTA-vSCs transition to SMC phenotype in response to TGF-β1, Jagged1-activated Notch, Sonic Hedgehog (Shh) and Wnt4 signalling factors, known to be in part implicated in vascular lesion progression *in vivo*.

5.2 Strategy

In order to study myogenic differentiation of the stem/progenitor cells isolated from two developmental discrete regions of the aortic tunica media (Chapter 4 of this thesis), the following strategy was adopted. Isolated vascular stem cells (vSCs) from the murine aortic arch (mAA; mAA-vSCs) and thoracic aorta (mTA; mTA-vSCs) were subjected to different myogenic inductive stimuli such as Transforming Growth Factor-β (TGF-β), the Notch ligand, Jagged1 (Jag1), Sonic Hedgehog (Shh), and Wnt4 to determine whether they exhibited similar responsiveness to the same stimuli.

The major objectives of this chapter are:

i) To determine whether mAA-vSCs are capable of undergoing myogenic differentiation following 1 week in myogenic differentiation media containing DMEM supplemented with non-stem cell certified 10% FBS- (DM).
ii) To compare the myogenic differentiation capacity of both isolated cell progenitors (mAA-vSCs and mTA-vSCs) when exposed to TGF-β1 and the Jagged1-activated Notch signalling.
iii) To determine the interplay between TGF-β1 and Jagged1/Notch-induced signalling in controlling myogenic differentiation of mAA-vSCs and mTA-vSCs.
iv) To determine the role of ligands, Sonic Hedgehog (Shh) and Wnt4 in myogenic differentiation of mAA-vSCs and mTA-vSCs.

5.2.1 Determine whether or not mAA-vSCs are capable of differentiating into mature SMC by culturing them for 7 days in 10%FBS-supplemented DMEM (DM).

The main focus of this section was to initially examine the myogenic differentiation capacity of the isolated cell progenitors when grown in regular SMC maintenance medium containing DMEM supplemented with 10% FBS (DM). DMEM and 10-15% FCS (or FBS) has been used in differentiation studies from progenitor cells into SMC (Hu et al., 2004; Passman et al., 2008; Tang et al., 2012). Additionally, Tang and colleagues (2012) reported spontaneous differentiation of MVSCs into mature SMCs ($CNN1^+$ and $SM\text{-}MHC^+$) 8 weeks after being cultured in DM (Tang et al., 2012). We performed a trial differentiation assay using 10% FBS-containing DMEM (DM) for 7

days to induce SMC differentiation of mouse aortic arch vascular stem cells (mAA-vSCs). A control sample consisting of mAA-vSCs grown in stem cells maintenance medium MM1 (Section 2.8.1) was prepared to compare changes in SMC differentiation marker expression analysed by real time RT-qPCR.

5.2.2 Compare the differentiation levels of both mAA-vSCs and mTA-vSCs to the SMC phenotype when exposed to TGF-β1 and the Jagged1-activated Notch signalling.

During vessel development expression of transforming growth factor-β1 (TGF-β1) in mesenchymal-derived cell progenitors induces their differentiation into SMCs resulting in the maturation of the vasculature (Wang et al., 2015; Jain, 2003; Cheung et al., 2012). Moreover, the Notch signalling pathway dictates SMC specification of neural crest progenitors during vasculogenesis (Shin, Nagai and Sheng, 2009; High et al., 2007; Wang et al., 2015). Both pathways have been intensively studied in murine models of vascular injury in order to elucidate a possible molecular mechanisms of SMC differentiation (Morrow et al., 2005b; Proweller, Pear and Parmacek, 2005; Havrda et al., 2006; Boucher et al., 2011; Doi et al., 2006; Wang et al., 2015; Cheung et al., 2014; Sinha, Iyer and Granata, 2014; Xie et al., 2011). Therefore, differentiation studies of mAA-vSCs and mTA-vSCs were performed using two different myogenic stimuli (i) 2 ng/ml of recombinant murine TGF-β1 (rmTGF-β1) or (ii) 500 ng/ml of immobilized Jagged1-Fc (Jag1-Fc) for 7 days in neuroectodermal maintenance medium (NE-MM) (Section 2.8.1, Table 2-17). This decision was made based on a medium screening trial performed to maximise the effect of each stimuli and also to control for most of the factors present in the induction medium. Control samples were also prepared, including NE-MM with vehicle or 500 ng/ml of immobilized IgG-Fc in NE-MM for the TGF-β1 or Jagged1-Fc treatment, respectively. Changes in the expression of the SMC markers, smooth muscle myosin heavy chain (SM-MHC; mature smooth muscle cell marker) and Calponin1 (Cnn1; intermediate smooth muscle cell marker), were analysed by Immunocytochemistry and real time RT-qPCR to assess differentiation levels (Campbell et al., 1979). Cell number was also determined by comparing the number of cells (DAPI nuclei) over the high-power field (HPF; visible area under the magnification power of the selected objective) between control and treatment.

5.2.3 To examine the effect of TGF-β1 on Jagged1/Notch-induced SMC differentiation, and vice versa.

The main aim of this section was to investigate the interactions between the TGF-β1 and Jagged1-dependent Notch signalling pathways in order to reveal a possible molecular mechanism for myogenic differentiation of vascular cell progenitors. Since the aortic arch is known to be susceptible to lesion formation (Cunningham and Gotlieb, 2005; Shah, 2003), only mAA-vSCs were used to carry out all the studies in this section. In this context, inhibition studies were conducted on cells treated with either rmTGF-β1 (TGβ1) or recombinant Jagged1-Fc (Jag1-Fc) and the effect on myogenic differentiation was analysed by immunocytochemistry and real time RT-qPCR.

In order to reassure that myogenic differentiation of the mAA-vSCs occurred through the TGF-β and Notch signalling pathways, acute (48 hours) and chronic (7 days) inhibition of TGF-β or Notch signalling pathways in TGβ1- or Jag1-Fc-treated mAA-vSCs was performed, respectively. Cells were preincubated with either 10 μM of SB431542 (SMAD/TGF-β signalling inhibitor) or 80 μM of DAPT (γ-secretase/Notch signalling inhibitor) followed by treatment of 2 ng/ml of rmTGF-β1 (TGβ1) or 500 ng/ml of immobilized Jagged1-Fc (Jag1-Fc), respectively, for 48 hours and 7 days. Changes in the expression of target genes were analysed by real time RT-qPCR at 48 hours, while expression of the smooth muscle cell genes/markers (CNN1 and SM-MHC) were determined by immunocytochemistry and real time RT-qPCR at day 7 (Campbell et al., 1979). Cell number was also determined by comparing the number of cells (DAPI nuclei) over the high-power field (HPF; visible area under the magnification power of the selected objective) between control and treatment.

Lastly, the interactions between the two pathways were studied by inhibiting Jag1-Fc-treated mAA-vSCs with 10 μM of SB431542, whereas TGβ1-treated cells were treated with DAPT (80 μM) for 7 days. Changes in the expression of the SMC genes (Cnn1 and Sm-mhc) were analysed by real time RT-qPCR (Campbell et al., 1979).

5.2.4 Determine whether or not mAA-vSCs are capable of differentiating into mature SMC upon activation of the Hh and Wnt/β-catenin signalling pathways

Compelling evidence suggests the involvement of Wnt/the β-catenin signalling and Hedgehog (Hh) signalling pathways in vascular remodelling and neointima formation *in vivo*(Kramann et al., 2016). Among the Wnt family proteins, Wnt4 signalling molecule was shown to be upregulated in proliferative vSMCs in culture, and *in vivo* studies using Wnt4-deficient transgenic mice revealed that these animals had a reduced intima thickening compared to the wild types 21 days after complete carotid artery ligation (Tsaousi et al., 2011; Ezan et al., 2004; Ackers and Malgor, 2018; Hua et al., 2014). Moreover, the Sonic Hedgehog (Shh) morphogen was demonstrated to contribute, in part to the formation and maintenance of adventitial Sca-1^+ cells during vascular development. *In vitro*, Shh treatment of rat vSMCs induced cell proliferation and interestingly increased the expression of notch target gene, Hrt1, Hrt2 and Hrt3 after 24 hours (Morrow et al., 2009; Hu et al., 2004; Passman et al., 2008; Hooper and Scott, 2005).

Based on these facts, we hypothesized that Wnt/the β-catenin and Hedgehog (Hh) signalling may induce myogenic differentiation of vascular stem cells (vSCs) into SMCs. Therefore, we performed trial differentiation studies of mAA-vSCs using two different treatments for 48 hours and 7 days involving 50 ng/ml of recombinant murine Wnt4 (rmWnt4) or 1 μg/ml of recombinant murine Shh (rmShh). Real time q-PCR technique was carried out to analyse SMC differentiation marker expression in these samples. Target gene expression was measured at 24 hours post treatment, while expression of the myogenic genes (Cnn1 and Sm-mhc) were determined at day 7. To ensure activation of the Wnt/the β-catenin signalling upon rmWnt4 treatment, the Wnt target gene runt related transcription actor1 (Runx1) was also examined. For the activation of the Hh signalling by Shh treatment, Gli1 expression was also analysed.

5.2.5 Methodology

In order to facilitate a clear understanding of the proceeding results, a brief summary of the steps taken within this *in vitro* study is presented below. Briefly, cells were analysed for SMC markers by immunocytochemistry and real time RT-qPCR as well

as cell number by using the image-analysis software ImageJ and Microsoft Office Excel 2011. Epigenetic changes such as histone modifications (H3K4me2 and H3K27me3) and DNA di-methylation (TET-2) at the SM-MHC locus by ChIP-PCR analysis. For full protocols refer to Materials and Methods Section, Chapter 2, as referenced below.

i) *Immunocytochemical analysis of SMC markers (Section 2.5)* –1° Abs were used to interrogate vSCs against the following phenotypic markers SM-MHC, and CNN1 to determine the levels of SMC specific markers. All images were taken and compiled using Olympus BX51 Fluorescence Microscope and Cell^{F} Multi-fluorescence and Imaging Software.
ii) *Cell number analysis (Section 2.5)* – Briefly, immunocytochemistry images were used to count the number of DAPI nuclei (cells) per high power field (HPF) using the image-analysis software ImageJ. GraphPad 6 Prism™ (GraphPad software, La Jalla, California, USA) was used to create the charts using the obtained cell counts.
iii) *Gene expression analysis by real time RT-qPCR (Section 2.3)* – Relative quantification of mRNA expression was performed on vSCs using specific primers for the following transcripts, Cnn1 and SM-MHC to determine the levels of SMC specific transcripts.
iv) *Chromatin Immunoprecipitation (ChIP) followed by real time PCR (ChIP-PCR) (Section 2.4)* – DNA samples were immunoprecipitated with anti-H3K4me2, H3K27me3 and TET-2 before real-time PCR was performed using a primer pair specific for the CpG island regions of the SM-MHC promoter. Fold enrichment of the histone modifications and TET-2 binding at the SM-MHC gene was calculated using the obtained Ct values.

5.3 Results

5.3.1 mAA-vSCs are capable of differentiating into SMC in 10% FBS-supplemented DMEM for 7 days

The mAA-vSCs were cultured in neuroectodermal maintenance medium (NE-MM) or 10% FBS-containing DMEM (DM) for 7 days as described in Section 5.3.5.

In accordance to the characterisation studies presented in Chapter 4, the typical dendritic-like morphology observed in mAA-vSCs changed towards a more spindle-shaped or stellar phenotype characteristic of smooth muscle cells (SMCs) 7 days after DM treatment (Figure 5.1, A).

Increased expression levels of Cnn1 and Sm-mhc transcripts were observed in treated cells compared to those in NE-MM (control). Cnn1 mRNA expression levels were significantly increased by 22.56 ± 4.77 fold change in DM-treated samples versus NE-MM 7 days after treatment (Figure 5.2, a). Although not significant, the relative expression levels of Sm-mhc mRNA were 4.28 ± 0.19 fold increased compared to the control sample at day 7 (Figure 5.1, B).

Concomitantly, immunocytochemical analysis (ICC) revealed an increase in the number of $CNN1^+$ and $SM\text{-}MHC^+$ in the DM-treated samples compared to the control cells cultured in NE-MM for 7 days. The fraction of cells expressing CNN1 and SM-MHC were 0.27 ± 1.39 and 0.16 ± 0.11, respectively (Figure 5.2, A and B). The data suggested that DM promoted myogenic differentiation of mAA-vSCs into mature SMCs after 7-day treatment.

The effects on cell number was also determined with a decrease in cell number observed after 7 days of DM treatment (Figure 5.3). The number of cells per μm^2 was 287.2 ± 125.5 in maintenance medium compared to 181.4 ± 81.41 cells/μm^2 for the 7-day DM treatment.

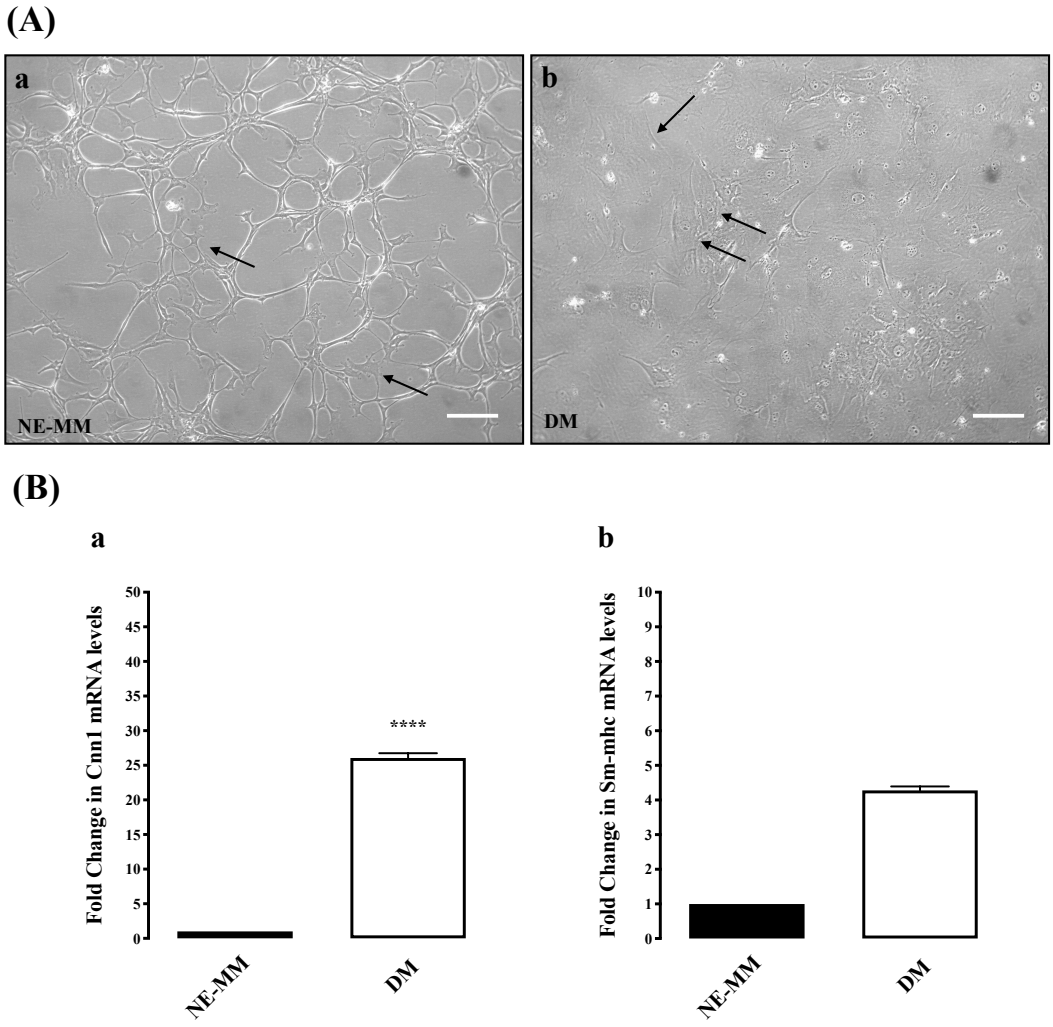

Figure 5.1. Myogenic differentiation of mouse aortic arch vascular stem cells (mAA-vSCs) in response to 10% FBS-containing DMEM (DM) for 7 days.

mAA-vSCs were cultured in neuroectodermal maintenance medium (NE-MM; control sample) and 10% FBS-containing DMEM (DM) for 7 days. SMC differentiation was analysed by PCR and immunocytochemistry.

(A) Phase-contrast images of mAA-vSCs cultured in (**a)** NE-MM and (**b)** DM for 7 days. Arrows indicate the typical morphology of (**a)** mAA-vSCs with a neural-like phenotype and (**b)** smooth muscle cells with spindle-shaped or stellar phenotypes.

(B) Relative mRNA expression levels of **(a)** Calponin1 (Cnn1) and **(b)** smooth muscle myosin heavy chain (Sm-mhc) were calculated using the Comparative C_T method ($\Delta\Delta C_T$). The data was normalised against the endogenous gene HPRT. The experiments were performed in triplicate, charts are representatives of three independent experiments. Data are mean ± S.E.M (n=3). Mann-Whitney test with significance value of $P \leq 0.05$. Results: ****$p<0.0001$.

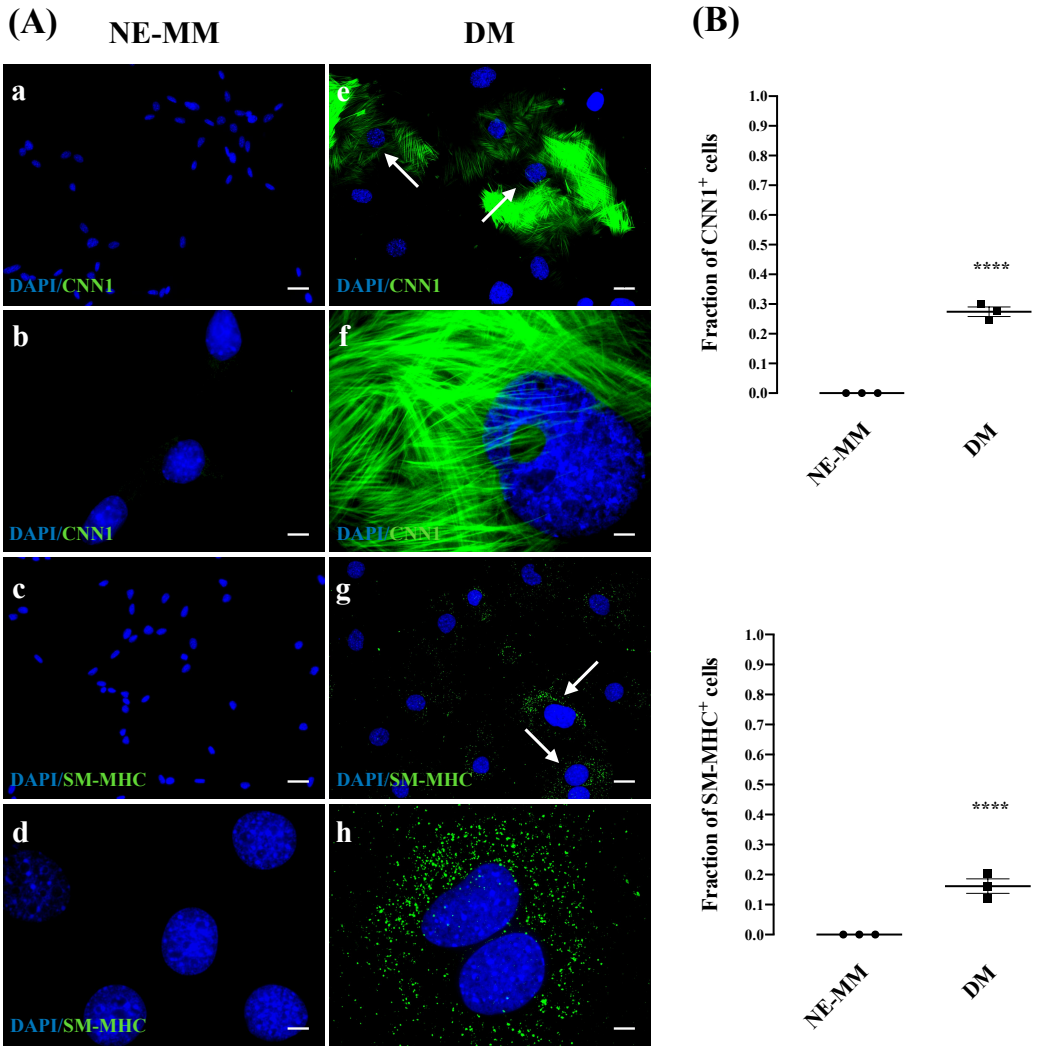

Figure 5.2. Myogenic differentiation of mouse aortic arch vascular stem cells (mAA-vSCs) in 10% FBS-containing DMEM (DM) for 7 days.

mAA-vSCs were cultured in neuroectodermal maintenance medium (NE-MM; control sample) and 10% FBS-containing DMEM (DM) for 7 days. SMC differentiation was analysed by PCR and immunocytochemistry.

(A) Immunocytochemical analysis was performed as descried in Section 2.4. Cell samples were immunostained for **(a, b, e, f)** Calponin1 (CNN1) and **(c, d, g, h)** smooth muscle myosin heavy chain (SM-MHC). Samples were probed with their corresponding AlexaFluor-488 secondary antibody. All images are representative of n ≥ 5. Scale bars, 20mm.

(B) Fraction of **(a)** CNN1-positive ($CNN1^+$) cells and **(b)** SM-MHC-positive ($SM\text{-}MHC^+$) cells in NE-MM versus DM after 7 days. The charts are representative of three independent experiments. Data are mean ± S.E.M. (n=3). Mann-Whitney test with significance value of $P \leq 0.05$. Results: ****$p < 0.0001$.

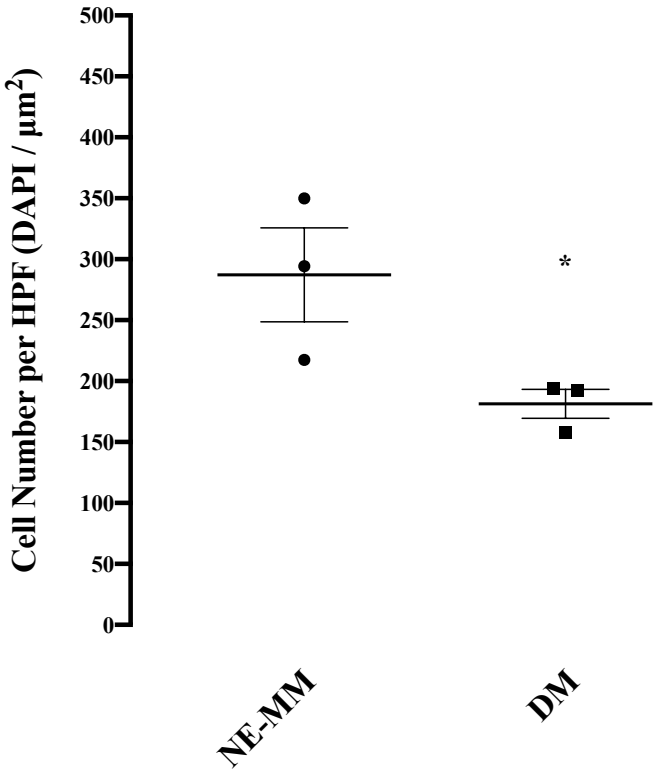

Figure 5.3. The cell number of mouse aortic arch vascular stem cells (mAA-vSCs) decreased 7 days after in 10% FBS-containing DMEM (DM).

mAA-vSCs were cultured in neuroectodermal maintenance medium (NE-MM; control sample) and 10% FBS-containing DMEM (DM) for 7 days. The number of cells per high-power field (HPF) was calculated using ImageJ™ and Excel Microsoft Office 2011. DAPI nuclear staining was used to count the number of cells per image in both NE-MM and DM group samples. The number of cells per HPF was calculated per image by dividing DAPI over the visible area under the magnification power of the selected objective, so values represent the number of cells per μm^2 were obtained. The chart is representative of three independent experiments. Data are mean ± S.E.M. (n=3). Unpaired t-test with significance value of $P \leq 0.05$. Results: *p=0.0106.

5.3.2 Jagged1-dependent Notch signaling but not TGF-β1 drives differentiation of mAA-vSCs and mTA-vSCs into mature SMCs.

5.3.2.1 Vascular stem cells from murine aortic arch and thoracic aorta respond similarly to TGF-β1 signalling.

Vascular stem cells isolated from the tunica media of murine aortic arch (mAA-vSCs) and thoracic aorta (mTA-vSCs) were cultured in NE-MM supplemented with 2 ng/ml of rmTGF-β1 or vehicle (control) for 7 days.

Real time RT-qPCR and immunocytochemistry analysis revealed that both cell lines responded in a similar manner to TGF-β1 treatment (TGβ1 treatment). At 7 days, the expression levels of Cnn1 transcript increased by 23.00 ± 0.14 (Figure 5.4, a) and 23.00 ± 1.98 (Figure 5.8, a) fold in mAA-vSCs and mTA-vSCs, respectively. On the other hand, no changes in the levels of Sm-mhc mRNA were observed in TGβ1-treated mAA-vSCs compared to control sample after 7 days (Figure 5.4, b). The mTA-vSCs seemed to have a reduction in the levels of Sm-mhc mRNA by 0.84 ± 0.03 fold change after 7-day treatment (Figure 5.8, b).

Immunocytochemical analysis revealed an increase in the fraction of cells staining positive for the intermediate smooth muscle marker, calponin1 (CNN1) 7 days after TGβ1 treatment (Figure 5.5 and 5.9). The fraction of positive cells was 0.33 ± 0.03 and 0.31 ± 0.03 in the mAA-vSCs (Figure 5.6) and mTA-vSCs (Figure 5.10), respectively, 7 days after TGβ1 treatment. In contrast, there was no increase in the mature smooth muscle marker, Sm-mhc transcript levels following TGβ1-treatment of cells after 7 days (Figure 5.4 and Figure 5.8).

There was a significant decrease in cell numbers per μm^2 for both vascular stem cell populations (mAA-vSCs and mTA-vSCs) after 7-day TGβ1 treatment. The number of cells per μm^2 decreased from 454.5 ± 45.37 to 78.20 ± 5.3 in TGβ1-treated mAA-vSCs (Figure 5.7). Similarly, the number of cells per μm^2 in the mTA-vSCs declined from 327.5 ± 155.6 to 92.30 ± 32.46 7 days after TGβ1 treatment (Figure 5.11).

5.3.2.2 Vascular stem cells from murine aortic arch and thoracic aorta respond similarly to Jagged1-activated Notch signalling

The mAA-vSCs and mTA-vSCs were cultured in plates pre-coated with either immobilised Jagged1-Fc (Jag1-Fc) or IgG-Fc (control) for 7 days in neuroectodermal maintenance medium (NE-MM) in order to induce myogenic differentiation.

Real time RT-qPCR and immunocytochemistry analysis demonstrated that both cell lines responded in a similar manner to SMC differentiation upon Jagged1-dependent Notch activation. 7 days after Jagged1 treatment of mAA-vSCs, a significant increase in the expression levels of the Notch target gene, Hey1 was detected by PCR analysis (293.8 ± 41.98 fold change) (Figure 5.12, a). Cnn1 and Sm-mhc transcript levels were also analysed by PCR exhibiting an increased expression of 9.63 ± 1.90 and 45.73 ± 3.26 (Figure 5.12, b and c) folds, respectively. Similarly, jagged1 treatment in mTA-vSCs increased the relative mRNA expression of Hey1, Cnn1, and Sm-mhc genes by 18.14 ± 1.79, 27.60 ± 7.41 and 14.01 ± 1.86 folds, respectively (Figure 5.19).

Concomitantly, immunocytochemical analysis demonstrated positive expression of CNN1 and SMC-MHC in both cell progenitors following Jagged1 treatment. In the mAA-vSCs Jagged1 treatment significantly increased the expression of CNN1 and SM-MHC proteins (Figure 5.13) by a fraction of 0.15 ± 0.03 and 0.10 ± 0.03 respectively (Figure 5.14). Similarly, the expression of the CNN1 protein in mTA-vSCs significantly incremented by a fraction of 0.12 ± 0.04 (Figure 5.20 and Figure 21) 7 days after Jagged1 treatment. Even though SM-MHC expressing cells were detected (Figure 5.20, c, d, g and h), the fraction of cells positive for this marker did not show relevant significance (0.02 ± 0.01) (Figure 5.21, b).

There was a significant decrease in cell numbers per μm^2 for both vascular stem cell populations (mAA-vSCs and mTA-vSCs) after 7-day Jagged1 treatment. The number of cells per μm^2 decreased from 454.5 ± 45.37 to 314.7 ± 37.09 in Jag1-Fc-treated mAA-vSCs (Figure 5.15). Similarly, the number of cells per μm^2 in the mTA-vSCs declined from 327.5 ± 40.18 to 182.0 ± 17.67 7 days after Jag1-Fc-treatment (Figure 5.22).

ChIP-PCR was performed on mAA-vSCs 7 days after Jagged1 treatment in order to

evaluate the level of enrichment of the histone modifications, H3K4me2 and H3K27me27 and the DNA di-methylase TET-2 at the SM-MHC promoter. Controls were used to calculate relative levels of enrichment including mouse embryonic stem cells (mESCs), mouse smooth muscle cells (mSMCs) and fresh mouse aortic tissue (mAorta). The results demonstrate that there was a large fold enrichment of H3K4me2 (95.32 ± 10.59) coincident with a reduction of the H3K27me3 (2.79 ± 0.47) at the Sm-mhc locus 7 days after treatment (Figure 5.16 and 5.17). The fold enrichment of TET-2 on the Jag1-treated cells was elevated after 7 days compared to the Fc control, 7.44 ± 1.24 and 4.16 ± 0.76, respectively; however, it was still low compared to mAorta (195.2 ± 9.03) and mSMC (19.33 ± 3.53) samples (Figure 5.18). The data suggested that activation of the Notch on AA-vSCs induced changes in the chromatin at the Sm-mhc promoter facilitating its transcription and thus SMC differentiation.

The data from this section is summarized Table 5-1 and Table 5-1 showed the level of gene expressions (as mean ± S.E.M.) in both mAA-vSCs and mTA-vSCs upon 7 days of rmTGF-β1 and recombinant Jagged1 treatment. Table 5-2 exhibited the level of protein expressions (fraction of positive cells as mean ± S.E.M.) in both mAA-vSCs and mTA-vSCs upon 7 days of rmTGF-β1 and recombinant Jagged1 treatment. In order to compare and make a final conclusion about the responsiveness of mAA-vSCs against mTA-vSCs to SMC induction, the data was interpreted by degree of expression namely, none, low, intermediate and high. The data revealed that TGF-β1 significantly increased the gene and protein expressions of the SMC marker Calponin1 (CNN1) in mAA-vSCs and mTA-vSCs but not those of the mature SMC marker, SM-MHC. Based on the protein expression profile of CNN1, TGF-β1 exerted high levels of expression on both cell progenitors, whereas Jag1-Fc induced an intermediate CNN1 expression on both cell types (Table 5-2). Cnn1 transcript levels in the mTA-vSCs showed an intermediate increment 7 days after TGF-β1 and Jag1-Fc treatment. The level of Cnn1 mRNA in mAA-vSCs was high in TGF-β1-treated cells, however Jagged1 treatment resulted in low levels of Cnn1 expression at 7 days.

Additionally, SM-MHC protein levels were intermediate for the mAA-vSCs and low for the mTA-vSCs, albeit the fraction of positive cells in the latter cell type was not significant. Similarly, the transcript levels of Sm-mhc in mAA-vSCs and mTA-vSCs after 7-day Jagged1 treatment, was intermediate and low, respectively. PCR analysis

was carried out on the Notch target gene, Hey1 to confirm activation of Notch by its ligand Jagged1 resulting in high and intermediate expression levels in mAA-vSCs and mTA-vSCs, respectively, post-treatment.

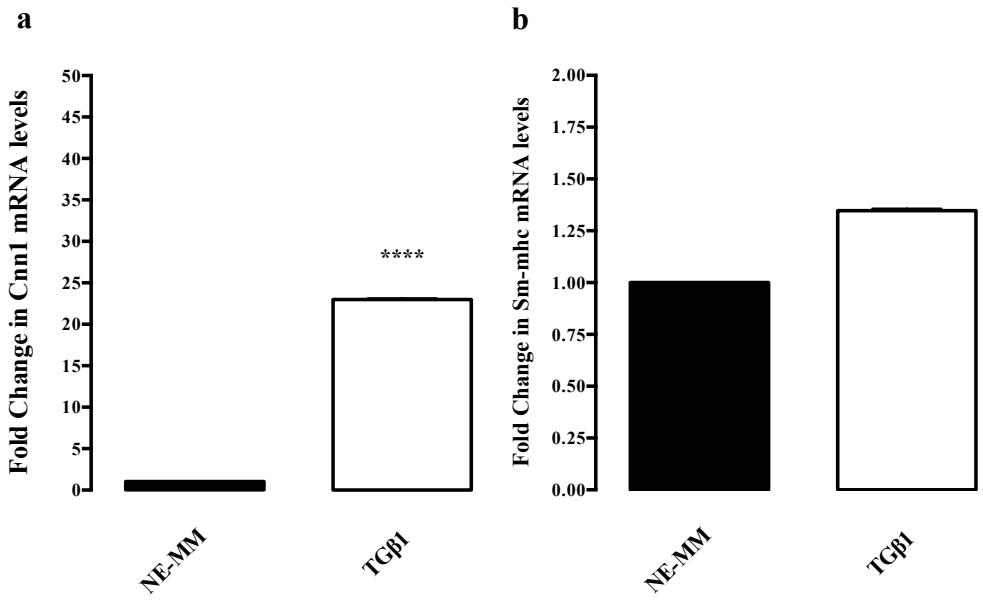

Figure 5.4. Calponin1 mRNA levels significantly increased on mAA-vSC 7 days after TGF-β1 treatment.

mAA-vSCs were cultured in neuroectodermal maintenance medium (NE-MM) supplemented with 2 ng/ml of TGF-β1 (TGβ1) or NE-MM (Control) for 7 days. Relative mRNA expression levels of **(a)** Calponin1 (Cnn1) and **(b)** smooth muscle myosin heavy chain (Sm-mhc) were calculated using the Comparative C_T method ($\Delta\Delta C_T$). The data was normalised against the endogenous gene HPRT. The experiments were performed in triplicate, charts are representatives of three independent experiments. Data are mean ± S.E.M (n=3). Mann-Whitney test with significance value of $P \leq 0.05$. Results: *$p<0.05$.

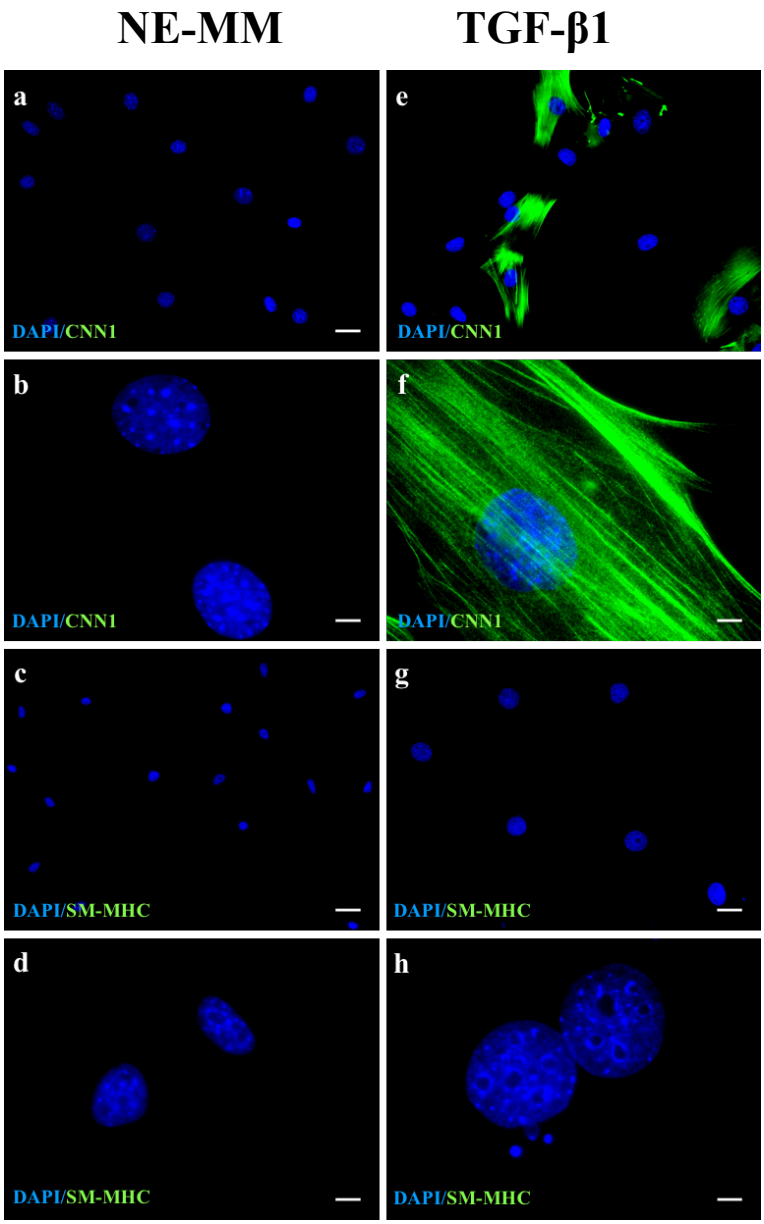

Figure 5.5. Calponin1 protein levels significantly increased on mAA-vSC 7 days after TGF-β1 treatment.

mAA-vSCs were cultured in neuroectodermal maintenance medium (NE-MM) supplemented with 2 ng/ml of TGF-β1 (TGβ1) or NE-MM (Control) for 7 days. Immunocytochemistry technique was performed as descried in Section 2.4. Cell samples were immunostained for **(a, b, e, f)** Calponin1 (CNN1) and **(c, d, g, h)** smooth muscle myosin heavy chain (SM-MHC). Samples were probed with their corresponding AlexaFluor-488 secondary antibody. Representative images are shown at **(a, c, e, g)** 20X and **(b, d, f, h)** 60X magnification power. All images are representative of n ≥ 5. Scale bars, 20mm.

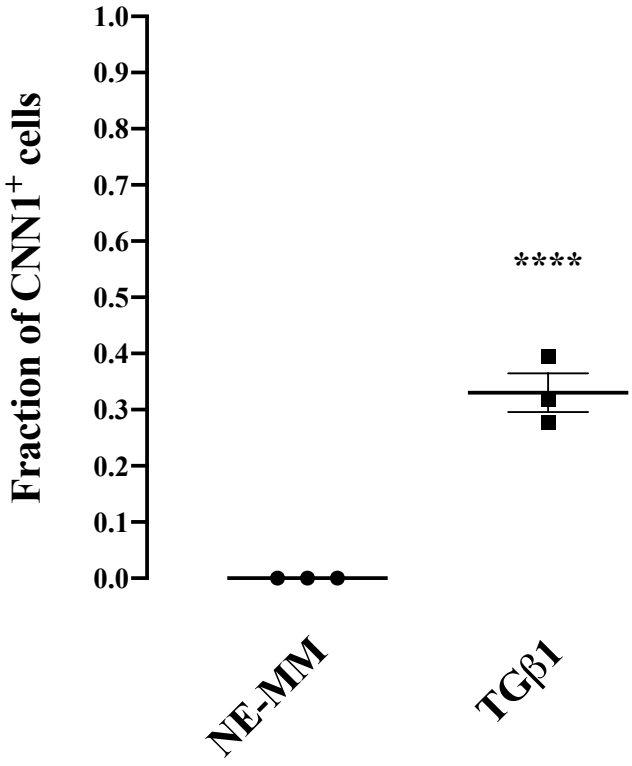

Figure 5.6. The fraction of cells positively expressing Calponin1 significantly increased on mAA-vSC 7 days after TGF-β1 treatment.

mAA-vSCs were cultured in neuroectodermal maintenance medium (NE-MM) supplemented with 2 ng/ml of TGF-β1 (TGβ1) or NE-MM (Control) for 7 days. Fraction of CNN1-positive ($CNN1^+$) cells in NE-MM (control) versus TGβ1-treated samples 7 days after treatment. The chart is representative of three independent experiments. Data are mean ± S.E.M. (n=3). Mann-Whitney test with significance value of $P \leq 0.05$. Results: ****$p<0.0001$.

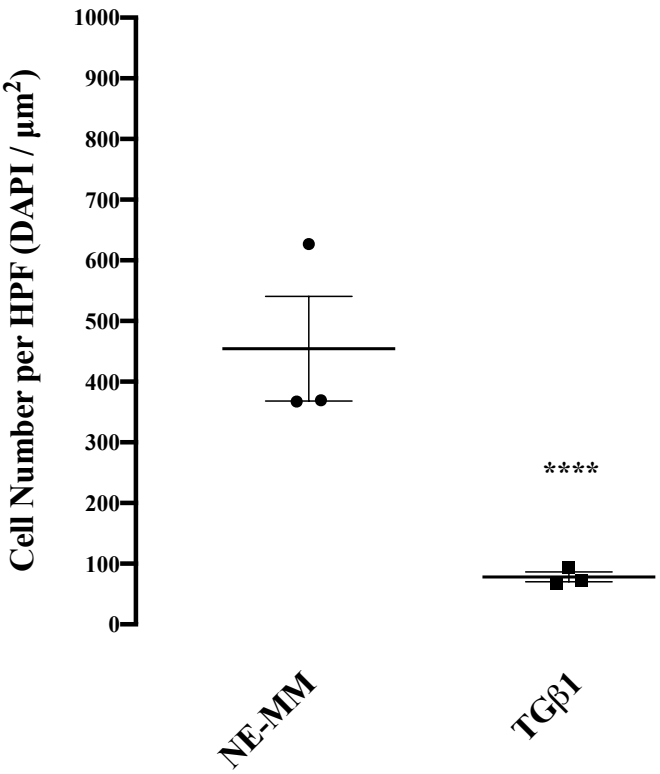

Figure 5.7. The cell number of mAA-vSCs decreased 7 days after TGF-□1 treatment.

mAA-vSCs were cultured in neuroectodermal maintenance medium (NE-MM) supplemented with 2 ng/ml of TGF-β1 (TGβ1) or NE-MM (Control) for 7 days. The number of cells per high-power field (HPF) was calculated using ImageJ™ and Excel Microsoft Office 2011. DAPI nuclear staining was used to count the number of cells per image in both NE-MM and TGβ1 group samples. The number of cells per HPF was calculated per image by dividing DAPI over the visible area under the magnification power of the selected objective, so values represent the number of cells per μm^2. The chart is representative of three independent experiments. Data are mean ± S.E.M. (n=3). Unpaired t-test with significance value of P≤0.05. Results: ****p<0.0001.

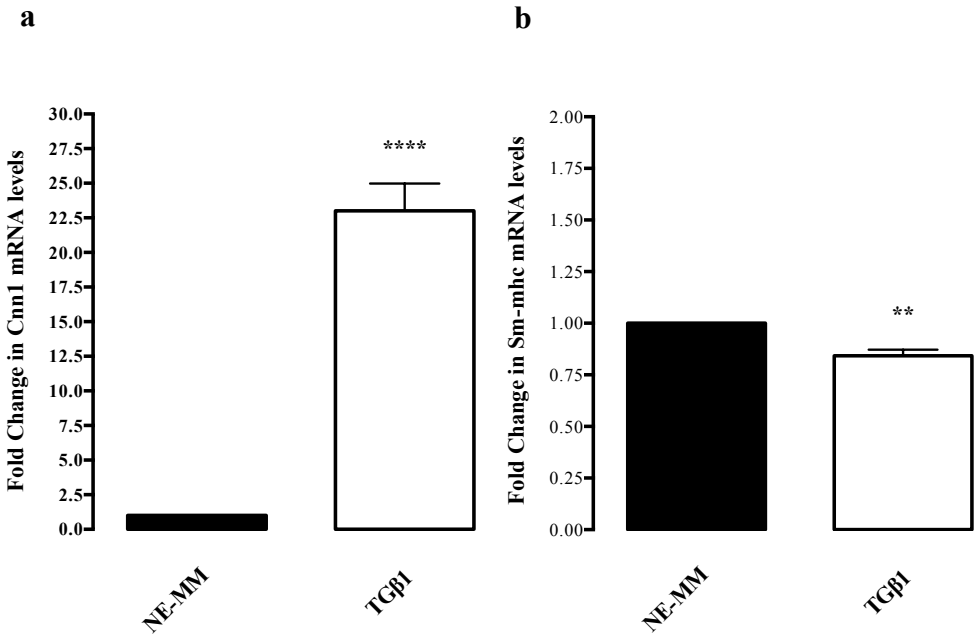

Figure 5.8. Calponin1 mRNA levels significantly increased on mTA-vSC 7 days after TGF-β1 treatment.

mTA-vSCs were cultured in neuroectodermal maintenance medium (NE-MM) supplemented with 2 ng/ml of TGF-β1 (TGβ1) or NE-MM (Control) for 7 days. Relative mRNA expression levels of **(a)** Calponin1 (Cnn1) and **(b)** smooth muscle myosin heavy chain (Sm-mhc) were calculated using the Comparative C_T method ($\Delta\Delta C_T$). The data was normalised against the endogenous gene HPRT. The experiments were performed in triplicate, charts are representatives of three independent experiments. Data are mean ± S.E.M (n=3). Mann-Whitney test with significance value of $P \leq 0.05$. Results: *$p<0.05$.

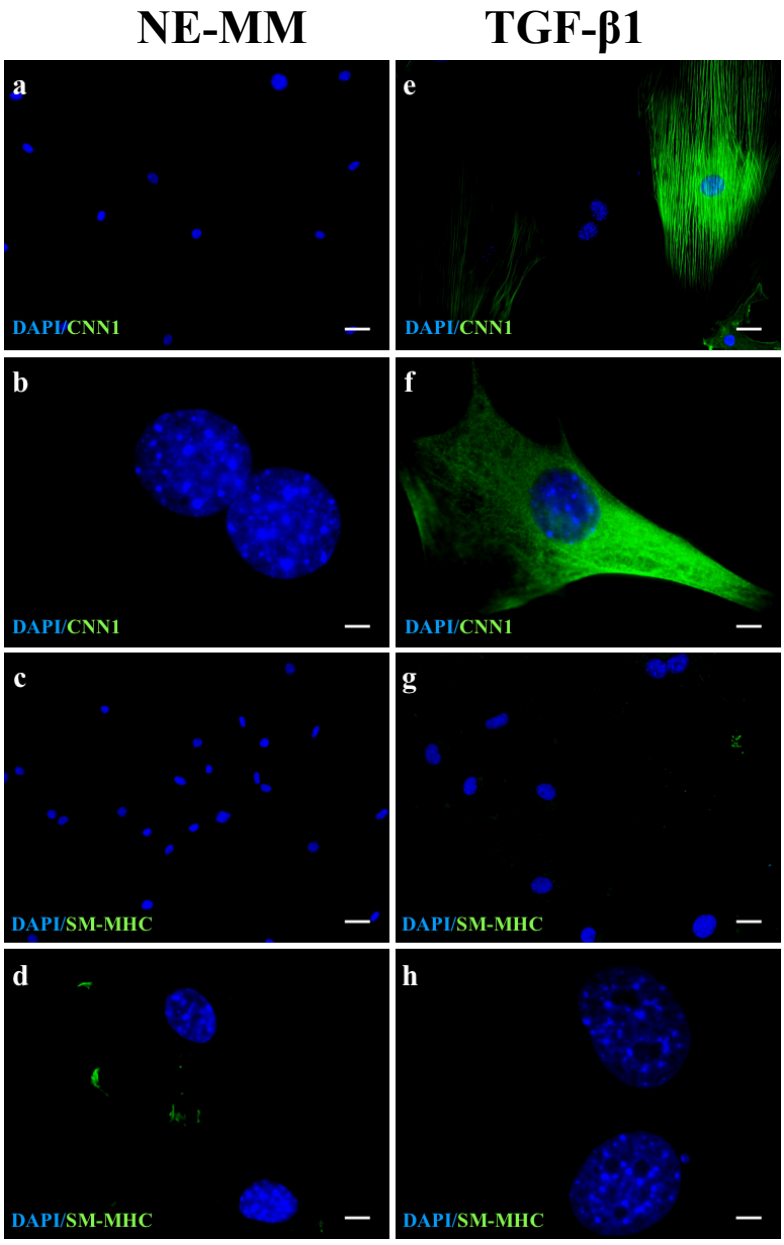

Figure 5.9. Calponin1 protein levels significantly increased on mTA-vSC 7 days after TGF-β1 treatment.

mTA-vSCs were cultured in neuroectodermal maintenance medium (NE-MM) supplemented with 2 ng/ml of TGF-β1 (TGβ1) or NE-MM (Control) for 7 days. Immunocytochemistry technique was performed as descried in Section 2.4. Cell samples were immunostained for **(a, b, e, f)** Calponin1 (CNN1) and **(c, d, g, h)** smooth muscle myosin heavy chain (SM-MHC). Samples were probed with their corresponding AlexaFluor-488 secondary antibody. Representative images are shown at **(a, c, e, g)** 20X and **(b, d, f, h)** 60X magnification power. All images are representative of $n \geq 5$. Scale bars, 20mm.

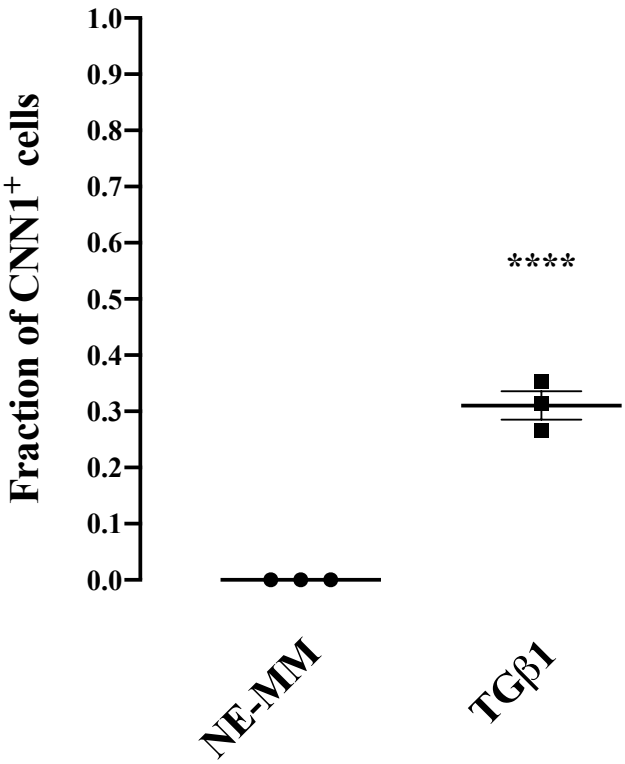

Figure 5.10. The fraction of cells positively expressing Calponin1 significantly increased on mTA-vSC 7 days after TGF-β1 treatment.

The mTA-vSCs were cultured in neuroectodermal maintenance medium (NE-MM) supplemented with 2 ng/ml of TGF-β1 (TGβ1) or NE-MM (Control) for 7 days. Fraction of CNN1-positive ($CNN1^+$) cells in TGβ1-treated versus NE-MM (control) samples 7 days after treatment. The chart is representative of three independent experiments. Data are mean ± S.E.M. (n=3). Mann-Whitney test with significance value of $P \leq 0.05$. Results: ****$p<0.0001$.

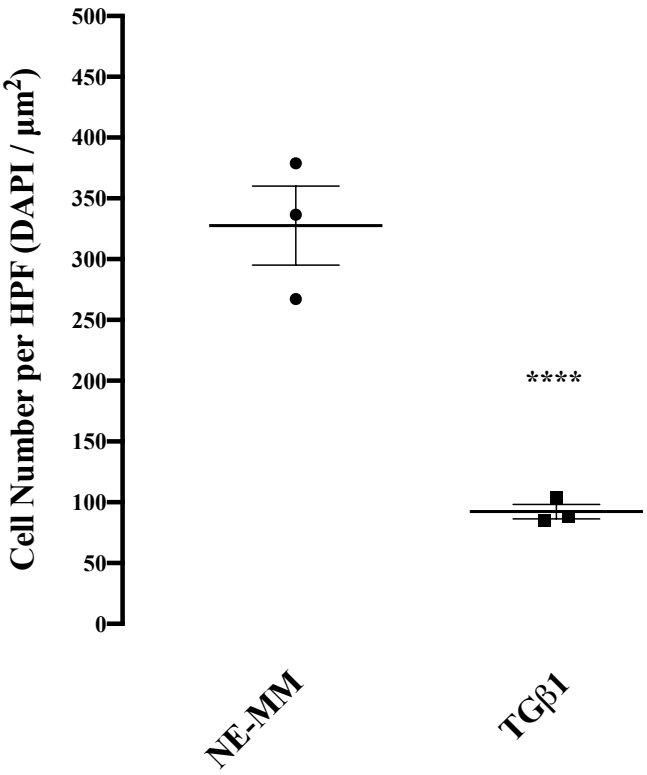

Figure 5.11. The cell number of mTA-vSCs decreased 7 days after TGF-β1 treatment.

mTA-vSCs were cultured in neuroectodermal maintenance medium (NE-MM) supplemented with 2 ng/ml of TGF-β1 (TGβ1) or NE-MM (Control) for 7 days. The number of cells per high-power field (HPF) was calculated using ImageJ™ and Excel Microsoft Office 2011. DAPI nuclear staining was used to count the number of cells per image in both NE-MM and TGβ1 group samples. The number of cells per HPF was calculated per image by dividing DAPI over the visible area under the magnification power of the selected objective, so values represent the number of cells per μm^2. The chart is representative of three independent experiments. Data are mean ± S.E.M. (n=3). Mann-Whitney t-test with significance value of $P \leq 0.05$. Results: ****$p<0.0001$.

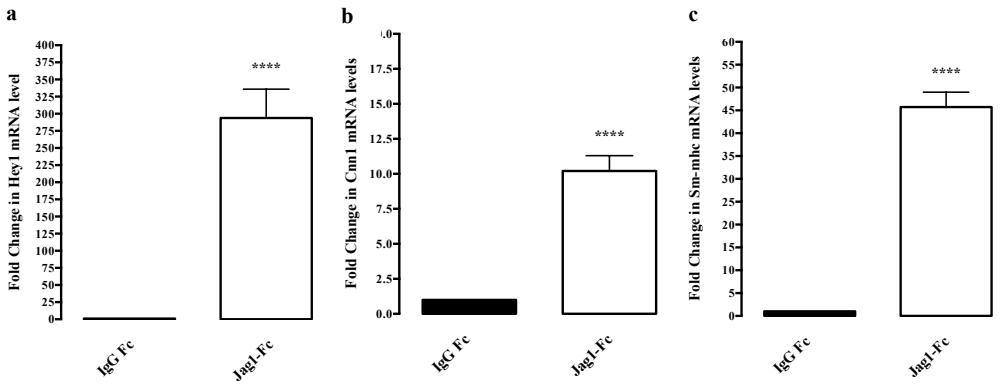

Figure 5.12. Hey1, Calponin1 and Sm-mhc mRNA levels significantly increased on mAA-vSC 7 days after Jagged1-activated Notch signalling.

mAA-vSCs were cultured on plates coated with immobilised 500 ng/ml of Jagged1-Fc (Jag1-Fc) or IgG-Fc (as control) in neuroectodermal maintenance medium (NE-MM) for 7 days. Relative mRNA expression levels of **(a)** Hey1, **(b)** Calponin1 (Cnn1) and **(c)** smooth muscle myosin heavy chain (Sm-mhc) were calculated using the Comparative C_T method ($\Delta\Delta C_T$). The data was normalised against the endogenous gene HPRT. The experiments were performed in triplicate, charts are representatives of three independent experiments. Data are mean ± S.E.M (n=3). Data are mean ± S.E.M (n=3). Mann-Whitney test with significance value of $P \leq 0.05$. Results: ****$p<0.0001$.

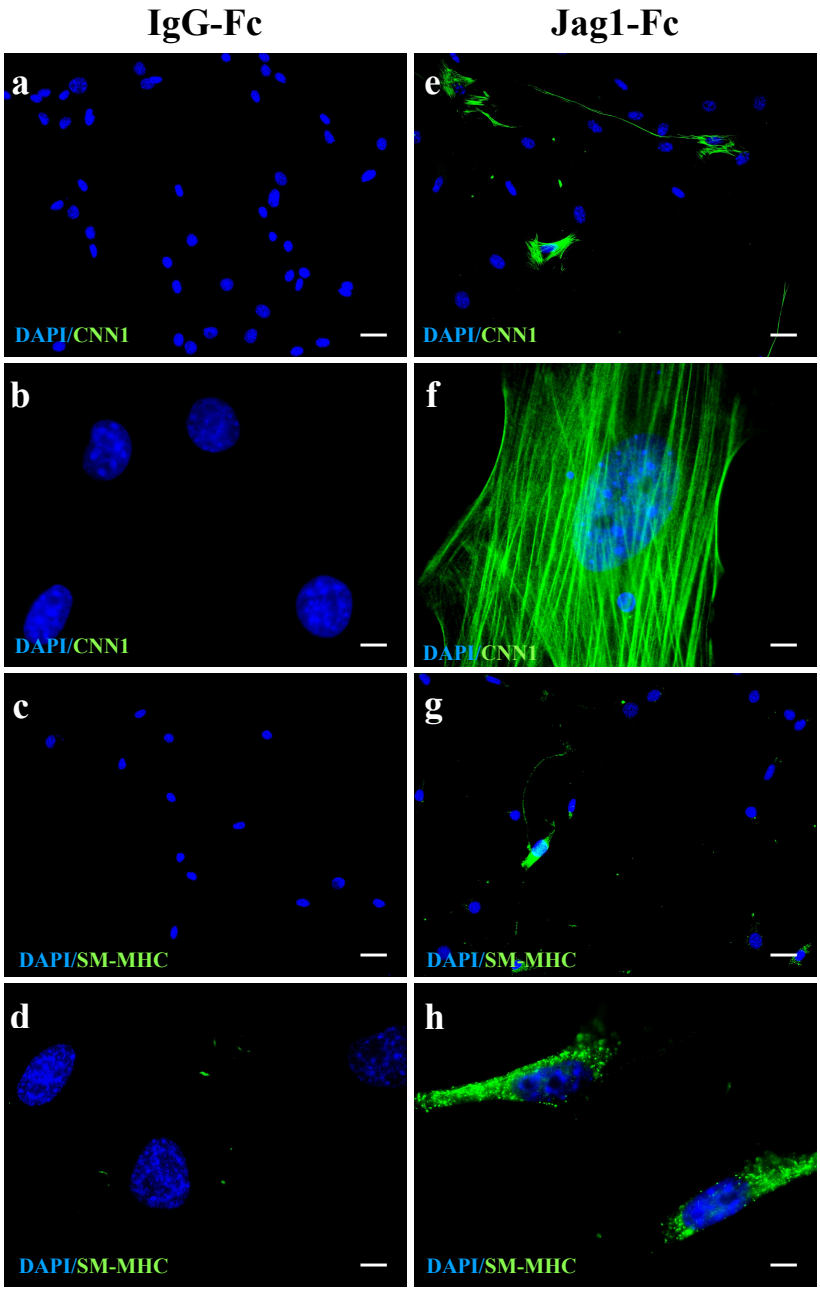

Figure 5.13. Calponin1 and SM-MHC protein levels significantly increased on mAA-vSC 7 days after Jagged1-activated Notch signalling.

mAA-vSCs were cultured on plates coated with immobilised 500 ng/ml of Jagged1-Fc (Jag1-Fc) or IgG-Fc (as control) in neuroectodermal maintenance medium (NE-MM) for 7 days. Immunocytochemistry technique was performed as descried in Section 2.4. Cell samples were immunostained for **(a, b, e, f)** Calponin1 (CNN1) and **(c, d, g, h)** smooth muscle myosin heavy chain (SM-MHC). Samples were probed with their corresponding AlexaFluor-488 secondary antibody. Representative images are shown at **(a, c, e, g)** 20X and **(b, d, f, h)** 60X magnification power. All images are representative of $n \geq 5$. Scale bars, 20mm.

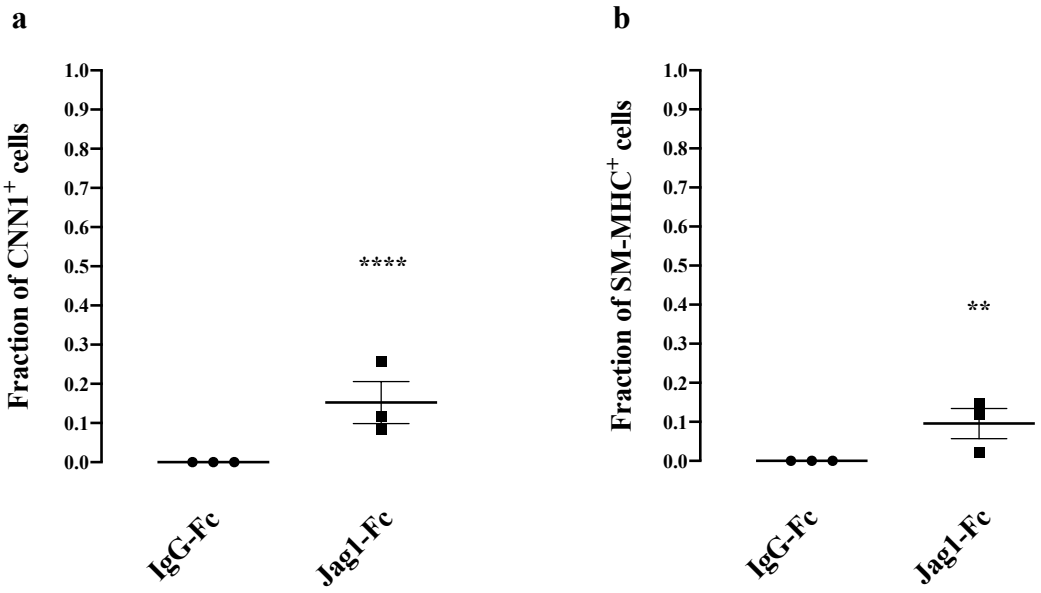

Figure 5.14. The fraction of cells positively expressing Calponin1 and SM-MHC significantly increased on mAA-vSC 7 days after Jagged1-activated Notch signalling.

mAA-vSCs were cultured on plates coated with immobilised 500 ng/ml of Jagged1-Fc (Jag1-Fc) or IgG-Fc (as control) in neuroectodermal maintenance medium (NE-MM) for 7 days. Fraction of **(a)** CNN1-positive ($CNN1^+$) and **(b)** SM-MHC-positive ($SM\text{-}MHC^+$) cells in Jag1-Fc-treated versus IgG-Fc (control) samples 7 days after treatment. The charts are representative of three independent experiments. Data are mean ± S.E.M. (n=3). Mann-Whitney test with significance value of $P \leq 0.05$. Results: **p<0.01 ****p<0.0001.

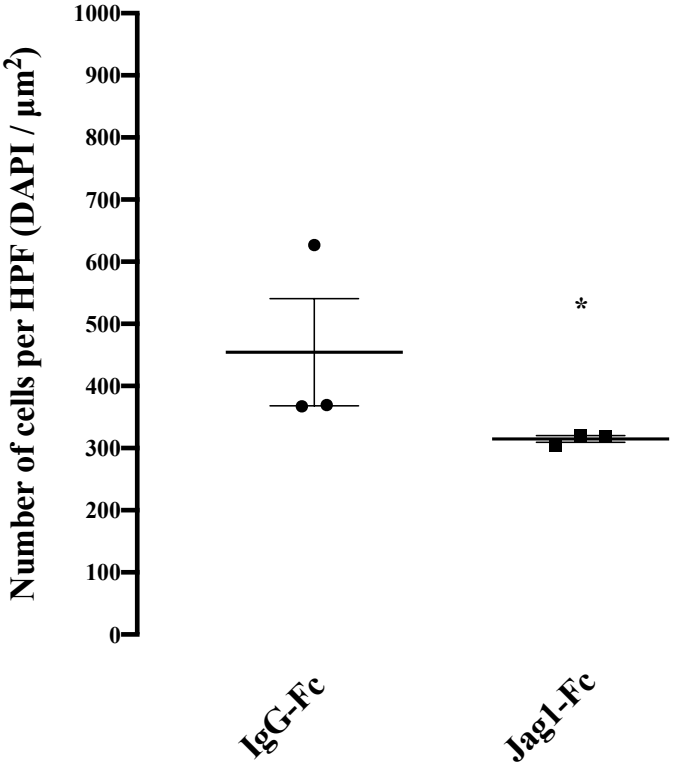

Figure 5.15. The cell number of mAA-vSCs decreased 7 days after Jagged1-activated Notch signalling.

mAA-vSCs were cultured on plates coated with immobilised 500 ng/ml of Jagged1-Fc (Jag1-Fc) or IgG-Fc (as control) in neuroectodermal maintenance medium (NE-MM) for 7 days. The number of cells per high-power field (HPF) was calculated using ImageJ™ and Excel Microsoft Office 2011. DAPI nuclear staining was used to count the number of cells per image in both Jag1-Fc and IgG-Fc group samples. The number of cells per HPF was calculated per image by dividing DAPI over the visible area under the magnification power of the selected objective, so values represent the number of cells per μm^2. The chart is representative of three independent experiments. Data are mean ± S.E.M. (n=3). Unpaired t-test with significance value of $P \leq 0.05$. Results: *$p<0.05$.

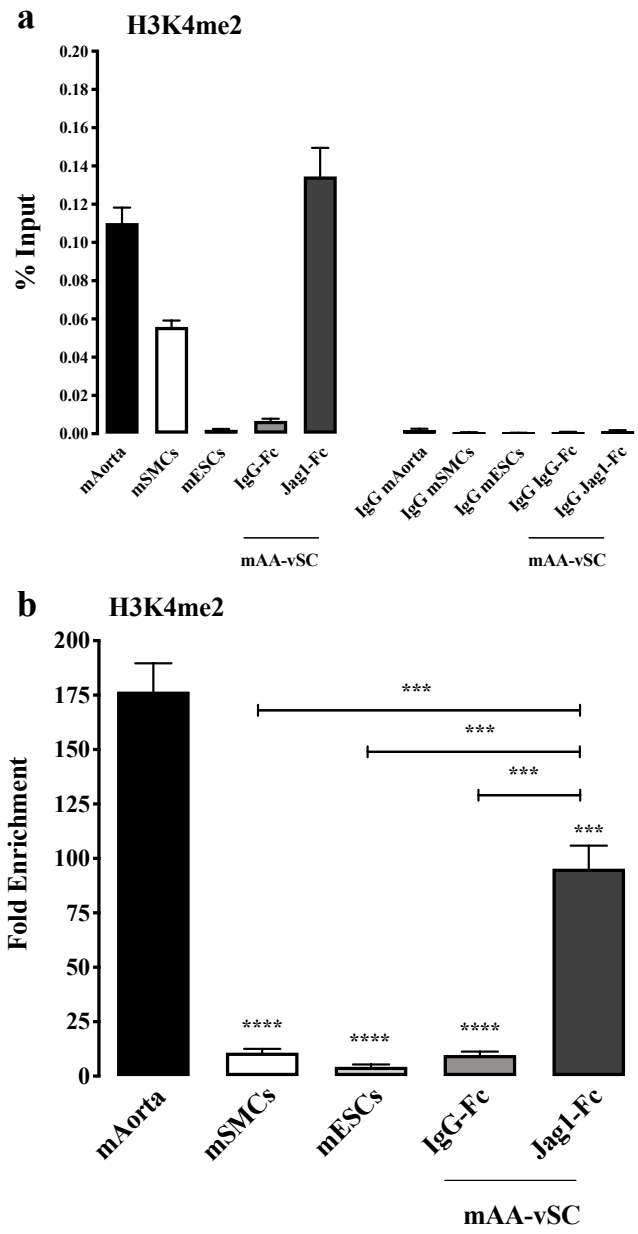

Figure 5.16. The histone modification H3K4me2 is enriched at the SM-MHC gene locus after Jagged1-activated Notch signalling on mAA-vSCs.

mAA-vSCs were cultured on plates coated with immobilised 500 ng/ml of Jagged1-Fc (Jag1-Fc) or IgG-Fc (as control) in neuroectodermal maintenance medium (NE-MM) for 7 days. **(a)** The % Input and **(b)** fold enrichment of dimethylation of lysine 4 on histone 3 (H3K4me2) in mAA-vSCs at the SM-MHC locus. The experiments were performed in triplicate and are representative of three independent experiments. Data are mean ± S.E.M (n=3). One-way ANOVA with significance value of $P \leq 0.05$. Results: ****$p < 0.0001$. Turkey's test for multiple comparisons with significance value of $P \leq 0.05$. Results: ***$p < 0.001$ and ****$p < 0.0001$. Significance are against the control sample (mAorta), unless indicated by a capped line.

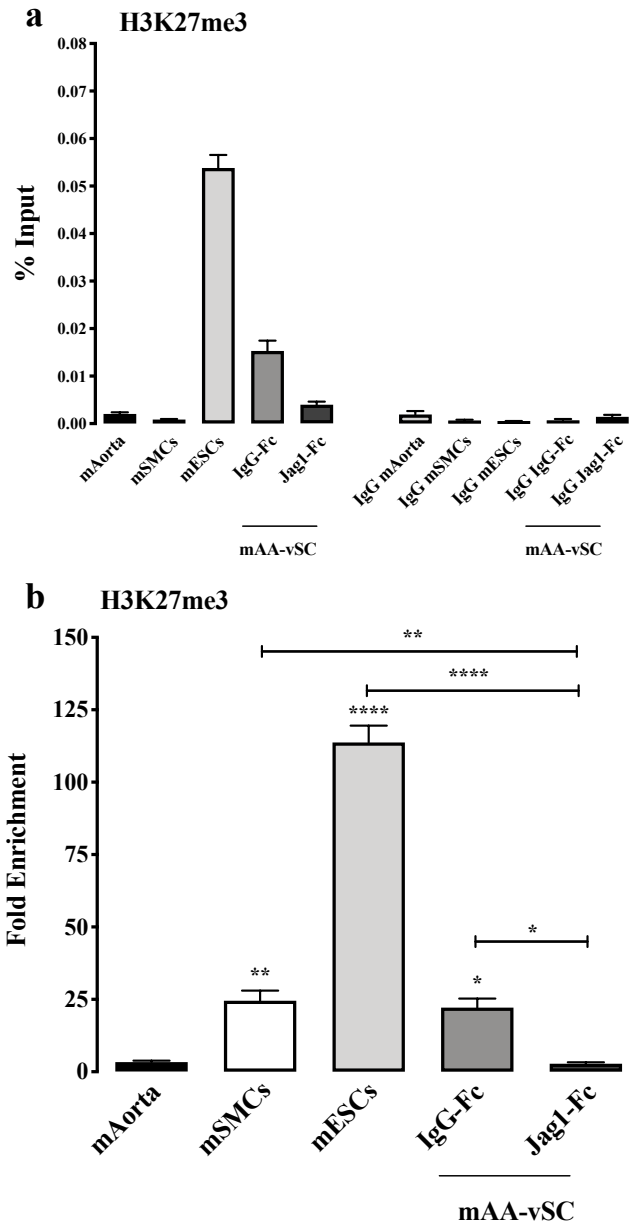

Figure 5.17. The histone modification H3K27me3 is enriched at the SM-MHC gene locus after Jagged1-activated Notch signalling on mAA-vSCs.

mAA-vSCs were cultured on plates coated with immobilised 500 ng/ml of Jagged1-Fc (Jag1-Fc) or IgG-Fc (as control) in neuroectodermal maintenance medium (NE-MM) for 7 days. **(a)** The % Input and **(b)** fold enrichment of trimethylation of lysine 27 on histone 3 (H3K27me3) in mAA-vSCs at the SM-MHC locus. The experiments were performed in triplicate and are representative of three independent experiments. Data are mean ± S.E.M (n=3). One-way ANOVA with significance value of $P \leq 0.05$. Results: ****$p<0.0001$. Turkey's test for multiple comparisons with significance value of $P \leq 0.05$. Results: ***$p<0.001$ and ****$p<0.0001$. Significance are against the control sample (mAorta), unless indicated by a capped line.

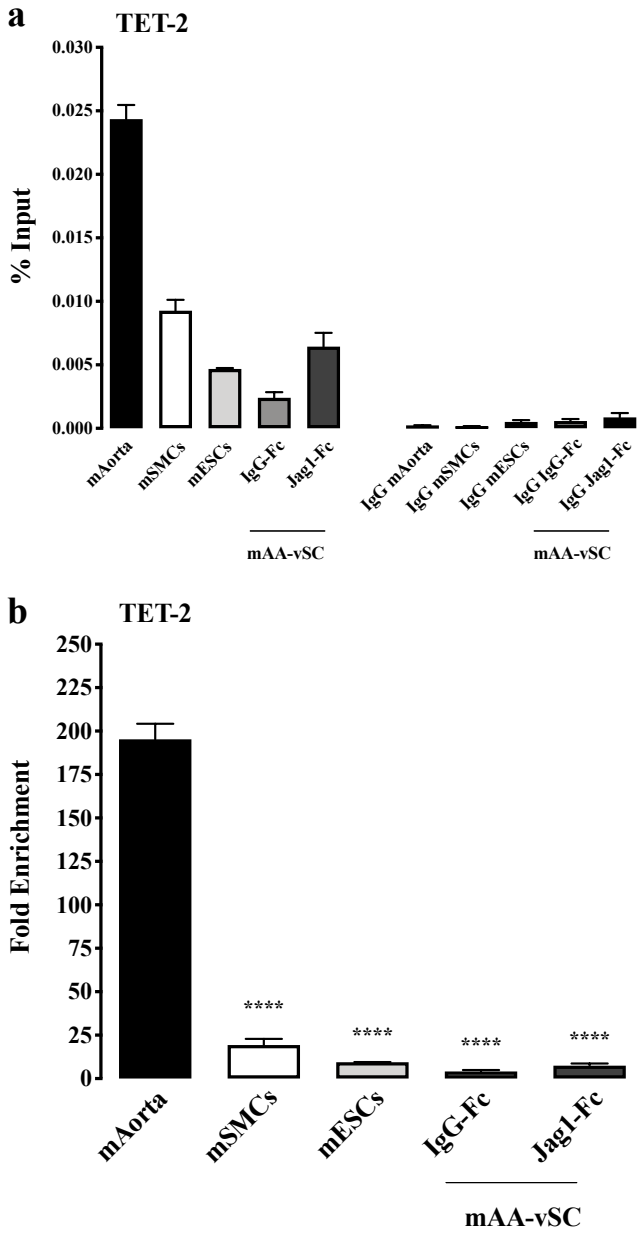

Figure 5.18. TET-2-binding at the SM-MHC gene locus after Jagged1-activated Notch signalling on mAA-vSCs.

mAA-vSCs were cultured on plates coated with immobilised 500 ng/ml of Jagged1-Fc (Jag1-Fc) or IgG-Fc (as control) in neuroectodermal maintenance medium (NE-MM) for 7 days. **(a)** The % Input and **(b)** fold enrichment of TET-2-binding in mAA-vSCs at the SM-MHC locus. The experiments were performed in triplicate and are representative of three independent experiments. Data are mean ± S.E.M (n=3). One-way ANOVA with significance value of $P \leq 0.05$. Results: ****$p<0.0001$. Turkey's test for multiple comparisons with significance value of $P \leq 0.05$. Results: ***$p<0.001$ and ****$p<0.0001$. Significance are against the control sample (mAorta), unless indicated by a capped line.

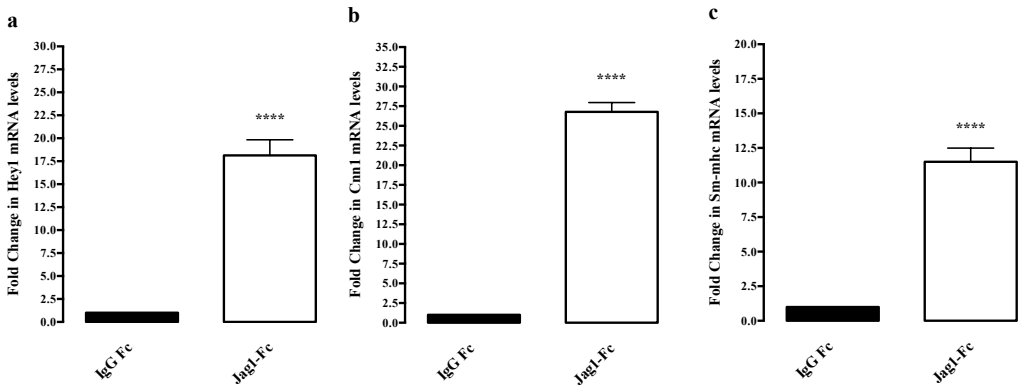

Figure 5.19. Hey1, Calponin1 and Sm-mhc mRNA levels significantly increased on mTA-vSC 7 days after Jagged1-activated Notch signalling.

mTA-vSCs were cultured on plates coated with immobilised 500 ng/ml of Jagged1-Fc (Jag1-Fc) or IgG-Fc (as control) in neuroectodermal maintenance medium (NE-MM) for 7 days. Relative mRNA expression levels of **(a)** Hey1, **(b)** Calponin1 (Cnn1) and **(c)** smooth muscle myosin heavy chain (Sm-mhc) were calculated using the Comparative C_T method ($\Delta\Delta C_T$). The data was normalised against the endogenous gene HPRT. The experiments were performed in triplicate, charts are representatives of three independent experiments. Data are mean ± S.E.M (n=3). Mann-Whitney test with significance value of $P \leq 0.05$. Results: ****$p<0.0001$.

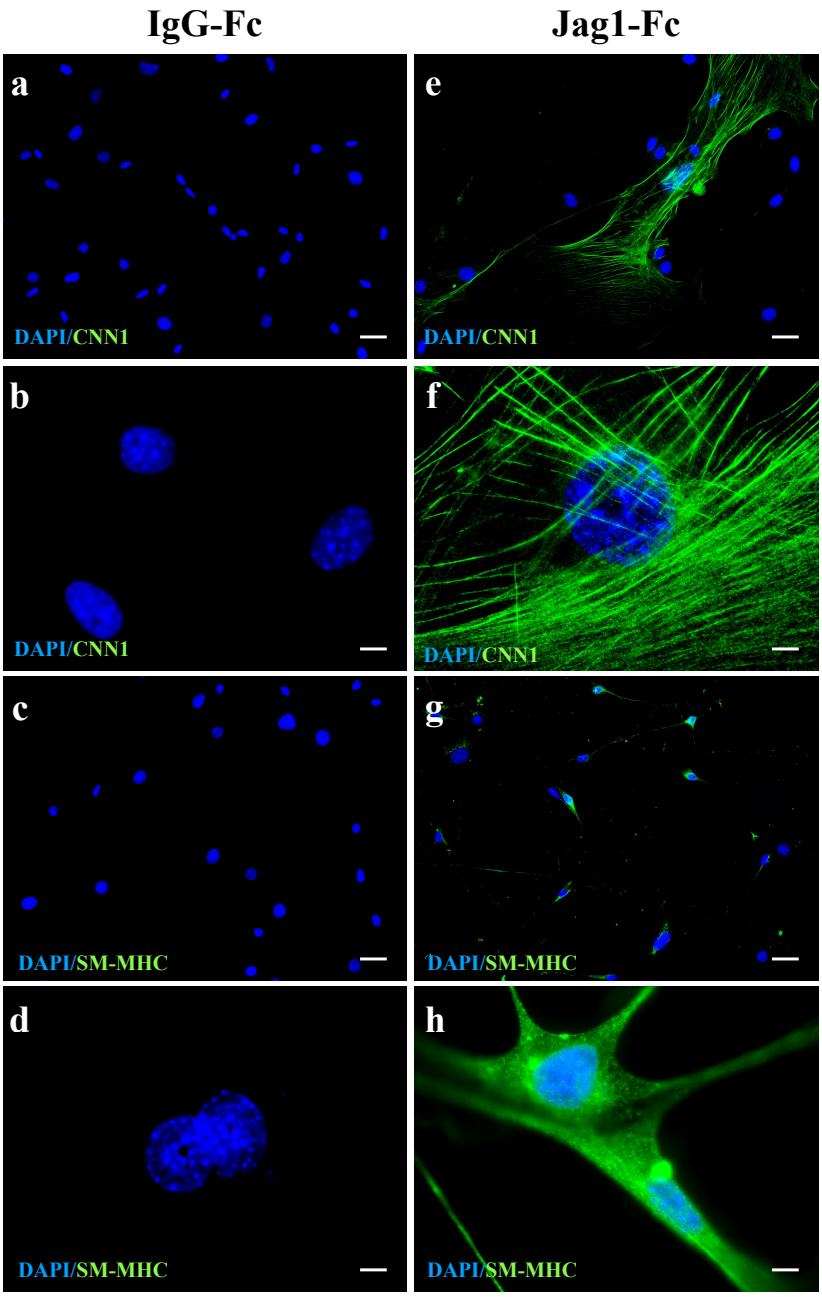

Figure 5.20. Calponin1 and SM-MHC protein levels significantly increased on mTA-vSC 7 days after Jagged1-activated Notch signalling.

mTA-vSCs were cultured on plates coated with immobilised 500 ng/ml of Jagged1-Fc (Jag1-Fc) or IgG-Fc (as control) in neuroectodermal maintenance medium (NE-MM) for 7 days. Immunocytochemistry technique was performed as descried in Section 2.4. Cell samples were immunostained for **(a, b, e, f)** Calponin1 (CNN1) and **(c, d, g, h)** smooth muscle myosin heavy chain (SM-MHC). Samples were probed with their corresponding AlexaFluor-488 secondary antibody. Representative images are shown at **(a, c, e, g)** 20X and **(b, d, f, h)** 60X magnification power. All images are representative of $n \geq 5$. Scale bars, 20mm.

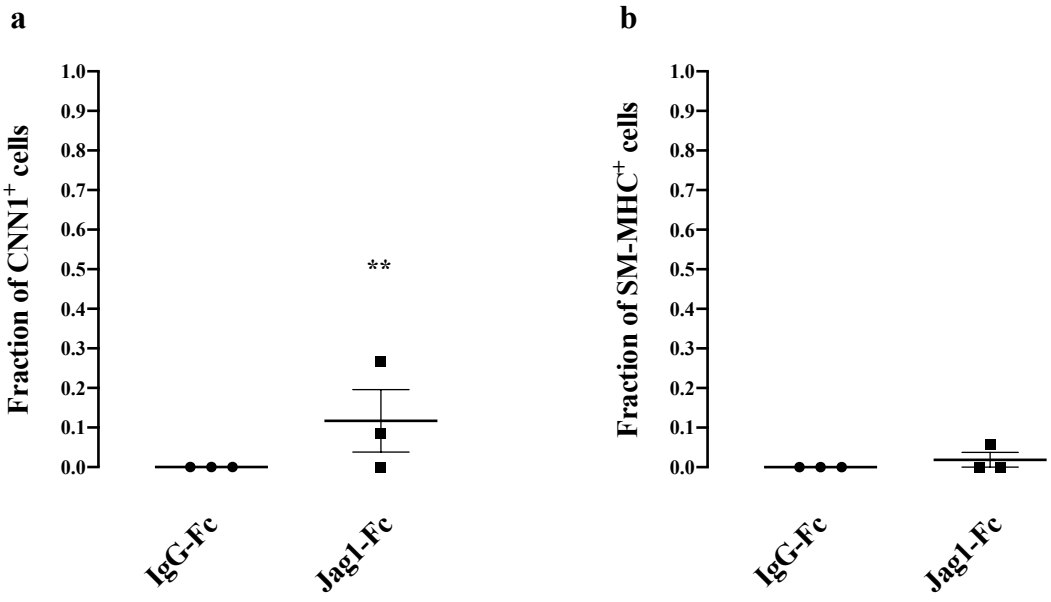

Figure 5.21. The fraction of cells positively expressing Calponin1 significantly increased on mTA-vSC 7 days after Jagged1-activated Notch signalling.

mTA-vSCs were cultured on plates coated with immobilised 500 ng/ml of Jagged1-Fc (Jag1-Fc) or IgG-Fc (as control) in neuroectodermal maintenance medium (NE-MM) for 7 days. Fraction of **(a)** CNN1-positive ($CNN1^+$) and **(b)** SM-MHC^+ cells in Jag1-Fc versus IgG-Fc (control) samples 7 days after treatment. The charts are representative of three independent experiments. Data are mean ± S.E.M. (n=3). Mann-Whitney test with significance value of $P \leq 0.05$. Results: $^{**}p<0.01$.

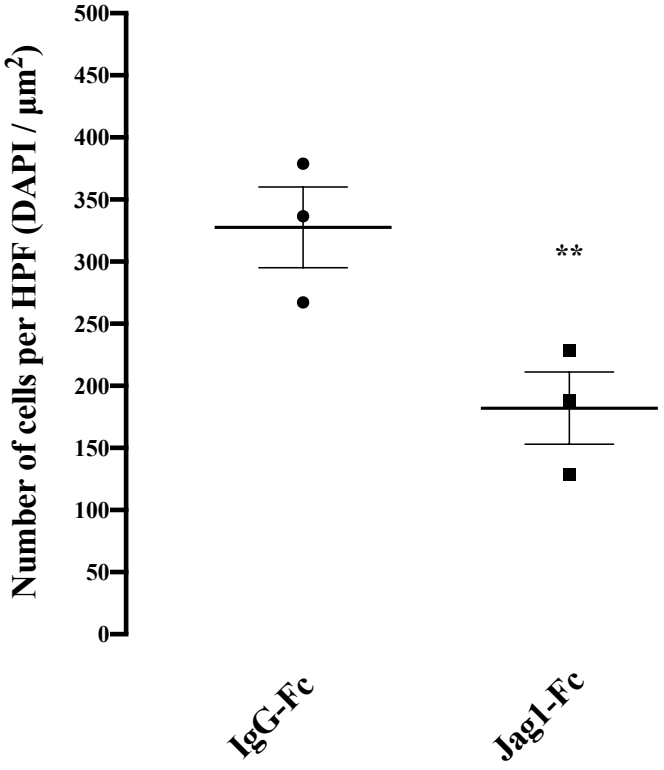

Figure 5.22. The cell number of mTA-vSCs decreased 7 days after Jagged1-activated Notch signalling.

mTA-vSCs were cultured on plates coated with immobilised 500 ng/ml of Jagged1-Fc (Jag1-Fc) or IgG-Fc (as control) in neuroectodermal maintenance medium (NE-MM) for 7 days. The number of cells per high-power field (HPF) was calculated using ImageJ™ and Excel Microsoft Office 2011. DAPI nuclear staining was used to count the number of cells per image in both Jag1-Fc and IgG-Fc group samples. The number of cells per HPF was calculated per image by dividing DAPI over the visible area under the magnification power of the selected objective, so values represent the number of cells per μm^2. The chart is representative of three independent experiments. Data are mean ± S.E.M. (n=3). Unpaired t-test with significance value of $P \leq 0.05$. Results: $^{**}p<0.01$.

Table 5-1. Responsiveness of mAA-vSCs and mTA-vSCs to myogenic differentiation according to gene expression.

Genes	Fold Change (mean ± S.E.M.)				Expression category			
	rmTGF-β1		rJagged1		rmTGF-β1		rJagged1	
	mAA-vSCs	mTA-vSCs	mAA-vSCs	mTA-vSCs	mAA-vSCs	mTA-vSCs	mAA-vSCs	mTA-vSCs
Cnn1	23.00 ± 0.14	23.00 ± 1.98	9.63 ± 1.90	27.60 ± 7.41	**	**	*	**
Sm-mhc	1.347 ± 0.01	0.84 ± 0.03	45.73 ± 3.26	14.01 ± 1.86	–	–	**	**
Hey1	———	———	293.8 ± 41.98	18.14 ± 1.79	———	———	***	**

Expression levels of Hey1, Calponin1 (Cnn1) and Smooth muscle myosin heavy chain (Sm-mhc) transcripts in mAA-vSCs and mTA-vSCs after myogenic differentiation. Cells were treated with either 2 ng/ml of rmTGF-β1 or 500 ng/ml of immobilized recombinant Jagged1-Fc protein in neuroectodermal maintenance medium (NE-MM) for 7 days. Fold changes were calculated using the Comparative C_T method ($\Delta\Delta C_T$). The data is representative of triplicate independent experiments. Data represent means ± S.E.M (n = 3). The level of responsiveness was given by categorising the mean expressions within the following ranges:

– ≤ 1 ≤ 3 fold change - None

* 3 ≤ 10 fold change – Low

** 10 ≤ 50 fold change – Intermediate

*** > 50 fold change – High

Table 5-2. Responsiveness of mAA-vSCs and mTA-vSCs to myogenic differentiation according to protein expression.

Protein	Fraction of positive cells (mean ± S.E.M.)				Expression category			
	rmTGF-β1		rJagged1		rmTGF-β1		rJagged1	
	mAA-vSCs	mTA-vSCs	mAA-vSCs	mTA-vSCs	mAA-vSCs	mTA-vSCs	mAA-vSCs	mTA-vSCs
CNN1	0.33 ± 0.03	0.31 ± 0.03	0.15 ± 0.03	0.12 ± 0.04	***	***	**	**
SM-MHC	None	None	0.10 ± 0.03	0.02 ± 0.01	–	–	**	*

Expression levels of Calponin1 (CNN1) and Smooth muscle myosin heavy chain (SM-MHC) proteins in mAA-vSCs and mTA-vSCs after myogenic differentiation. Cells were treated with either 2 ng/ml of rmTGF-β1 or 500 ng/ml of immobilized recombinant Jagged1-Fc protein in neuroectodermal maintenance medium (NE-MM) for 7 days. The fraction of positive cells expressing a marker was calculated over the total number of cells per image. The data is representative of triplicate independent experiments. Data represent means ± S.D. (n = 3). The level of responsiveness was given by categorising the mean expressions within the following ranges:

– 0.0 – None

* 0 ≤ 0.05 – Low

** 0.05 ≤ 0.20 – Intermediate

*** > 0.20 – High

5.3.3 Interaction studies between the TGF-β1 and Jagged1 signalling suggested that both pathways may be required for SMC induction, but Jagged1 activation is directly involved in SMC differentiation of vSCs.

5.3.3.1 TGF-β1-induced myogenic differentiation of vascular stem cells from murine aortic arch is prevented by the SMAD/TGF-β signalling inhibitor, SB431542

Vascular stem cells isolated from the tunica media of murine aortic arch were treated with either DMSO (control) or DMSO/rmTGF-β1 (2 ng/ml) or SB431542 (10 μM)/rmTGF-β1 (2 ng/ml) and cultured in NE-MM at 37°C, 5% CO_2 for 48 hours (hrs) and 7 days.

Real time RT-qPCR was performed to measure the expression levels of the TGF-β target gene, BCL2-like 11 (Bcl2l11) in each treatment group after 48 hrs. The expression levels of the apoptotic facilitator, Bcl2l11 decreased by 0.19 ± 0.4 fold change in rmTGF-β1-treated cells compared to the control sample (Figure 5.23, a). However, when rmTGF-β signalling was blocked with 10 μM of SB431542 the transcript levels of Bcl2l11 (0.85 ± 0.02) recovered to levels similar to the control sample (Figure 5.23, a). Moreover, the expression levels of Cnn1 mRNA increased in rmTGF-β1-treated cells by 11.33 ± 0.56 7 days after treatment compared to the control. On the other hand, when rmTGF-β1-treated cells were pre-incubated with 10 μM of SB431542 the transcript levels of Cnn1 (1.38 ± 0.03) decreased to levels similar to the control sample (Figure 5.23, b).

Immunocytochemical analysis revealed that 0.35 ± 0.04 fraction of cells were positively stained for the intermediate smooth muscle marker, calponin1 (CNN1) 7 days after rmTGF-β1 treatment (Figure 5.25). However, no significant $CNN1^+$ cells were observed in the rmTGF-β1/SB431542 after 7-day treatment. As previously shown in Section 5.2.2 TGF-β1 did not affect the levels of the mature smooth muscle cell marker, SM-MHC (Figure 5.24).

Concomitantly, the cell number in rmTGF-β1-treated mAA-vSCs decreased from 130.8 ± 7.2 to 92.30 ± 8.85 at day 7 (Figure 5.26). Once again 10 μM of SB431542 treatment inhibited the effect of rmTGF-β1 and thus increasing cell number to 131.7 ± 9.83 comparable to the control sample (Figure 5.26). All together the data suggest that activation of the TGF-β signalling pathway, results in decreased levels of Bcl2l11 transcript concomitant with induced differentiation of mAA-vSCs into SMC by increasing the gene and protein expression levels of CNN1. The myogenic effect of rmTGF-β1 was attenuated by treatment with the SMAD/TGF-β signalling, SB431542.

5.3.3.2 Jagged1-induced myogenic differentiation of vascular stem cells from murine aortic arch is prevented by the secretase inhibitor, DAPT

Vascular stem cells isolated from the tunica media of murine aortic arch were treated with either DMSO/IgG-Fc (500 ng/ml) (control) or DMSO/Jag1-Fc (500 ng/ml) (Jag1) or DAPT (80μM) /Jag1-Fc (500 ng/ml) (DT/Jag1) and cultured in NE-MM at 37°C, 5% CO_2 for 7 days.

Real time RT-qPCR was performed to measure the expression levels of the Notch target gene Hey1 in each treatment group after 7 days to confirm activation of the Notch signalling pathway by the Notch ligand, Jagged1. There was an increase in the expression of Hey1 mRNA by 289.8 ± 78.02 fold change in Jag1-treated cells compared to the control sample (Figure 5.27). However, when Jag1-activated Notch signalling was blocked with 80 μM of DAPT the transcript levels of Hey1 (0.84 ± 0.11) recovered to levels similar to the control sample (Figure 5.27). Moreover, the expression levels of Cnn1 and Sm-mhc mRNA increased in Jag1-treated cells by 41.94 ± 11.75 and 30.33 ± 3.59 fold change, respectively, 7 days after treatment compared to the control (Figure 5.28 and Figure 5.29). However, when Jag1-treated cells were pre-incubated with 80 μM of DAPT the transcript levels of Cnn1 and Sm-mhc decreased to 0.46 ± 0.05 and 0.40 ± 0.06 fold change, respectively (Figure 5.28. and Figure 5.29).

Immunocytochemical analysis revealed that the fraction of cells positively staining for the intermediate and mature smooth muscle markers, CNN1 and SM-MHC, respectively, significantly increased 7 days after Jag1 treatment. $CNN1^+$ cells

accounted for 0.20 ± 0.03 cell fraction, whereas SM-MHC$^+$ cells represented 0.04 ± 0.01 cell fraction. Jag1-treated cells that were pre-incubated with DAPT (DT/Jag1) did not show an increment in the number of cells staining positive for either CNN1 or SM-MHC suggesting that DAPT inhibited Jag1-activated Notch signalling at day 7 (Figure 5.30, Figure 5.31 and Figure 5.32).

Concomitantly, the cell number in the Jag1-treated mAA-vSCs decreased from 466.3 ± 49.88 to 195.2 ± 22.66 at day 7 (Figure 5.33). Once again 80 μM of DAPT treatment inhibited the effect of Jag1 and thus increasing cell number to 289.7 ± 31.32. All together the data suggested that activation of the Jagged1/Notch signalling pathway, confirmed by increased levels of Hey1 transcript, induced differentiation of mAA-vSCs into SMC by increasing the gene and protein expression levels of CNN1 and SM-MHC. The myogenic effect of recombinant Jagged1-Fc was revoked by treatment with the γ-secretase inhibitor, DAPT (Figure 5.33).

5.3.3.3 The TGF-β and Jagged1-dependent Notch signalling pathways work synergistically to transition vascular stem cells (vSCs) to SMCs, but Jagged1-activated Notch is critical in the SMC maturation process of vSCs.

Significant myogenic differentiation in mAA-vSCs was observed upon activation of the TGF-β and Notch signalling pathways by rmTGF-β1 and recombinant Jagged1-Fc treatment. However, gene and protein expression of the mature smooth muscle cells marker, SM-MHC was only seen in Jag1-treated cells compared to those incubated with rmTGF-β1. This result was comparable to mAA-vSCs treated in DM (10% FBS-containing DMEM) for 7 days. Therefore, we hypothesised that Jagged1-dependent Notch activation is directly involved in myogenic differentiation and SMC maturation by increasing the expression of the SM-MHC gene/marker.

Vascular stem cells isolated from the tunica media of murine aortic arch (mAA-vSCs) were treated with in either DMSO (control) or DMSO/rmTGF-β1 (2 ng/ml) (TGβ1) or DAPT (80 μM)/rmTGF-β1 (2 ng/ml) (DT/TGβ1), and cultured in NE-MM at 37°C, 5% CO_2 for 7 days. Results showed that the expression of Cnn1 mRNA increased by

43.94 ± 10.40 fold change in TGβ1-treated cells compared to the control sample. Even though Cnn1 mRNA expression levels in the DT/TGβ1-treated cells were still higher (12.73 ± 1.51), incubation with DAPT did reduce the expression of Cnn1 mRNA 3.45 times to the TGβ1 sample. The levels of Sm-mhc mRNA were not affected in any of the samples (Figure 5.34 and Figure 5.35).

mAA-vSCs were also treated with either DMSO/IgG-Fc (500 ng/ml) (Fc; control) or DMSO/Jag1-Fc (500 ng/ml) (Jag1) or SB431542 (10μM)/Jag1-Fc (500 ng/ml) (SB/Jag1) and cultured in NE-MM at 37°C, 5% CO_2 for 7 days. The expression of Hey1 mRNA increased by 11.27 ± 0.86 fold change in Jag1-treated cells compared to the control sample (Figure 5.36). However, when Jag1-treated cells were incubated with the SMAD/TGF-β inhibitor (SB431542), the transcript levels of Hey1 incremented to 15.81 ± 1.09 compared to the control (Figure 5.36). Moreover, the expression levels of Cnn1 and Sm-mhc mRNA increased in Jag1-treated cells by 3.90 ± 0.50 (Figure 5.37). and 78.65 ± 26.48 (Figure 5.38) fold change, respectively, 7 days after treatment compared to the control. On the other hand, when Jag1-treated cells were pre-incubated with 10 μM of SB431542 the transcript levels of Cnn1 and Sm-mhc increased to 4.75 ± 0.70 and 528.6 ± 80.29 fold change (Figure 5.9, b and c), respectively (Figure 5.37 and Figure 3.38).

The results suggested that the mRNA expression of Sm-mhc was directly upregulated upon activation of the Notch signalling pathway by Jagged1 but not by the TGF-β signalling. Interestingly, inhibition of the SMAD/TGF-β signalling increased expression of Sm-mhc on Jag1-treated cells, implying that TGF-β1 treatment in mAA-vSCs may be preventing the maturation of this progenitor cells towards the contractile SMC phenotype. In this context, the relative expression levels of Tgf-β1 mRNA was measured by PCR 24 hours (hrs), 72 hours (hrs) and 7 days post-treatment with Fc or Jag1 or SB/Jag1. Results showed that Tgf-β1 transcript expression fluctuated with fold change values of 2.84 ± 0.02, 0.33 ± 0.003 and 2.70 ± 0.06 at 24 hrs, 72 hrs and 7 days (Figure 5.39), respectively. The transcript levels of Collagen type II, alpha 1 (Col3a1) and the notch target gene Hey1 were also analysed by PCR. The relative expression levels of Col3a1 gene peaked at 72 hrs with a fold change of 4.09 ± 0.04 compared to the control. At day 7, Col3a1 transcripts were still upregulated by 2.39 ± 0.04 fold

change (Figure 5.40). Hey1 mRNA levels were upregulated at each time point with increasing expression levels including 17.03 ± 0.83, 44.18 ± 0.75 and 314.2 ± 5.98 24 hrs, 72 hrs and 7 days post-treatment, respectively (Figure 5.41). The expression levels of the myogenic genes, Cnn1 and Sm-mhc were examined by PCR at 72 hrs and 7 days post-treatment. Coincidently, at 72 hrs the relative expression levels of Cnn1 transcripts were unaffected when levels of Tgf-β1 mRNA were significantly reduced (Figure 5.42 and Figure 5.43). Additionally, the expression of Sm-mhc mRNA peaked by 129.4 ± 4.96 fold change at this time point (72 hrs) compared to the control. However, although still high, the levels of Sm-mhc transcripts were reduced to 46.44 ± 0.91 fold change by day 7 compared to the control sample. This dropped of Sm-mhc fold change expression 7 days after Jag1-treatment occurred in parallel with an increase in Cnn1 and Tgf-β1 transcript level by 15.74 ± 1.07 and 2.70 ± 0.06, respectively (Figure 5.42 and Figure 5.43).

Lastly, the relative expression levels of Jag1 and Col3a1 mRNAs were measured by qRT-PCR 24 hrs and 7 days post-treatment with DMSO or TGβ1 or SB/ TGβ1. This experiment was performed in order to complement the data obtained above. The expression levels of Jag1 mRNA increased by 9.95 ± 0.35 and 2.39 ± 0.03 fold change (Figure 5.44) at 24 hrs and 7 days, respectively. In contrast, Col3a1 mRNA expression levels gradually decreased by 0.39 ± 0.005 and 0.11 ± 0.002 (Figure 5.44) 24 hrs and 7 days post-treatment, respectively (Figure 5.45).

Collectively, the data suggest that both stimuli were necessary to initially induce SMC differentiation in vascular stem cells (mAA-vSCs) as the transcription levels of Tgf-β1 and Jag1 mRNA increased 24 hrs after Jag1 and Tgf-β1 treatment, respectively. However, TGβ1 signalling seemed to be necessary for the initial expression levels of Cnn1 gene, but also it seemed to negatively regulate its expression through a feedback loop. This, paired with the fact that expression of Sm-mhc was not upregulated by TGβ1 signalling, implied that TGβ1 may drive mAA-vSCs to an intermediate cell defined as a mesenchymal-like (MSC-like) cell. Instead, Jag1 treatment of mAA-vSCs directly resulted in SMC differentiation with increased expression levels of Cnn1 and Sm-mhc genes. Also, inhibition of the SMAD/TGF-β signalling pathway in Jag1-treated cells resulted in a higher expression of Cnn1 and Sm-mhc transcripts

suggesting that TGβ pathway had a regulatory effect on the Jagged1-dependent Notch pathway.

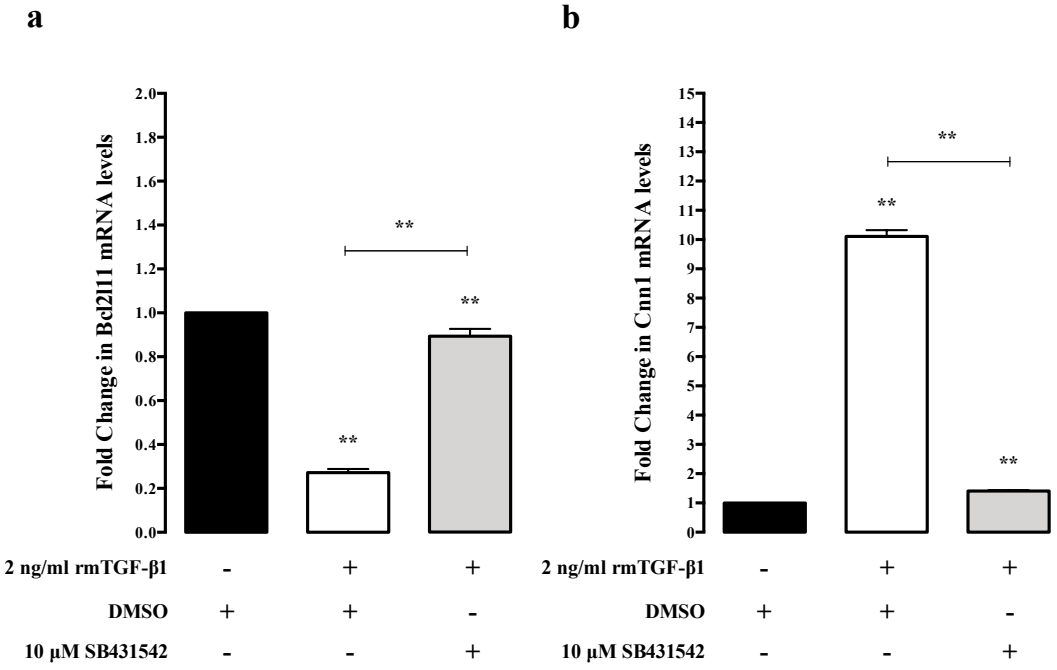

Figure 5.23. The SMAD/TGF-β signalling inhibitor, SB431542 attenuates the effect of TGF-β1 on the Bcl2l1 and Cnn1 gene expression in mAA-vSC.

mAA-vSCs were preincubated in 10 μM of SB431542 or DMSO at 37°C, 5% CO_2 for 30 min. Pre-treated cells were then cultured in neuroectodermal maintenance medium (NE-MM) supplemented with 2 ng/ml of TGF-β1 (TGβ1) or NE-MM (Control) for 48 hours and 7 days. Relative mRNA expression levels of **(a)** BCL2-like 11 (Bcl2l11) at 48 hours and **(b)** Calponin1 (Cnn1) in mAA-vSCs at day 7 after SB431542/TGβ1, DMSO/TGβ1 or DMSO/NE-MM (control) treatment. The data was normalised against the endogenous gene HPRT. The experiments were performed in duplicate, charts are representatives of two independent experiments. Data are mean ± S.E.M (n=2). One-way ANOVA with significance value of P≤0.05. Results: ****p<0.0001. Mann-Whitney test with significance value of P≤0.05. Results: **p<0.01. Significance are against the control sample (DMSO), unless indicated by a capped line.

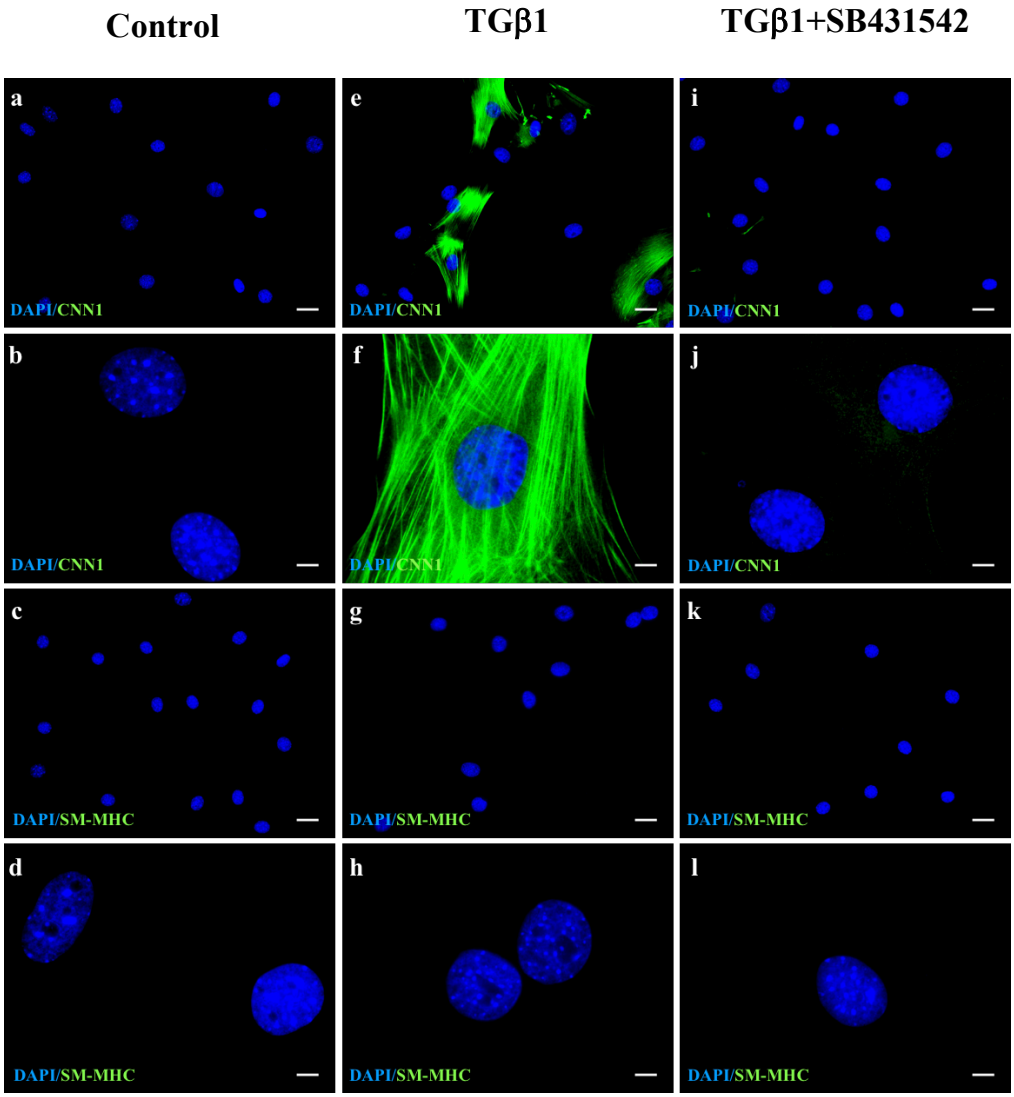

Figure 5.24. The SMAD/TGF-β signalling inhibitor, SB431542 attenuates the effect of TGF-β1 on the CNN1 protein expression in mAA-vSC.

mAA-vSCs were preincubated in 10 μM of SB431542 or DMSO at 37°C, 5% CO_2 for 30 min. Pre-treated cells were then cultured in neuroectodermal maintenance medium (NE-MM) supplemented with 2 ng/ml of TGF-β1 (TGβ1) or NE-MM (Control) for 48 hours and 7 days. Immunocytochemical analysis was performed 7 days post-treatment (Section 2.4). Cell samples were immunostained for **(a, b, e, f, I, j)** Calponin1 (CNN1) and **(c, d, g, h, k, l)** smooth muscle myosin heavy chain (SM-MHC). Samples were probed with their corresponding AlexaFluor-488 secondary antibody. Representative images are shown at **(a, c, e, g, i, k)** 20X and **(b, d, f, h, j, l)** 60X magnification power. All images are representative of n ≥ 10 (duplicate experiment). Scale bars, 20mm.

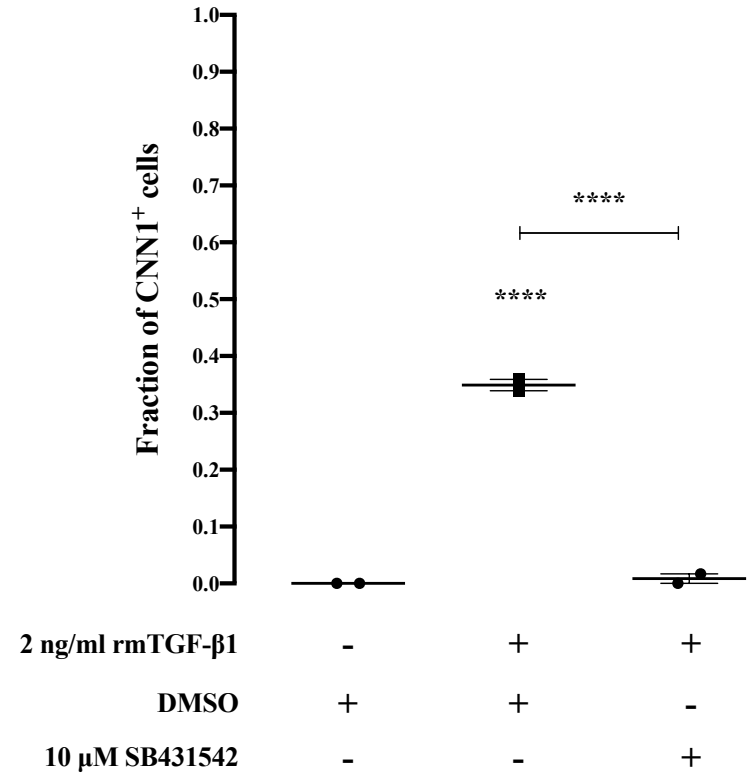

Figure 5.25. The SMAD/TGF-β1 signalling inhibitor, SB431542 reduces the effect of TGF-β1 on the fraction of CNN1$^+$ cells in mAA-vSC.

mAA-vSCs were preincubated in 10 µM of SB431542 or DMSO at 37°C, 5% CO_2 for 30 min. Pre-treated cells were then cultured in neuroectodermal maintenance medium (NE-MM) supplemented with 2 ng/ml of TGF-β1 (TGβ1) or NE-MM (Control) for 48 hours and 7 days. Fraction of CNN1-positive (CNN1$^+$) cells in mAA-vSCs 7 days after SB431542/TGβ1, DMSO/TGβ1 or DMSO/NE-MM (control) treatment. The chart is representative of two independent experiments. Data are mean ± S.E.M. (n=2). Mann-Whitney test with significance value of P≤0.05. Results: ****p<0.0001. Significance are compared to the control unless specified with a capped line.

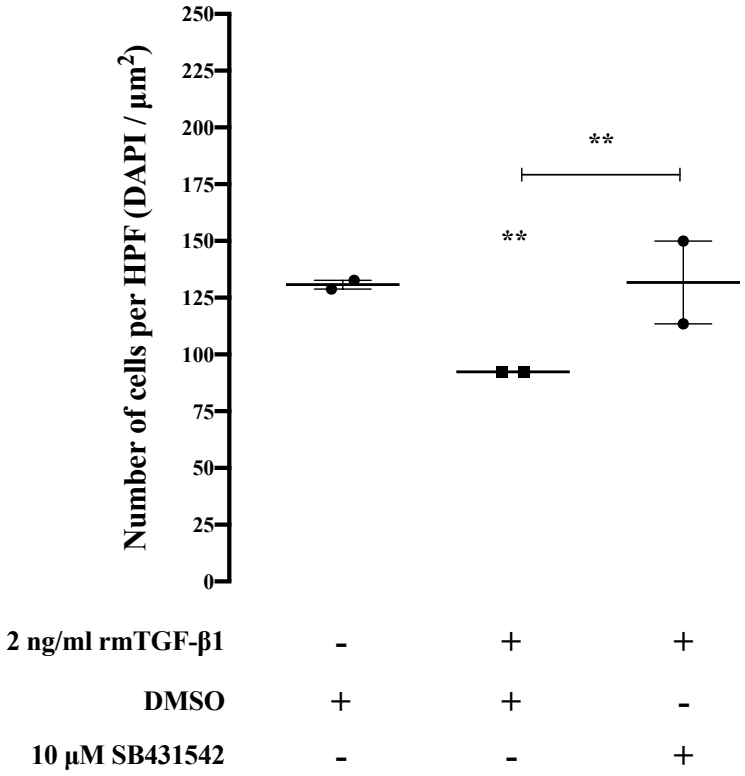

Figure 5.26. The SMAD/TGF-β1 signalling inhibitor, SB431542 reduces the effect of TGF-β1 on cell number in mAA-vSC.

mAA-vSCs were preincubated in 10 µM of SB431542 or DMSO at 37°C, 5% CO_2 for 30 min. Pre-treated cells were then cultured in neuroectodermal maintenance medium (NE-MM) supplemented with 2 ng/ml of TGF-β1 (TGβ1) or NE-MM (Control) for 48 hours and 7 days. The number of cells per high-power field (HPF) was calculated at day 7 post-treatment using ImageJ™ and Excel Microsoft Office 2011. DAPI nuclear staining was used to count the number of cells per image in SB431542/TGβ1, DMSO/TGβ1 or DMSO/NE-MM (control) group samples. The number of cells per HPF was calculated per image by dividing DAPI over the visible area under the magnification power of the selected objective, so values represent the number of cells per μm^2. The chart is representative of two independent experiments. Data are mean ± S.E.M. (n=2). Unpaired t-test with significance value of $P \leq 0.05$. Results: ****$p<0.0001$. Significance are compared to the control unless specified with a capped line.

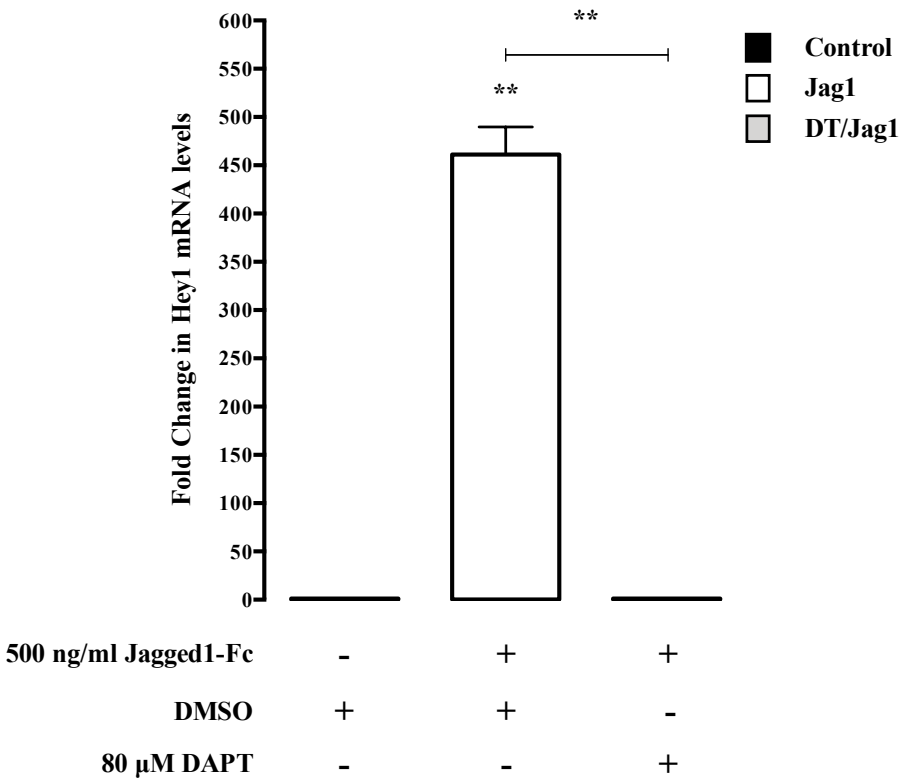

Figure 5.27. The γ-secretase inhibitor, DAPT downregulates the effect of Jag1-Fc on Hey1 gene expression in mAA-vSC.

mAA-vSCs were preincubated in 80 µM of DAPT or DMSO at 37°C, 5% CO_2 for 30 min. Pre-treated cells were then cultured in neuroectodermal maintenance medium (NE-MM) supplemented with 500 ng/ml of Jagged1-Fc (Jag1-Fc) or IgG-Fc (Control) for 7 days. Relative mRNA expression levels of Hey1 7 days after DAPT/Jag1-Fc (DT/Jag1), DMSO/Jag1-Fc (Jag1) or DMSO/IgG-Fc (Control) treatment. The data was normalised against the endogenous gene HPRT. The experiments were performed in duplicate, chart is representatives of two independent experiments. Data are mean ± S.E.M (n=2). Mann-Whitney t-test with significance value of $P \leq 0.05$. Results: **$p<0.01$. Significance are compared to the control unless specified with a capped line.

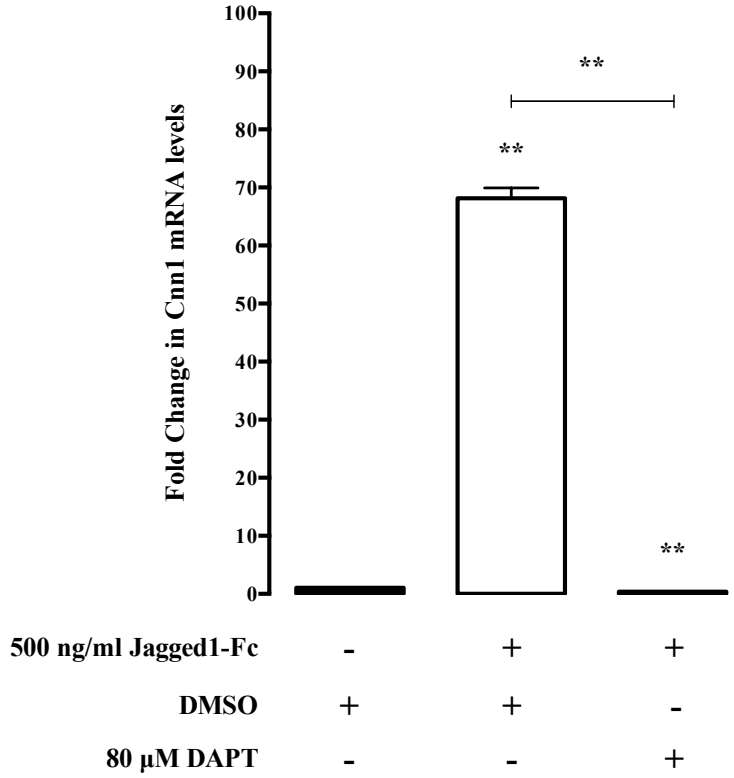

Figure 5.28. The γ-secretase inhibitor, DAPT downregulates the effect of Jag1-Fc on Cnn1 gene expression in mAA-vSC.

mAA-vSCs were preincubated in 80 µM of DAPT or DMSO at 37°C, 5% CO_2 for 30 min. Pre-treated cells were then cultured in neuroectodermal maintenance medium (NE-MM) supplemented with 500 ng/ml of Jagged1-Fc (Jag1-Fc) or IgG-Fc (Control) for 7 days. Relative mRNA expression levels of Calponint1 (Cnn1) 7 days after DAPT/Jag1-Fc (DT/Jag1), DMSO/Jag1-Fc (Jag1) or DMSO/IgG-Fc (Control) treatment. The data was normalised against the endogenous gene HPRT. The experiments were performed in duplicate, chart is representatives of two independent experiments. Data are mean ± S.E.M (n=2). Mann-Whitney t-test with significance value of $P \leq 0.05$. Results: **$p<0.01$. Significance are compared to the control unless specified with a capped line.

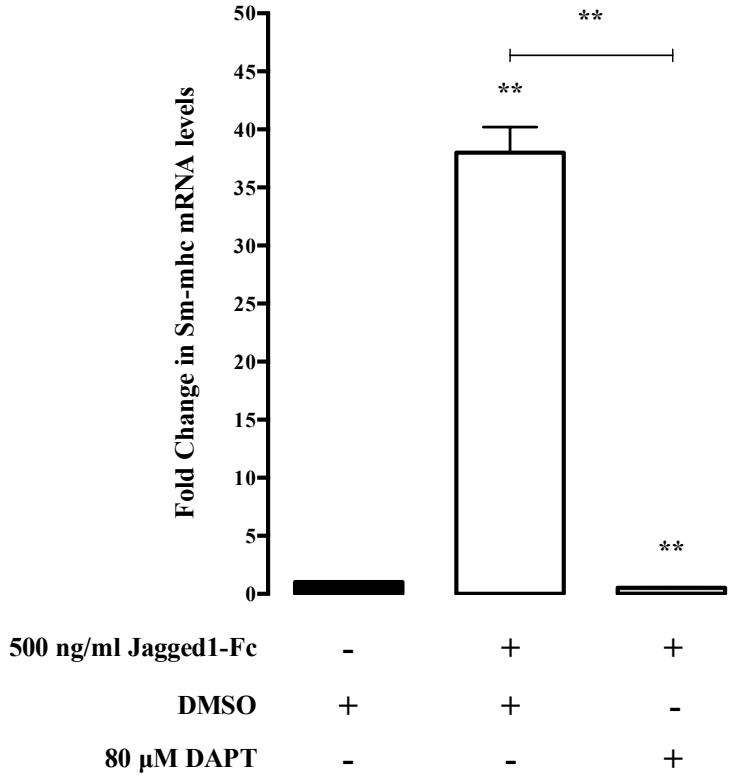

Figure 5.29. The γ-secretase inhibitor, DAPT downregulates the effect of Jag1-Fc on Sm-mhc gene expression in mAA-vSC.

mAA-vSCs were preincubated in 80 µM of DAPT or DMSO at 37°C, 5% CO_2 for 30 min. Pre-treated cells were then cultured in neuroectodermal maintenance medium (NE-MM) supplemented with 500 ng/ml of Jagged1-Fc (Jag1-Fc) or IgG-Fc (Control) for 7 days. Relative mRNA expression levels of smooth muscle myosin heavy chain (Sm-mhc) 7 days after DAPT/Jag1-Fc (DT/Jag1), DMSO/Jag1-Fc (Jag1) or DMSO/IgG-Fc (Control) treatment. The data was normalised against the endogenous gene HPRT. The experiments were performed in duplicate, chart is representatives of two independent experiments. Data are mean ± S.E.M (n=2). Mann-Whitney t-test with significance value of $P \leq 0.05$. Results: **$p < 0.01$. Significance are compared to the control unless specified with a capped line.

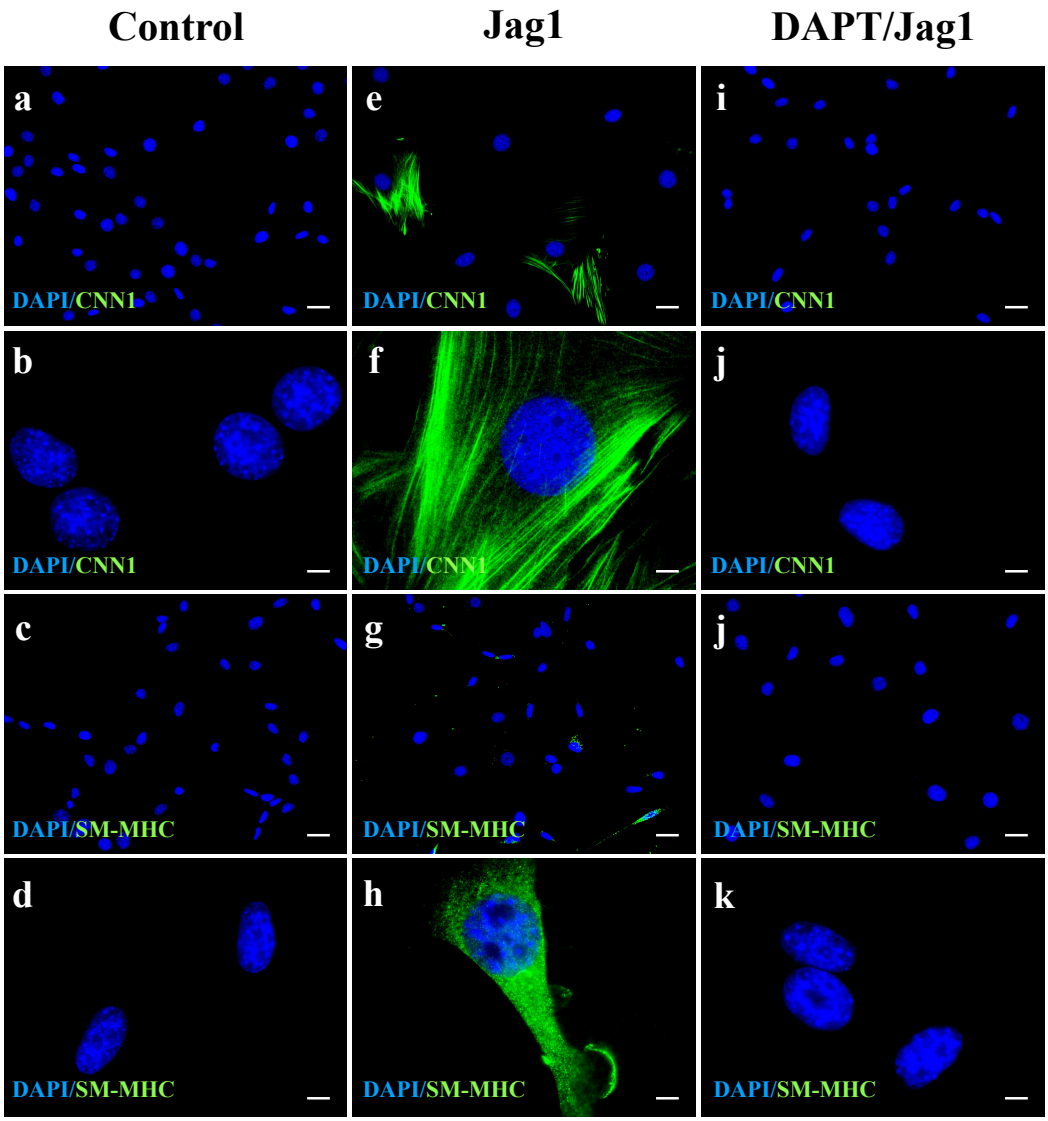

Figure 5.30. The γ-secretase inhibitor, DAPT downregulates the effect of Jag1-Fc on CNN1 and SM-MHC protein expression in mAA-vSC.

mAA-vSCs were preincubated in 80 μM of DAPT or DMSO at 37°C, 5% CO_2 for 30 min. Pre-treated cells were then cultured in neuroectodermal maintenance medium (NE-MM) supplemented with 500 ng/ml of Jagged1-Fc (Jag1-Fc) or IgG-Fc (Control) for 7 days. Immunocytochemical analysis was performed 7 days after DAPT/Jag1-Fc (DAPT/Jag1), DMSO/Jag1-Fc (Jag1) or DMSO/IgG-Fc (Control) treatment. Cell samples were immunostained for **(a, b, e, f, I, j)** Calponin1 (CNN1) and **(c, d, g, h, k, l)** smooth muscle myosin heavy chain (SM-MHC). Samples were probed with their corresponding AlexaFluor-488 secondary antibody. Representative images are shown at **(a, c, e, g, i, k)** 20X and **(b, d, f, h, j, l)** 60X magnification power. All images are representative of n ≥ 10 (duplicate experiment). Scale bars, 20mm.

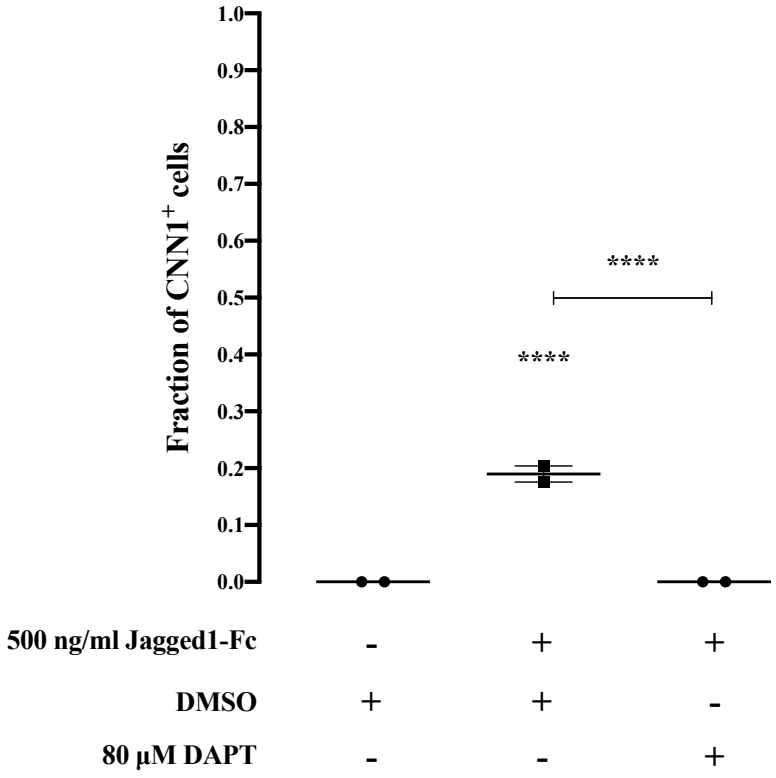

Figure 5.31. The γ-secretase inhibitor, DAPT reduces the effect of Jag1-Fc on the fraction of CNN1$^+$ cells in mAA-vSC.

mAA-vSCs were preincubated in 80 µM of DAPT or DMSO at 37°C, 5% CO_2 for 30 min. Pre-treated cells were then cultured in neuroectodermal maintenance medium (NE-MM) supplemented with 500 ng/ml of Jagged1-Fc (Jag1-Fc) or IgG-Fc (Control) for 7 days. Fraction of **(a)** CNN1-positive (CNN1$^+$) and **(b)** SM-MHC-positive (SM-MHC$^+$) cells in mAA-vSCs 7 days after DAPT/Jag1-Fc (DAPT/Jag1), DMSO/Jag1-Fc (Jag1) or DMSO/IgG-Fc (Control) treatment. The chart is representative of two independent experiments. Data are mean ± S.E.M. (n=2). Mann-Whitney t-test with significance value of $P \leq 0.05$. Results: ****$p < 0.0001$. Significance are compared to the control unless specified with a capped line.

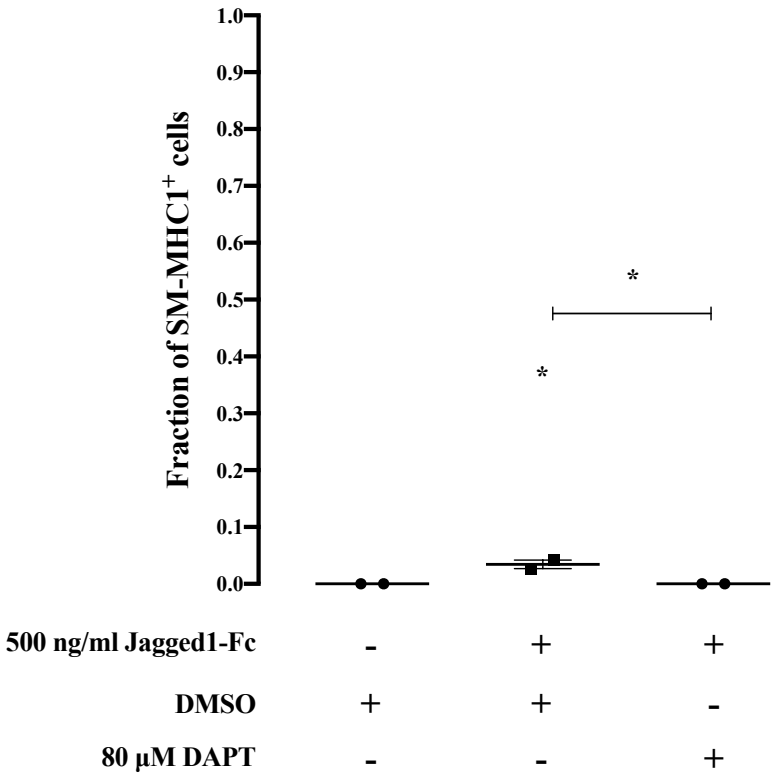

Figure 5.32. The γ-secretase inhibitor, DAPT reduces the effect of Jag1-Fc on the fraction of SM-MHC$^+$ cells in mAA-vSC.

mAA-vSCs were preincubated in 80 µM of DAPT or DMSO at 37°C, 5% CO_2 for 30 min. Pre-treated cells were then cultured in neuroectodermal maintenance medium (NE-MM) supplemented with 500 ng/ml of Jagged1-Fc (Jag1-Fc) or IgG-Fc (Control) for 7 days. Fraction of **(a)** CNN1-positive (CNN1$^+$) and **(b)** SM-MHC-positive (SM-MHC$^+$) cells in mAA-vSCs 7 days after DAPT/Jag1-Fc (DT/Jag1), DMSO/Jag1-Fc (Jag1) or DMSO/IgG-Fc (Control) treatment. The chart is representative of two independent experiments. Data are mean ± S.E.M. (n=2). Mann-Whitney t-test with significance value of $P \leq 0.05$. Results: *$p<0.05$. Significance are compared to the control unless specified with a capped line.

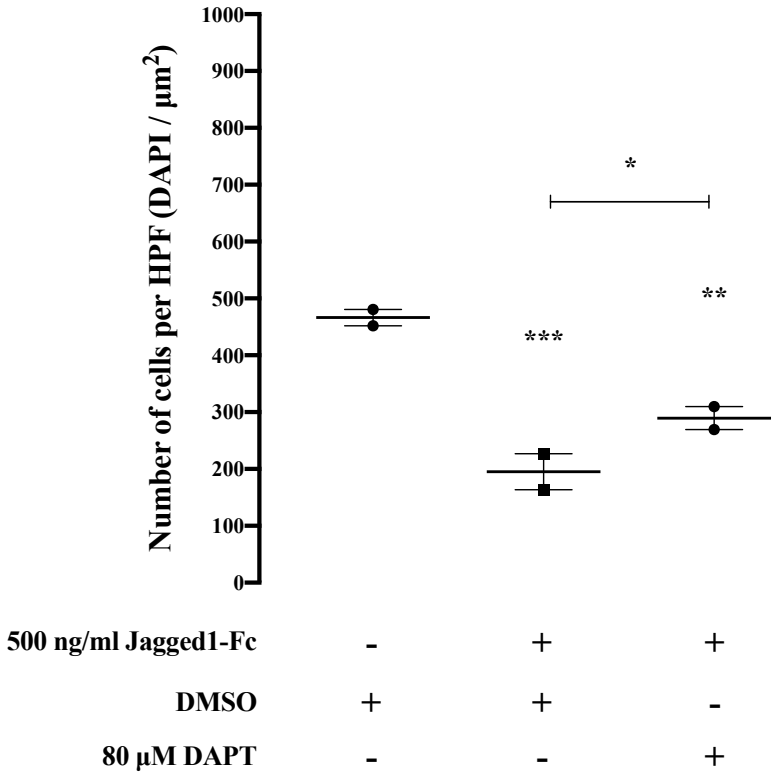

Figure 5.33. The γ-secretase inhibitor, DAPT reduces the effect of Jag1-Fc on cell number in mAA-vSC.

mAA-vSCs were preincubated in 80 µM of DAPT or DMSO at 37°C, 5% CO_2 for 30 min. Pre-treated cells were then cultured in neuroectodermal maintenance medium (NE-MM) supplemented with 500 ng/ml of Jagged1-Fc (Jag1-Fc) or IgG-Fc (Control) for 7 days. The number of cells per high-power field (HPF) was calculated at day 7 post-treatment using ImageJ™ and Excel Microsoft Office 2011. DAPI nuclear staining was used to count the number of cells per image in DAPT/Jag1-Fc (DT/Jag1), DMSO/Jag1-Fc (Jag1) or DMSO/IgG-Fc (Control) group samples. The number of cells per HPF was calculated per image by dividing DAPI over the visible area under the magnification power of the selected objective, so values represent the number of cells per μm^2. The chart is representative of two independent experiments. Data are mean ± S.E.M. (n=2). Unpaired t-test with significance value of $P \leq 0.05$. Results: *$p<0.05$, **$p<0.01$ and ***$p<0.001$. Significance are compared to the control unless specified with a capped line.

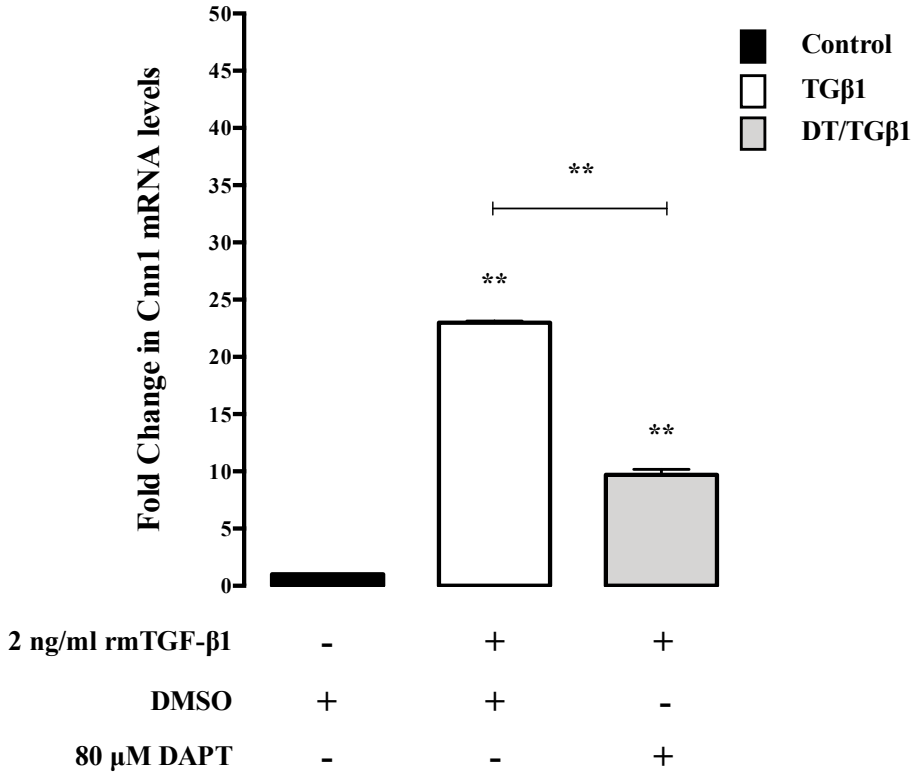

Figure 5.34. The γ-secretase inhibitor, DAPT attenuates the effect of TGF-β1 on Cnn1 gene expression in mAA-vSC.

mAA-vSCs were preincubated in 80 µM of DAPT or DMSO at 37°C, 5% CO_2 for 30 min. Pre-treated cells were then cultured in neuroectodermal maintenance medium (NE-MM) supplemented with 2 ng/ml of TGF-β1 (TGβ1) or NE-MM (Control) for 7 days Relative mRNA expression levels of Calponint1 (Cnn1) 7 days after DAPT/rmTGF-β1 (DT/TGβ1), DMSO/rmTGF-β1 (TGβ1), or DMSO (Control) treatment. The data was normalised against the endogenous gene HPRT. The experiments were performed in duplicate, chart is representatives of two independent experiments. Data are mean ± S.E.M (n=2). Mann-Whitney t-test with significance value of $P \leq 0.05$. Results: **$p < 0.01$. Significance are compared to the control unless specified with a capped line.

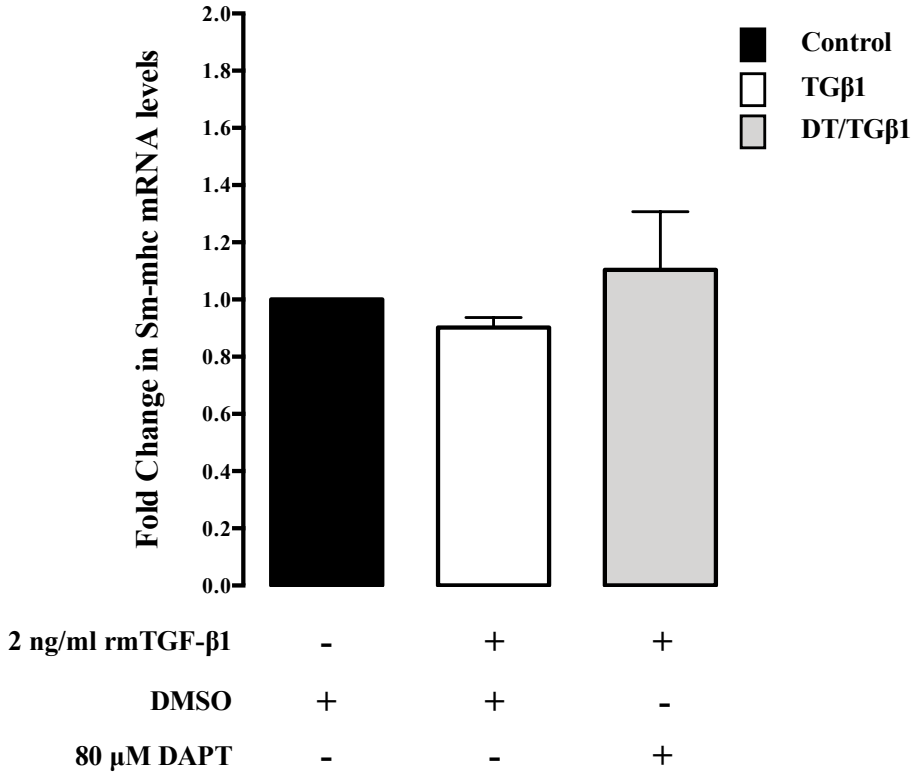

Figure 5.35. The γ-secretase inhibitor, DAPT does not alter the effect of TGF-β1 on Sm-mhc gene expression in mAA-vSC.

mAA-vSCs were preincubated in 80 µM of DAPT or DMSO at 37°C, 5% CO_2 for 30 min. Pre-treated cells were then cultured in neuroectodermal maintenance medium (NE-MM) supplemented with 2 ng/ml of TGF-β1 (TGβ1) or NE-MM (Control) for 7 days. Relative mRNA expression levels of smooth muscle myosin heavy chain (Sm-mhc) 7 days after DAPT/rmTGF-β1 (DT/TGβ1), DMSO/rmTGF-β1 (TGβ1), or DMSO (Control) treatment. The data was normalised against the endogenous gene HPRT. The experiments were performed in duplicate, chart is representatives of two independent experiments. Data are mean ± S.E.M (n=2). Mann-Whitney t-test with significance value of $P \leq 0.05$.

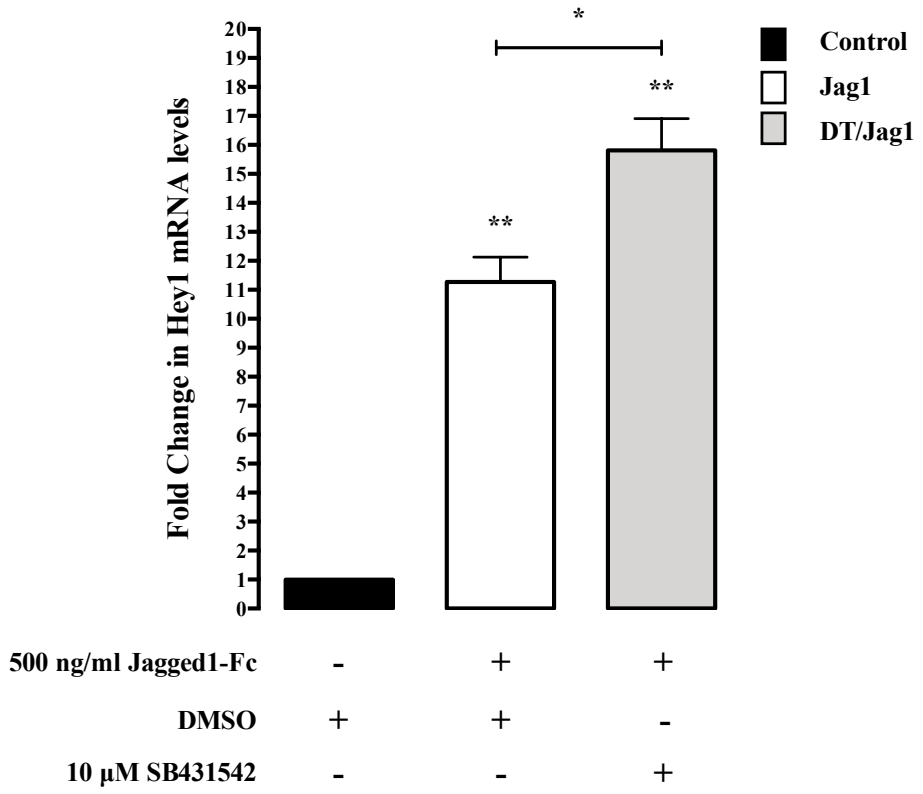

Figure 5.36. The SMAD/TGF-β inhibitor, SB431542 enhances the effect of Jag1-Fc on Hey1 gene expression in mAA-vSC.

mAA-vSCs were preincubated in 10 µM of SB431542 or DMSO at 37°C, 5% CO_2 for 30 min. Pre-treated cells were then cultured in neuroectodermal maintenance medium (NE-MM) supplemented with 500 ng/ml of Jagged1-Fc (Jag1-Fc) or IgG-Fc (Control) for 7 days. Relative mRNA expression levels of Hey1 7 days after SB4315/Jag1-Fc (SB/Jag1), DMSO/Jag1-Fc (Jag1) or DMSO/IgG-Fc (Control) treatment. The data was normalised against the endogenous gene HPRT. The experiments were performed in duplicate, chart is representatives of two independent experiments. Data are mean ± S.E.M (n=2). Mann-Whitney t-test with significance value of $P \leq 0.05$. Results: *$p<0.05$ and **$p<0.01$. Significance are compared to the control unless specified with a capped line.

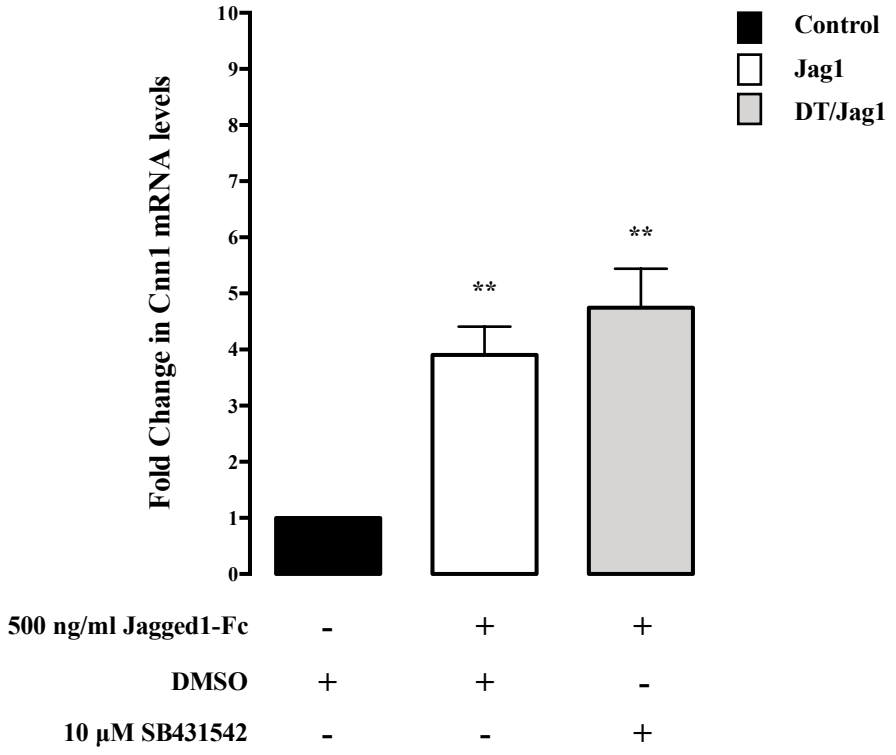

Figure 5.37. The SMAD/TGF-β inhibitor, SB431542 enhances the effect of Jag1-Fc on Cnn1 gene expression in mAA-vSC.

mAA-vSCs were preincubated in 10 µM of SB431542 or DMSO at 37°C, 5% CO_2 for 30 min. Pre-treated cells were then cultured in neuroectodermal maintenance medium (NE-MM) supplemented with 500 ng/ml of Jagged1-Fc (Jag1-Fc) or IgG-Fc (Control) for 7 days. Relative mRNA expression levels of Calponin1 (Cnn1) 7 days after SB4315/Jag1-Fc (SB/Jag1), DMSO/Jag1-Fc (Jag1) or DMSO/IgG-Fc (Control) treatment. The data was normalised against the endogenous gene HPRT. The experiments were performed in duplicate, chart is representatives of two independent experiments. Data are mean ± S.E.M (n=2). Mann-Whitney t-test with significance value of $P \leq 0.05$. Results: **$p<0.01$. Significance are compared to the control unless specified with a capped line.

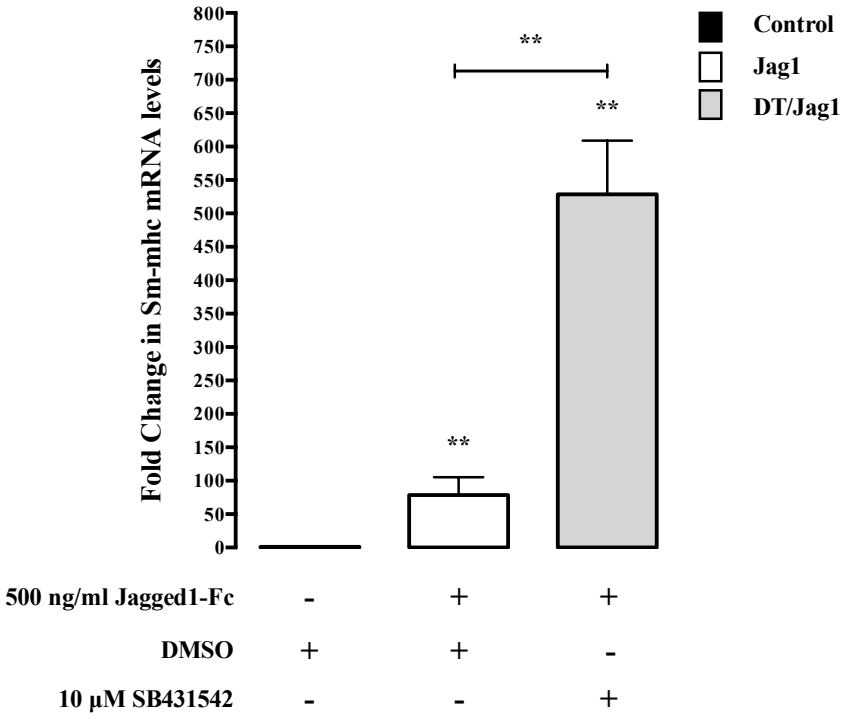

Figure 5.38. The SMAD/TGF-β inhibitor, SB431542 enhances the effect of Jag1-Fc on Sm-mhc gene expression in mAA-vSC.

mAA-vSCs were preincubated in 10 µM of SB431542 or DMSO at 37°C, 5% CO_2 for 30 min. Pre-treated cells were then cultured in neuroectodermal maintenance medium (NE-MM) supplemented with 500 ng/ml of Jagged1-Fc (Jag1-Fc) or IgG-Fc (Control) for 7 days. Relative mRNA expression levels of smooth muscle myosin heavy chain (Sm-mhc) 7 days after SB4315/Jag1-Fc (SB/Jag1), DMSO/Jag1-Fc (Jag1) or DMSO/IgG-Fc (Control) treatment. The data was normalised against the endogenous gene HPRT. The experiments were performed in duplicate, chart is representatives of two independent experiments. Data are mean ± S.E.M (n=2). The Mann-Whitney t-test with significance value of $P \leq 0.05$. Results: **$p<0.01$. Significance are compared to the control unless specified with a capped line.

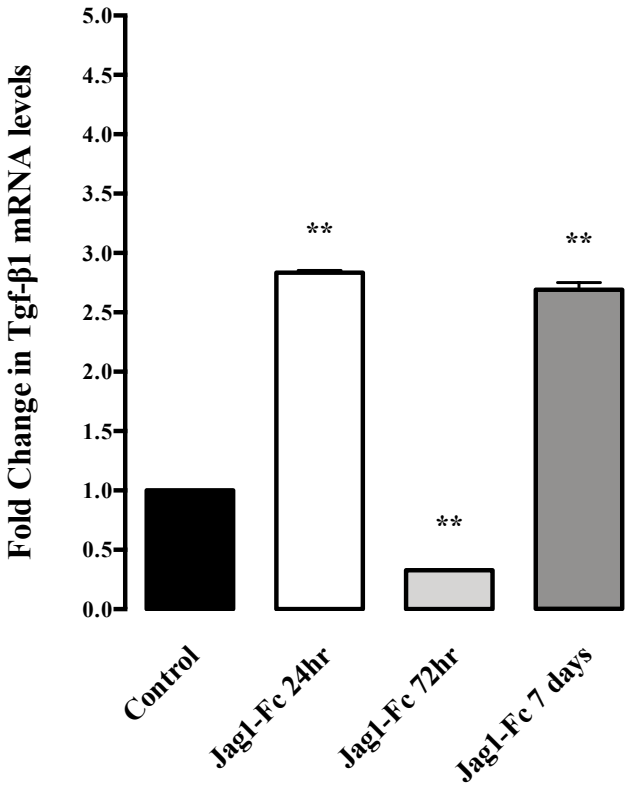

Figure 5.39. Relative Tgf-β1 gene expression in mAA-vSCs at different time points after Jag1-Fc treatment.

mAA-vSCs were cultured on plates coated with immobilised 500 ng/ml of Jagged1-Fc (Jag1-Fc) or IgG-Fc (as control) in neuroectodermal maintenance medium (NE-MM) for 24 hours, 72 hours and 7 days. Relative mRNA expression levels of Tgf-β1 72 hours (72hr) and 7 days post-treatment. The data was normalised against the endogenous gene HPRT. The experiments were performed in duplicate, chart is representatives of two independent experiments. Data are mean ± S.E.M (n=2). Mann-Whitney t-test with significance value of $P \leq 0.05$. Results: **$p < 0.01$. Significance are compared to the control unless specified with a capped line.

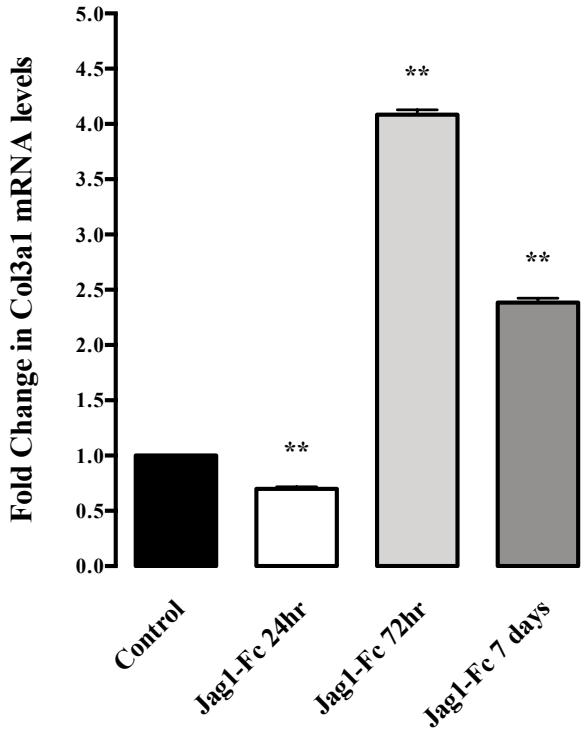

Figure 5.40. Relative Col3a1 gene expression in mAA-vSCs at different time points after Jag1-Fc treatment.

mAA-vSCs were cultured on plates coated with immobilised 500 ng/ml of Jagged1-Fc (Jag1-Fc) or IgG-Fc (as control) in neuroectodermal maintenance medium (NE-MM) for 24 hours, 72 hours and 7 days. Relative mRNA expression levels of Col3a11 72 hours (72hr) and 7 days post-treatment. The data was normalised against the endogenous gene HPRT. The experiments were performed in duplicate, chart is representatives of two independent experiments. Data are mean ± S.E.M (n=2). Mann-Whitney t-test with significance value of $P \leq 0.05$. Results: **$p < 0.01$. Significance are compared to the control unless specified with a capped line.

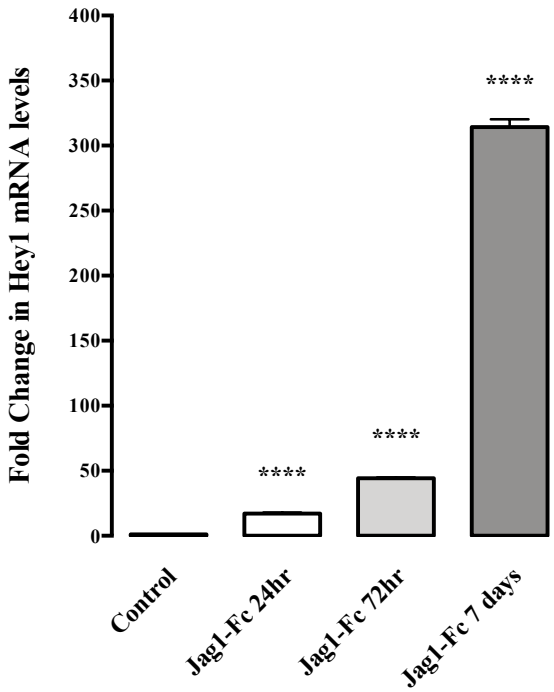

Figure 5.41. Relative Hey1 gene expression in mAA-vSCs increases with time after Jag1-Fc treatment.

mAA-vSCs were cultured on plates coated with immobilised 500 ng/ml of Jagged1-Fc (Jag1-Fc) or IgG-Fc (as control) in neuroectodermal maintenance medium (NE-MM) for 24 hours, 72 hours and 7 days. Relative mRNA expression levels of Hey1 72 hours (72hr) and 7 days post-treatment. The data was normalised against the endogenous gene HPRT. The experiments were performed in triplicate, chart is representatives of two independent experiments. Data are mean ± S.E.M (n=3). Mann-Whitney t-test with significance value of $P \leq 0.05$. Results: ****$p<0.0001$. Significance are compared to the control unless specified with a capped line.

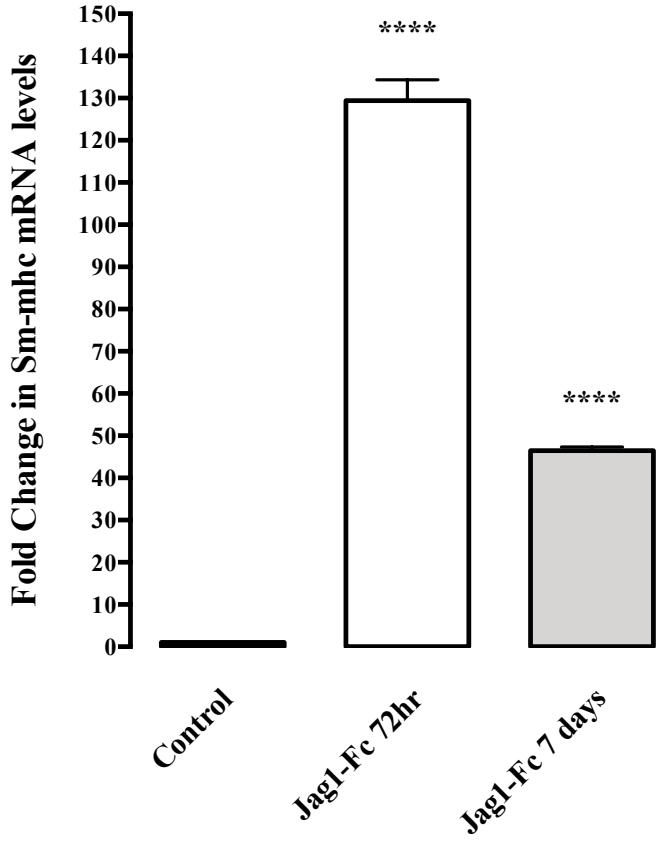

Figure 5.42. Relative Sm-mhc gene expression in mAA-vSCs peaks 72 hours after Jag1-Fc treatment.

mAA-vSCs were cultured on plates coated with immobilised 500 ng/ml of Jagged1-Fc (Jag1-Fc) or IgG-Fc (as control) in neuroectodermal maintenance medium (NE-MM) for 24 hours, 72 hours and 7 days. Relative mRNA expression levels of Sm-mhc 72 hours (72hr) and 7 days post-treatment. The data was normalised against the endogenous gene HPRT. The experiments were performed in triplicate, chart is representatives of two independent experiments. Data are mean ± S.E.M (n=3). Mann-Whitney t-test with significance value of $P \leq 0.05$. Results: ****$p < 0.0001$. Significance are compared to the control unless specified with a capped line.

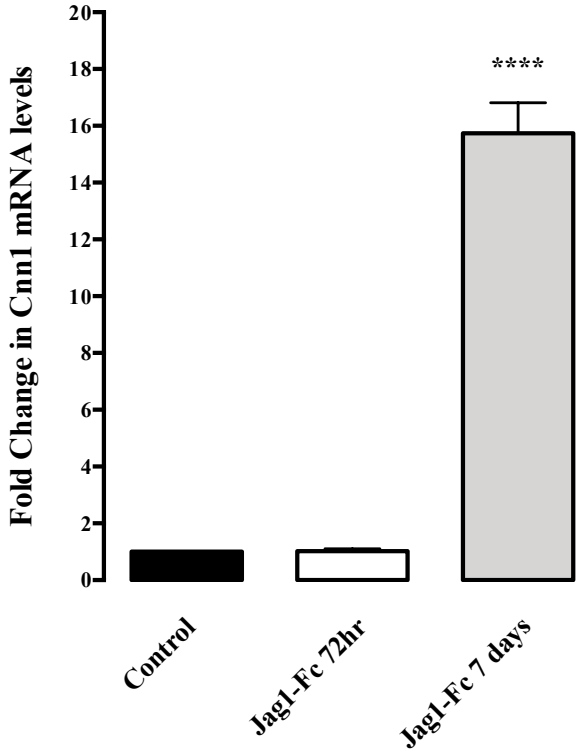

Figure 5.43. Relative Cnn1 gene expression in mAA-vSCs increases 7 days after Jag1-Fc treatment.

The mAA-vSCs were cultured on plates coated with immobilised 500 ng/ml of Jagged1-Fc (Jag1-Fc) or IgG-Fc (as control) in neuroectodermal maintenance medium (NE-MM) for 24 hours, 72 hours and 7 days. Relative mRNA expression levels of Cnn1 72 hours (72hr) and 7 days post-treatment. The data was normalised against the endogenous gene HPRT. The experiments were performed in triplicate, chart is representatives of two independent experiments. Data are mean ± S.E.M (n=3). Mann-Whitney t-test with significance value of $P \leq 0.05$. Results: ****$p < 0.0001$. Significance are compared to the control unless specified with a capped line.

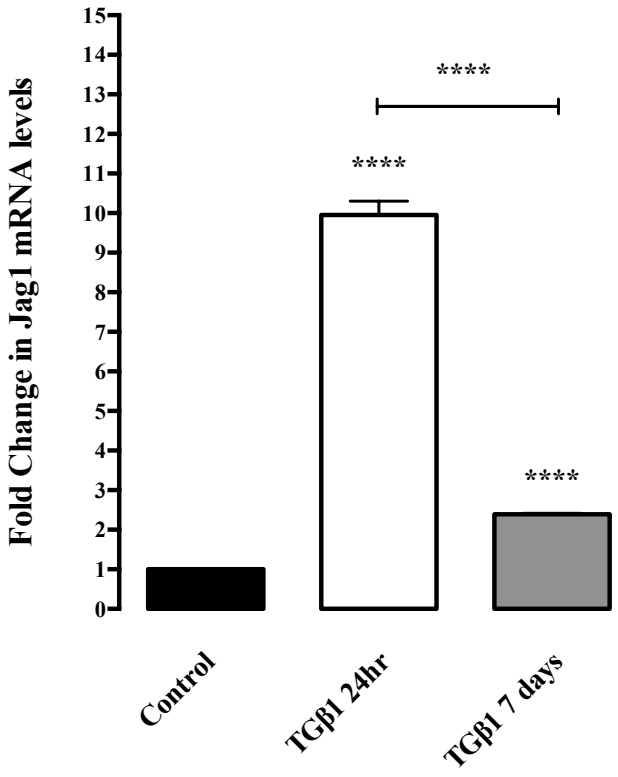

Figure 5.44. Relative Jag1 gene expression in mAA-vSCs 24 hour and 7 days after TGβ1 treatment.

mAA-vSCs were cultured in neuroectodermal maintenance medium (NE-MM) supplemented with 2 ng/ml of TGF-β1 (TGβ1) or NE-MM (Control) for 24 hours and 7 days. Relative mRNA expression levels of Jagged1 (Jag1) 24 hours (24hr) and 7 days post-treatment. The data was normalised against the endogenous gene HPRT. The experiments were performed once, chart represents a single experiment. Data are mean ± S.E.M (n=3). Unpaired T-test with significance value of $P \leq 0.05$. Results: ****$p<0.0001$. Significance are compared to the control unless specified with a capped line.

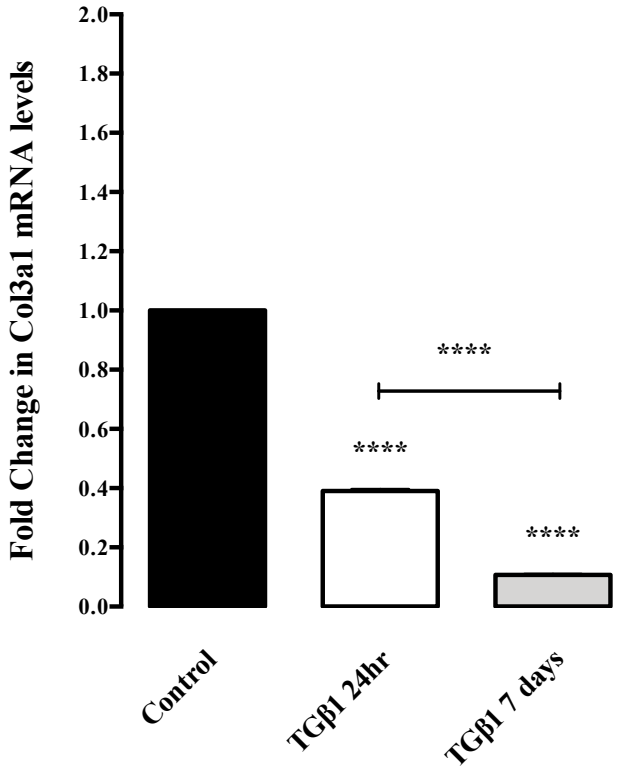

Figure 5.45. Relative Col3a1 gene expression in mAA-vSCs 24 hour and 7 days after TGβ1 treatment.

mAA-vSCs were cultured in neuroectodermal maintenance medium (NE-MM) supplemented with 2 ng/ml of TGF-β1 (TGβ1) or NE-MM (Control) for 24 hours and 7 days. Relative mRNA expression levels of Collagen type III, alpha 1 (Col3a1) 24 hours (24hr) and 7 days post-treatment. The data was normalised against the endogenous gene HPRT. The experiments were performed once, chart represents a single experiment. Data are mean ± S.E.M (n=3). Unpaired T-test with significance value of $P \leq 0.05$. Results: ****$p<0.0001$. Significance are compared to the control unless specified with a capped line.

5.3.4 Wnt4 and Sonic Hedgehog treatment on mAA-vSCs

5.3.4.1 Murine recombinant Wnt4 does not induce myogenic differentiation of vascular stem cells from murine aortic arch

Vascular stem cells isolated from the tunica media of murine aortic arch were cultured in NE-MM supplemented with 50 ng/ml of rmWnt4 or none (control) for 48 hours and 7 days.

Real time RT-qPCR was performed to measure the expression levels of the canonical Wnt signalling target gene runt related transcription factor1 (Runx1) in treatment group versus the control sample after 48 hrs. The expression level of Runx1 was slightly but significantly increased by 1.38 ± 0.12 fold change in rmWnt4-treated cells compared to the control sample (Figure 5.46). Moreover, the expression levels of Cnn1 mRNA significantly increased in rmWnt4-treated cells by 1.32 ± 0.06 7 days after treatment compared to the control (Figure 5.47). On the other hand, no changes in the levels of Sm-mhc mRNA were observed in the rmWnt4-treated samples compared to control sample after 7 days (Figure 5.48). PCR analysis was also performed to measure the relative expression levels of the Wnt receptor, Frizzled-1 (Fzd-1) in Wnt4-treated versus control samples. Results showed that Fzd-1 mRNA levels significantly increased by 1.98 ± 0.17 in the treatment group compared to the control (Figure 5.49).

The results suggest that activation of the Wnt/β-catenin signalling pathway was achieved by increased expression levels of Runx1 transcript. However, the level of expression was modest. Therefore, double experiments using 100 ng/ml of rmWnt4 for 48 hours and 7 days on mAA-vSCs were conducted in order to evaluate if the concentration of 50 ng/ml used in the above experiments was too low to induce a strong Wnt/β-catenin signalling and thus myogenic differentiation. Results showed that gene expression levels of Runx1 and Fzd1 were 1.01 ± 0.0.04 and 1.29 ± 0.08 fold change, respectively, in rmWnt4-treated cells compared to the control sample (Figure 5.50). Moreover, the expression levels of both Cnn1 and Sm-mhc mRNA significantly decreased in rmWnt4-treated cells by 0.92 ± 0.02 and 0.87 ± 0.009 fold change, respectively, 7 days after treatment compared to the control (Figure 5.51).

5.3.4.2 Murine recombinant Shh does not induce myogenic differentiation of vascular stem cells from murine aortic arch

Vascular stem cells isolated from the tunica media of murine aortic arch were cultured in NE-MM supplemented with 1 μg/ml of rmShh or none (control) for 24 hours and 7 days. The experiment was performed once as part of a preliminary investigation.

Real time RT-qPCR was performed to measure the expression levels of the Hh signalling target gene, Gli1 in treatment group versus the control sample after 24 hrs. The gene expression level of Gli1 increased by 2.70 ± 0.24 fold change in rmShh-treated cells compared to the control sample (Figure 5.52). Moreover, the expression levels of both Cnn1 and Sm-mhc mRNA decreased in rmShh-treated cells by 0.39 ± 0.04 and 0.71 ± 0.007 fold change, respectively, 7 days after treatment compared to the control (Figure 5.53 and Figure 5.54).

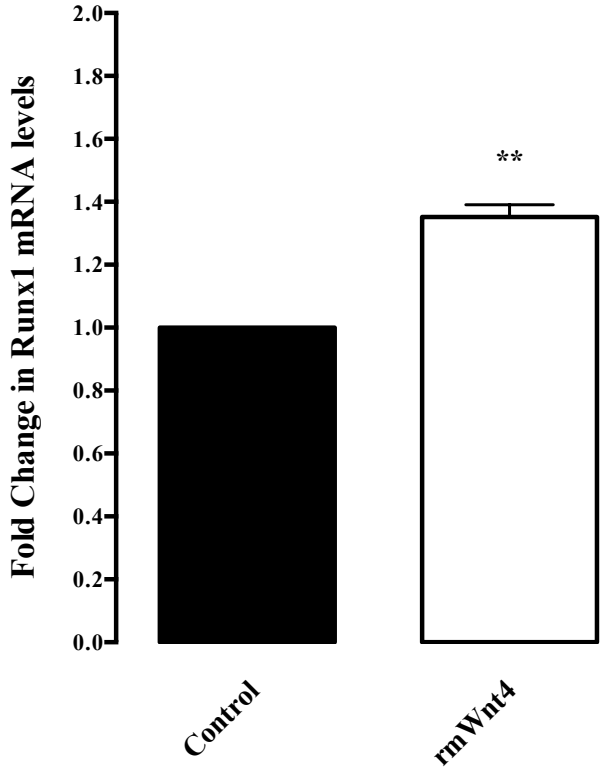

Figure 5.46. Wnt4 signalling increases the expression levels of the Wnt target gene Runx1 in mAA-vSC 7 days post-treatment.

mAA-vSCs were cultured in neuroectodermal maintenance medium (NE-MM) supplemented with 50 ng/ml recombinant murine Wnt4 (rmWnt4) or NE-MM (Control) for 48 hours. Relative mRNA expression levels of Runt related transcription factor1 (Runx1) 48 hours after treatment. The data was normalised against the endogenous gene HPRT. The experiments were performed in triplicate, chart is representatives of three independent experiments. Data are mean ± S.E.M (n=3). Mann-Whitney t-test with significance value of $P \leq 0.05$. Results: $^{**}p<0.01$.

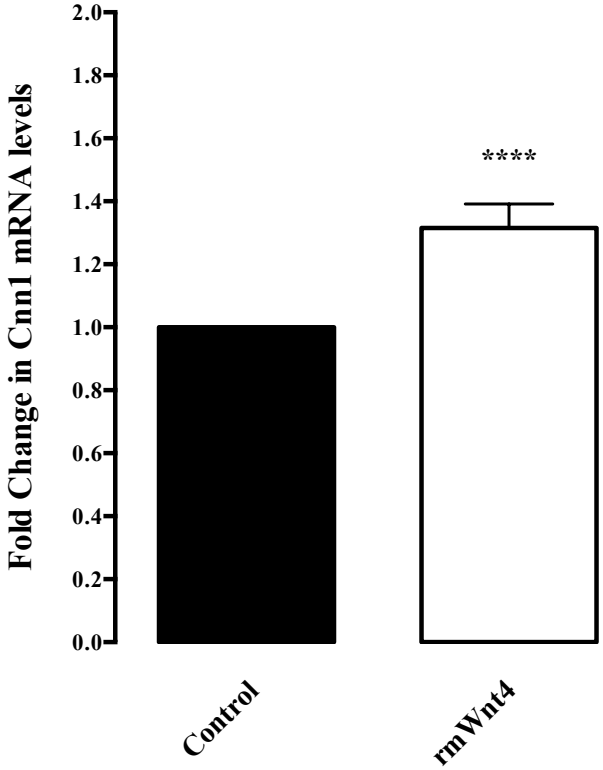

Figure 5.47. Wnt4 signalling increases the expression levels of Cnn1 in mAA-vSC 7 days post-treatment.

mAA-vSCs were cultured in neuroectodermal maintenance medium (NE-MM) supplemented with 50 ng/ml recombinant murine Wnt4 (rmWnt4) or NE-MM (Control) for 7 days. Relative mRNA expression levels of Calponin1 (Cnn1) 7 days post-treatment. The data was normalised against the endogenous gene HPRT. The experiments were performed in triplicate, chart is representatives of three independent experiments. Data are mean ± S.E.M (n=3). Mann-Whitney t-test with significance value of $P \leq 0.05$. Results: ****$p < 0.0001$.

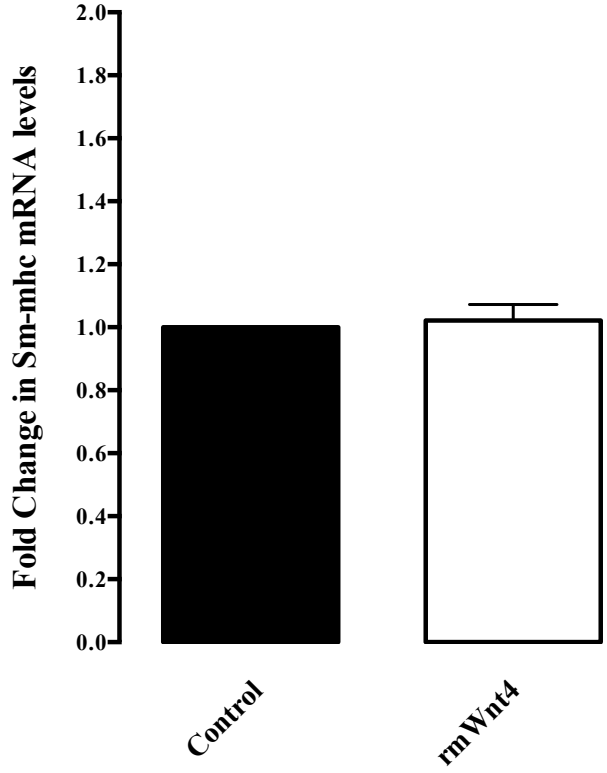

Figure 5.48. Wnt4 signalling does not have an effect on the expression levels of Sm-mhc in mAA-vSC 7 days post-treatment.

mAA-vSCs were cultured in neuroectodermal maintenance medium (NE-MM) supplemented with 50 ng/ml recombinant murine Wnt4 (rmWnt4) or NE-MM (Control) for 7 days. Relative mRNA expression levels of Sm-mhc 7 days post-treatment. The data was normalised against the endogenous gene HPRT. The experiments were performed in triplicate, chart is representatives of three independent experiments. Data are mean ± S.E.M (n=3). Mann-Whitney t-test with significance value of $P \leq 0.05$.

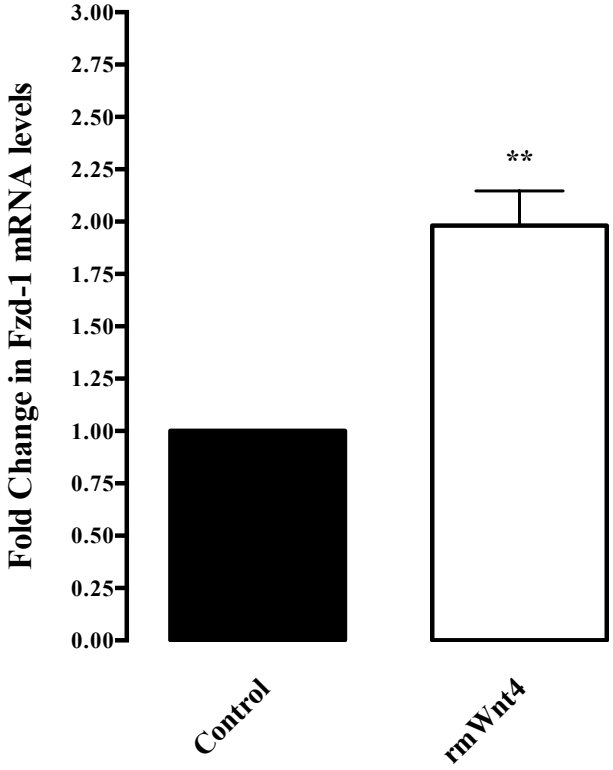

Figure 5.49. Wnt4 signalling increases the expression levels of Fzd-1 in mAA-vSC 7 days post-treatment.

mAA-vSCs were cultured in neuroectodermal maintenance medium (NE-MM) supplemented with 50 ng/ml recombinant murine Wnt4 (rmWnt4) or NE-MM (Control) for 48 hours. Relative mRNA expression levels of the Wnt receptor, Frizzled-1 (Fzd-1). The data was normalised against the endogenous gene HPRT. The experiments were performed once, chart represents a single experiment. Data are mean ± S.E.M (n=3). Unpaired t-test with significance value of $P \leq 0.05$. Results: $^{**}p<0.01$.

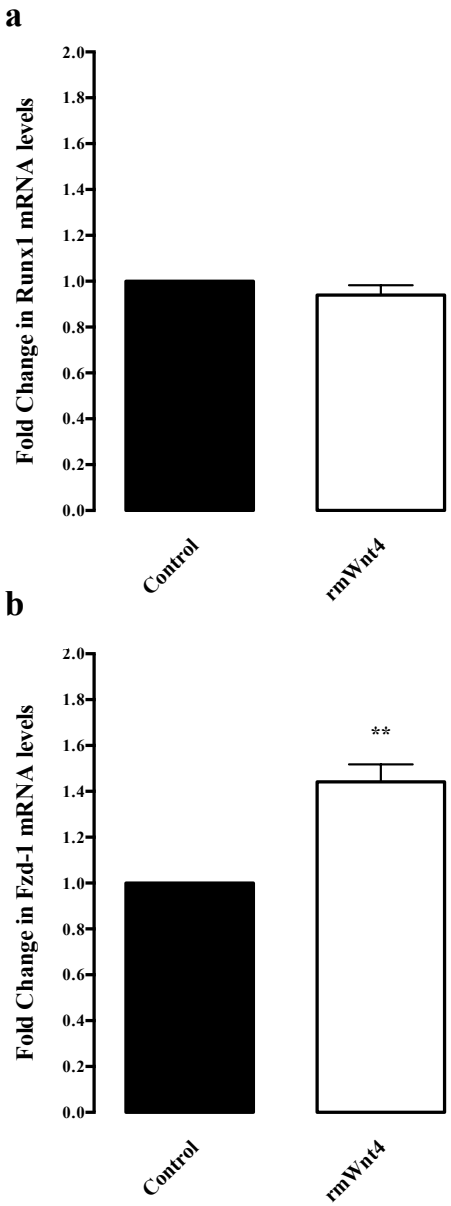

Figure 5.50. The effect of rmWnt4 on the Wnt target genes Runx1 and Fzd-1 in mAA-vSCs 48 hours after treatment.

mAA-vSCs were cultured in neuroectodermal maintenance medium (NE-MM) supplemented with 100 ng/ml recombinant murine Wnt4 (rmWnt4) or NE-MM (Control) for 48 hours. Relative mRNA expression levels of **(a)** Runt related transcription factor1 (Runx1) and **(b)** Frizzled-1 receptor (Fzd-1) 48 hours after treatment. The data was normalised against the endogenous gene HPRT. The experiments were performed in duplicate, charts are representatives of two independent experiments. Data are mean ± S.E.M (n=3). Mann-Whitney t-test with significance value of $P \leq 0.05$. Results: $^{**}p<0.01$.

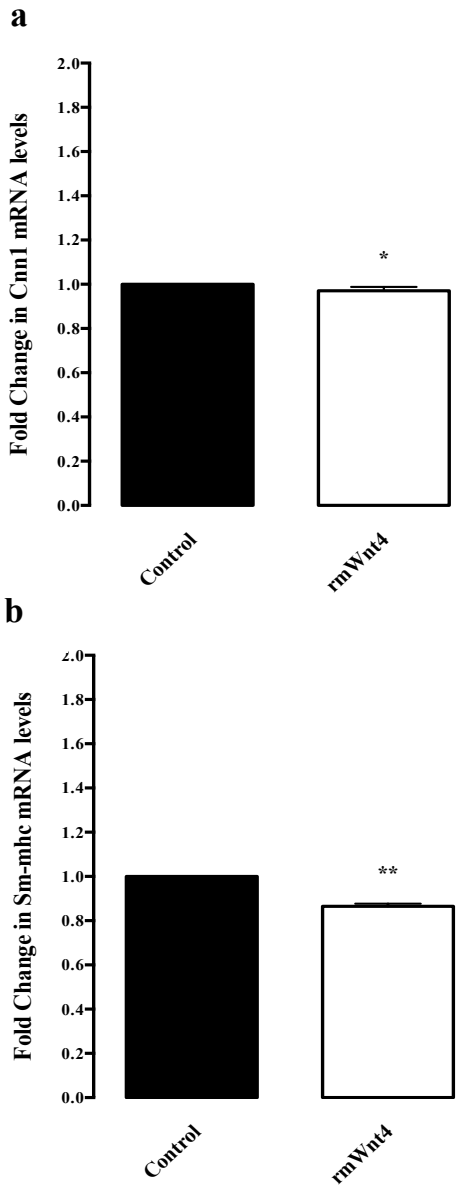

Figure 5.51. The effect of rmWnt4 on the SMC genes Cnn1 and Sm-mhc in mAA-vSCs 7 days after treatment.

mAA-vSCs were cultured in neuroectodermal maintenance medium (NE-MM) supplemented with 100 ng/ml recombinant murine Wnt4 (rmWnt4) or NE-MM (Control) for 7 days. Relative mRNA expression levels of **(a)** Calponin1 (Cnn1) and **(b)** smooth muscle myosin heavy chain (Sm-mhc) 7 days post-treatment. The data was normalised against the endogenous gene HPRT. The experiments were performed in duplicate, charts are representatives of two independent experiments. Data are mean ± S.E.M (n=3). Mann-Whitney t-test with significance value of $P \leq 0.05$. Results: *$p<0.05$ and **$p<0.01$.

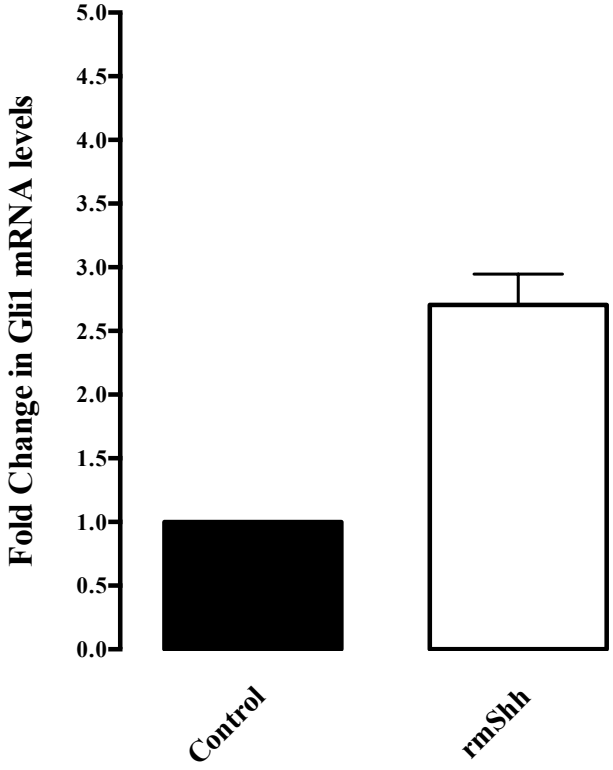

Figure 5.52. The effect of rmShh on the Shh target gene Gli1 in mAA-vSCs 48 hours after treatment.

mAA-vSCs were cultured in neuroectodermal maintenance medium (NE-MM) supplemented with 1 µg/ml recombinant murine Shh (rmShh) or NE-MM (Control) for 48 hours. Relative mRNA expression levels of Gli1 48 hours after treatment. The data was normalised against the endogenous gene HPRT. The experiments were performed in duplicate, chart is representatives of two independent experiments. Data are mean ± S.E.M (n=3). Mann-Whitney t-test with significance value of $P \leq 0.05$.

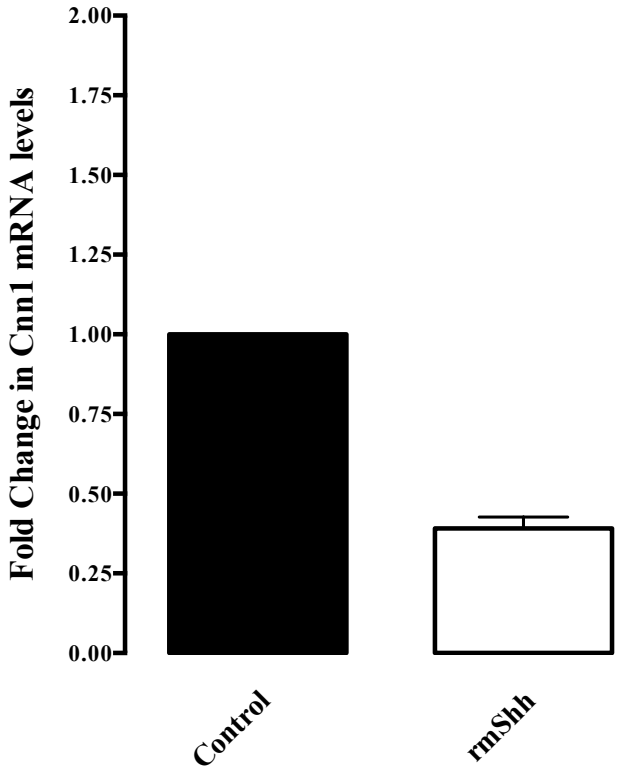

Figure 5.53. The effect of rmShh on the SMC target gene Cnn1 in mAA-vSCs 7days after treatment.

mAA-vSCs were cultured in neuroectodermal maintenance medium (NE-MM) supplemented with 1 μg/ml recombinant murine Shh (rmShh) or NE-MM (Control) for 7 days. Relative mRNA expression levels of Calponin1 (Cnn1) 7 days post-treatment. The data was normalised against the endogenous gene HPRT. The experiments were performed in duplicate, chart is representatives of two independent experiments. Data are mean ± S.E.M (n=3). Mann-Whitney t-test with significance value of $P \leq 0.05$.

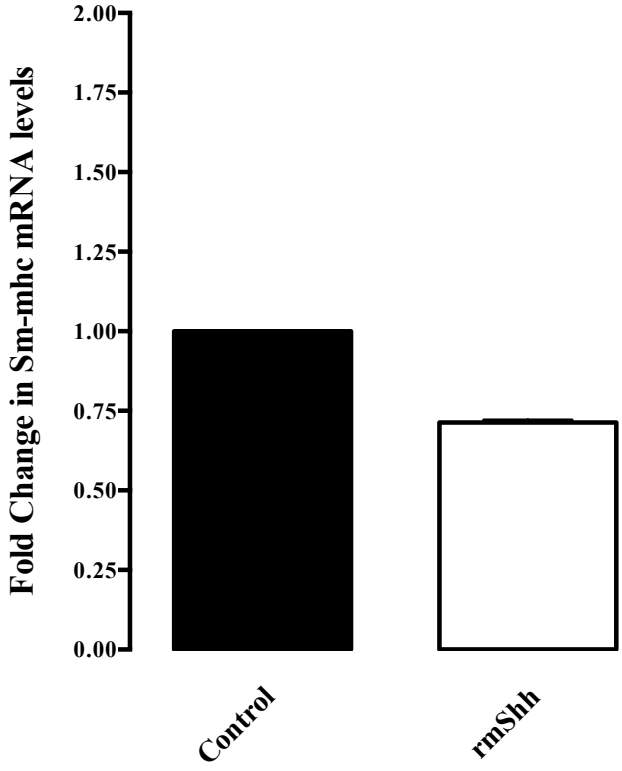

Figure 5.54. The effect of rmShh on the SMC target gene Sm-mhc in mAA-vSCs 7days after treatment.

mAA-vSCs were cultured in neuroectodermal maintenance medium (NE-MM) supplemented with 1 µg/ml recombinant murine Shh (rmShh) or NE-MM (Control) for 48 hours and 7 days. Relative mRNA expression levels of smooth muscle myosin heavy chain (Sm-mhc) 7 days post-treatment. The data was normalised against the endogenous gene HPRT. The experiments were performed in duplicate, chart is representatives of two independent experiments. Data are mean ± S.E.M (n=3). Mann-Whitney t-test with significance value of $P \leq 0.05$.

5.3.5 Summary

- The mAA-vSCs had the potential to spontaneously become mature smooth muscle cells (SMCs) following treatment with SMC differentiation media containing 10%FBS-supplemented DMEM (DM) after 1 week. Immunocytochemistry and transcriptional analysis confirmed increased expression of the SMC differentiation markers/genes, smooth muscle myosin heavy chain (SM-MHC) and Calponin1 (CNN1). Morphologically, cells adopted a spindle-shaped-like phenotype characteristic of mature SMCs. Cell number analysis showed a reduction in the number of cells per high power field (HPF) after 1-week treatment.
- TGF-β1 treatment similarly induced myogenic differentiation of mAA-vSCs and mTA-vSCs to a SMC phenotype by increasing the transcript and protein levels of the intermediate SMC marker, CNN1, however expression of the mature SMC marker, SM-MHC was not upregulated by TGF-β1 signalling. Concomitant with cell specification, the number of cells was attenuated after 1-week treatment. This suggested that factors other than TGF may be involved in the maturation of vascular stem cells to SMCs.
- Jagged1 treatment similarly induced myogenic differentiation of mAA-vSCs and mTA-vSCs to a mature SMC phenotype by increasing the transcript and protein levels of both SMC differentiation markers/genes, SM-MHC and CNN1. Concomitant with cell differentiation, the number of cells was reduced after 1-week treatment. Jagged1 treatment induced epigenetic changes in both vSCs by increasing the fold enrichment of the SMC signature H3K4me2 facilitating SMC differentiation. This result suggested that Jag1-activated Notch signalling is directly involved in SMC differentiation of vascular stem cells.
- The myogenic effect of rmTGF-β1 on mAA-vSCs was confirmed by analysing the gene expression of the TGF-β target gene, BCL2-like 11 (Bcl2l11) after 48 hours. However, pre-incubation of rmTGF-β1-treated cells with the SMAD/TGF-β signalling, SB431542 revoked the levels of Bcl2l11 and the SMC differentiation markers/genes (SM-MHC and CNN1) comparable to control samples. Concomitantly, the effect of TGF-β1 on reduced cell number was cancelled by treatment with SB431542.

- The myogenic effect of Jagged1 on mAA-vSCs was confirmed by inhibition studies carried out using the γ-secretase inhibitor, DAPT. Pre-treatment of DAPT on Jag1-treated cells revoked the levels of the Notch target gene Hey1 and the SMC differentiation markers/genes (SM-MHC and CNN1) comparable to control samples. Concomitantly, the effect of Jag1 on reduced cell number was cancelled by treatment with DAPT.
- Interaction studies carried out by inhibition of the TGF-β1 and the Jagged1 signalling with DAPT and SB431542, respectively, implied that both pathways may be required to initiate SMC induction of vSCs. While TGF-β1 alone may transition vSCs to an intermediate state of differentiation, Jagged1-activated seems to be critical for complete SMC differentiation.
- Transcriptional analysis demonstrated that mAA-vSCs can be activated by Wnt4 signalling as increased mRNA fold changes of Wnt target gene runt related transcription factor1 (Runx1) and Wnt receptor Frizzled-1 (Fzd-1) were observed. However, Wnt4 signalling did not induce robust myogenic differentiation in vSCs, suggesting that other factors may be required to synergistically work with Wnt/β-catenin signalling pathway.
- Preliminary data on Sonic Hedgehog treatment suggested that activation of the Hh signalling pathway did not induce myogenic differentiation of mAA-vSCs after 7 days.

5.4 Discussion

The biological mechanisms governing the process of neointima hyperplasia after PCI procedure is still under investigation. The factors as well as the progenitor cells that contribute to intima thickening have been intensively studied. Herein, we investigated the role of different signalling pathways, known to be involved in the development of the cardiovascular system, in isolated vascular stem cell transition and differentiation into smooth muscle cells (SMCs).

In order to achieve this, we firstly examined the differentiation potential of isolated vascular stem cells from aortic arch (mAA-vSCs) to become SMCs upon 7-day treatment with 10% FBS-containing DMEM (DM). In agreement with previously reported stem cell differentiation studies, mAA-vSCs spontaneously differentiated into mature SMCs as confirmed by increased expression levels of the smooth muscle cell genes/markers, Calponin1 (CNN1) and smooth muscle myosin heavy chain (SM-MHC). Proliferative mAA-vSCs treated with DM for 7 days exhibited a reduction in cell number accompanying with increased differentiation and morphological changes towards a spindle-shaped phenotype (Hao, Gabbiani and Bochaton-Piallat, 2003; Rensen, Doevendans and van Eys, 2007; Tang et al., 2012; Kennedy et al., 2014; Hu et al., 2004; Passman et al., 2008).

Given these results and the fact that mAA-vSCs and mTA-vSCs possessed a single neuroectodermal origin as described in Chapter 4, it is tempting to speculate that these cells may respond in a similar manner to factors known to be recapitulated during vascular injury and remodelling (Rensen, Doevendans and van Eys, 2007; Havrda et al., 2006; Yamashita et al., 2000; Hao, Gabbiani and Bochaton-Piallat, 2003; Morrow et al., 2005a; 2009). Therefore, the responsiveness levels of mAA-vSCs and mTA-vSCs to myogenic differentiation were studied and compared after induction of the TGF-β1 and Jagged1/Notch signalling. The results showed that mAA-vSCs and mTA-vSCs treated with 2 ng/ml of recombinant murine TGF-β1 (rmTGF-β1) for 7 days transitioned to an intermediate SMC phenotype determined by increased gene and protein levels of the intermediate smooth muscle cell marker CNN1. On the other hand, vSCs treated with 500 ng/ml of recombinant Jagged1-Fc (Jag1-Fc) exhibited myogenic differentiation into mature SMCs after 7 days. Tang *et al.* (2012) proposed

a differentiation pathway, where multipotent vascular stem cells (MVSCs) ultimately differentiate into SMCs by transition to an intermediate or mesenchymal-like cell. This differentiation model was proposed based on the data obtained from a long-term experiment carried out on MVSCs cultured in 10% FBS-containing DMEM (DM). MVSCs were observed to gradually lose and consequently gain the expression of the stem cell and smooth muscle cell markers, respectively, accompanying with reduction in their differentiation potential. 8 weeks after MVSCs spontaneously differentiated into mature SMCs confirmed by the expression of CNN1 and SM-MHC markers (Tang et al., 2012). Given these facts, it was suggested that Jagged1/Notch signaling alone but not rmTGF-β1 was sufficient to induce SMC differentiation by the expression of the mature SMC marker, SM-MHC, positioning Jagged1/Notch signaling as the direct activator of SMC differentiation *in vitro*.

In order to determine whether or not mAA-vSCs and mTA-vSCs responded similar to both TGF-β1 and Jagged1/Notch signalling, the levels of gene and protein expressions were given a category for that particular marker and an arbitrarily value as low, intermediate or high. Overall, the results showed that both cell progenitors responded similarly to the myogenic stimuli and considering that these cells have a common protein profile as outlined in Chapters 4 of this thesis, it was proposed that these cells were a unique progenitor cell type.

Epigenetic modifications related to SMC differentiation including di-methylation of lysine 4 on histone 3 (H3K4me2) and the DNA di-methylase ten-eleven translocation-2 (TET-2) were analysed at the SM-MHC locus on mAA-vSCs in order to study the chromatin changes that facilitate gene transcription. Indeed, Jagged1-dependent Notch activation mAA-vSCs acquired the SMC epigenetic signature H3K4me2 at the SM-MHC promoter consistent with reduction of H3K27me3, which is associated to transcriptional silencing and maintenance of pluripotency in embryonic stem cells (McDonald et al., 2006; Gomez et al., 2013; Gomez, Swiatlowska and Owens, 2015). Although, the DNA di-methylase TET-2 showed a small enrichment at the SM-MHC gene locus compared to the mAorta and mSMC samples, its fold enrichment was higher than in the Fc-treated vSCs suggesting that TET-2 may contribute to myogenic differentiation of mAA-vSCs upon Jagged1/Notch signaling.

Given these findings, the interaction between the TGF-β1 and Jagged1/Notch signalling on mAA-vSCs was evaluated by administering DAPT to TGF-β1-treated cells and SB431542 to Jag1-treated cells. The interaction of TGF-β and Notch signalling has been previously observed probably due to their extensive roles in embryonic development and adult tissue homeostasis. The outcome effects of the cross-talk between these two pathways depend on the cell type and the *in vitro* conditions used to perform the experiments since other morphogens and factors can also interfere with their overall response (Luo, 2017). In our hands and under the defined experimental conditions, TGF-β1 signalling negatively regulated the expression of the SMC differentiation genes in jagged1-treated mAA-vSCs. Conversely, Jagged1 enhanced the myogenic effect of TGFβ confirmed by the reduction of CNN1 after DAPT treatment. Overall, the data suggested that TGF-β1 may be negatively regulating the myogenic effect of Jagged1/Notch signalling owing to i) TGF-β1-treated cells achieved an intermediate state, ii) Jagged1 is sufficient to drive vSCs to mature SMCs and iii) inhibition of Tgf-β1 factor increased the SMC differentiation effect of vSCs in culture.

Surprisingly, cell number on mAA-vSCs and mTA-vSCs was attenuated when cultured under three different SMC differentiation conditions (DM, TGF-β1 and immobilised Jagged1). The number of cells in control and treated-vSCs cultures was larger at 7 days compared to that of 24 hours after initial seeding. However, cells defined by their nuclei and plasma membrane became very large in size and in some cases, it was not possible to image more than 6-7 cells per low magnification field (20X), which were then used to calculate the number of cells per μm^2. This phenomenon was more pronounce in DM and TGF-β1 compared to those on immobilised Jagged1-Fc. During embryogenesis, stem cells undergo a number of both asymmetrical and symmetrical division ultimately giving rise to an entire organism. Symmetric divisions occur when a stem cell self-renews resulting in the generation of two daughter stem cells. In contrast, asymmetric division refers to when a stem cell becomes polarised and thus divides into two daughter cells in which one remains stem and the other one becomes a more specialised or differentiated cell. During asymmetric division the number of stem cells can then remain constant while the number of differentiated cells increases. Asymmetric division is critical during development and

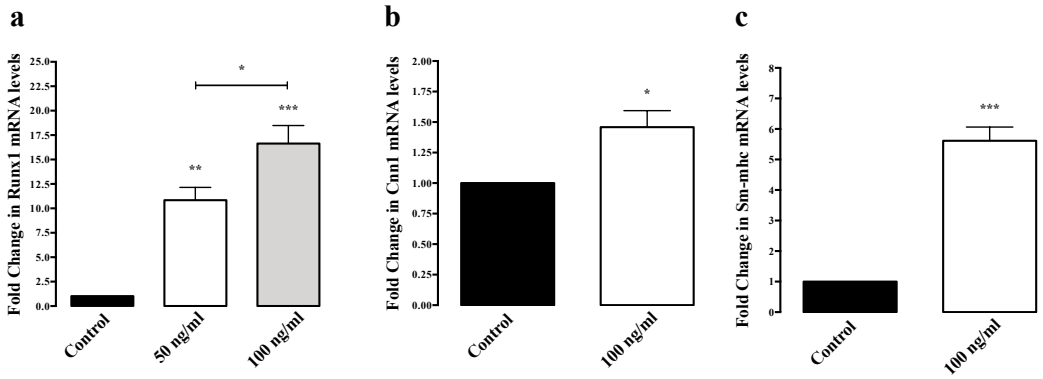

Figure 5.55. The myogenic effect of Wnt4 signalling on mTA-vSC cultured in 10% FBS-containing medium.

mTA-vSCs were cultured in a neuroectodermal maintenance medium used for the growth of murine neuroectodermal stem cells (mNE-4Cs) as outlined in Section 2.8.1. Relative mRNA expression levels of **(a)** Runx1 using 50 ng/ml and 100 ng/ml of rmWnt4 after 48 hours incubation (One-Way ANOVA). 7-day treatment was performed with 100 ng/ml of rmWnt4 and the relative expression levels of **(b)** Cnn1 and **(c)** Sm-mhc mRNA were measured by PCR analysis (Unpaired t-test). The data was normalised against the endogenous gene HPRT. The experiments were performed once, charts represent a single experiment. Data are mean ± S.E.M (n=3). One-way ANOVA with significance value of P≤0.05. Results: *p<0.05. Tukey's test for multiple comparisons with significance value of P≤0.05. Results: *p<0.05, **p<0.01 and ***p<0.001. Unpaired t-test with significance value of P≤0.05. Results: *p<0.05 and ***p<0.001.

the replacement of cells in adult organisms (Morrison and Kimble, 2006; Knoblich, 2008).

Given this fact, the decreased cell number observed in treated vSCs may be due to asymmetric division, where a slower but steady increase in cell number was observed compared to untreated stem cell sample (data not shown).

Lastly, the myogenic effect of Wnt4 and Sonic Hedgehog (Shh) signalling were evaluated on mAA-vSCs. The proliferative role of Wnt4 in vascular smooth muscle cells *in vitro* and *in vivo* has been previously reported (Hua et al., 2014; Tsaousi et al., 2011; Ezan et al., 2004; Ackers and Malgor, 2018), therefore we investigated whether Wnt4 stimulation in mAA-vSCs could promote myogenic differentiation. The data showed that Wnt4 under the defined culture conditions did not have any effect on the

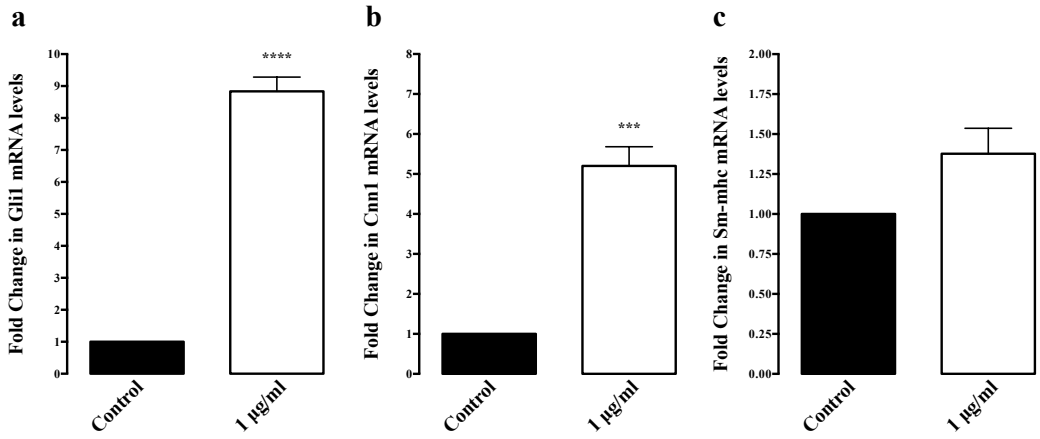

Figure 5.56. The myogenic effect of Shh signalling on mTA-vSC cultured in 10% FBS-containing medium.

mTA-vSCs were cultured in a neuroectodermal maintenance medium used for the growth of murine neuroectodermal stem cells (mNE-4Cs) as outlined in Section 2.8.1. This medium was supplemented with 1 µg/ml of rmShh and cells were incubated for 48 hours and 7 days. Relative mRNA expression levels of **(a)** Gli1 after 48 hours as well as **(b)** Cnn1 and **(c)** Sm-mhc after 7 days incubation were calculated by PCR. The data was normalised against the endogenous gene HPRT. The experiments were performed once, charts represent a single experiment. Data are mean ± S.E.M (n=3). Unpaired t-test with significance value of P≤0.05. Results: ***p<0.001 and **** p<0.0001.

myogenesis of vascular stem cells. Given this finding and results obtained on a preliminary study carried out on mTA-vSCs cultured in a medium used for the growth and maintenance of mouse neuroectodermal stem cells (mNE-4Cs), we speculated that Wnt signaling may require other factors to induce lineage specificity before myogenesis via the Wnt signaling pathway. Figure 5.55 demonstrated that when mTA-vSCs were exposed to either 50 ng/ml or 100 ng/ml of rmWnt4 for 48 hours in a 10% FBS-containing medium, the level of Runx1 mRNA were significantly upregulated. The data also showed that Cnn1 but more pronounced Sm-mhc gene expression was significantly elevated after 7-day treatment. These results suggested that Wnt signaling may require other factors to exert myogenesis.

Despite the fact that Hedgehog (Hh) signalling has been shown to be recapitulated during arterial remodelling in response to vascular injury *in vivo,* and the sonic

hedgehog (Shh) morphogen has been implicated in SMC differentiation of stem cells *in vitro* (Fitzpatrick et al., 2017; Mooney et al., 2015; Passman et al., 2008; Morrow et al., 2009), this work showed that Shh treatment of mAA-vSCs did not increase the transcript levels of Cnn1 and Sm-mhc under the described experimental conditions. However, when the condition of the medium in where vSCs were treated with Shh changed, the expression levels of the Shh target gene Gli1 and the SMC gene maker Cnn1 were significantly elevated compared to the control sample after 48 hours and 7 days, respectively (Figure 5.56). The growth medium used to culture and treat mTA-vSCs in Figure 5.56 had a higher percentage of FBS (10%) compared to the 1% FBS-containing medium used in all the rest of the experiments in this Chapter. Therefore, these results might suggest that Shh signaling may require other factors to exert myogenesis.

Overall, these results suggested that Wnt4 and Shh signalling may require other factors to stimulate myogenic differentiation. Conversely, TGF-β1 was able to induce SMC specification, perhaps by transitioning vascular stem cells towards a mesenchymal-like cell phenotype; however, Jagged1 was sufficient to drive myogenic differentiation alone and thus suggesting that Jagged1-activated Notch is directly involved SMC maturation of vSCs.

Chapter 6

General Discussion

Cardiovascular disease (CVD) remains the leading cause of death globally (Benjamin et al., 2019). Current treatment options include preventative therapy (diet and exercise), and medications such as statins and anti-hypertensives, in addition to revascularization and stenting of obstructed arteries to reduce ischemia and improve quality of life. Despite these treatment options, morbidity and mortality from CVD remain unacceptably high (Benjamin et al., 2019).

A hallmark of arterial pathology in CVD is the accumulation of neointimal cells, primarily vascular smooth muscle (SMC)-like cells, leading to intimal thickening (Bennett, Sinha and Owens, 2016). Vascular smooth muscle cell (SMC) accumulation is a key event leading to the development of early adaptive lesions (Sakamoto et al., 2018) and an essential marker of subclinical disease yet the fundamental aspects of vascular cell accumulation, proliferation and the phenotypic changes within the vessel wall remain unresolved (Bennett, Sinha and Owens, 2016). Lineage tracing analysis has provided substantial evidence of the involvement of stem cell-derived progeny(Wan et al., 2012; Tang et al., 2012; Kramann et al., 2016) in addition to 'reprogrammed' differentiated SMCs (Nemenoff et al., 2011; Herring et al., 2014; Chappell et al., 2016; Albarrán-Juárez et al., 2016), SMC-derived from endothelial-mesenchymal transition (EndMT) (Cooley et al., 2014) and minimal SMC derived from bone-marrow stem cells (Skowasch et al., 2003) in initiating and progressing adaptive intimal thickening as these cells become activated/reprogrammed, differentiate down vascular and myeloid lineages and subsequently dictate, in part, vessel remodelling.

The focus of this thesis was on the complex and widely debated topic around the various cell populations that may contribute to the pathology of intimal thickening, typical of arteriolosclerosis, atherosclerosis, and clinical ISR after angioplasty and stenting. In doing so, this study specifically examined whether S100β^{+}/Sca-1^{+} progenitors and their progeny contributed to intimal thickening following iatrogenic flow-restriction using transgenic reporter mice and genetic cell fate mapping *in vivo.* Further studies successfully isolated S100β^{+}/Sca-1^{+} progenitors isolated from athero-prone (aortic arch) and athero-resistant (thoracic aorta) regions of the murine aorta *in vitro* and determined whether these cell populations shared a similar origin before assessing their responsiveness to known myogenic inductive factors implicated in the

progression of intimal thickening.

The present study has provided significant evidence for S100β$^+$ and Sca-1$^+$ progenitor cells within the tunica adventitia and/media participating in intimal thickening following iatrogenic flow-restriction in mice. Although a modified enzymatic protocol was utilised to isolate these progenitor cells from the medial layer of the aortic tissue, our evidence suggests that these cells may predominantly reside within the adventitial rather than the medial layer of the artery. Isolated vascular progenitor cells from both athero-prone (aortic arch) and athero-resistant (thoracic aorta) regions of the murine aorta exhibited a neuroectodermal phenotype characterised by their persistent expression of markers including S100β, SOX10/17, and Sca-1. Both isolated vascular stem cells (vSCs) also showed an epigenetic signature (H3K27me3) at the SM-MHC promoter typical of undifferentiated stem cells and ESCs. In addition, the stable signature epigenetic mark H3K4me3 of SMCs at the same locus was not observed. Most importantly, *in vitro* differentiation studies performed with myogenic factors known to be upregulated in vascular disease progression revealed a mechanistic pathway where Jagged1-activated Notch signalling is the ultimate arbiter that drives myogenic differentiation of these cells *in vitro* and is accompanied by enrichment of SMC epigenetic mark at the SM-MHC locus and enhanced expression of smooth muscle cell differentiation markers (CNN1 and SM-MHC).

These results reinforce the contention that resident vascular stem cells are in part responsible for the progression of pathologic intimal thickening.

6.1 The Involvement of S100β$^+$ and Sca-1$^+$ in Vascular Disease

The origin of intimal cells has recently been challenged. Over the last decade, two significant possibilities for the source of intimal lesional cells have emerged: somatic cell re-programming following de-differentiation (and in some cases within calcified lesions, trans-differentiation) of mature differentiated SMCs or differentiation from immature multipotent mesenchymal-like vascular progenitors that reside within the vessel wall or migrate from the circulation. Substantial evidence now suggests that vascular stem cells in addition to de-differentiated SMCs may become activated following vascular injury by transitioning to SMC-like cells. It is believed that these SMC-like cells, in part, contribute to the deleterious remodelling event that leads to

vascular disease progression(Yuan et al., 2017).

The long-standing dogma is that neointimal SMC-like cells are derived from resident medial differentiated vascular SMCs that undergo ‘phenotypic switching' and ‘re-programming', migration into the intima where they proliferate, produce extracellular matrix and participate in intimal thickening, including fibrous cap formation (Gomez et al., 2013). However, until recently, the evidence for this was circumstantial predominantly driven from studies utilising SMCs in culture (Sandison et al., 2016).

Recent lineage tracing studies using *Myh11CreERT* transgenic mice have since provided substantial evidence that neointimal SMCs(Nemenoff et al., 2011; Herring et al., 2014; Shankman et al., 2015) and a considerable number of neointimal macrophages(Shankman et al., 2015; Albarrán-Juárez et al., 2016) are derived from ‘marked' medial differentiated SMC *in vivo* that are thought to ‘re-programme’ to a more plastic ‘de-differentiated’ phenotype following vascular injury (Shankman et al., 2015; Majesky et al., 2017; Chappell et al., 2016). Furthermore, multi-colour lineage tracing analysis in *Myh11-CreERT-Confetti* reporter mice suggests that not all ‘marked’ differentiated SMCs are responsible for the accumulation of neointimal SMCs or macrophages but rather a discrete subpopulation of ‘plastic’ medial SMCs (Chappell et al., 2016). Finally, epigenetic signatures (H3K4me2: histone 3 lysine 4 dimethylation) at the Myh11 locus and their retention in de-differentiated SMCs that are no longer transcriptionally active have also been used to mark differentiated SMCs *in vivo* and validate the origin of neointimal SMCs and macrophages *in vivo* as SMC using parallel lineage tracing with *Myh11CreERT2-YFP* mice (Gomez, Swiatlowska and Owens, 2015; Shankman et al., 2015).

Key research groups supporting the de-differentiation of vascular smooth muscle cells (vSMCs) have employed tamoxifen-inducible SM-MHC-cre/Rose26 animals with either wire-injured femoral artery or complete carotid artery ligation. For instance, Nemenoff *et al.* showed that vSMCs became proliferative thus contributing to the cellularization of the lesion in injured animals (Nemenoff et al., 2011). Herring *et al.* (2014) demonstrated that approx. 80% of the lesional cells were derived from resident vascular SMCs (Herring et al., 2014). This study was challenged by Yang *et al.* (2016) using adult animals (11 weeks old) in contrast to the juvenile mice (younger than 6 weeks old) used in Herring’s study. The findings showed that less than 30% of the

lesional cells were originated from vSMCs as opposed to the 80% reported by Herring *et al.* (2014) (Yang et al., 2016). The interesting work carried out by Chappell *et al.* (2016) using the multicolour conditional reporter mice provided compelling evidence that neointimal cells are derived from a discrete subpopulation of vSMCs (Chappell et al., 2016). Also, since a large number of adventitial progenitor cells originate from resident vSMCs during development, this has led some investigators to hypothesize that vSMCs were indirectly involved in neointimal thickening by contributing to resident vascular progenitor cells in the adventitia (Majesky et al., 2017).

This original paradigm of vascular SMC 'phenotypic switching' and re-programming *in vitro* and *in vivo* has been since challenged by numerous studies that demonstrate the presence of stem cell markers within rodent and human vascular lesions and the isolation and the characterization of these cells as multipotent *in vitro* (Hu et al., 2004). Subsequent lineage tracing analysis has also provided compelling evidence that a significant subset, if not the majority of neointimal SMC and macrophages may be derived from medial progenitors (Tang et al., 2012; Wan et al., 2012), adventitial progenitors(Kramann et al., 2016; 2015), endothelial-mesenchymal stem cells (EndMT) (Cooley et al., 2014) or from bone-marrow derived stem cells(Sata et al., 2002) using various models of vascular injury in mice.

Whereas some authors support the contribution of bone-marrow cells to vascular pathology (Wan et al., 2012; Chen et al., 2018), their role has been since clarified (Hoglund, Dong and Majesky, 2010). Initial studies demonstrated that resident vascular stem cells are the primary cell present in intimal lesions (Hu et al., 2004; Tang et al., 2012; Passman et al., 2008; Fitzpatrick et al., 2017; Sainz et al., 2006). Indeed, it is widely purported that resident stem cell antigen-1 positive ($Sca1^+$) (Hu et al., 2004) and $Sox10^+$/S100β stem cells (Tang et al., 2012; Yuan et al., 2017) may contribute significantly to neointimal formation *in vivo,* at least in rodent models. Their recruitment is regulated by matrix metalloproteinase-8, and stromal-cell-derived factor (Zhang and Xu, 2017) and their differentiation towards a myogenic lineage was controlled by *c-myb* regulation of the myocardin promoter (Shikatani et al., 2016).

Nevertheless, the specific origin of neointimal cells remains controversial, and the spatiotemporal pattern of S100β/$Sca1^+$ cells and their overall contribution to intimal thickening is less well characterized. Lastly, the studies carried out by Cooley *et al.*

(2014) in an injury model of vein grafting proposed that venous endothelial cells contributed in part to the SMC-like cells within the lesion by transitioning through a mesenchymal phenotype (EndoMT) (Cooley et al., 2014).

It is clear that recent lineage tracking experiments in mice provide significant evidence for a stem cell origin of lesional cells(Yuan et al., 2017; Tang et al., 2012; Kramann et al., 2016; Wan et al., 2012) in addition to the contributory role of endothelial cells through endothelial-mesenchymal transition (EndoMT) (Yuan et al., 2017; Cooley et al., 2014) and medial differentiated SMC(Nemenoff et al., 2011; Herring et al., 2014; Chappell et al., 2016). However, these studies that tracked resident stem cells using Nestin(Wan et al., 2012) and Sox10(Yuan et al., 2017) Cre-LoxP transgenic mice relied specifically on constitutive Cre recombinase to mark these cells from birth. As these cells might also be expressed during embryonic development, the temporal and spatial control of Cre recombinase activity can be more efficiently controlled with inducible recombination to selectively activate Cre in resident vascular stem cells of adult mice via a stem cell-specific promoter. This is particularly important when analysing carotid arteries before and after vascular injury as carotid SMC are derived from a neural stem cell background (Wang et al., 2015). In this context, the work presented within this thesis is the first to mark and track S100β resident stem cells in atheroprone vessels using an inducible Cre-loxP reporter system in mice.

Using Sca1-EGFP and S100 β-EGFP transgenic mice to detect $Sca1^{+}$ and S100β positive cells during the development of intimal thickening, respectively, a significant proportion of intimal lesional cells were Sca1/$S100\beta^{+}$ after iatrogenic flow-restriction in mice when compared to sham controls. Moreover, using lineage tracing analysis of S100β marked cells, this population of intimal lesional cells originated from a resident $S100\beta^{+}$, non-SMC parent population. Indeed, freshly isolated differentiated SMCs do not express stem cell markers (Sox10/Sox17/ S100β/Nestin/Sca1) but when sub-cultured *in vitro,* these stem cell markers appear in cultured cells (Kennedy et al., 2014). It is possible that de-differentiation and re-programming of differentiated SMCs to a more plastic de-differentiated SMC phenotype typical of sub-cultured cells could account for the appearance of these stem cell markers. However, no direct evidence has ever been presented to show that 'marked' differentiated SMC from uninjured *Myh11CreERT2* mice *in vivo* were retained when cultured *in vitro* when phenotypic

switching is predicted to occur. Recent studies using marked differentiated SMCs isolated from the aorta of *Myh11CreERT*-Rosa26-EGFP transgenic mice and cultured *in vitro* suggest that these marked cells are eventually lost in culture as the cells begin to proliferate and expand (Yuan et al., 2017). A similar phenomenon for marked differentiated β-islet cells has been reported (*insulin-CreZ/AP* mice and *insulin-CreER mice*) where marked differentiated β-cells rarely proliferate under standard culture conditions and are eventually lost in culture with the remaining β-islet cells, not of a β-cell 'marked' origin (Weinberg et al., 2007).

The reason(s) for the conflicting results on the source of intimal lesion cells in murine models of intimal thickening remain unresolved. Nevertheless, a common feature of all these *in vivo* lineage tracing studies is the use of inducible Cre transgenic mice in combination with reporter animals. This technology is widely used in lineage-tracing studies, however, experimental evidence regarding the use of tamoxifen (Cre-recombination inducer) is not described. An important issue addressed by Reinert *et al.* (2012) (Reinert et al., 2012) was the lack of established parameters such as dose titre, and administration time length for the use of Tamoxifen, critically for 'pulse-chase' lineage tracing experiments. In this system, the Cre enzyme is expressed under the activity of a specific promoter, however, in the absence of tamoxifen Cre is inactive and sequestered in the cell cytoplasm by an estrogen receptor (ER). Once tamoxifen is administered to the animals, cells expressing the Cre-ER fusion protein mediate recombination of the LoxP sites, and the reporter gene becomes transcribed. Cells expressing Cre-recombination will then be indelibly marked as will their progeny. Pulse is referred to as the time when cells under the desired promoter are being marked. It is vital that during this period tamoxifen is wholly eliminated before the injury. If tamoxifen is still present in the tissue after injury (chase period) cells acquiring the protein under which the Cre is expressed will undergo tamoxifen-induced recombination and create false positive. Importantly, tamoxifen-induced Cre-LoxP recombination in adult mice occurred for weeks after the last drug administration and that the extent of recombination was dose-dependent. This group developed a novel bioassay that allowed them to measure Cre recombination at any point after Tamoxifen (Tm) treatment using a transgenic mouse model to target β-cells ($Pdx1^{PB}$-$CreER^{Tm}$/$R26R^{LacZ}$). Pancreatic islet cells from $Pdx1^{PB}$-$CreER^{Tm}$ Tm-free mice were then transplanted into Tm recipient wildtype animals 48hr, 1 week, 2 weeks and 4

weeks after tamoxifen administration. Overall, their experimental data revealed the importance of the parameters involved in Cre recombination is key to avoid false positives by residual tamoxifen-induced recombination remaining within tissues (Reinert et al., 2012).

Even though the *in vivo* studies carried out by Nemenoff *et al.,* Herring *et al.* and Yang *et al.* concluded that differentiated SMCs were the main contributor to intimal thickening following injury, it is notable that the extent of their contribution was significantly different. These discrepancies could in part be due to the various parameters set when designing the cell fate mapping experiment, including the dose of tamoxifen, tamoxifen degradation time and even the age of the animals. These considerations are important when interpreting their findings (Nemenoff et al., 2011; Herring et al., 2014; Yang et al., 2016). Moreover, when multicolor tamoxifen-inducible Cre-Loxp mice were employed to reveal a subpopulation of vSMCs that were responsible for the lesional intimal cells after vascular injury, the mice were subjected to carotid ligation 1 week after the last dose of tamoxifen administration (Chappell et al., 2016). Therefore, it is highly likely that any resident vascular stem cell that acquired the SM-MHC promoter driving the Cre following flow-restriction would be marked due to the presence of tamoxifen remaining with a tissue compartment, thereby confounding the interpretation.

Finally, the importance of optimization of the tamoxifen dose for the use of the Cre-LoxP system to carry out fate-mapping studies has recently been addressed in the mouse brain (Valny et al., 2016). Degradation times for tamoxifen were strongly dependent on the initial tamoxifen dose concentration and was more pronounced using aged animals with a higher mortality rate after the administration of a high dose. The strain of the mice is also crucial as they can display different degradation rates (e.g., FVB/NJ mice had a significantly higher degradation rate than mice of a C577BL/6J background) (Valny et al., 2016).

Overall, it is clear that the tamoxifen dosage regime and recovery times after administration ceases are vital parameter to consider maximizing the level of Cre recombination while minimizing extended recombination due to the presence of residual tamoxifen within the tissue. The age of the animals as well as the specific strain used should always be considered when assessing their metabolic rates of

tamoxifen. Although, tamoxifen-inducible Cre-LoxP transgenic animals have been widely used in studies addressing the origin of intimal lesional cells during disease, the conflicting data to date could be due to variations in these parameters that critically control Cre-recombination.

One final consideration not addressed in any previous studies is the potential role of extracellular vesicles (EVs) and their likely release of the Cre enzyme from Cre^+ positive cells to a Cre^- negative cell that expresses the Rosa26 reporter gene thereby driving recombination in that cell (Zomer, Steenbeek, Maynard and van Rheenen, 2016). It is clear that EC and SMC release distinct EVs which are likely to have different impacts on neighbouring cells. EC dysfunction and apoptosis generates the release of EVs that are implicated in arteriosclerotic disease (Schiro et al., 2014) and during the aging process (Uryga and Bennett, 2016). EVs derived from SMCs are involved in vascular calcification, a hallmark of atherosclerotic lesions (Kapustin et al., 2015). Indeed, it is also known that endothelial dysfunction due to disturbed blood flow is associated with the release of EVs in athero-prone vessels (Hromada et al., 2017).

The data from the lineage tracing study presented in Chapter 3 of this thesis demonstrated that the majority of the cells in the neointima after iatrogenic flow-restriction are derived from an $S100\beta^+$ parent stem/progenitor cell resident within the vessel wall. This data was generated using an experimental design that consisted of 1 x 1 mg/kg of tamoxifen for 5 consecutive days followed by complete carotid artery ligation 2 weeks after the last dose of tamoxifen. Our group has also analysed cross-sections from injured vessel 4 weeks after the last tamoxifen administration and our preliminary data suggests that S100β-derived cells are still present in the lesions 21 days post-ligation (data not shown).

6.2 Isolated vascular progenitor cells from the athero-prone (aortic arch) and athero-resistant (thoracic aorta) regions of the murine aorta are neuroectodermal in origin

The presence of vascular stem cells within the tunica adventitia and tunica media has

been reported by different research groups supporting the existence of an adventitia progenitor cell (Hu et al., 2004; Passman et al., 2008; Fitzpatrick et al., 2017). On the other hand, the presence of a medial stem cell characterized by the expression of the Sox10 marker has been reported (Tang et al., 2012; Yuan et al., 2017). These cells express markers associated with neural crest stem cells and could potentially be the source of cells causing intimal thickening by transitioning to a SMC phenotype in vitro under different myogenic conditions such as TGF-β1 and Sonic Hedgehog (Fitzpatrick et al., 2017; Hu et al., 2004; Tang et al., 2012). Lineage tracing studies support the role for an S100β+ parent population within the vessel wall that contributes in part to intimal thickening after iatrogenic flow-restriction in mice. These cells were, therefore, isolated to characterize their phenotype and assess their myogenic differentiation potential *in vitro.*

In vivo studies have demonstrated that disease development was intrinsic to their embryological origin rather than haemodynamic conditions (DeBakey and Glaeser, 2000; Haimovici and Maier, 1964; Trigueros-Motos et al., 2013). In this context, SMCs of the aortic arch and carotid artery are of neuroectodermal (NE) origin compared to the paraxial-mesoderm (PM) cells within the thoracic aorta. Hence, it was essential to evaluate the embryological origin of isolated vascular stem cells from NE and PM tunica medial regions of the aorta and determine how these cells respond to myogenic stimuli that could ultimately dictate their role in specific vascular disease.

Vascular stem cells were isolated from the two regions (thoracic aorta and aortic arch) known to be disease-specific. Susceptibility to atherosclerosis along the aorta is not equal, for instance, stretches with blood flow disturbance such as curvatures and angles (aortic arch and arterial branches) are more prone to develop this vascular disease than others where the blood flow is laminar (thoracic and abdominal aorta) (Wasilewski, Głowacki and Poloński, 2013). Therefore, as vascular beds display differential disease susceptibility (Haimovici, 1991), it is likely that their embryological origin (S100β neuroectoderm [NE] vs Pax1 paraxial mesoderm [PM]) in addition to endothelial dysfunction (Wasilewski, Głowacki and Poloński, 2013; Majesky, 2007; 2003; Rensen, Doevendans and van Eys, 2007) may influence disease localisation and progression (Trigueros-Motos et al., 2013).

We demonstrated that vascular stem cells (vSCs) isolated from the aortic arch (mAA-

vSCs) and the thoracic aorta (mTA-vSCs) expressed neural crest stem cell markers including S100β, Sox10, and Nestin in agreement with other previous studies (Yuan et al., 2017; Tang et al., 2012). Transcriptional studies of specific genes associated to germ layer specification (neuroectodermal [NE] versus mesodermal [M]) revealed their neuroectodermal origin by the enrichment of the neural crest marker (Pax6) gene (Sinha, Iyer and Granata, 2014). Surprisingly, vSCs were persistently positive for the Sca-1 marker previously reported in adventitial stem cells (Hu et al., 2004; Passman et al., 2008; Majesky et al., 2017; Fitzpatrick et al., 2017). Considering that in our *in vivo* studies, both S100β and Sca-1 were only found in the adventitia of sham-operated animals, we determined the fidelity of the protocol for the isolation of medial vSCs from aortic tissue utilised by us and others (Sinha, Iyer and Granata, 2014; Yuan et al., 2017). Results from the immunohistochemical analysis performed in Chapter 4 suggests that the enzymatic removal of the adventitia layer was not 100% efficient as some cells remained on the external elastic lamina at the adventitial side. These data strongly suggested that the niche of the isolated mAA-vSCs and mTA-vSCs may also reside within the tunica adventitia and not exclusively in the medial layer of the aorta.

Previous studies have suggested that "de-differentiated" cultured SMCs *in vitro* and intimal lesional cells *in vivo* may retain the stable epigenetic histone mark, H3K4me2 at the SM-MHC promoter and this property can be used to ascertain the origin of stem cells from SMCs *in vitro* and *in vivo* (Shankman et al., 2015; Gomez et al., 2013; Gomez, Swiatlowska and Owens, 2015). Indeed, previous studies have noted that a proportion of adventitial Sca-1 population were derived from vSMCs and enrich for this mark *in vitro* (Majesky et al., 2017). Hence, isolated mAA-vSCs cells were interrogated by ChIP for the presence of the SMC signature H3K4me2 at the SM-MHC. Our results indicate that isolated mAA-vSCs do not enrich for this epigenetic mark H3K4me2 when compared to aortic tissue and mouse smooth muscle cells (mSMCs) in culture suggesting that these cells are not de-differentiated SMC, or a stem cell-like cell derived from mature SMCs. In support of this conclusion, the demethylase enzyme TET-2, which is predominantly enriched in smooth muscle tissue and associated with gene activation (Liu et al., 2013), was not present at the SM-MHC locus in these vascular stem cells compared to the aortic tissue and cultured mSMCs. Nevertheless, the epigenetic modification H3K27me3 typically present in embryonic stem cells and associated with transcriptional repression (Juan et al., 2016) was

enriched at the SM-MHC gene locus in isolated mAA-vSCs reaffirming their stemness.

Collectively, these data suggest that isolated vascular stem cells from both athero-prone (aortic arch) and athero-resistant (thoracic aorta) regions of the aortic wall possessed a common neuroectodermal origin and most importantly, they did not originate from resident differentiated vascular SMCs. We further hypothesised that these cells are a unique stem cell population resident within the aortic wall which becomes activated under different pathological conditions. To address this question, the myogenic responsiveness of mAA-vSCs and mTA-vSCs to the same inductive stimuli their level of responsiveness was assessed.

6.3 Jagged1-activated Notch signaling directly mediates SMC differentiation in vascular stem cells

Cell fate mapping studies have provided compelling evidence for the involvement of 'reprogrammed' de-differentiated SMC resident stem cell-derived progeny and SMCs derived from endothelial-mesenchymal-transition in progressing subclinical atherosclerosis (Chappell et al., 2016; Yuan et al., 2017; Kramann et al., 2016), yet the factors that dictate phenotypic changes, reprogramming and/or differentiation of these discrete cell populations and their progeny remain unknown.

Genetic predetermination of arterial vessels during development occurs through the pleiotropic signalling pathways (Lawson et al., 2002). Previous studies using murine injury models have shown that different signalling pathways such as Transforming Growth Factor-β (TGF-β), Notch, Hedgehog (Hh) and Wnt/β-catenin signalling played an important role in smooth muscle cell (SMC) recruitment and proliferation during vascular remodelling and repair. TGF-β signalling is a versatile pathway that exerts a pleiotropic effect on the cells. In human vascular smooth muscles (SMCs) activation of TGF-β signalling induces a contractile phenotype in these cells (Massagué, 2012; Pardali, Goumans and Dijke, 2010). *In vivo,* TGF-β signalling induces proliferation and migration of SMCs to complete vessel assembly and thus the stabilisation of the newly formed vasculature. Depletion of TGF-β R2 are lethal due to

the improper interaction between endothelial cells and smooth muscle cells causing the formation of immature vessels (Massagué, 2012; Pardali, Goumans and Dijke, 2010). On the other hand, Notch signalling is recapitulated in neointimal lesions following carotid-ligated animals since the expression of various Notch components are exaggerated, including Notch 1 and 3, Jagged1 and Notch target genes (Hrt 1 and 2) (Redmond et al., 2014).

Under normal homeostasis, Notch and Hh signalling are relatively silent but can become reactivated during regeneration (Morrow, Cullen, Cahill and Redmond, 2008a; Morrow et al., 2009; Mooney et al., 2015). Mutations of components of these pathways exhibit important vascular pathologies, e.g. NOTCH3 [cerebral autosomal dominant arteriopathy with subcortical infarcts and leukoencephelopathy (CADASIL) (Coupland, Lendahl and Karlström, 2018)], JAG/NOTCH2 [Alagille Syndrome (Hakimjavadi et al., 2017) and hedgehog interacting protein-like 1 (HHIPL1) [Atherosclerosis] (Aravani et al., 2016). During arterial specification, the majority of Notch1 signalling is silent until after flow begins (Jahnsen et al., 2015). In adult cells, flow promotes intracellular clustering of the Notch ligand, JAG1 and enhances the signalling potential of endothelial cells while DII4 expression decreases (Driessen et al., 2018). Similarly, Sonic, Indian and Desert (Shh, Ihh and Dhh) hedgehogs are released with lipid modifications that underlie their dispersion range and signalling function in response to flow (Walshe et al., 2011) (Hall et al., 2019).

Given these findings, isolated vascular stem cells from aortic arch (mAA-vSCs) and thoracic aorta (mTA-vSCs) were treated with TGF-β1 or Jagged1/Notch and their myogenic differentiation capacity assessed by determining the expression of SMC differentiation markers. The vSCs underwent myogenic differentiation towards the SMC phenotype; however, unlike the TGF-β1treated cells, Jagged1-activated Notch signalling was sufficient to drive the expression of the SMC mature marker SM-MHC in treated vSCs. Additionally, when the myogenic responsiveness levels of both cell types are compared, it was evident that these cells did not qualitatively differ from each other in the way they responded to myogenic inductive stimuli.

The TGF-β1 signalling pathway also controls many processes that are regulated by Notch signalling. Therefore, cross-talk experiments between TGF-β1 and Jagged1-activated Notch signalling was performed on mAA-vSCs. The data suggest that

Jagged1 was required by TGF-β1 to induce myogenic differentiation of vSCs in vitro since TGF-β1 stimulated Jag1 mRNA levels after 24h. Moreover, upon Jagged1/Notch inhibition, TGF-β1-induced myogenic differentiation was attenuated. Surprisingly, Jagged1-treated cells pre-treated with a TGF-β1 inhibitor significantly increased the level of the mature SMC maker (SM-MHC) implying a negative regulatory effect of TGF-β1 on Notch signalling. The interaction between Notch and the TGF-β ligands has been reported before in the literature; however, the outcomes and the mechanisms involved during their interaction is dependent on the cellular content and conditions (Luo, 2017). For instance, Smad3, a component of the TGF-β1 signalling pathway, associated with notch intracellular domain (NICD) synergistically enhanced the transcriptional activation of Notch target genes. In other cases, the Smad3-NICD complex antagonised each other to regulate the regenerative competence of stem cells. While active Smad3 (phosphorylated-Smad3) inhibited the proliferation and differentiation of stem cells by the upregulation of cyclin-dependent kinase (CDK) inhibitors, Notch attenuates this effect by sequestering p-Smad3 from their promoter regions (Luo, 2017; Carlson, Hsu and Conboy, 2008). Although, the precise interactions between the TGF-β1 and Jagged1/Notch signalling in isolated vascular stem cells remains unknown, our results may suggest that TGF-β1 attenuated the myogenic effect of Jagged1-activated Notch, in order to control excessive proliferation and differentiation of these SMC progenitors since Jagged1 was the only stimulus driving vSCs to mature SMCs differentiation.

The enrichment of the SMC epigenetic histone mark, H3K4me2 at the SM-MHC promoter by Jagged1 treatment in mAA-vSCs confirmed that Notch promotes SMC specification in these resident vascular stem cells. Concomitantly, the levels of H3K27me3 at the SM-MHC promoter decreased to levels lower than cultured SMC and similar to the aortic sample. Unexpectedly, the levels of TET-2 binding did not significantly change at the same SM-MHC gene locus. Perhaps, the role of TET-2 in murine vascular SCs is not as pronounced as previously reported in human coronary artery SMCs (Liu, Leslie and Martin, 2015; Liu et al., 2013).

Collectively, the data strongly suggested a direct role of Jagged1-activated Notch signalling in the myogenic differentiation of S100β vascular stem cells *in vitro* and further suggests that these cells may be the direct target for local knockdown of Notch1

receptors *in situ* using siRNA's (Redmond et al., 2014) thereby decreasing the accumulation of lesional cells contributing to intimal thickening during arteriosclerosis. Further work is required to confirm this hypothesis using S100β specific Notch1 Floxed mice to knockout Notch1 receptors on these vSC cells. This work is now ongoing.

The role of Wnt4 (Hua et al., 2014; Tsaousi et al., 2011) and Sonic hedgehog (Shh) (Fitzpatrick et al., 2017; Redmond et al., 2013) in vascular remodelling has been demonstrated in several *in vivo* studies using different injury models of neointima hyperplasia such as balloon-wired and complete/partial ligation of the carotid arteries (Mooney et al., 2015). Additionally, *in vitro* studies on smooth muscle cells showed increased cell proliferation and survival upon Wnt or Shh treatment (Ezan et al., 2004; Morrow et al., 2009). The failure of Wnt4 and Shh ligands to promote myogenic differentiation of mAA-vSCs (Chapter 5) may suggest that the degree of stemness of a cell may influence its response under certain conditions. In this context, a pathway may exist whereby vSCs become mesenchymal stem cell (MSC)-like before transitioning into smooth muscle cells (Tang et al., 2012). Therefore, our results may imply that for Wnt4 and Shh ligands to promote myogenic differentiation of vSCs, these cells may have to first transition to an intermediate cell or a mesenchymal-like cell.

Although the clinical implications of these results are under investigation, several important conclusions can be drawn. Firstly, there exists a perivascular location for a presumptive S100β/Sca1^{+} stem cell population that is distinct from the Sca1 cells derived from SMCs, previously reported (Majesky et al., 2017) within the adventitia of larger normal adult vessels, and importantly, concentrated around a 'high' susceptibility region for vascular disease (arch, ascending aorta). Secondly, purified adventitial S100β/Sca1^{+} cells in culture possess the expected myogenic differentiation capacity of bona fide stem cells and undergo myogenic differentiation upon Notch and TGF-β1 activation *in vitro.* Thirdly, and importantly, these S100β/Sca1^{+} cells directly contribute to intimal thickening and support the existence of a ''niche'' of Notch-responsive plastic vascular progenitor cells in addition to Gli-responsive progenitors (Kramann et al., 2015). Moreover, targeting these cells *in vivo* using Notch inhibitors may be responsible for the significant attenuation of intimal thickening following

Notch1 knockdown (Redmond et al., 2014). Indeed, the numerous phenotypes reported within advanced arteriosclerotic and atherosclerotic lesions may represent the different stages of stem cell-mediated myogenic, osteogenic, vasculogenic and myeloid differentiation (Zhang et al., 2018). Therefore, regulating both the differentiation and renewal capacity of these S100β/Sca1^{+} cell population(s) may represent a novel approach to modulate intimal thickening in humans.

Future Work

The Tamoxifen issue and the likelihood that tamoxifen is still present in the tissue marking cells that acquire the expression of the promoter that drives the Cre enzyme can no longer be neglected. While extending the tamoxifen elimination period will definitely lead to improve fidelity of results, ideally a tamoxifen administration scheme as conducted by Valny *et al.* should be performed in order to standardise the method and also make the data across different research groups more comparable. Objectives should include defining the correct degradation time of tamoxifen and metabolites while also maximising cre recombination levels in the specific tissue under study. In addition, the strain and age of the animal and the corresponding effects should be considered (Valny et al., 2016).

We and others have shown that the Notch signalling pathway is recapitulated in lesions during medial-intimal thickening after injury and that inhibition of Notch 1 significantly reduced lesion formation. Moreover, Notch signalling was shown to become activated in human vascular endothelial cells (HUVECs) when exposed to physiological levels of cyclic strain (Morrow et al., 2010; Redmond et al., 2014; Morrow et al., 2007a; 2009). Endothelial cell (EC) injury is a key element in the complex pathophysiology of atherogenesis and triggers the release of EC-derived extracellular vesicles (EVs). Since endothelial cells modulate the proliferation state of vSMC during pathophysiological conditions, we speculate that Notch ligands may be released in EVs for cell-cell communication (Jansen, Li, Pfeifer and Werner, 2017). Therefore, we propose to investigate the presence of the Notch ligand Jagged1 in exosomes by performing the following experiments: 1) Flow cytometry analysis – to evaluate the co-localisation of Jagged1 with endothelial EV markers (CD62E and CD144, CD31, CD54, CD105, CD146), will be determined with PE-conjugated antibodies. 2) Flow Cytometry, Immunocytochemistry and real time RT-qPCR to determine the myogenic differentiation of murine vSCs when exposed to isolated EVs from mouse endothelial cells. 3) Validate these findings in human *in vitro* models using human iPS-derived neuroectodermal cell progenitors and human vascular endothelial cells (HUVECs).

Our data suggests that neither Wnt4 nor Shh are potent inducers of myogenic

differentiation on their own; however, they may be active in the presence of other inducers like TGF-β1 or Notch ligands. We know that KO of either pathways ameliorates intimal medial thickening (Morrow et al., 2010; b; a; Redmond et al., 2014), therefore we propose to investigate the interaction of these morphogens with TGFb1 and Jagged1/Notch signalling in mouse vSCs by performing the following experiments: Loss-and-gain-of-function strategies to manipulate Notch and TGF-β1 signalling in combination with Wnt4 and Shh includes recombination ligands/proteins and ectopic expression of the Notch1 intracellular domain (NCID) with pharmacological inhibitors of Notch (DAPT and Compound E), TGF-β1 (SB431542), Wnt4 (Calbiochem) and Shh (Cyclopamine). Additionally, siRNA depletion experiments can be carried out in vSCs following Jagged1 and TGF-β1 treatment to study cross-talk effects between pathways. For instance, siRNA against specific receptors of Wnt4 (e.g.: Frizddle1) and Shh (e.g.: Pach1 and Smoothened) may be used in vSCs treated with Jagged1 and TGFb1. Initially, real time RT-qPCR could be performed to evaluate transcriptional changes. ChIP analysis of the SMC specification genetic mark H3K4me2 and the embryonic stem cell mark H3K27me3 on the SM-MHC promoter can be analysed in Wnt4 and Shh treated cells in order to investigate if these morphogens induce changes in the chromatin and thus preparing the cell for differentiation.

The importance of cell modulation in dictating cell plasticity (cell proliferation, migration and differentiation) has become of great importance especially during disease (Lin et al., 2018). We and others have shown that stem cells resident of the vessel wall can adopt a SMC phenotype typically of cells comprising arteriosclerotic lesions such as neointima hyperplasia. Moreover, various pathways such as Notch, TGFβ, Hh and Wnt have been shown to recapitulate during arteriosclerosis *in vivo* resulting in neointima formation and vascular remodelling. However, these lesions were attenuated with the administration of an appropriate inhibitor. Therefore, a better understanding on how these factors/pathways regulate cell fate through cell modulation will impact on the way cardiovascular diseases are treated, potentially developing the next-generation therapeutics.

Bibliography

Abe, T. and Fujimori, T., 2013. Reporter Mouse Lines for Fluorescence Imaging. *Development, Growth & Differentiation*, 55(4), pp.390–405.

Ackers, I. and Malgor, R., 2018. Interrelationship of canonical and non-canonical Wnt signalling pathways in chronic metabolic diseases. *Diabetes & vascular disease research*, 15(1), pp.3–13.

Albarrán-Juárez, J., Kaur, H., Grimm, M., Offermanns, S. and Wettschureck, N., 2016. Lineage tracing of cells involved in atherosclerosis. *Atherosclerosis*, 251, pp.445–453.

Aoki, Y. and De Gregorio, J., 2018. Optimal Approach for Treating In-Stent Restenosis. *Cardiac Interventions Today*, 12, pp.49–52.

Aravani, D., Karamanavi, E., Andrews, S.L., Samani, N.J., Stringer, E.J., and Webb, T.R. 2016. A The Coronary Artery Disease Associated Gene HHIPL1 Promotes Atherosclerosis. *Heart* 102, A145–A146.

Bargehr, J., Low, L., Cheung, C., Bernard, W.G., Iyer, D., Bennett, M.R., Gambardella, L. and Sinha, S., 2016. Embryological Origin of Human Smooth Muscle Cells Influences Their Ability to Support Endothelial Network Formation. *Stem cells translational medicine*, 5(7), pp.946–959.

Beckers, L., Heeneman, S., Wang, L., Burkly, L.C., Rousch, M.M.J., Davidson, N.O., Gijbels, M.J.J., de Winther, M.P.J., Daemen, M.J.A.P. and Lutgens, E., 2007. Disruption of hedgehog signalling in ApoE - /- mice reduces plasma lipid levels, but increases atherosclerosis due to enhanced lipid uptake by macrophages. *The Journal of pathology*, 212(4), pp.420–428.

Bellosta, S., Mahley, R.W., Sanan, D.A., Murata, J., Newland, D.L., Taylor, J.M. and Pitas, R.E., 1995. Macrophage-specific expression of human apolipoprotein E reduces atherosclerosis in hypercholesterolemic apolipoprotein E-null mice. *Journal of Clinical Investigation*, 96(5), pp.2170–2179.

Benjamin, E.J., Muntner, P., Alonso, A., Bittencourt, M.S., Callaway, C.W., Carson, A.P., Chamberlain, A.M., Chang, A.R., Cheng, S., Das, S.R., et al. 2019. Heart Disease and Stroke Statistics—2019 Update: A Report From the American Heart Association. *Circulation 139*, e56–e66

Bennett, M.R., Sinha, S. and Owens, G.K., 2016. Vascular Smooth Muscle Cells in Atherosclerosis. *Circulation research*, 118(4), pp.692–702.

Bennett, M.R., Sinha, S., Owens, G.K., Libby, P., Bornfeldt, K.E., and Tall, A.R. (2016). Atherosclerosis Compendium Vascular Smooth Muscle Cells in Atherosclerosis. *Circ. Res.* 118:, 692–702.

Boucher, J.M., Peterson, S.M., Urs, S., Zhang, C. and Liaw, L., 2011. The miR-143/145 cluster is a novel transcriptional target of Jagged-1/Notch signaling in vascular smooth muscle cells. *The Journal of biological chemistry*, 286(32), pp.28312–28321.

Bray, S.J., 2016. Notch signalling in context. *Nature reviews. Molecular cell biology*, 17(11), pp.722–735.

Breckenridge, R.A., 2013. Animal Models of Myocardial Disease. In: *Animal Models for the Study of Human Disease*. Elsevier, pp.145–171.

Briscoe, J. and Thérond, P.P., 2013. The mechanisms of Hedgehog signalling and its roles in development and disease. *Nature reviews. Molecular cell biology*, 14(7), pp.416–429.

Campbell, G.R., Chamley-Campbell, J., Gröschel-Stewart, U., Small, J.V. and Anderson, P., 1979. Antibody staining of 10-nm (100-A) filaments in cultured smooth, cardiac and skeletal muscle cells. *Journal of cell science*, 37, pp.303–322.

CARDIoGRAMplusC4D Consortium, Deloukas, P., Kanoni, S., Willenborg, C., Farrall, M., Assimes, T.L., Thompson, J.R., Ingelsson, E., Saleheen, D., Erdmann, J., Goldstein, B.A., Stirrups, K., König, I.R., Cazier, J.-B., Johansson, A., Hall, A.S., Lee, J.-Y., Willer, C.J., Chambers, J.C., Esko, T., Folkersen, L., Goel, A., Grundberg, E., Havulinna, A.S., Ho, W.K., Hopewell, J.C., Eriksson, N., Kleber, M.E., Kristiansson, K., Lundmark, P., Lyytikäinen, L.-P., Rafelt, S., Shungin, D., Strawbridge, R.J., Thorleifsson, G., Tikkanen, E., Van Zuydam, N., Voight, B.F., Waite, L.L., Zhang, W., Ziegler, A., Absher, D., Altshuler, D., Balmforth, A.J., Barroso, I., Braund, P.S., Burgdorf, C., Claudi-Boehm, S., Cox, D., Dimitriou, M., Do, R., DIAGRAM Consortium, CARDIOGENICS Consortium, Doney, A.S.F., Mokhtari, El, N., Eriksson, P., Fischer, K., Fontanillas, P., Franco-Cereceda, A., Gigante, B., Groop, L., Gustafsson, S., Hager, J., Hallmans, G., Han, B.-G., Hunt, S.E., Kang, H.M., Illig, T., Kessler, T., Knowles, J.W., Kolovou, G., Kuusisto, J., Langenberg, C., Langford, C., Leander, K., Lokki, M.-L., Lundmark, A., McCarthy, M.I., Meisinger, C., Melander, O., Mihailov, E., Maouche, S., Morris, A.D., Müller-Nurasyid, M., MuTHER Consortium, Nikus, K., Peden, J.F., Rayner, N.W., Rasheed, A., Rosinger, S., Rubin, D., Rumpf, M.P., Schäfer, A., Sivananthan, M., Song, C., Stewart, A.F.R., Tan, S.-T., Thorgeirsson, G., van der Schoot, C.E., Wagner, P.J., Wellcome Trust Case Control Consortium, Wells, G.A., Wild, P.S., Yang, T.-P., Amouyel, P., Arveiler, D., Basart, H., Boehnke, M., Boerwinkle, E., Brambilla, P., Cambien, F., Cupples, A.L., de Faire, U., Dehghan, A., Diemert, P., Epstein, S.E., Evans, A., Ferrario, M.M., Ferrières, J., Gauguier, D., Go, A.S., Goodall, A.H., Gudnason, V., Hazen, S.L., Holm, H., Iribarren, C., Jang, Y., Kähönen, M., Kee, F., Kim, H.-S., Klopp, N., Koenig, W., Kratzer, W., Kuulasmaa, K., Laakso, M., Laaksonen, R., Lee, J.-Y., Lind, L., Ouwehand, W.H., Parish, S., Park, J.E., Pedersen, N.L., Peters, A., Quertermous, T., Rader, D.J., Salomaa, V., Schadt, E., Shah, S.H., Sinisalo, J., Stark, K., Stefansson, K., Trégouët, D.-A., Virtamo, J., Wallentin, L., Wareham, N., Zimmermann, M.E., Nieminen, M.S., Hengstenberg, C., Sandhu, M.S., Pastinen, T., Syvänen, A.-C., Hovingh, G.K., Dedoussis, G., Franks, P.W., Lehtimäki, T., Metspalu, A., Zalloua, P.A., Siegbahn, A., Schreiber, S., Ripatti, S., Blankenberg, S.S., Perola, M., Clarke, R., Boehm, B.O., O'Donnell, C., Reilly, M.P., März, W., Collins, R., Kathiresan, S., Hamsten, A., Kooner, J.S., Thorsteinsdottir, U., Danesh, J., Palmer, C.N.A., Roberts, R., Watkins, H., Schunkert, H. and Samani, N.J., 2013. Large-scale association analysis identifies new risk loci for coronary artery disease. *Nature genetics*, 45(1), pp.25–33.

Carlson, M.E., Hsu, M. and Conboy, I.M., 2008. Imbalance between pSmad3 and Notch induces CDK inhibitors in old muscle stem cells. *Nature*, 454(7203), pp.528–532.

Chamley-Campbell, J., Campbell, G.R. and Ross, R., 1979. The smooth muscle cell in culture. *Physiological reviews*, 59(1), pp.1–61.

Chappell, J., Harman, J.L., Narasimhan, V.M., Yu, H., Foote, K., Simons, B.D., Bennett, M.R. and Jørgensen, H.F., 2016. Extensive Proliferation of a Subset of Differentiated, yet Plastic, Medial Vascular Smooth Muscle Cells Contributes to Neointimal Formation in Mouse Injury and Atherosclerosis Models. *Circulation research*, 119(12), pp.1313–1323.

Chen, L., Shannon, R.P. and Shen, Y.-T., 2013. Animal Models for Cardiovascular Research. In: *Animal Models for the Study of Human Disease*. Elsevier, pp.173–194.

Chen, Q., Yang, M., Wu, H., Zhou, J., Wang, W., Zhang, H., Zhao, L., Zhu, J., Zhou, B., Xu, Q. and Zhang, L., 2018. Genetic lineage tracing analysis of c-kit+ stem/progenitor cells revealed a contribution to vascular injury-induced neointimal lesions. *Journal of Molecular and Cellular Cardiology*, 121, pp.277–286.

Cheung, C., Bernardo, A.S., Pedersen, R.A. and Sinha, S., 2014. Directed differentiation of embryonic origin-specific vascular smooth muscle subtypes from human pluripotent stem cells. *Nature protocols*, 9(4), pp.929–938.

Cheung, C., Bernardo, A.S., Trotter, M.W.B., Pedersen, R.A. and Sinha, S., 2012. Generation of human vascular smooth muscle subtypes provides insight into embryological origin-dependent disease susceptibility. *Nature biotechnology*, 30(2), pp.165–173.

Chorro, F.J., Such-Belenguer, L. and López-Merino, V., 2009. Animal Models of Cardiovascular Disease. *Revista Española de Cardiología (English Edition)*, 62(1), pp.69–84.

Choudhry, Z., Rikani, A.A., Choudhry, A.M., Tariq, S., Zakaria, F., Asghar, M.W., Sarfraz, M.K., Haider, K., Shafiq, A.A. and Mobassarah, N.J., 2014. Sonic hedgehog signalling pathway: a complex network. *Annals of neurosciences*, 21(1), pp.28–31.

Chung, I.M., Schwartz, S.M. and Murry, C.E., 1998. Clonal architecture of normal and atherosclerotic aorta: implications for atherogenesis and vascular development. *The American journal of pathology*, 152(4), pp.913–923.

Colombo, A., Guha, S., Mackle, J.N., Cahill, P.A. and Lally, C., 2013. Cyclic strain amplitude dictates the growth response of vascular smooth muscle cells in vitro: role in in-stent restenosis and inhibition with a sirolimus drug-eluting stent. *Biomechanics and modeling in mechanobiology*, 12(4), pp.671–683.

Cooley, B.C., 2004. Murine model of neointimal formation and stenosis in vein grafts. *Arteriosclerosis, Thrombosis, and Vascular Biology*, 24(7), pp.1180–1185.

Cooley, B.C., 2005. Model of murine interpositional vein grafting. *Microsurgery*, 25(3), pp.209–212.

Cooley, B.C., Nevado, J., Mellad, J., Yang, D., St Hilaire, C., Negro, A., Fang, F., Chen, G., San, H., Walts, A.D., Schwartzbeck, R.L., Taylor, B., Lanzer, J.D., Wragg, A., Elagha, A., Beltran, L.E., Berry, C., Feil, R., Virmani, R., Ladich, E., Kovacic, J.C. and Boehm, M., 2014. TGF- Signaling Mediates Endothelial-to-Mesenchymal Transition (EndMT) During Vein Graft Remodeling. *Science Translational Medicine*, 6(227), pp.227ra34–227ra34.

Corjay, M.H., Blank, R.S. and Owens, G.K., 1990. Platelet-derived growth factor-induced destabilization of smooth muscle alpha-actin mRNA. *Journal of cellular physiology*, 145(3), pp.391–397.

Corjay, M.H., Thompson, M.M., Lynch, K.R. and Owens, G.K., 1989. Differential effect of platelet-derived growth factor- versus serum-induced growth on smooth muscle alpha-actin and nonmuscle beta-actin mRNA expression in cultured rat aortic smooth muscle cells. *The Journal of biological chemistry*, 264(18), pp.10501–10506.

Coupland, K., Lendahl, U. and Karlström, H., 2018. Role of NOTCH3 Mutations in the Cerebral Small Vessel Disease Cerebral Autosomal Dominant Arteriopathy With Subcortical Infarcts and Leukoencephalopathy. *Stroke*, 49(11), pp.2793–2800.

Cunningham, K.S. and Gotlieb, A.I., 2005. The role of shear stress in the pathogenesis of atherosclerosis. *Laboratory investigation; a journal of technical methods and pathology*, 85(1), pp.9–23.

Daniel, J.-M. and Sedding, D.G., 2011. Circulating smooth muscle progenitor cells in arterial remodeling. *Journal of Molecular and Cellular Cardiology*, 50(2), pp.273–279.

DeBakey, M.E. and Glaeser, D.H., 2000. Patterns of atherosclerosis: effect of risk factors on recurrence and survival-analysis of 11,890 cases with more than 25-year follow-up. *The American Journal of Cardiology*, 85(9), pp.1045–1053.

DeBakey, M.E., Lawrie, G.M., and Glaeser, D.H. (1985). Patterns of atherosclerosis and their surgical significance. *Ann. Surg*. 201, 115–131.

Demeter, K., Zádori, A., Agoston, V.A. and Madarász, E., 2005. Studies on the use of NE-4C embryonic neuroectodermal stem cells for targeting brain tumour. *Neuroscience research*, 53(3), pp.331–342.

Derynck, R. and Zhang, Y.E., 2003. Smad-dependent and Smad-independent pathways in TGF-beta family signalling. *Nature*, 425(6958), pp.577–584.

Doevendans, P.A., Daemen, M.J., de Muinck, E.D. and Smits, J.F., 1998. Cardiovascular phenotyping in mice. *Cardiovascular Research*, 39, pp.34–49.

Doi, H., Iso, T., Sato, H., Yamazaki, M., Matsui, H., Tanaka, T., Manabe, I., Arai, M., Nagai, R. and Kurabayashi, M., 2006. Jagged1-selective notch signaling induces smooth muscle differentiation via a RBP-Jkappa-dependent pathway. *The Journal of biological chemistry*, 281(39), pp.28555–28564.

Driessen, R.C.H., Stassen, O.M.J.A., Sjöqvist, M., Suarez Rodriguez, F., Grolleman, J., Bouten, C.V.C. and Sahlgren, C.M., 2018. Shear stress induces expression,

intracellular reorganization and enhanced Notch activation potential of Jagged1. *Integrative biology : quantitative biosciences from nano to macro*, 10(11), pp.719–726.

Dutzmann, J., Koch, A., Weisheit, S., Sonnenschein, K., Korte, L., Haertlé, M., Thum, T., Bauersachs, J., Sedding, D.G. and Daniel, J.-M., 2017. Sonic hedgehog-dependent activation of adventitial fibroblasts promotes neointima formation. *Cardiovascular Research*, 113(13), pp.1653–1663.

Ezan, J., Leroux, L., Barandon, L., Dufourcq, P., Jaspard, B., Moreau, C., Allières, C., Daret, D., Couffinhal, T. and Duplàa, C., 2004. FrzA/sFRP-1, a secreted antagonist of the Wnt-Frizzled pathway, controls vascular cell proliferation in vitro and in vivo. *Cardiovascular Research*, 63(4), pp.731–738.

Farese, R.V., Véniant, M.M., Cham, C.M., Flynn, L.M., Pierotti, V., Loring, J.F., Traber, M., Ruland, S., Stokowski, R.S., Huszar, D. and Young, S.G., 1996. Phenotypic analysis of mice expressing exclusively apolipoprotein B48 or apolipoprotein B100. *Proceedings of the National Academy of Sciences*, 93(13), pp.6393–6398.

Farooq, V., Gogas, B.D. and Serruys, P.W., 2011. Restenosis: delineating the numerous causes of drug-eluting stent restenosis. *Circulation. Cardiovascular interventions*, 4(2), pp.195–205.

Fishbein, M.C. and Fishbein, G.A., 2015. Arteriosclerosis: facts and fancy. *Cardiovascular pathology: the official journal of the Society for Cardiovascular Pathology*, 24(6), pp.335–342.

Fitzpatrick, E., Han, X., Liu, W., Corcoran, E., Burtenshaw, D., Morrow, D., Helt, J.-C., Cahill, P.A. and Redmond, E.M., 2017. Alcohol Reduces Arterial Remodeling by Inhibiting Sonic Hedgehog-Stimulated Stem Cell Antigen-1 Positive Progenitor Stem Cell Expansion. *Alcoholism, clinical and experimental research*, 41(12), pp.2051–2065.

Freeman, S., 2011. *Biological Science*. 4th edn. Place of publication: Pearson.

Fuster, J.J., Castillo, A.I., Zaragoza, C., Ibáñez, B. and Andrés, V., 2012. Animal models of atherosclerosis. *Progress in molecular biology and translational science*, 105, pp.1–23.

Galkina, E. and Ley, K., 2009. Immune and inflammatory mechanisms of atherosclerosis (*). *Annual review of immunology*, 27(1), pp.165–197.

Gammill, L.S. and Bronner-Fraser, M., 2003. Neural crest specification: migrating into genomics. *Nature reviews. Neuroscience*, 4(10), pp.795–805.

Gaydos, L.J., Wang, W., and Strome, S. (2014). H3K27me and PRC2 transmit a memory of repression across generations and during development. *Science* (80-.). 345, 1515–1518.

Getz, G.S. and Reardon, C.A., 2006. Diet and murine atherosclerosis. *Arteriosclerosis, Thrombosis, and Vascular Biology*, 26(2), pp.242–249.

Giustino, G., Baber, U., Sartori, S., Mehran, R., Mastoris, I., Kini, A.S., Sharma, S.K., Pocock, S.J. and Dangas, G.D., 2015. Duration of dual antiplatelet therapy after drug-eluting stent implantation: a systematic review and meta-analysis of randomized controlled trials. *Journal of the American College of Cardiology*, 65(13), pp.1298–1310.

Gomez, D., Shankman, L.S., Nguyen, A.T. and Owens, G.K., 2013. Detection of histone modifications at specific gene loci in single cells in histological sections. *Nature Methods*, 10(2), pp.171–177.

Gomez, D., Shankman, L.S., Nguyen, A.T., and Owens, G.K. (2013). Detection of histone modifications at specific gene loci in single cells in histological sections. *Nat. Methods* 10, 171–177.

Gomez, D., Swiatlowska, P. and Owens, G.K., 2015. Epigenetic Control of Smooth Muscle Cell Identity and Lineage Memory. *Arteriosclerosis, Thrombosis, and Vascular Biology*, 35(12), pp.2508–2516.

Gridley, T., 2007. Notch signaling in vascular development and physiology. *Development*, 134(15), pp.2709–2718.

Haimovici, H. (1991). The role of arterial tissue susceptibility in atherogenesis. *Texas Hear. Inst.* J. 18, 81–83.

Haimovici H. and Maier R, N., 1964. Fate of aortic homografts in canine atherosclerosis. 3. Study of fresh abdominal and thoracic aortic implants into thoracic aorta: role of tissue susceptibility in atherogenesis. *Archives of surgery (Chicago, Ill. : 1960)*, 89, pp.961–969.

Hakimjavadi, R., Olayinka, A., Luca, M. Di, Guha, S., Walls, D., Redmond, E.M., and Cahill, P.A. (2017). Pathogenetic Mechanisms in Alagille Syndrome. In ELS, (Chichester, UK: *John Wiley & Sons, Ltd*), pp. 1–10.

Hall, E.T., Cleverdon, E.R., and Ogden, S.K. (2019). Dispatching Sonic Hedgehog: Molecular Mechanisms Controlling Deployment. *Trends Cell Biol. (in press)*

Handy, D.E., Castro, R. and Loscalzo, J., 2011. Epigenetic modifications: basic mechanisms and role in cardiovascular disease. *Circulation*, 123(19), pp.2145–2156.

Hao, H., Gabbiani, G. and Bochaton-Piallat, M.-L., 2003. Arterial smooth muscle cell heterogeneity: implications for atherosclerosis and restenosis development. *Arteriosclerosis, Thrombosis, and Vascular Biology*, 23(9), pp.1510–1520.

Hasenfuss, G., 1998. Animal models of human cardiovascular disease, heart failure and hypertrophy. *Cardiovascular Research*, 39(1), pp.60–76.

Havrda, M.C., Johnson, M.J., O'Neill, C.F. and Liaw, L., 2006. A novel mechanism of transcriptional repression of p27kip1 through Notch/HRT2 signaling in vascular smooth muscle cells. *Thrombosis and haemostasis*, 96(3), pp.361–370.

Hellström, M., Kalén, M., Lindahl, P., Abramsson, A. and Betsholtz, C., 1999. Role of PDGF-B and PDGFR-beta in recruitment of vascular smooth muscle cells and pericytes during embryonic blood vessel formation in the mouse. *Development*, 126(14), pp.3047–3055.

Herring, B., Hoggatt, A.M., Burlak, C. and Offermanns, S., 2014. Previously differentiated medial vascular smooth muscle cells contribute to neointima formation following vascular injury. *Vascular Cell*, 6(1), p.21.

High, F.A., Zhang, M., Proweller, A., Tu, L., Parmacek, M.S., Pear, W.S. and Epstein, J.A., 2007. An essential role for Notch in neural crest during cardiovascular development and smooth muscle differentiation. *Journal of Clinical Investigation*, 117(2), pp.353–363.

Hirschi, K.K., Rohovsky, S.A. and D'Amore, P.A., 1998. PDGF, TGF-beta, and heterotypic cell-cell interactions mediate endothelial cell-induced recruitment of 10T1/2 cells and their differentiation to a smooth muscle fate. *The Journal of Cell Biology*, 141(3), pp.805–814.

Hoglund, V.J., Dong, X.R. and Majesky, M.W., 2010. Neointima formation: a local affair. *Arteriosclerosis, Thrombosis, and Vascular Biology*, 30(10), pp.1877–1879.

Hooper, J.E. and Scott, M.P., 2005. Communicating with Hedgehogs. *Nature reviews. Molecular cell biology*, 6(4), pp.306–317.

Hromada, C., Mühleder, S., Grillari, J., Redl, H. and Holnthoner, W., 2017. Endothelial Extracellular Vesicles-Promises and Challenges. *Frontiers in physiology*, 8, p.275.

Hu, Y., Zhang, Z., Torsney, E., Afzal, A.R., Davison, F., Metzler, B. and Xu, Q., 2004. Abundant progenitor cells in the adventitia contribute to atherosclerosis of vein grafts in ApoE-deficient mice. *Journal of Clinical Investigation*, 113(9), pp.1258–1265.

Hua, J., Xu, Y., He, Y., Jiang, X., Ye, W. and Pan, Z., 2014. Wnt4/β-catenin signaling pathway modulates balloon-injured carotid artery restenosis via disheveled-1. *International journal of clinical and experimental pathology*, 7(12), pp.8421–8431.

Huang, J. and Kalderon, D., 2014. Coupling of Hedgehog and Hippo pathways promotes stem cell maintenance by stimulating proliferation. *The Journal of Cell Biology*, 205(3), pp.325–338.

Indolfi, C., Mongiado, A., Curcio, A. and Torella, D., 2003. Molecular Mechanisms of In-Stent Restenosis and Approach to Therapy with Eluting Stents. *Trends Cardiovasc Med*, 13, pp.142–148.

Ingham, P.W. and McMahon, A.P., 2001. Hedgehog signaling in animal development: paradigms and principles. *Genes & development*, 15(23), pp.3059–3087.

Ishibashi, S., Brown, M.S., Goldstein, J.L., Gerard, R.D., Hammer, R.E. and Herz, J., 1993. Hypercholesterolemia in low density lipoprotein receptor knockout mice and its reversal by adenovirus-mediated gene delivery. *Journal of Clinical Investigation*, 92(2), pp.883–893.

Iso, T., Kedes, L. and Hamamori, Y., 2003. HES and HERP families: multiple effectors of the Notch signaling pathway. *Journal of cellular physiology*, 194(3), pp.237–255.

Jahnsen, E.D., Trindade, A., Zaun, H.C., Lehoux, S., Duarte, A. and Jones, E.A.V., 2015. Notch1 is pan-endothelial at the onset of flow and regulated by flow. *PloS one*, 10(4), p.e0122622.

Jain, R.K., 2003. Molecular regulation of vessel maturation. *Nature medicine*, 9(6), pp.685–693.

Jansen, F., Li, Q., Pfeifer, A. and Werner, N., 2017. Endothelial- and Immune Cell-Derived Extracellular Vesicles in the Regulation of Cardiovascular Health and Disease. *JACC. Basic to translational science*, 2(6), pp.790–807.

Jones, P.A. and Takai, D., 2001. The role of DNA methylation in mammalian epigenetics. *Science (New York, N.Y.)*, 293(5532), pp.1068–1070.

Juan, A.H., Wang, S., Ko, K.D., Zare, H., Tsai, P.-F., Feng, X., Vivanco, K.O., Ascoli, A.M., Gutierrez-Cruz, G., Krebs, J., Sidoli, S., Knight, A.L., Pedersen, R.A., Garcia, B.A., Casellas, R., Zou, J. and Sartorelli, V., 2016. Roles of H3K27me2 and H3K27me3 Examined during Fate Specification of Embryonic Stem Cells. *Cell reports*, 17(5), pp.1369–1382.

Kapustin, A.N., Chatrou, M.L.L., Drozdov, I., Zheng, Y., Davidson, S.M., Soong, D., Furmanik, M., Sanchis, P., De Rosales, R.T.M., Alvarez-Hernandez, D., Shroff, R., Yin, X., Muller, K., Skepper, J.N., Mayr, M., Reutelingsperger, C.P., Chester, A., Bertazzo, S., Schurgers, L.J. and Shanahan, C.M., 2015. Vascular smooth muscle cell calcification is mediated by regulated exosome secretion. *Circulation research*, 116(8), pp.1312–1323.

Kennedy, E., Mooney, C.J., Hakimjavadi, R., Fitzpatrick, E., Guha, S., Collins, L.E., Loscher, C.E., Morrow, D., Redmond, E.M. and Cahill, P.A., 2014. Adult vascular smooth muscle cells in culture express neural stem cell markers typical of resident multipotent vascular stem cells. *Cell and tissue research*, 358(1), pp.203–216.

Kinner, B., Zaleskas, J.M. and Spector, M., 2002. Regulation of smooth muscle actin expression and contraction in adult human mesenchymal stem cells. *Experimental cell research*, 278(1), pp.72–83.

Knoblich, J.A., 2008. Mechanisms of asymmetric stem cell division. *Cell*, 132(4), pp.583–597.

Konstantinov, I.E. and Jankovic, G.M., 2013. Alexander I. Ignatowski. *Texas Heart Institute Journal*, 40, pp.246–249.

Kopan, R. and Ilagan, M.X.G., 2009. The canonical Notch signaling pathway: unfolding the activation mechanism. *Cell*, 137(2), pp.216–233.

Korshunov, V.A. and Berk, B.C., 2003. Flow-induced vascular remodeling in the mouse: a model for carotid intima-media thickening. *Arteriosclerosis, Thrombosis, and Vascular Biology*, 23(12), pp.2185–2191.

Kramann, R., Goettsch, C., Wongboonsin, J., Iwata, H., Schneider, R.K., Kuppe, C., Kaesler, N., Chang-Panesso, M., Machado, F.G., Gratwohl, S., Madhurima, K., Hutcheson, J.D., Jain, S., Aikawa, E. and Humphreys, B.D., 2016. Adventitial MSC-like Cells Are Progenitors of Vascular Smooth Muscle Cells and Drive Vascular Calcification in Chronic Kidney Disease. *Cell stem cell*, 19(5), pp.628–642.

Kramann, R., Schneider, R.K., DiRocco, D.P., Machado, F., Fleig, S., Bondzie, P.A., Henderson, J.M., Ebert, B.L. and Humphreys, B.D., 2015. Perivascular Gli1+ progenitors are key contributors to injury-induced organ fibrosis. *Cell stem cell*, 16(1), pp.51–66.

Kumar, A. and Lindner, V., 1997. Remodeling With Neointima Formation in the Mouse Carotid Artery After Cessation of Blood Flow. *Arteriosclerosis, Thrombosis, and Vascular Biology*, 17(10), pp.2238–2244.

Kurpinski, K., Lam, H., Chu, J., Wang, A., Kim, A., Tsay, E., Agrawal, S., Schaffer, D.V. and Li, S., 2010. Transforming growth factor-beta and notch signaling mediate stem cell differentiation into smooth muscle cells. *Stem cells (Dayton, Ohio)*, 28(4), pp.734–742.

Lawson, N.D., Vogel, A.M., and Weinstein, B.M. (2002). Sonic hedgehog and vascular endothelial growth factor act upstream of the Notch pathway during arterial endothelial differentiation. *Dev. Cell* 3, 127–136

Li, G., Chen, S.-J., Oparil, S., Chen, Y.-F. and Thompson, J.A., 2000. Direct In Vivo Evidence Demonstrating Neointimal Migration of Adventitial Fibroblasts After Balloon Injury of Rat Carotid Arteries. *Circulation*, 101, pp.1362–1365.

Liao, J., Huang, W. and Liu, G., 2017. Animal models of coronary heart disease. *Journal of Biomedical Research*, pp.3–10.

Lin, B., Srikanth, P., Castle, A.C., Nigwekar, S., Malhotra, R., Galloway, J.L., Sykes, D.B. and Rajagopal, J., 2018. Modulating Cell Fate as a Therapeutic Strategy. *Cell stem cell*, 23(3), pp.329–341.

Lindner, V., Fingerle, J. and Reidy, M.A., 1993. Mouse model of arterial injury. *Circulation research*, 73(5), pp.792–796.

Liu W, Redmond EM, Morrow D, Cullen JP. 2011. Differential effects of daily-moderate versus weekend-binge alcohol consumption on atherosclerotic plaque development in mice. *Atherosclerosis* **219**:448–454.

Liu, R., Jin, Y., Tang, W.H., Qin, L., Zhang, X., Tellides, G., Hwa, J., Yu, J. and Martin, K.A., 2013. Ten-eleven translocation-2 (TET2) is a master regulator of smooth muscle cell plasticity. *Circulation*, 128(18), pp.2047–2057.

Liu, R., Leslie, K.L. and Martin, K.A., 2015. Epigenetic regulation of smooth muscle cell plasticity. *Biochimica et biophysica acta*, 1849(4), pp.448–453.

Livet, J., Weissman, T.A., Kang, H., Draft, R.W., Lu, J., Bennis, R.A., Sanes, J.R. and Lichtman, J.W., 2007. Transgenic strategies for combinatorial expression of fluorescent proteins in the nervous system. *Nature*, 450(7166), pp.56–62.

López-Sánchez, C. and García-Martínez, V., 2011. Molecular determinants of cardiac specification. *Cardiovascular Research*, 91(2), pp.185–195.

Luna, G., Paez, J. and Cardier, J.E., 2004. Expression of the hematopoietic stem cell antigen Sca-1 (LY-6A/E) in liver sinusoidal endothelial cells: possible function of Sca-1 in endothelial cells. *Stem cells and development*, 13(5), pp.528–535.

Luo, K., 2017. Signaling Cross Talk between TGF-β/Smad and Other Signaling Pathways. *Cold Spring Harbor perspectives in biology*, 9(1), p.a022137.

Majesky, M.W., 2003. Vascular smooth muscle diversity: insights from developmental biology. *Current atherosclerosis reports*, 5(3), pp.208–213.

Majesky, M.W., 2007. Developmental basis of vascular smooth muscle diversity. *Arteriosclerosis, Thrombosis, and Vascular Biology*, 27(6), pp.1248–1258.

Majesky, M.W., Horita, H., Ostriker, A., Lu, S., Regan, J.N., Bagchi, A., Dong, X.R., Poczobutt, J., Nemenoff, R.A. and Weiser-Evans, M.C.M., 2017. Differentiated Smooth Muscle Cells Generate a Subpopulation of Resident Vascular Progenitor Cells in the Adventitia Regulated by Klf4. *Circulation research*, 120(2), pp.296–311.

Massagué, J., 2012. TGFβ signalling in context. *Nature reviews. Molecular cell biology*, 13(10), pp.616–630.

McDonald, O.G., Wamhoff, B.R., Hoofnagle, M.H. and Owens, G.K., 2006. Control of SRF binding to CArG box chromatin regulates smooth muscle gene expression in vivo. *Journal of Clinical Investigation*, 116(1), pp.36–48.

MD, K.D.B., MPH, R.T., PhD, T.R.M., PhD, L.X., MSPH, J.G., MD, I.B.-D., MD, W.O.S., MD, L.F.S. and MD, R.W., 2018. In-Stent Restenosis of Drug-Eluting Stents Compared With a Matched Group of Patients With De Novo Coronary Artery Stenosis. *The American Journal of Cardiology*, 121(12), pp.1512–1518.

Metzger, D. and Chambon, P., 2001. Site- and Time-Specific Gene Targeting in the Mouse. *Methods*, 24(1), pp.71–80.

Mooney, C.J., Hakimjavadi, R., Fitzpatrick, E., Kennedy, E., Walls, D., Morrow, D., Redmond, E.M. and Cahill, P.A., 2015. Hedgehog and Resident Vascular Stem Cell Fate. *Stem cells international*, 2015(6), pp.468428–16.

Morrison, S.J. and Kimble, J., 2006. Asymmetric and symmetric stem-cell divisions in development and cancer. *Nature*, 441(7097), pp.1068–1074.

Morrow, D., Cullen, J.P., Cahill, P.A. and Redmond, E.M., 2007a. Cyclic strain regulates the Notch/CBF-1 signaling pathway in endothelial cells: role in angiogenic activity. *Arteriosclerosis, Thrombosis, and Vascular Biology*, 27(6), pp.1289–1296.

Morrow, D., Cullen, J.P., Cahill, P.A. and Redmond, E.M., 2008a. Ethanol stimulates endothelial cell angiogenic activity via a Notch- and angiopoietin-1-dependent pathway. *Cardiovascular Research*, 79(2), pp.313–321.

Morrow, D., Cullen, J.P., Liu, W., Cahill, P.A. and Redmond, E.M., 2010. Alcohol inhibits smooth muscle cell proliferation via regulation of the Notch signaling pathway. *Arteriosclerosis, Thrombosis, and Vascular Biology*, 30(12), pp.2597–2603.

Morrow, D., Cullen, J.P., Liu, W., Guha, S., Sweeney, C., Birney, Y.A., Collins, N., Walls, D., Redmond, E.M. and Cahill, P.A., 2009. Sonic Hedgehog induces Notch target gene expression in vascular smooth muscle cells via VEGF-A. *Arteriosclerosis, Thrombosis, and Vascular Biology*, 29(7), pp.1112–1118.

Morrow, D., Guha, S., Sweeney, C., Birney, Y., Walshe, T., O'Brien, C., Walls, D., Redmond, E.M. and Cahill, P.A., 2008b. Notch and vascular smooth muscle cell phenotype. *Circulation research*, 103(12), pp.1370–1382.

Morrow, D., Scheller, A., Birney, Y.A., Sweeney, C., Guha, S., Cummins, P.M., Murphy, R., Walls, D., Redmond, E.M. and Cahill, P.A., 2005a. Notch-mediated CBF-1/RBP-J{kappa}-dependent regulation of human vascular smooth muscle cell phenotype in vitro. *American journal of physiology. Cell physiology*, 289(5), pp.C1188–96.

Morrow, D., Sweeney, C., Birney, Y.A., Cummins, P.M., Walls, D., Redmond, E.M. and Cahill, P.A., 2005b. Cyclic strain inhibits Notch receptor signaling in vascular smooth muscle cells in vitro. *Circulation research*, 96(5), pp.567–575.

Morrow, D., Sweeney, C., Birney, Y.A., Guha, S., Collins, N., Cummins, P.M., Murphy, R., Walls, D., Redmond, E.M. and Cahill, P.A., 2007b. Biomechanical regulation of hedgehog signaling in vascular smooth muscle cells in vitro and in vivo. *American journal of physiology. Cell physiology*, 292(1), pp.C488–96.

Nakagawa, K., and Nakashima, Y. (2018). Pathologic intimal thickening in human atherosclerosis is formed by extracellular accumulation of plasma-derived lipids and dispersion of intimal smooth muscle cells. *Atherosclerosis* 274, 235–242.

Nemenoff, R.A., Horita, H., Ostriker, A.C., Furgeson, S.B., Simpson, P.A., VanPutten, V., Crossno, J., Offermanns, S. and Weiser-Evans, M.C.M., 2011. SDF-1α Induction in Mature Smooth Muscle Cells by Inactivation of PTEN Is a Critical Mediator of Exacerbated Injury-Induced Neointima Formation. *Arteriosclerosis, Thrombosis, and Vascular Biology*, 31(6), pp.1300–1308.

Newby, A.C. and Zaltsman, A.B., 2000. Molecular mechanisms in intimal hyperplasia. *The Journal of pathology*, 190(3), pp.300–309.

Nguyen, A.T., Gomez, D., Bell, R.D., Campbell, J.H., Clowes, A.W., Gabbiani, G., Giachelli, C.M., Parmacek, M.S., Raines, E.W., Rusch, N.J., Speer, M.Y., Sturek, M., Thyberg, J., Towler, D.A., Weiser-Evans, M.C., Yan, C., Miano, J.M. and Owens, G.K., 2013. Smooth muscle cell plasticity: fact or fiction? *Circulation research*, 112(1), pp.17–22.

Okabe, M., Ikawa, M., Kominami, K., Nakanishi, T. and Nishimune, Y., 1997. 'Green mice' as a source of ubiquitous green cells. *Federation of European Biochemical Societies*, 407, pp.313–319.

Orban, P.C., Chui, D. and Marth, J.D., 1992. Tissue- and site-specific DNA recombination in transgenic mice. *Genetics*, 89, pp.6861–6865.

Owens, G.K. (2007). Molecular Control of Vascular Smooth Muscle Cell Differentiation and Phenotypic Plasticity. (John Wiley & Sons, Ltd), pp. 174–193.

Parameswaran, M. and Tam, P.P., 1995. Regionalisation of cell fate and morphogenetic movement of the mesoderm during mouse gastrulation. *Developmental genetics*, 17(1), pp.16–28.

Pardali, E., Goumans, M.-J. and Dijke, Ten, P., 2010. Signaling by members of the TGF-beta family in vascular morphogenesis and disease. *Trends in cell biology*, 20(9), pp.556–567.

Passman, J.N., Dong, X.R., Wu, S.P., Maguire, C.T., Hogan, K.A., Bautch, V.L. and Majesky, M.W., 2008. A sonic hedgehog signaling domain in the arterial adventitia supports resident Sca1+ smooth muscle progenitor cells. *Proceedings of the National Academy of Sciences*, 105(27), pp.9349–9354.

Peterson, S.M., Liaw, L. and Lindner, V., 2016. Ligation of the Mouse Common Carotid Artery. In: *Mouse Models of Vascular Diseases*. Tokyo: Springer, Tokyo, pp.43–68.

Petrova, R. and Joyner, A.L., 2014. Roles for Hedgehog signaling in adult organ homeostasis and repair. *Development*, 141(18), pp.3445–3457.

Polizio, A.H., Chinchilla, P., Chen, X., Kim, S., Manning, D.R. and Riobo, N.A., 2011. Heterotrimeric Gi proteins link Hedgehog signaling to activation of Rho small GTPases to promote fibroblast migration. *The Journal of biological chemistry*, 286(22), pp.19589–19596.

Pratumvinit, B., Reesukumal, K., Janebodin, K., Ieronimakis, N. and Reyes, M., 2013. Isolation, characterization, and transplantation of cardiac endothelial cells. *BioMed research international*, 2013(8), pp.359412–18.

Provost & Wallert Research (2015) *Haemocytometer Cell Counting Protocol*. Available at: http://home.sandiego.edu/~josephprovost/Hemocytometer%20Cell%20Counting%20Protocol.pdf

Proweller, A., Pear, W.S. and Parmacek, M.S., 2005. Notch signaling represses myocardin-induced smooth muscle cell differentiation. *The Journal of biological chemistry*, 280(10), pp.8994–9004.

Redmond, E.M., Hamm, K., Cullen, J.P., Hatch, E., Cahill, P.A. and Morrow, D., 2013. Inhibition of Patched-1 Prevents Injury-Induced Neointimal Hyperplasia. *Arteriosclerosis, Thrombosis, and Vascular Biology*, 33(8), pp.1960–1964.

Redmond, E.M., Liu, W., Hamm, K., Hatch, E., Cahill, P.A. and Morrow, D., 2014. Perivascular delivery of Notch 1 siRNA inhibits injury-induced arterial remodeling. *PloS one*, 9(1), p.e84122.

Reinert, R.B., Kantz, J., Misfeldt, A.A., Poffenberger, G., Gannon, M., Brissova, M. and Powers, A.C., 2012. Tamoxifen-Induced Cre-loxP Recombination Is Prolonged in Pancreatic Islets of Adult Mice. *PloS one*, 7(3), p.e33529.

Rensen, S.S.M., Doevendans, P.A.F.M. and van Eys, G.J.J.M., 2007. Regulation and characteristics of vascular smooth muscle cell phenotypic diversity. *Netherlands Heart Journal*, 15(3), pp.100–108.

Rivera-Pérez, J.A., and Hadjantonakis, A.K. (2015). The dynamics of morphogenesis in the early mouse embryo. *Cold Spring Harb. Perspect. Biol*. 7.11: :a015867 17

Romagnani, P., Rinkevich, Y. and Dekel, B., 2015. The use of lineage tracing to study kidney injury and regeneration. *Nature reviews. Nephrology*, 11(7), pp.420–431.

Ross, R., 1999. Atherosclerosis--an inflammatory disease. *The New England journal of medicine*, 340(2), pp.115–126.

Sainz, J., Haj Zen, Al, A., Caligiuri, G., Demerens, C., Urbain, D., Lemitre, M. and Lafont, A., 2006. Isolation of 'side population' progenitor cells from healthy arteries of adult mice. *Arteriosclerosis, Thrombosis, and Vascular Biology*, 26(2), pp.281–286.

Saiura, A., Sata, M., Hirata, Y., Nagai, R. and Makuuchi, M., 2001. Circulating smooth muscle progenitor cells contribute to atherosclerosis. *Nature medicine*, 7(4), pp.382–383.

Sakamoto, A., Torii, S., Jinnouchi, H., Finn, A.V., Virmani, R. and Kolodgie, F.D., 2018. Pathologic intimal thickening: Are we any closer to understand early transitional plaques that lead to symptomatic disease? *Atherosclerosis*, 274, pp.227–229.

Sanan, D.A., Newland, D.L., Tao, R., Marcovina, S., Wang, J., Mooser, V., Hammer, R.E. and Hobbs, H.H., 1998. Low density lipoprotein receptor-negative mice expressing human apolipoprotein B-100 develop complex atherosclerotic lesions on a chow diet: no accentuation by apolipoprotein(a). *Proceedings of the National Academy of Sciences*, 95(8), pp.4544–4549.

Sandison, M.E., Dempster, J., and McCarron, J.G. (2016). The transition of smooth muscle cells from a contractile to a migratory, phagocytic phenotype: direct demonstration of phenotypic modulation. *J. Physiol.* 594, 6189.

Santos, A., Fernández-Friera, L., Villalba, M., López-Melgar, B., España, S., Mateo, J., Mota, R.A., Jiménez-Borreguero, J. and Ruiz-Cabello, J., 2015. Cardiovascular imaging: what have we learned from animal models? *Frontiers in Pharmacology*, 6(149), pp.239–25.

Sartore, S., Chiavegato, A., Faggin, E., Franch, R., Puato, M., Ausoni, S. and Pauletto, P., 2001. Contribution of adventitial fibroblasts to neointima formation and vascular remodeling: from innocent bystander to active participant. *Circulation research*, 89(12), pp.1111–1121.

Sata, M., 2003. Molecular strategies to treat vascular diseases: circulating vascular progenitor cell as a potential target for prophylactic treatment of atherosclerosis.

Circulation journal: official journal of the Japanese Circulation Society, 67(12), pp.983–991.

Sata, M., Maejima, Y., Adachi, F., Fukino, K., Saiura, A., Sugiura, S., Aoyagi, T., Imai, Y., Kurihara, H., Kimura, K., Omata, M., Makuuchi, M., Hirata, Y. and Nagai, R., 2000. A mouse model of vascular injury that induces rapid onset of medial cell apoptosis followed by reproducible neointimal hyperplasia. *Journal of Molecular and Cellular Cardiology*, 32(11), pp.2097–2104.

Sata, M., Saiura, A., Kunisato, A., Tojo, A., Okada, S., Tokuhisa, T., Hirai, H., Makuuchi, M., Hirata, Y. and Nagai, R., 2002. Hematopoietic stem cells differentiate into vascular cells that participate in the pathogenesis of atherosclerosis. *Nature medicine*, 8(4), pp.403–409.

Sata, M., Sugiura, S., Yoshizumi, M., Ouchi, Y., Hirata, Y. and Nagai, R., 2001. Acute and chronic smooth muscle cell apoptosis after mechanical vascular injury can occur independently of the Fas-death pathway. *Arteriosclerosis, Thrombosis, and Vascular Biology*, 21(11), pp.1733–1737.

Sauer, B. and Henderson, N., 1988. Cre-stimulated recombination at loxP-containing DNA sequences placed into the mammalian genome. *Nucleic Acids Research*, 17, pp.147–161.

Sauer, B., 1987. FunctionalExpressionofthecre-loxSite-SpecificRecombination System in the Yeast Saccharomyces cerevisiae. *Molecular and Cellular Biology*, pp.2087–2096.

Schiro, A., Wilkinson, F.L., Weston, R., Smyth, J.V., Serracino-Inglott, F. and Alexander, M.Y., 2014. Endothelial microparticles as conveyors of information in atherosclerotic disease. *Atherosclerosis*, 234(2), pp.295–302.

Schneider, C.A., Rasband, W.S. and Eliceiri, K.W., 2012. NIH Image to ImageJ: 25 years of image analysis. *Nature Methods*, 9(7), pp.671–675.

Scott Freeman (2011) *Biological Science*. 4th Edn. San Francisco: Pearson Benjamin Cummings

Shah, P.K., 2003. Mechanisms of plaque vulnerability and rupture. *Journal of the American College of Cardiology*, 41(4), pp.S15–S22.

Shankman, L.S., Gomez, D., Cherepanova, O.A., Salmon, M., Alencar, G.F., Haskins, R.M., Swiatlowska, P., Newman, A.A.C., Greene, E.S., Straub, A.C., Isakson, B., Randolph, G.J. and Owens, G.K., 2015. KLF4-dependent phenotypic modulation of smooth muscle cells has a key role in atherosclerotic plaque pathogenesis. *Nature medicine*, 21(6), pp.628–637.

Shi, Y., O'Brien, J.E., Fard, A., Mannion, J.D., Wang, D. and Zalewski, A., 1996. Adventitial Myofibroblasts Contribute to Neointimal Formation in Injured Porcine Coronary Arteries. *Circulation*, 94(7), pp.1655–1664.

Shikatani, E.A., Chandy, M., Besla, R., Li, C.C., Momen, A., El-Mounayri, O., Robbins, C.S., and Husain, M. (2016). c-Myb Regulates Proliferation and Differentiation of Adventitial Sca1 + Vascular Smooth Muscle Cell Progenitors by Transactivation of Myocardin. *Arterioscler. Thromb. Vasc. Biol*. 36, 1367–1376.

Shimizu, K., Sugiyama, S., Aikawa, M., Fukumoto, Y., Rabkin, E., Libby, P. and Mitchell, R.N., 2001. Host bone-marrow cells are a source of donor intimal smooth-muscle-like cells in murine aortic transplant arteriopathy. *Nature medicine*, 7(6), pp.738–741.

Shin, M., Nagai, H. and Sheng, G., 2009. Notch mediates Wnt and BMP signals in the early separation of smooth muscle progenitors and blood/endothelial common progenitors. *Development*, 136(4), pp.595–603.

Shoji, M., Koba, S. and Kobayashi, Y., 2014. Roles of bone-marrow-derived cells and inflammatory cytokines in neointimal hyperplasia after vascular injury. *BioMed research international*, 2014(14), pp.945127–8.

Sinha, S., Hoofnagle, M.H., Kingston, P.A., McCanna, M.E. and Owens, G.K., 2004. Transforming growth factor-beta1 signaling contributes to development of smooth muscle cells from embryonic stem cells. *American journal of physiology. Cell physiology*, 287(6), pp.C1560–8.

Sinha, S., Iyer, D. and Granata, A., 2014. Embryonic origins of human vascular smooth muscle cells: implications for in vitro modeling and clinical application. *Cellular and molecular life sciences: CMLS*, 71(12), pp.2271–2288.

Skowasch, D., Jabs, A., Andrié, R., Dinkelbach, S., Lüderitz, B., and Bauriedel, G. (2003). Presence of bone-marrow- and neural-crest-derived cells in intimal hyperplasia at the time of clinical in-stent restenosis. *Cardiovasc. Res.* 60, 684–691.

Steinhart, Z. and Angers, S., 2018. Wnt signaling in development and tissue homeostasis. *Development*, 145(11), p.dev146589.

Stenmark, K.R. and Mecham, R.P., 1997. Cellular and molecular mechanisms of pulmonary vascular remodeling. *Annual review of physiology*, 59(1), pp.89–144.

Stocker, R. and Keaney, J.F., 2004. Role of oxidative modifications in atherosclerosis. *Physiological reviews*, 84(4), pp.1381–1478.

Takayama, T., Shi, X., Wang, B., Franco, S., Zhou, Y., DiRenzo, D., Kent, A., Hartig, P., Zent, J. and Guo, L.-W., 2015. A murine model of arterial restenosis: technical aspects of femoral wire injury. *Journal of visualized experiments: JoVE*, (97), p.e52561.

Talele, N.P., Fradette, J., Davies, J.E., Kapus, A. and Hinz, B., 2015. Expression of α-Smooth Muscle Actin Determines the Fate of Mesenchymal Stromal Cells. *Stem cell reports*, 4(6), pp.1016–1030.

Tang, Z., Wang, A., Wang, D. and Li, S., 2013. Smooth muscle cells: to be or not to be? Response to Nguyen et Al. *Circulation research*, 112(1), pp.23–26.

Tang, Z., Wang, A., Yuan, F., Yan, Z., Liu, B., Chu, J.S., Helms, J.A. and Li, S., 2012. Differentiation of multipotent vascular stem cells contributes to vascular diseases. *Nature Communications*, 3(1), pp.875–13.

Torsney, E. and Xu, Q., 2011. Resident vascular progenitor cells. *Journal of Molecular and Cellular Cardiology*, 50(2), pp.304–311.

Torsney, E., Hu, Y. and Xu, Q., 2005. Adventitial progenitor cells contribute to arteriosclerosis. *Trends Cardiovasc Med*, 15(2), pp.64–68.

Touboul P-J. Intima-media thickness of carotid arteries. *Front Neurol Neurosci*. 2015;36:31–39.

Trigueros-Motos, L., González-Granado, J.M., Cheung, C., Fernández, P., Sánchez-Cabo, F., Dopazo, A., Sinha, S. and Andrés, V., 2013. Embryological-origin-dependent differences in homeobox expression in adult aorta: role in regional phenotypic variability and regulation of NF-κB activity. *Arteriosclerosis, Thrombosis, and Vascular Biology*, 33(6), pp.1248–1256.

Tsaousi, A., Williams, H., Lyon, C.A., Taylor, V., Swain, A., Johnson, J.L. and George, S.J., 2011. Wnt4/β-catenin signaling induces VSMC proliferation and is associated with intimal thickening. *Circulation research*, 108(4), pp.427–436.

Uchida, K., Sasahara, M., Morigami, N., Hazama, F. and Kinoshita, M., 1996. Expression of platelet-derived growth factor B-chain in neointimal smooth muscle cells of balloon injured rabbit femoral arteries. *Atherosclerosis*, 124(1), pp.9–23.

Uryga, A.K. and Bennett, M.R., 2016. Ageing induced vascular smooth muscle cell senescence in atherosclerosis. *The Journal of Physiology*, 594(8), pp.2115–2124.

Valny, M., Honsa, P., Kirdajova, D., Kamenik, Z. and Anderova, M., 2016. Tamoxifen in the Mouse Brain: Implications for Fate-Mapping Studies Using the Tamoxifen-Inducible Cre-loxP System. *Frontiers in cellular neuroscience*, 10(e78236), p.243.

Varjosalo, M. and Taipale, J., 2008. Hedgehog: functions and mechanisms. *Genes & Development*, 22, pp.2454-2472.

Walshe, T.E., Connell, P., Cryan, L., Ferguson, G., Gardiner, T., Morrow, D., Redmond, E.M., O'Brien, C., and Cahill, P.A. (2011). Microvascular Retinal Endothelial and Pericyte Cell Apoptosis In Vitro: Role of Hedgehog and Notch Signaling. *Investig. Opthalmology Vis. Sci*. 52, 4472.

Wan, M., Li, C., Zhen, G., Jiao, K., He, W., Jia, X., Wang, W., Shi, C., Xing, Q., Chen, Y.-F., Jan De Beur, S., Yu, B. and Cao, X., 2012. Injury-activated transforming growth factor β controls mobilization of mesenchymal stem cells for tissue remodeling. *Stem cells (Dayton, Ohio)*, 30(11), pp.2498–2511.

Wang, G., Jacquet, L., Karamariti, E. and Xu, Q., 2015. Origin and differentiation of vascular smooth muscle cells. *The Journal of Physiology*, 593(14), pp.3013–3030.

Wang, X., Chai, H., Lin, P.H., Lumsden, A.B., Yao, Q. and Chen, C., 2006. Mouse models of neointimal hyperplasia: techniques and applications. *Medical science*

monitor: international medical journal of experimental and clinical research, 12(9), pp.RA177–85.

Wang, Y., Cao, W., Cui, J., Yu, Y., Zhao, Y., Shi, J., Wu, J., Xia, Z., Yu, B. and Liu, J., 2018. Arterial Wall Stress Induces Phenotypic Switching of Arterial Smooth Muscle Cells in Vascular Remodeling by Activating the YAP/TAZ Signaling Pathway. *Cellular physiology and biochemistry: international journal of experimental cellular physiology, biochemistry, and pharmacology*, 51(2), pp.842–853.

Wasilewski, J., Głowacki, J. and Poloński, L., 2013. Not at random location of atherosclerotic lesions in thoracic aorta and their prognostic significance in relation to the risk of cardiovascular events. *Polish journal of radiology*, 78(2), pp.38–42.

Weinberg, N., Ouziel-Yahalom, L., Knoller, S., Efrat, S., and Dor, Y. (2007). Lineage Tracing Evidence for In Vitro Dedifferentiation but Rare Proliferation of Mouse Pancreatic -Cells. *Diabetes* 56, 1299–1304.

Weissman, T.A. and Pan, Y.A., 2015. Brainbow: new resources and emerging biological applications for multicolor genetic labeling and analysis. *Genetics*, 199(2), pp.293–306.

Westermark, B., Siegbahn, A., Heldin, C.H. and Claesson-Welsh, L., 1990. B-type receptor for platelet-derived growth factor mediates a chemotactic response by means of ligand-induced activation of the receptor protein-tyrosine kinase. *Proceedings of the National Academy of Sciences*, 87(1), pp.128–132.

Xiao, Q., Zeng, L., Zhang, Z., Hu, Y. and Xu, Q., 2007. Stem cell-derived Sca-1+ progenitors differentiate into smooth muscle cells, which is mediated by collagen IV-integrin alpha1/beta1/alphav and PDGF receptor pathways. *American journal of physiology. Cell physiology*, 292(1), pp.C342–52.

Xie, C., Ritchie, R.P., Huang, H., Zhang, J. and Chen, Y.E., 2011. Smooth muscle cell differentiation in vitro: models and underlying molecular mechanisms. *Arteriosclerosis, Thrombosis, and Vascular Biology*, 31(7), pp.1485–1494.

Xu, C., Gao, X., Wei, Q., Nakahara, F., Zimmerman, S.E., Mar, J. and Frenette, P.S., 2018. Stem cell factor is selectively secreted by arterial endothelial cells in bone marrow. *Nature Communications*, 9(1), p.2449.

Yamashita, J., Itoh, H., Hirashima, M., Ogawa, M., Yurugi, T., Naito, M., Nakao, K. and Nishikawa, S., 2000. Flk1-positive cells derived from embryonic stem cells serve as vascular progenitors. *Nature*, 408(6808), pp.92–96.

Yang, P., Hong, M.S., Fu, C., Schmit, B.M., Su, Y., Berceli, S.A. and Jiang, Z., 2016. Preexisting smooth muscle cells contribute to neointimal cell repopulation at an incidence varying widely among individual lesions. *Surgery*, 159(2), pp.602–612.

Yu H., Stoneman V, Clarke M, Figg N, Xin H-B, Kotlikoff M, Littlewood T, Bennett M. Bone marrow-derived smooth muscle-like cells are infrequent in advanced primary atherosclerotic plaques but promote atherosclerosis. *Arterioscler Thromb Vasc Biol*. 2011;31:1291–1299.

Yu, Q.C., Song, W., Wang, D. and Zeng, Y.A., 2016. Identification of blood vascular endothelial stem cells by the expression of protein C receptor. *Cell research*, 26(10), pp.1079–1098.

Yuan, F., Wang, D., Xu, K., Wang, J., Zhang, Z., Yang, L., Yang, G.-Y. and Li, S., 2017. Contribution of Vascular Cells to Neointimal Formation. *PloS one*, 12(1), p.e0168914.

Zaniboni, A., Bernardini, C., Bertocchi, M., Zannoni, A., Bianchi, F., Avallone, G., Mangano, C., Sarli, G., Calzà, L., Bacci, M.L. and Forni, M., 2015. In vitro differentiation of porcine aortic vascular precursor cells to endothelial and vascular smooth muscle cells. *American journal of physiology. Cell physiology*, 309(5), pp.C320–31.

Zaragoza, C., Gomez-Guerrero, C., Martin-Ventura, J.L., Blanco-Colio, L., Lavin, B., Mallavia, B., Tarin, C., Mas, S., Ortiz, A. and Egido, J., 2011. Animal models of cardiovascular diseases. *Journal of biomedicine & biotechnology*, 2011(2), pp.497841–13.

Zhang, L., and Xu, Q. (2017). Vascular Progenitors and Smooth Muscle Cells Chicken and Egg? *Circ. Res.* 120, 246–248.

Zomer, A., Steenbeek, S.C., Maynard, C. and van Rheenen, J., 2016. Studying extracellular vesicle transfer by a Cre-loxP method. *Nature protocols*, 11(1), pp.87–101.